NASA/CR—2003-212317

Analysis of Combustion Systems

Daniel B. Bain and Clifford E. Smith
CFD Research Corporation, Huntsville, Alabama

August 2003

The NASA STI Program Office . . . in Profile

Since its founding, NASA has been dedicated to the advancement of aeronautics and space science. The NASA Scientific and Technical Information (STI) Program Office plays a key part in helping NASA maintain this important role.

The NASA STI Program Office is operated by Langley Research Center, the Lead Center for NASA's scientific and technical information. The NASA STI Program Office provides access to the NASA STI Database, the largest collection of aeronautical and space science STI in the world. The Program Office is also NASA's institutional mechanism for disseminating the results of its research and development activities. These results are published by NASA in the NASA STI Report Series, which includes the following report types:

- TECHNICAL PUBLICATION. Reports of completed research or a major significant phase of research that present the results of NASA programs and include extensive data or theoretical analysis. Includes compilations of significant scientific and technical data and information deemed to be of continuing reference value. NASA's counterpart of peer-reviewed formal professional papers but has less stringent limitations on manuscript length and extent of graphic presentations.

- TECHNICAL MEMORANDUM. Scientific and technical findings that are preliminary or of specialized interest, e.g., quick release reports, working papers, and bibliographies that contain minimal annotation. Does not contain extensive analysis.

- CONTRACTOR REPORT. Scientific and technical findings by NASA-sponsored contractors and grantees.

- CONFERENCE PUBLICATION. Collected papers from scientific and technical conferences, symposia, seminars, or other meetings sponsored or cosponsored by NASA.

- SPECIAL PUBLICATION. Scientific, technical, or historical information from NASA programs, projects, and missions, often concerned with subjects having substantial public interest.

- TECHNICAL TRANSLATION. English-language translations of foreign scientific and technical material pertinent to NASA's mission.

Specialized services that complement the STI Program Office's diverse offerings include creating custom thesauri, building customized databases, organizing and publishing research results . . . even providing videos.

For more information about the NASA STI Program Office, see the following:

- Access the NASA STI Program Home Page at ***http://www.sti.nasa.gov***

- E-mail your question via the Internet to help@sti.nasa.gov

- Fax your question to the NASA Access Help Desk at 301–621–0134

- Telephone the NASA Access Help Desk at 301–621–0390

- Write to:
  NASA Access Help Desk
  NASA Center for AeroSpace Information
  7121 Standard Drive
  Hanover, MD 21076

NASA/CR—2003-212317

Analysis of Combustion Systems

Daniel B. Bain and Clifford E. Smith
CFD Research Corporation, Huntsville Alabama

Prepared under Contract NAS3–25967

National Aeronautics and
Space Administration

Glenn Research Center

August 2003

Document History

This research was originally published internally as HSR043 in August 1996.

Available from

NASA Center for Aerospace Information
7121 Standard Drive
Hanover, MD 21076

National Technical Information Service
5285 Port Royal Road
Springfield, VA 22100

Available electronically at http://gltrs.grc.nasa.gov

PREFACE

This report is the final report of the project entitled "Analysis of Combustion Systems". The project was funded under NASA Lewis Contract NAS3-25967. The NASA-LeRC technical monitor was Dr. James D. Holdeman.

Mr. Clifford E. Smith was the Program Manager at CFD Research Corporation (CFDRC). The CFDRC Principal Investigator (PI) was Mr. Daniel B. Bain. Ms. Marni Kent prepared all documentation at CFDRC.

Additional engineering support at CFDRC was supplied by Dr. Scott Crocker and Dr. Andy Leonard. Software support at CFDRC was supplied by Mr. Milind Talpallikar, Mr. Fritz Owens, Mr. Gary Hufford, Dr. Vincent Harrand and Mr. Lyle Johnson. Many others at CFDRC also aided in the success of this project.

Strong interaction and useful discussions were held with Mr. David S. Liscinsky and Dr. Alexander Vranos at United Technology Research Center; their cooperation is greatly appreciated. Discussions and feedback were also held with Dr. G. Scott Samuelsen and Dr. William Sowa (especially for the NIC code); University of California, Irvine; and Dr. Hukam Mongia and Mr. Victor L. Oechsle of Allison Engine.

EXECUTIVE SUMMARY

As part of the NASA High-Speed Research Program, low emission combustors are being studied and demonstrated. One combustor concept that is currently being studied and evaluated is the Rich burn-Quick mix-Lean burn (RQL) combustor. The quick-mix zone of the RQL combustor is extremely important in reducing NO_x emissions; rapid mixing of the bypass airflow with rich-burn effluent is essential. The basic challenge can be described as rapid jet-in-crossflow mixing. Although jet-in-crossflow mixing is not new, this RQL application is unique in that the jet-to-mainstream mass-flow ratios are higher than studied previously (~3 in RQL applications versus ~0.5 in dilution zone studies), plus the emphasis is on reducing NO_x emissions (i.e. good mixing might not necessarily produce low emissions).

This five-year project focused on identifying quick-mix methods that would reduce NO_x emissions in RQL combustors. The work included study of mixing concepts, and the development of design methodology. 3D CFD analysis was the primary tool used in assessing concepts and developing design methodology for low emissions. Isothermal and reacting CFD calculations were performed on cylindrical, rectangular, and annular generic geometries. Systematic parametric studies were performed to isolate key design parameters and their influence on mixing and emissions. Some of the parametric studies were:

1. the effect of rich burn-to-quick mix neckdown ratio;
2. the effect of jet-to-mainstream momentum-flux ratio (J);
3. the effect of number of orifices;
4. the effect of slot aspect ratio;
5. comparison of slanted versus straight slots;
6. comparison of inline versus staggered orifices for rectangular geometries;
7. effect of jet-to-mainstream mass-flow ratio;
8. the effect of orifice shape;
9. the effect of spacing-to-duct height (S/H) in rectangular geometries;
10. the effect of increased pressure drop across orifice;
11. the effect of orifice blockage;

12. comparison of optimum annular and can geometries;
13. the effect of plenum-to-mainstream flow coupling; and
14. the effect of orifice length-to-diameter ratio.

In addition to the CFD analysis, software was written to interpret experimental isothermal mixing results in terms of NO_x emissions. The software, called NO_x Inference Code (NIC), took planar experimental jet mass fraction data and inferred NO_x emissions assuming: 1) the jet mass fraction fields were the same for reacting and non-reacting flows if the momentum-flux ratio and mass-flow ratio were maintained, and 2) fast equilibrium chemistry occurred for heat release. Thermal NO_x was predicted using the extended Zeldovich mechanism. The code was validated using the experimental data of Anderson. NIC was then used to assess the effect of jet penetration on NO_x emissions and to compare emission for optimum inline and staggered orifices in a rectangular geometry.

Important conclusions in this project are:

1. Optimum mixing and lowest NO_x emissions occur when jets from orifices penetrate to an optimum location. For a can geometry, the jets should penetrate to the mid-radius (based on area); for a rectangular or annular geometry, the jets should penetrate to 1/4 of the duct height (for two-sided injection).

2. Orifice shape and/or slot orientation does not seem to affect NO_x emissions as long as optimum jet penetration is achieved.

3. Optimum penetration is generally achieved when designs meet the following correlation:

$$C = (S/H)\sqrt{J}$$

This correlation is in general agreement with Holdeman's correlation, except the correlation constant is approximately doubled for two-sided jet injection for rectangular or annular geometries.

4. Necking down the quick-mix zone decreases residence time, therefore decreasing NO_x emissions. There is a limit on the amount of neckdown, based on the total pressure drop across the quick-mix zone.

5. In RQL quick-mix sections, NO_x is produced in the jet shear layers at near stoichiometric flame temperatures.

6. Two-sided, inline round orifices seem to produce the lowest NO_x emissions. This configuration has orifices with the least amount of jet surface area (i.e. jet shear layer area).

7. Rectangular or annular geometries will produce lower NO_x emissions than can geometries for optimized jet configurations.

8. Increasing the pressure drop across the orifices will reduce NO_x emissions if the jet penetration is optimized.

9. For orifice blockage as high as 90%, orifice blockage did not affect jet penetration or mixing.

Overall, this project produced an improved understanding of the jet-in-crossflow mixing process and emission production in RQL combustor applications. Improved design methodology was developed that assisted in the design and evaluation of RQL combustors for High-Speed Civil Transport Aircraft engines. Close interaction was maintained with United Technology Research Center (UTRC) and Pratt & Whitney (P&W) for the duration of the project.

TABLE OF CONTENTS

TABLE OF CONTENTS (continued)

LIST OF ILLUSTRATIONS

LIST OF ILLUSTRATIONS (continued)

1.0 INTRODUCTION

As today's society becomes more aware of their continuing destruction of the environment, efforts have increased to understand and reduce the effects of technology and the ongoing deterioration of the planet. One main area of concern that has surfaced recently is the continuing deterioration of the ozone layer. One of the key contributors to the disappearing ozone layer is the emissions exhausted from present day aircraft and proposed supersonic aircraft. The environmental effects of carbon monoxide (CO), oxides of nitrogen (NO_x), and unburned hydrocarbon (UHC) have been identified as having a close relation with the causes of the reduction in the ozone layer.

The goal of reduced emission signatures of advance combustors is one of increasing importance. Recent advances of gas turbine technology have focussed on increasing both the engine pressure ratio and turbine inlet temperature levels. These advances will realize a gain in the overall thermodynamic cycle efficiency which in turn reduces the specific fuel consumption. Unfortunately, these gains cannot be achieved without adversely affecting gaseous emissions. The production of nitrogen oxides (NO and NO_2) formed in gas turbine engines is proportional to the cycle temperature and are thought to cause the most problems. The nitrogen oxides can be characterized by two main groups;

1. prompt NO_x, which is generally associated with lower temperatures and having fuel fragments present. Typically prompt NO_x is formed near the fuel injector and in the primary zone of the combustor; and
2. thermal NO_x which is present in regions of high temperatures and stoichiometric fuel-air ratios. In combustors where the fuel and the air are not premixed, the thermal NO_x mechanism produces the most significant NO_x .

The necessity of developing new ways of controlling NO_x has led to radical changes in combustor design. Typical combustors has been created employing a single-staged combustion process where the fuel and air are allowed to enter the combustion chamber and react at near stoichiometric temperatures. To compensate for the high

operating temperatures on NO_x production, staged combustion is being explored as an alterative method. One staged combustion concept is the Rich burn-Quick mix-Lean burn (RQL) combustor.[1] This combustor utilizes the staged burning concept in which the primary zone is designed to operate fuel-rich.[2] The combustion products high in carbon monoxide concentration (but low in NO_x concentrations) enter the quick mix section where mixing is initiated with bypass air. The combustion process is then completed in the lean-burn section. Figure 1-1 shows a typical RQL combustor.

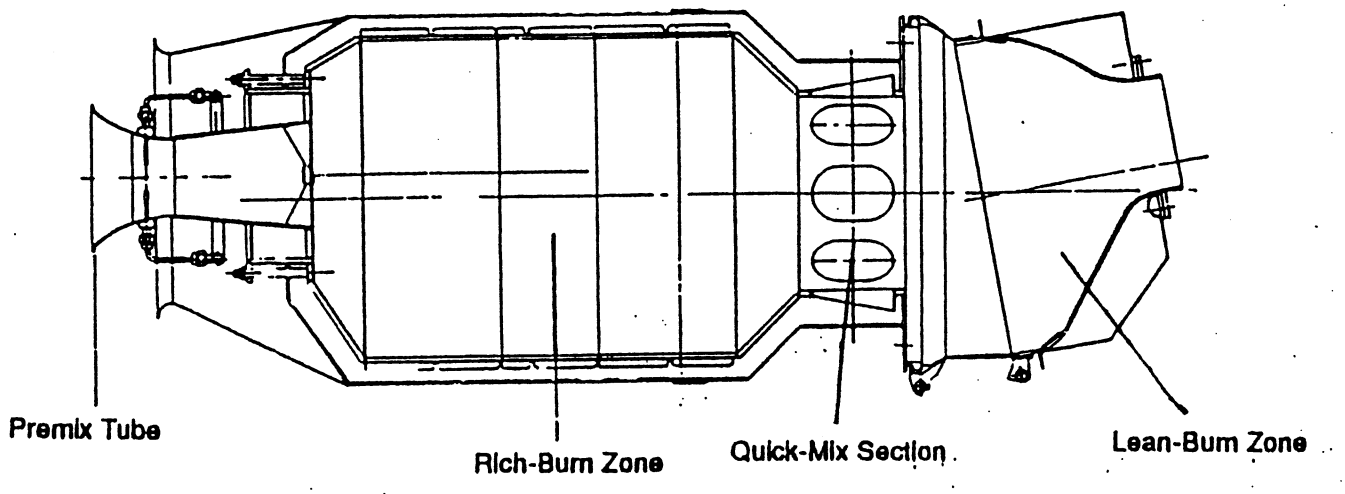

Figure 1-1. Typical RQL Combustor

The successful performance (i.e. low NO_x emission) of the RQL combustor relies on the ability to attain rapid and uniform mixing of the bypass airflow and combustion products in the quick-mix section. For the flowfields to have low NO_x, the mixing taking place at stoichiometric fuel-air ratios must occur very quickly (i.e. low residence times). Therefore a good design of the mixing section is essential to the overall success of the RQL concept.

The mixing that takes place in the RQL quick-mix section can be generically described as jet mixing in confined crossflow. For some time now, the importance of research on jet mixing in a confined crossflow has been recognized as having a significant impact on a variety of practical applications. Within the gas turbine industry, jet mixing is especially important in the combustor dilution zone. The dilution zone represents the aft section of the combustor where the combustion products are mixed with bypass air to produce a temperature profile acceptable to the combustor.[3,4] The typical range of jet-to-mainstream mass-flow ratio (MR) varies from 0.25 to 0.50.

In sharp contrast to conventional combustor dilution zones, the RQL mixing zone has a number of significant differences. Typical jet-to-mainstream mass-flow ratios are on the order of 3.0 or higher. The increase in jet mass flow potentially leads to larger orifices. With the use of larger orifices, slots may be needed rather than round holes in order to fit the orifices in the liner. In addition, the blockage effects associated with larger orifices is unknown. Another major difference for RQL quick-mix zones is that emissions levels become the main design driver, rather than temperature profile and "hot" spots.

Over the years, significant research has been performed on dilution zone mixing studies. These studies have been performed using cylindrical, rectangular, and annular geometries. This research has identified two key parameters that determine jet penetration and mixing characteristics; 1) jet-to-mainstream momentum-flux ratio (J), and 2) orifice spacing-to-duct height ratio (S/H). Single-sided injection was extensively studied while two-sided injection was studied to a lesser extent. Optimum mixing was determined to be a function of the product of S/H and the square root of J for the range of conditions tested and analyzed[4]:

$$C = (S/H)\sqrt{J} \tag{1}$$

where C = 2.5 for can geometries
2.5 for single-sided injection in rectangular geometries
1.25 for inline two-sided injection in rectangular geometries
5.0 for staggered two-sided injection in rectangular geometries.

The best mixing was found to occur when the jets penetrated to one-quarter duct height for two-sided injection in rectangular geometries and one-half duct height for single-sided injection in rectangular geometries. Optimum penetration for can geometries occurred when the jets penetrated to mid-radius (based on area). The optimum number of orifices can be expressed as:

$$n = \sqrt{2J} / C \tag{2}$$

where n = optimum number of holes
C = experimentally derived constant (2.5)
J = momentum-flux ratio.

It is important to note that in deriving this equation it was assumed that the orifice spacing for a rectangular duct would be appropriate for a can when applied at the radius that divides the can into equal area can and annular sections.

Current NASA programs have been funding studies that focus on identifying improved mixing and emission concepts pertaining to RQL applications.[5-41]

2.0 TECHNICAL OBJECTIVE AND APPROACH

The overall goal of this project was to numerically determine and evaluate mixing concepts that reduced overall RQL combustor emissions. The technical objectives were to:

a. perform 3-D non-reacting and reacting flow calculations to investigate the effects of flow and geometric variations that promote and enhance the mixing of two gas streams in cylindrical, rectangular, and annular configurations;

b. to develop design methodology for low emission quick-mix zones; and

c. to develop a software program that infers NO_x emissions from experimental isothermal jet mass fraction fields.

3D CFD analysis was the primary tool used to perform the work. Two flow solvers were employed: REFLEQS[42,43,44,45] (used in years 1, 2 and 3) and CFD-ACE[42,43,46,47] (used in years 4 and 5). CFD-ACE represents a newer technology than REFLEQS. The grids were generated using an in-house orthogonal grid generator (in years 1, 2 and 3) and CFD-GEOM[48] (in years 4 and 5), a multi-block, body-fitted-coordinate grid generator. The CFD results were graphically viewed and interpreted using PLOT3D[49] (in years 1, 2 and 3) and CFD-VIEW[50] (in years 4 and 5). Non-graphical post-processing was performed using CFD-POST.[51]

The flow conditions used in the analysis were chosen to maintain close commonality with HSCT operating conditions. Likewise, geometric dimensions were chosen to be similar to HSCT combustor dimensions.

All technical objectives were achieved in this project.

3.0 ISOTHERMAL FLOW CALCULATIONS FOR CYLINDRICAL GEOMETRIES

3.1 Study of the Jet Mixing from Slanted Slots

In this analysis, slanted slots in a confined cylindrical crossflow were examined. Specifically, the mixing of 45 deg. slanted slot jets in a confined crossflow were studied. A six-slot, 2.5 inch diameter model of United Technologies Research Center's (UTRC's) experimental configuration was analyzed. To validate the CFD analysis, numerical predictions were first compared to UTRC experimental results. Then, a total of three parametric studies was performed. Two parametric studies were performed to assess the effect of jet-to-mainstream momentum-flux ratio (J) on mixing, one maintaining constant slot area and the other maintaining constant jet mass flow. The third parametric study studied the effect of density ratio (ρ_j/ρ_m).

3.1.1 Model Specifications

The numerical model is shown in Figure 3-1. The cylinder was 2.5 inches (0.0635 m) in diameter. All other pertinent dimensions of the geometry are shown in Figure 3-1. Six equally spaced slots were positioned on the perimeter of the cylinder. The leading edges of the slots were located 6.43 inches (0.1633 m) from the inlet of the cylinder. The aspect ratio of each slot was 4-to-1, with the largest geometric dimension of 0.620 inches (0.0157 m) angled 45 degrees to the direction of the mainstream flow. The numerical model assumed a discharge coefficient of 0.8, thus giving a physical slot with dimensions of 0.555 inches by 0.1395 inches (0.0141 m by 0.0035 m).

3.1.2 Grid

The grid consisted of a pie section that twisted at a 45 degree angle through the slot (see Figure 3-2). A twisted grid was chosen instead of a straight pie section grid to reduce grid skewness and to be able to handle overlapping slanted slots tested at UTRC. The grid had 24,192 cells (72×16×21 cells in x, r, θ directions). The grid distribution was non-uniform with greater grid density in the vicinity of the slot as well as the combustor wall.

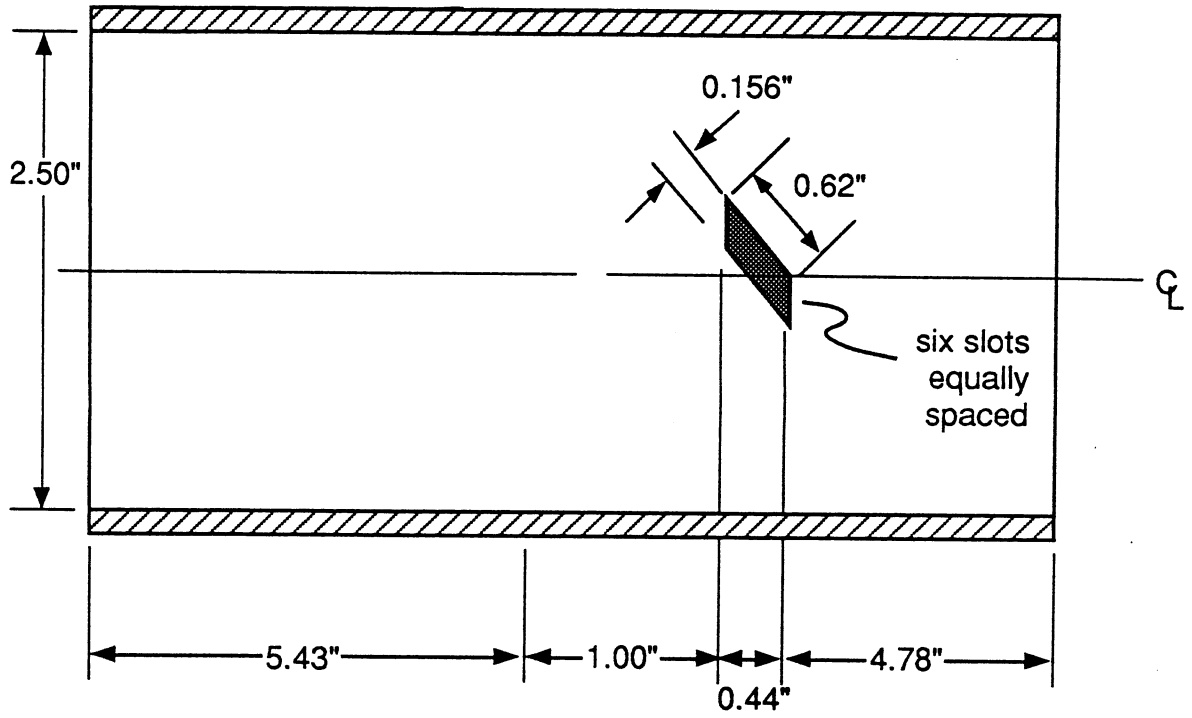

Figure 3-1. Cylindrical Mixing Configuration

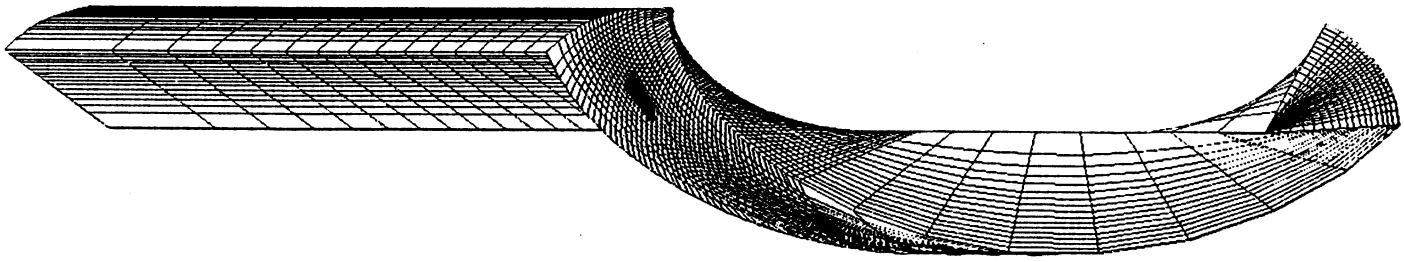

Figure 3-2. Grid Employed in CFD Computations

3.1.3 Numerical Details

The numerical details of the 3-D CFD calculations included:

a. wholefield solution of u momentum, v momentum, w momentum, pressure correction, turbulent kinetic energy (k), turbulence dissipation (ε), and mixture fraction of jet;

b. first order upwind differencing of convective fluxes and second order central differencing of diffusive fluxes;

c. standard k-ε model with wall functions; and

d. turbulent Prandtl number of 0.9.

3.1.4 Boundary Conditions

Jet flow and mainstream flow were assumed to be air. The baseline case had a jet-to-mainstream momentum-flux ratio (J) of 20.8 and a jet-to-mainstream mass-flow ratio of 0.435. Specific boundary conditions for the baseline case are stated below.

Mainstream Flow:

Axial Velocity	=	4.39 m/s (14.39 ft/s)
Temperature	=	300 K (80 °F)
Density	=	1.0 kg/m^3 (0.062 lbm/ft^3)
Turbulent kinetic energy, k	=	2.889×10^{-3} m^2/s^2 (3.109×10^{-2} ft^2/sec^2)
Dissipation of turbulent kinetic energy, ε	=	7.514×10^{-5} m^2/sec (8.085×10^{-4} ft^2/sec^2)

Jet Flow (Slot):

Radial Velocity	=	20.02 m/s (65.64 ft/sec)
Temperature	=	300 K (80 °F)
Density	=	1.0 kg/m^3 (0.062 lbm/ft^3)
Turbulent kinetic energy, k	=	5.411×10^{-1} m^2/s^2 (5.820 ft^2/sec^2)
Dissipation of turbulent kinetic energy, ε	=	2.635 m^2/s^2 (28.353 ft^2/sec^2)

Exit Boundary:

The exit boundary condition was a fixed pressure boundary with pressure set at 14.7 psia (1.0×10^5 N/m^2). All other variables (velocity components, physical properties, turbulence variables, species concentrations, etc.) were zero gradient.

Transverse Boundaries:

The transverse boundaries were assumed to be periodic planes.

Combustor Wall:

The combustor wall was treated as a no-slip adiabatic wall. Wall functions were used for the calculation of wall shear stress and near wall turbulent quantities (k and ε).

Centerline:

The computational boundary at the centerline was assumed to be a symmetry plane.

3.1.5 Convergence

The summations of all error residuals were reduced four orders of magnitude, and continuity was conserved in each axial plane. Typically convergence required approximately 300 iterations. Approximately 40 CPU minutes were required on an CRAY YMP.

3.1.6 Calculation of Unmixedness

In order to quantify the mixing effectiveness, the mass-averaged spatial concentration variance of jet flow (C_{var}) was calculated in each axial plane. The mas-averaged unmixedness (U_s)[52] is defined as

$$U_s = C_{var}/[C_{avg}(1-C_{avg})] \tag{3}$$

where C_{var} =

m_{TOT} = total mass flow in each axial plane

m_i = mass flow of cell i

C_i = jet mass fraction in cell i

3.1.7 Results

Comparison with UTRC Measurements: Figure 3-3 presents jet mass fraction color maps at X/d of 0.6. Figure 3-3 has a 1/16 inch annulus removed from the outer diameter during post-processing. Removal of this flow area allowed better comparison with UTRC's data since measurements could not be performed any closer than 1/16 inch to the outer wall. For comparison, Figure 3-4 presents UTRC's experimental results along with the comparable numerical results. It can be seen for the three momentum-flux ratios the numerical and experimental results show very good agreement. The numerical results do a very good job of predicting the flow structures and capturing the corresponding jet mass fraction levels across the diameter.

Another method of comparing predictions and measurements is shown in Figure 3-5. Unmixedness (U_s) is plotted as a function of J for both numerical and experimental results. The computational results show the same trends as the experimental results, although the unmixedness is slightly higher for the calculations. The optimum J appears to be 20 for this configuration but little difference in unmixedness is seen between a J of 20 and 30.

Parametric Study of J (Constant Jet Mass Flow): The previous calculations maintained constant slot area, thus varying J by varying jet mass flow. To better isolate the effect of J on unmixedness, a parametric study was performed in which the jet mass flow was maintained by varying the slot area. Figure 3-7 shows jet mass fraction color maps for J=4.5, 12.4, 20.8 and 29.25 where the jet mass flow is held constant. Notice that the color band is different for Figure 3-7 compared to Figures 3-3 and 3-4. Figure 3-6 shows the unmixedness results for both constant slot area and constant jet mass flow. It can be seen that the trends are the same, and both parametrics showed that J=20.8 was the optimum mixer. However, there are differences, and these differences are probably due to mass-flow ratio differences. This is in contrast mixing studies reported in the NASA Jet Mixing Program[53,54] where mass-flow ratio had little impact on mixing results.

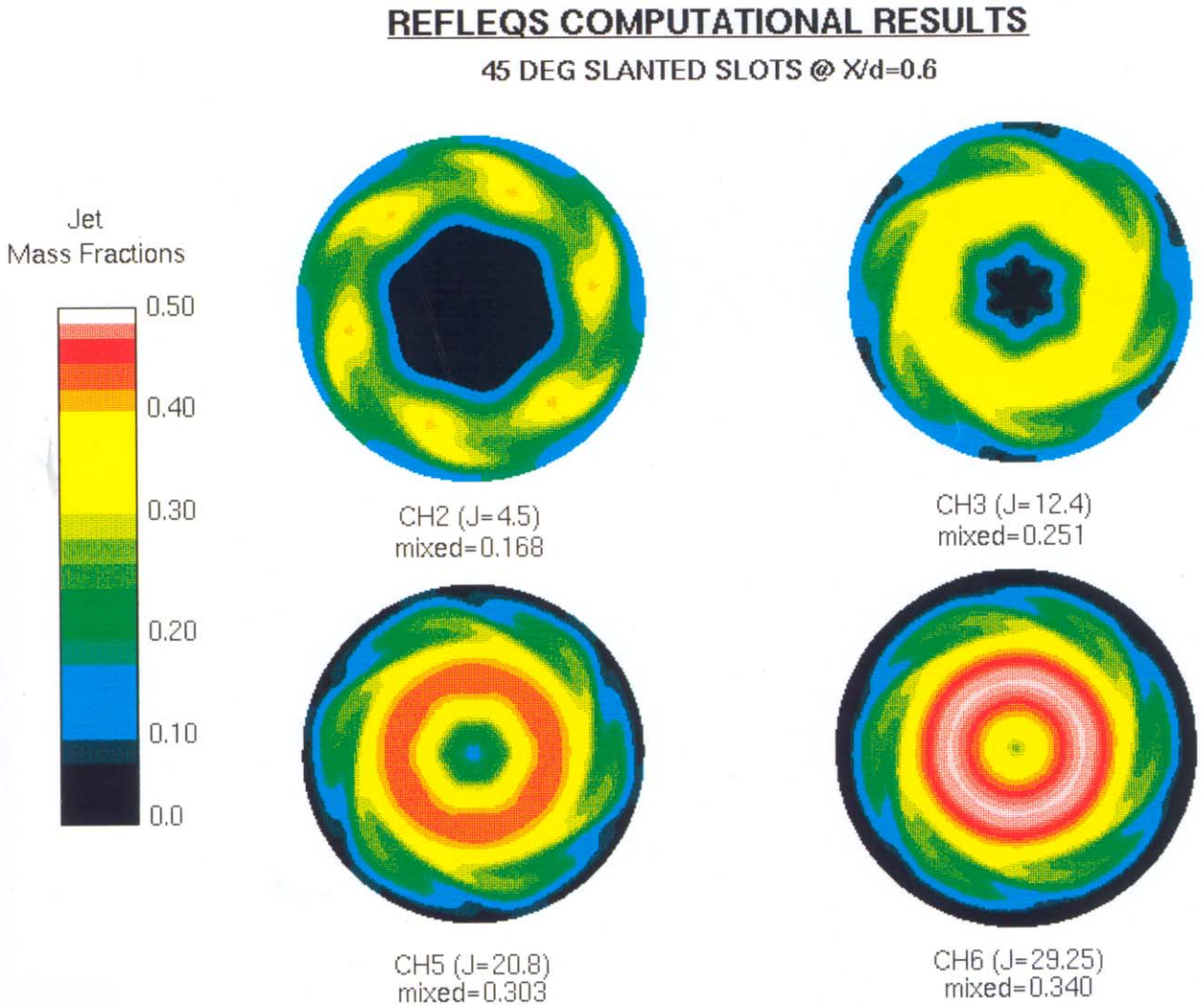

Figure 3-3. Numerical Results for UTRC CHX Configuration; Jet Discharge Coefficient of 0.80

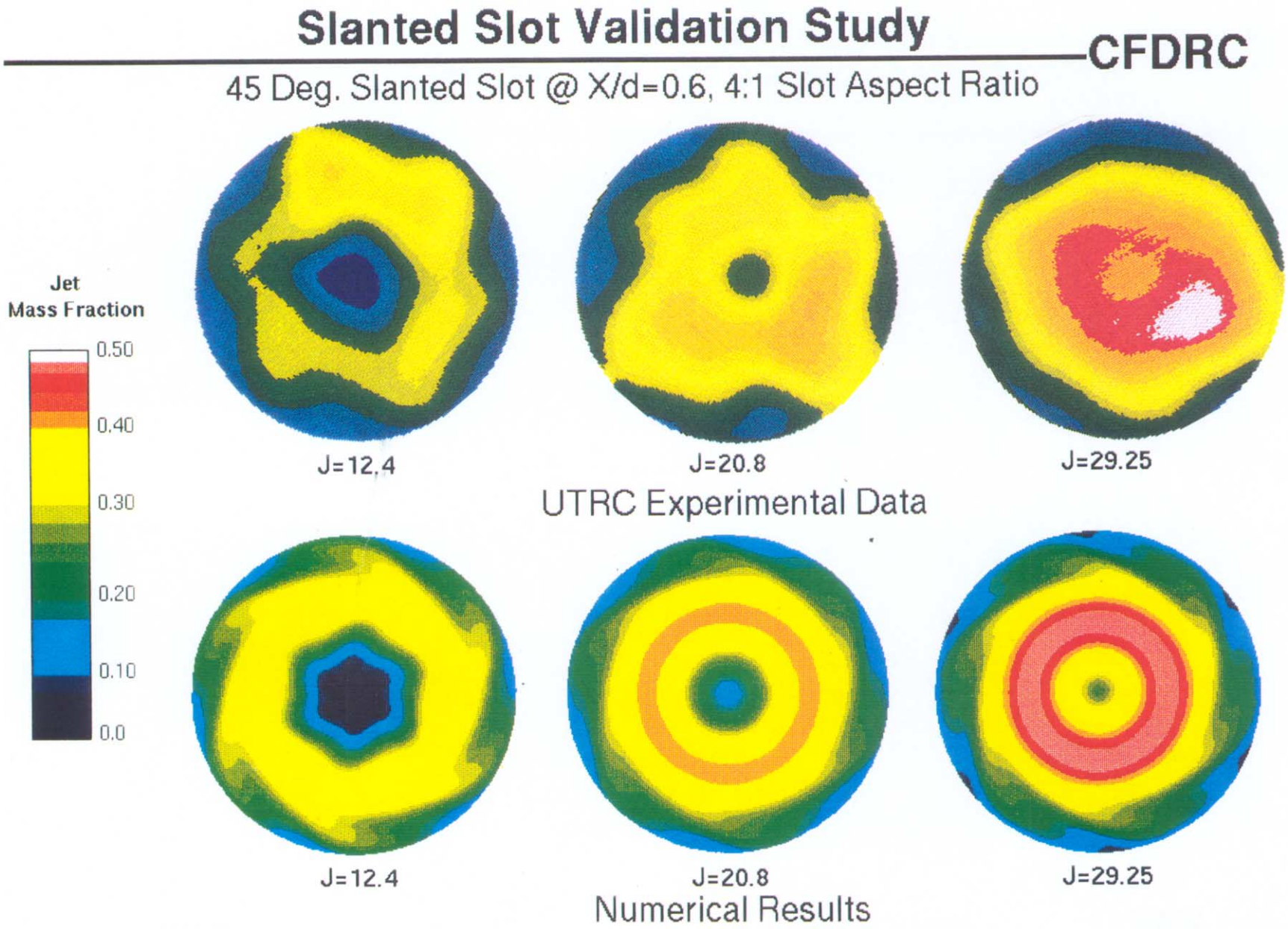

Figure 3-4. Comparison of Numerical Results and Experimental Data for Slanted Slot Configuration

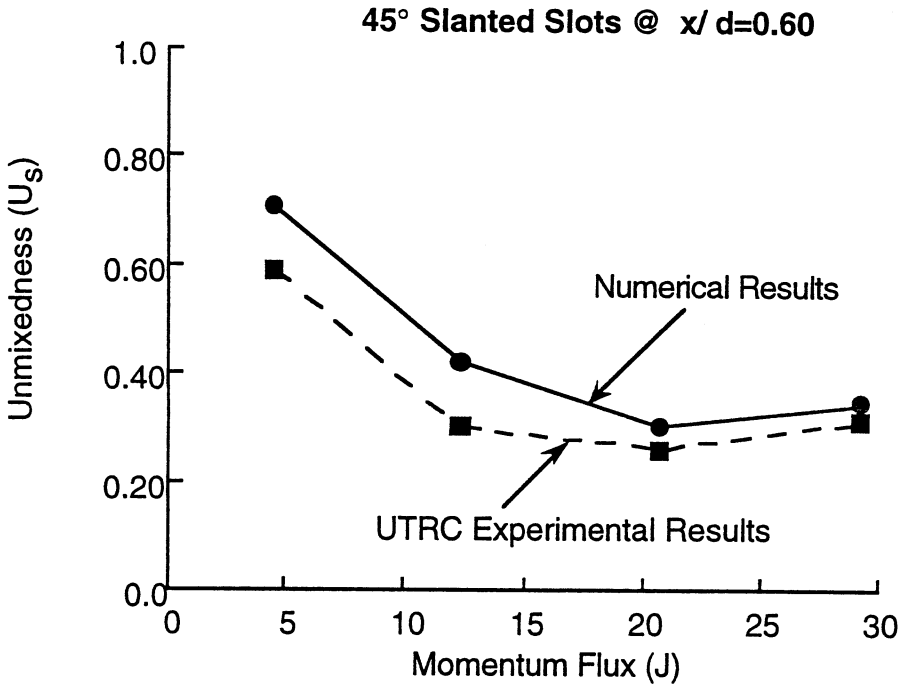

Figure 3-5. Unmixedness Comparison of Numerical Results and Experimental Data

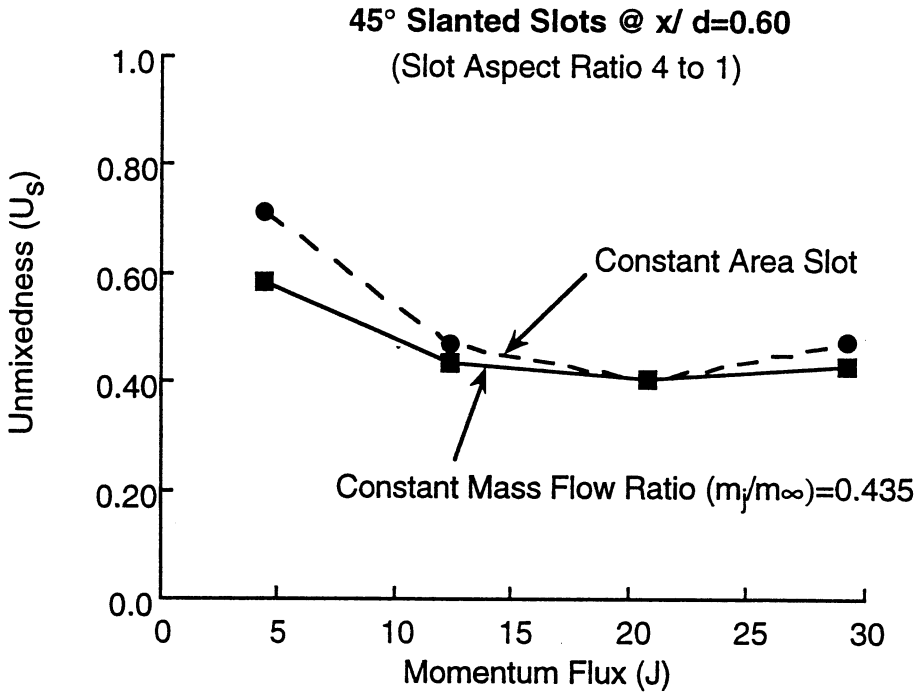

Figure 3-6. Numerical Unmixedness Results for Constant Area Slot and Constant Mass Flow Ratio

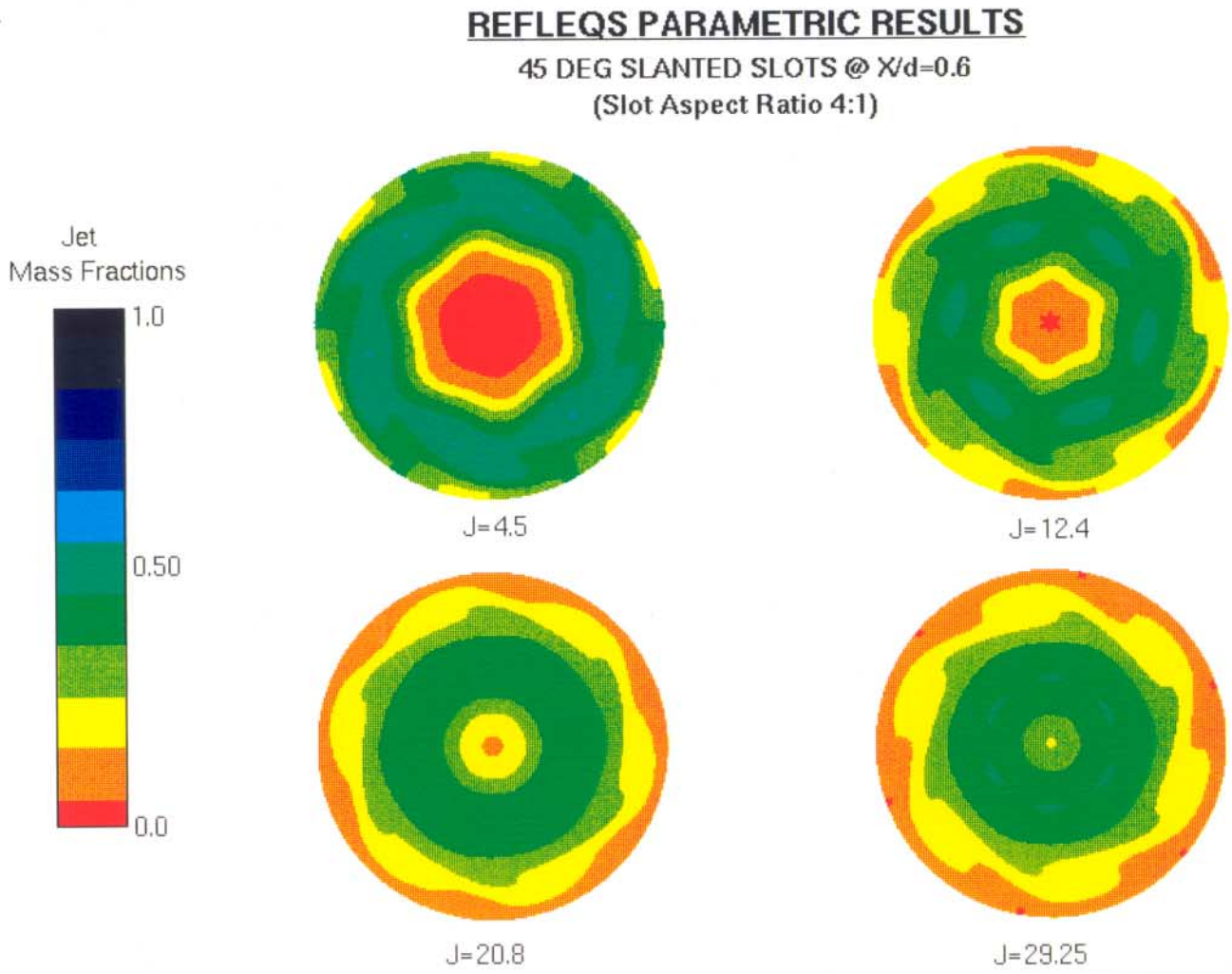

Figure 3-7. Parametric Variation of Momentum Flux Ratio with Constant Mass Flow Ratio (0.435)

Parametric Study of Density Ratio: Calculations were performed to show the effect of density ratio on mixedness. To simulate the density ratio, the ρ_{jet} was increased to a value of 2.77 while maintaining the mainstream density at unity. This yielded a density ratio (ρ_{jet}/ρ_{main}) of 2.77 typically seen in combustors. Figure 3-8 illustrates the unmixedness values (U_s) plotted over a momentum-flux ratio (J) range for the two density curves. The two curves show very little difference especially over the lower J values.

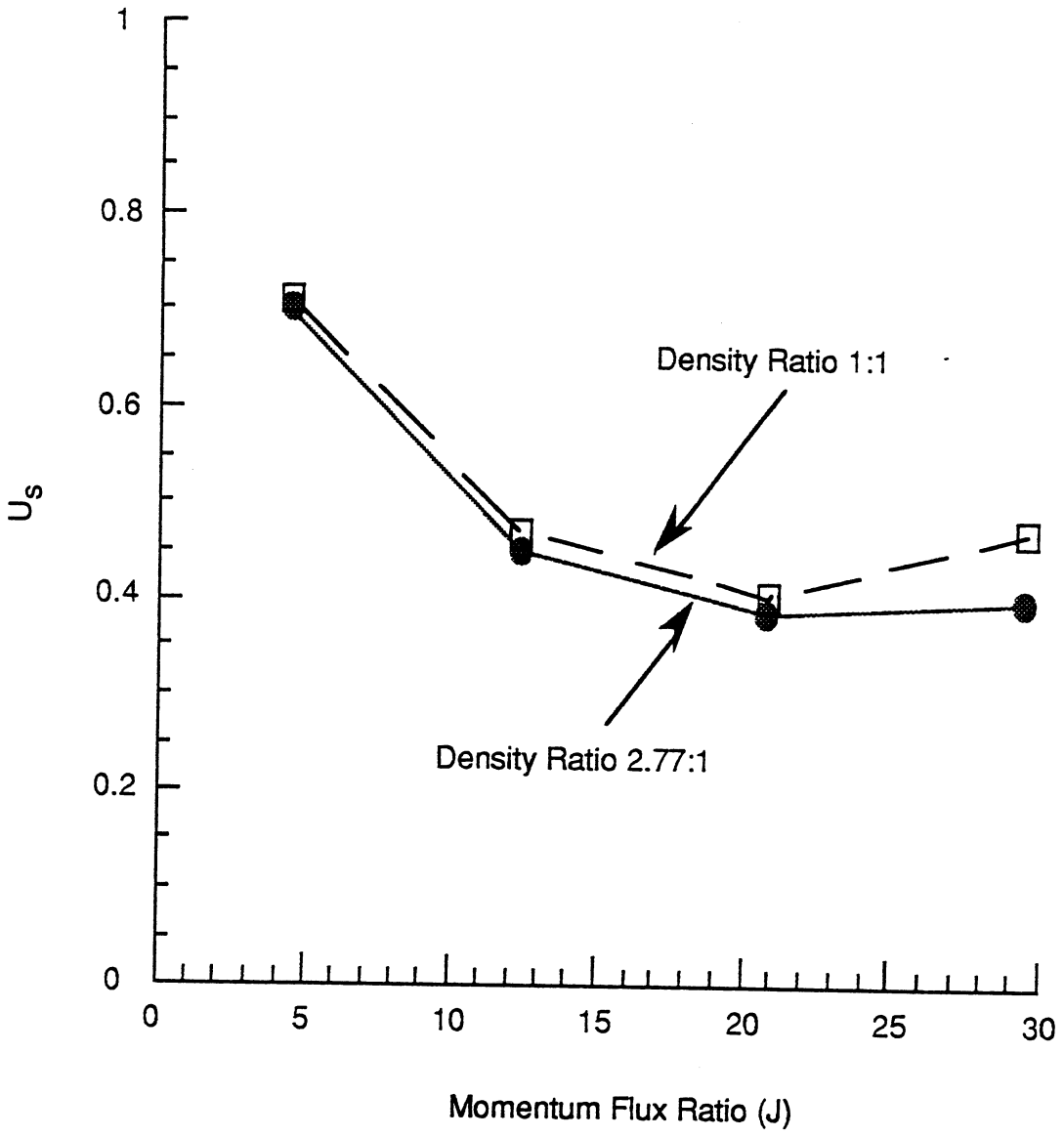

Figure 3-8. Density Effect on Unmixedness

4.0 ISOTHERMAL FLOW CALCULATIONS FOR RECTANGULAR GEOMETRIES

4.1 Slanted Slots

Slanted slots were identified as a possible way to enhance mixing. Slanted slots were thought to introduce bulk swirl that might supplement conventional jet-in-crossflow mixing. Therefore, a systematic numerical analysis was performed to determine if slanted slot configurations had better mixing characteristics than straight (in the flow direction) slots. The work performed in this analysis was published in AIAA paper 92-3087 titled "CFD Mixing Analysis of Jets Injected from Straight and Slanted Slots into Confined Crossflow in Rectangular Ducts" by Bain et al. (1992).[5]

4.2 Inline vs. Staggered

The question that continues to arise in the development of combustors is which lateral arrangement of orifice geometry produces the best mixing: inline or staggered? A systematic parametric CFD analysis was performed to address the lateral arrangement and determine which is better in RQL applications. The results of this study were published in AIAA-93-2044 paper titled "CFD Mixing Analysis of Axially Opposed Rows of Jets Injected Into Confined Crossflow" by Bain et al. (1995).[7]

4.3 Effect of Mass Flow and Aspect Ratio

In contrast to conventional combustor dilution zones, the jet-to-mainstream mass-flow levels in the quick-mix section of the RQL combustor are much larger (MR ~ 3.0 vs. MR ~ 0.5 for conventional combustor dilution zones). In terms of size constraints, the higher mass-flow ratios can lead to the use of slots vs. holes in the combustor liner. It was unclear if the increased blockage caused from the use of larger orifices could lead to differences in jet penetration. Furthermore, the effect of the increased mass-flow ratio on Holdeman's design correlations for jet mixing was unknown. Therefore by the use of a rigorous computational investigation, these design parameter issues were addressed. The results of this analysis were published

in AIAA-94-0218 paper titled "CFD Assessment of Orifice Aspect Ratio and Mass Flow Ratio on Jet Mixing in Rectangular Ducts" by Bain et al. (1994).[6]

5.0 REACTING FLOW CALCULATIONS FOR CYLINDRICAL GEOMETRIES

5.1 The Effect of Design Parameters on Jet Mixing and NOx Reduction

A number of design variables affect jet mixing and NO_x emissions in RQL combustor applications. Some of these include:

a. jet-to-mainstream momentum-flux ratio (J);
b. number of orifices;
c. slot aspect ratio; and
d. neckdown of mainstream flow area.

Numerical studies were performed to isolate the effects of these design variables. Two separate papers were written on this subject: 1) ASME-91-GT-217 paper entitled "CFD Analysis of Jet Mixing in Low NO_x Flametube Combustors" by Talpallikar et al. (1990)[39] and 2) AIAA-91-2460 paper entitled "A CFD Study of Jet Mixing in Reduced Flow Areas for Lower Combustor Emissions" by Smith et al. (1991).[34]

6.0 REACTING FLOW CALCULATIONS FOR ANNULAR GEOMETRIES

6.1 Comparison of Emissions Results for Annular and Cylindrical Geometries

The geometry of the mixing section can follow two different paths. One path employs a full annular geometry, while the other employs a can geometry. Many unanswered questions exist as to which geometry is the best design for low emissions. Other factors will play a role in the selection of the best design, but the input of geometry on emission signature also plays a significant role. A systematic computational study was performed to identify emission and mixing potential of each geometry. The results of this study were published in AIAA-95-2995 paper entitled "Jet Mixing and Emission Characteristics of Transverse Jets in Annular and Cylindrical Confined Crossflow" by Bain et al. (1995).[8]

6.2 Flow Coupling Effects

Typical CFD calculations are performed on the interior of the combustor with inlet boundary conditions specified by the designer. The jets are typically input with uniform velocity profiles and turbulence levels. An effective orifice flow area (geometric area times C_d) is usually assumed as the jet orifice area. In real combustors, there is evidence that the airflow through the orifices is not uniform (i.e. that there are flow coupling effects).[55-60] To better understand flow coupling effects, a CFD study was performed in which the external airflow and interior combustor flowfield were analyzed together. The results of this analysis were published in AIAA-96-2762 paper entitled "Flow Coupling Effects in Jet-In-Crossflow Flowfields" by Bain et al. (1996).[9]

7.0 NOx INFERENCE CODE (NIC)

For cost considerations, jet mixing relevant to gas turbine combustors has usually been studied experimentally under isothermal flow conditions. Design correlations have been developed, and these correlations are useful for designing dilution zones that produce acceptable temperature radial profiles, pattern factor, etc.

For assessing RQL quick-mix designs, mixing data alone are not enough. A software tool is needed to infer NO_x emissions from isothermal mixing data. Such a tool was written, validated and applied in this project. A computational code, named the NO_x Inference Code (NIC), was developed to take planes of experimental jet mass fraction data and infer NO_x and CO emissions at various downstream locations.

7.1 Background of the NOx Inference Code

In this section, an overview of the NIC will be discussed. Following are the assumptions and descriptions of the input and models in the NIC. A general flowchart of the NIC is illustrated in Figure 7-1.

Assumptions

The following are major assumptions made in the development of the NIC.

a. Only planar scalar data (jet mass fraction) will be used. No fluid dynamics information is assumed available.

b. The jet mass fraction fields are the same for reacting and non-reacting flows if momentum-flux ratio (J) and mass-flow ratio (MR) are maintained. Recent CFD computations by Oechsle et al.[29] have shown that the jet mass fraction fields of non-reacting and reacting flows are very similar.

c. Uniform composition and temperature at the mainstream inlet was assumed.

d. Fast equilibrium chemistry for heat release is assumed.

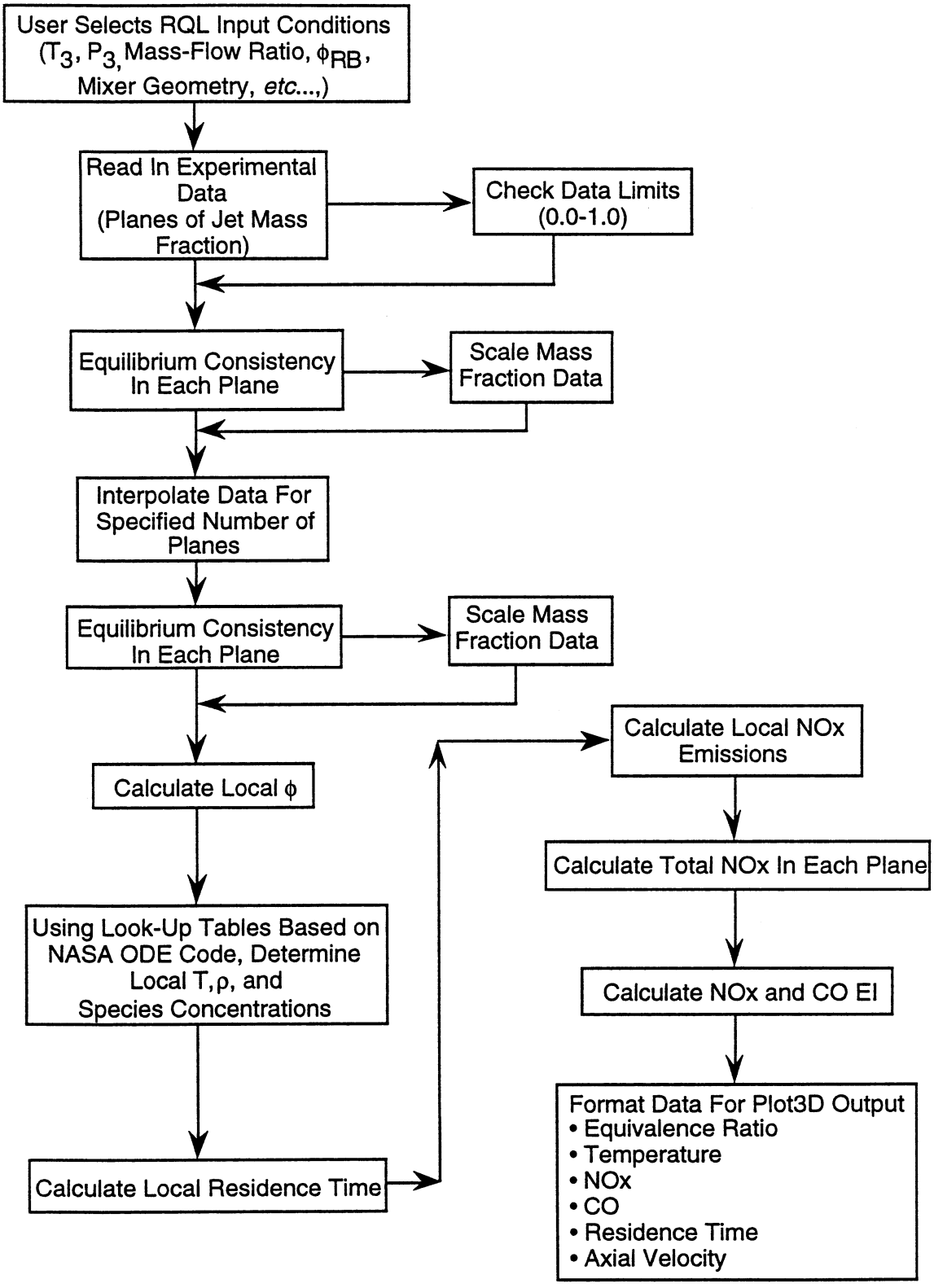

Figure 7-1. Flow Chart for NO_x Inference Algorithm

e. Only the thermal NO_x mechanism is important; the formation of NO_x is assumed irreversible.

f. Only axial fluid motion impacts residence time (i.e., vertical and transverse velocities are assumed to be zero.) This is a good assumption except in the orifice region, or near the orifice in the case of slanted slots due to the transverse nature of the injected velocities.

Data Input

The data input coding is divided into two sections. The first section reads a user defined input file which specifies RQL combustor initial conditions and mixer geometry. The second input section is responsible for reading the formatted experimental mass fraction data.

Check Mass Fraction Limits

The mass checking coding is designed to read all the mass fraction experimental data points and then proceeds to check for values greater than 1.0 (100% jet flow) or less than zero (100% mainstream flow). If any values are located that exceed these upper and lower limits, they are reset to either 1.0 or zero respectively.

Check Average Jet Mass Fraction In a Given Plane

In each plane, the area-averaged jet mass fraction is calculated from the local measurements. The average jet mass fraction is also calculated based on the axial plane location and the amount of jet mass flow that has entered the flowfield. If the average jet mass fraction calculated from the experimental measurements does not equal the average jet mass fraction calculated from global flow considerations, the experimental measurements are scaled accordingly. Note that in any plane downstream of the orifice the average jet mass fraction is easily determined by:

$$\theta_{EB} = m_j/(m_j + m_\infty) \tag{4}$$

where: θ_{EB} = Average Jet Mass Fraction

$\dot{m}_j$ = Total Jet Mass Flow

$\dot{m}_\infty$ = Total Mainstream Mass Flow

Interpolated Planes

Experimental data are taken in only a limited number of planes, typically eight to ten locations. NIC divides the entire flowfield into a user specified number of equally spaced planes. The experimental data are then interpolated to provide values of jet mass fraction in each computational plane. The interpolation routine, named UNBAR, has provisions for 1st, 2nd, and 3rd order interpolation.

Chemistry Subroutine

The chemistry subroutine serves the vital function of calculating:

1. The local equivalence ratio based on jet mass fraction.

2. The local temperature based on the local equivalence ratio and chemical equilibrium.

3. The NO_x production rate based on the thermal NO_x mechanism.

Local Equivalence Ratio:

The local equivalence ratio is calculated from the equation:

$$\phi_{local} = \frac{\left[\left(1 - \frac{\dot{m}_j}{\dot{m}_{tot}}\right)\frac{1}{FASTOGY}\right]}{\left[\frac{\dot{m}_j}{\dot{m}_{tot}} + \frac{1}{(FASTOGY)\,\phi_{RB}}\right]} \tag{5}$$

where $\frac{\dot{m}_j}{\dot{m}_{tot}}$ = Local Jet Mass Fraction

FASTOGY = Stoichiometric Fuel/Air Ratio

ϕ_{RB} = Rich-Burn Equivalence Ratio

Local Temperature:

The NASA ODE (One Dimensional Equilibrium)[61] code was executed to generate look-up tables of temperature, O, N_2, and CO versus equivalence ratio. The initial pressure and temperature were assumed to be 207 psia and 1250 K respectively. The liquid fuel was assumed to be $C_{12}H_{26}$ at a temperature of 400 °F. These conditions correspond to Pratt & Whitney's supersonic cruise conditions. Other look-up tables can easily be generated if required. Indeed, for the Anderson validation case to be discussed later, another set of look-up tables were generated and used.

NO_x:

The NO_x production in a cell was calculated based on the extended Zeldovich mechanism.[62]

$$O + N_2 \Leftrightarrow NO + N \quad (6)$$

$$N + O_2 \Leftrightarrow NO + O \quad (7)$$

$$N + OH \Leftrightarrow NO + H \quad (8)$$

A prompt NO_x mechanism was not considered because the products of the rich-burn section in all likelihood do not contain HCN, an intermediate product of fuel pyrolysis. The nitrous oxide NO_x mechanism was also not considered because previous research[63] has shown the nitrous oxide mechanism to only be important during fuel-lean combustion (ϕ ~ 0.5-0.6).

Invoking a steady-state approximation for the N-atom concentration, and assuming the oxygen atom is in equilibrium, the NO formation rate can be expressed as:

$$\frac{d(NO)}{dt} = 2k_3(O)(N_2)\frac{1-\frac{(NO)^2}{K(O_2)(N_2)}}{1+\frac{k_{-3}(NO)}{[k_4(O_2)+k_5(OH)]}} \quad (9)$$

where $K = \left(\frac{k_3}{k_{-3}}\right)\left(\frac{k_4}{k_{-4}}\right)$ = equilibrium constant for the reaction $N_2 + O_2 \Leftrightarrow 2NO$.

If NO is far from equilibrium, the NO formation rate can be expressed as:

$$\frac{d(NO)}{dt} = 2k_3(O)(N_2)$$

where $k_3 = 1.82\text{x}10^{14} e^{\frac{(-3.8\text{x}10^4)}{T}}$ $cm^3\ mol^{-1}\ s^{-1}$.

The local residence time is calculated from the local axial velocity (assumed constant in each plane) and the local density. The NO_x formed in each cell is calculated by multiplying the NO_x formation rate times the local residence time. The NO_x formed in a plane is determined by summing the NO_x concentrations in each cell of the plane. An overall NO_x concentration is calculated by summing the planar values of NO_x.

The amount of CO in each cell is determined from equilibrium considerations based on the local equivalence ratio. Due to the assumption of fast heat release chemistry, any CO remaining in the flowfield downstream of the jet orifice is due to the unmixedness of the jet airflow with the rich-burn mainstream. Thus, CO will be quite high at downstream locations if the airflow jets significantly underpenetrate into the mainstream flow.

Output

Two forms of output are printed from NIC. The first form of output is a PLOT3D file containing data sets of equivalence ratio, temperature, NO_x, CO, residence time, and axial velocity. The PLOT3D files can be read into graphics packages such as PLOT3D or CFD-VIEW to visually observe the computed results. The second form of output is a file containing input parameters and tabulated output parameters such as NO and CO concentrations at each axial (x/H) location and NO_x and CO emission indices.

Initial Validation Case

An initial check-out case was conducted to show the code's capability to quantitatively predict NO_x and CO. A simple case was set-up to model Anderson's flametube experiment.[64] All of the heat release was assumed to occur in the first cell, and NO_x and CO were predicted as the flow preceded down the flametube. NIC calculations were performed at various overall equivalence ratios as tested by Anderson.

Figure 7-2 presents the predicted and measured NO_x results for 2 msec. The predicted NO_x EI was lower than measured for very lean equivalence ratios, but higher than measured for ϕ greater than 0.8. The poor agreement at low ϕ may be due to prompt or nitrous oxide NO_x mechanisms being important, but not being modeled. The overprediction for ϕ's greater than 0.8 may be due to experimental error (reported by Anderson). However, overall there was good qualitative agreement in an engineering sense.

Comparison of predicted and measured CO emission indices in shown in Figure 7-3. The equilibrium assumption appears to be quite accurate in this case, and good agreement is seen.

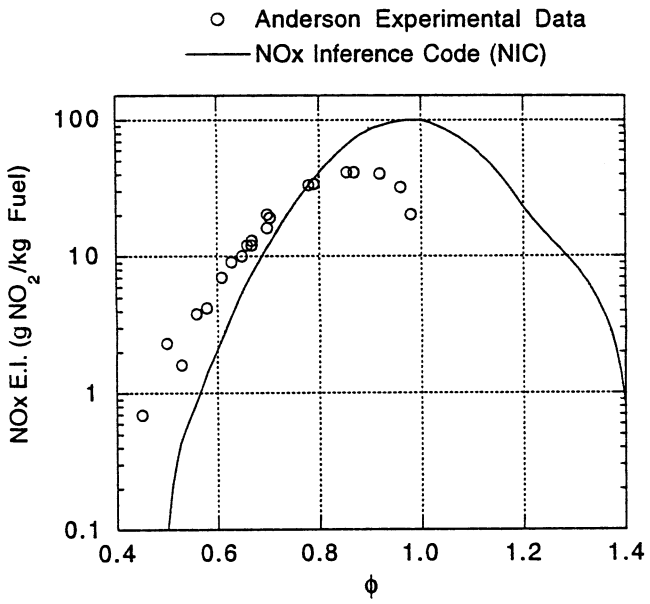

Figure 7-2. Comparison of NO_x EI for Anderson's Experimental Data and NIC

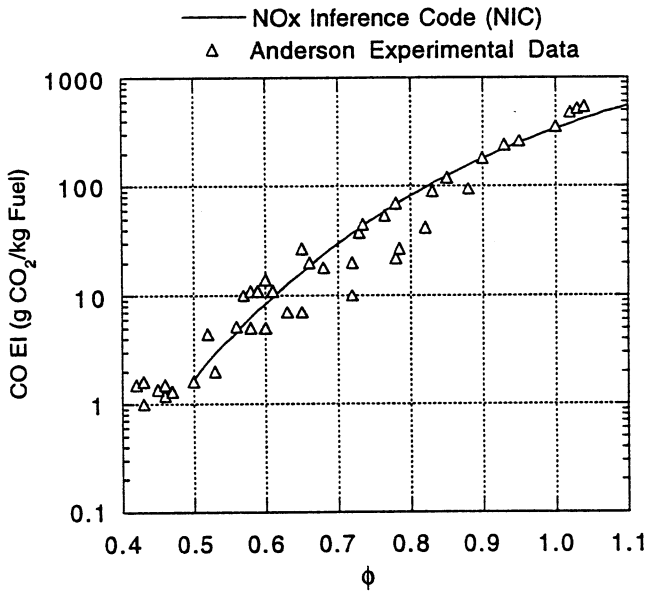

Figure 7-3. Comparison of CO EI for Anderson's Experimental Data and NIC

7.2 NOx Inferred from UTRC Experimental Data

One of the key motivations behind the development of the NO_x Inference Code (NIC) was to determine if the best mixing configuration was also the lowest NO_x configuration. To help address this issue, UTRC provided sets of experimental isothermal mass fraction data for use in the NIC. The experimental mass fraction data sets represented an optimum and two off-optimum mixing designs for inline orifices based on Holdeman's correlation. The three cases were chosen based on previously performed experimental and numerical analyses. The optimum mixing geometry was chosen to have 1/4 duct height jet penetration while the other two configurations selected represented an over- and under-penetrated configuration.

The three cases used are shown below in Table 7-1.

Table 7-1. UTRC Experimental Test Cases

Case	S/H	MR	J	$C=S/H \bullet \sqrt{J}$
Case 1. "Optimum"	0.425	2.0	36	2.55
Case 2. Over-Penetrated	↓	↓	70	3.55
Case 3. Under-Penetrated	↓	↓	15	1.65

The product of $\sqrt{J}$ and S/H is listed as C in Table 7-1. From this product, Case 1 would be considered near optimum, Case 2 would be slightly over-penetrated, and Case 3 would be slightly under-penetrated. The Case 2 geometry used a circular orifice in place of a square orifice due to the lack of square mass fraction data at the desired conditions. It was possible to make this substitution because previous numerical and experimental mixing results showed very little mixing differences between the two types of orifices.

The data provided by UTRC were taken at 10 selected planes. Figure 7-4 shows the various plane locations selected for each configuration. For each case, the individual data planes were combined to form one large data set. The data were then read into the NIC and interpolated into 100 planes from x/H = 0.0 to 1.0 The input parameters assumed in the NIC were representative of HSCT cruise conditions. Listed in Table 7-2 are the input parameters assumed for the NIC analysis.

Data Plane Locations: Case 1

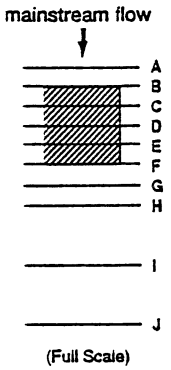

Plane	Relative	Absolute Inches
A	-25% of L	-0.1625
B	Leading Edge	0
C	25% of L	0.1625
D	50% of L	0.325
E	75% of L	0.4875
F	Trailing Edge (L)	0.65
G	TE + (H/2 - TE)/2	0.825
H	50% of H	1
I	75% of H	1.5
J	H	2

Data Plane Locations: Case 2

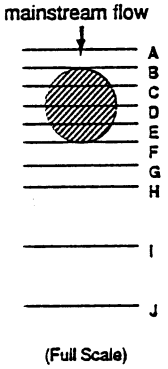

Plane	Relative	Absolute Inches
A	-25% of L	-0.15625
B	Leading Edge	0
C	25% of L	0.15625
D	50% of L	0.3125
E	75% of L	0.46875
F	Trailing Edge (L)	0.625
G	TE + (H/2 - TE)/2	0.8125
H	50% of H	1
I	75% of H	1.5
J	H	2

Data Plane Locations: Case 3

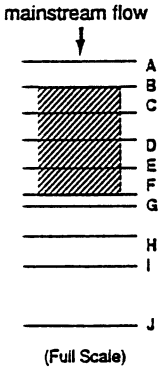

Plane	Relative	Absolute Inches
A	-25% of L	-0.2275
B	Leading Edge	0
C	25% of L	0.2275
D	50% of L	0.455
E	75% of L	0.6825
F	Trailing Edge (L)	0.91
G	50% of H	1
H	62.5% of H	1.25
I	75% of H	1.5
J	H	2

Figure 7-4. Data Plane Locations for UTRC Experimental Data Sets

Table 7-2. NIC Input Parameters

Parameter	NIC Test Conditions 1	NIC Test Conditions 2	Pratt & Whitney Supersonic Cruise
Jet-To-Mainstream Mass Flow Ratio (MR)	2.00	2.00	2.88
ϕ_{rb} (Rich-Burn Exit)	1.8	1.35	1.8
ϕ_{lb} (Quick-Mix Exit)	0.55	0.425	0.425
Reference Inlet Velocity	35 m/sec	35 m/sec	35 m/sec
Rich-Burn Temperature	2165 K	2504 K	2165 K
Jet Temperature	950 K	950 K	950 K
Combustor Pressure	207 PSIA	207 PSIA	207 PSIA
Fuel	Jet A	Jet A	Jet A
Equilibrium Species Considered	CO,CO_2,H_2O,H_2,N_2	CO,CO_2,H_2O,H_2,N_2	

Two different conditions were analyzed by the NIC. The first condition was run at a rich-burn ϕ of 1.8 and a jet-to-mainstream mass-flow ratio of 2.0. The corresponding lean-zone ϕ was 0.55. The second condition had at rich-burn ϕ of 1.35 and a lean-burn ϕ of 0.425. The second condition was selected to approximate the lean-burn ϕ for the Pratt & Whitney RQL supersonic cruise point. All the input conditions except for the ϕ_{rb} were identical to the Pratt & Whitney supersonic cruise conditions. The basis for the ϕ_{rb} difference is due to the experimental data being taken at a mass flow split (jet/mainstream) of 2:1, whereas typical RQL mass flow splits are on the order of 3:1. In order to model the RQL 3:1 mass flow split, the experimental data would have to be scaled, thus potentially compromising the integrity of the mass fraction data. Therefore the approach chosen was to match up the ϕ_{lb} and determine the corresponding ϕ_{rb} from the mass flow split. This approach was felt to be valid based on Rosfjord's data[65] shown in Figure 7-5. Rosfjord's experimental results show that varying the ϕ_{rb} has little impact on the NO_x formation.

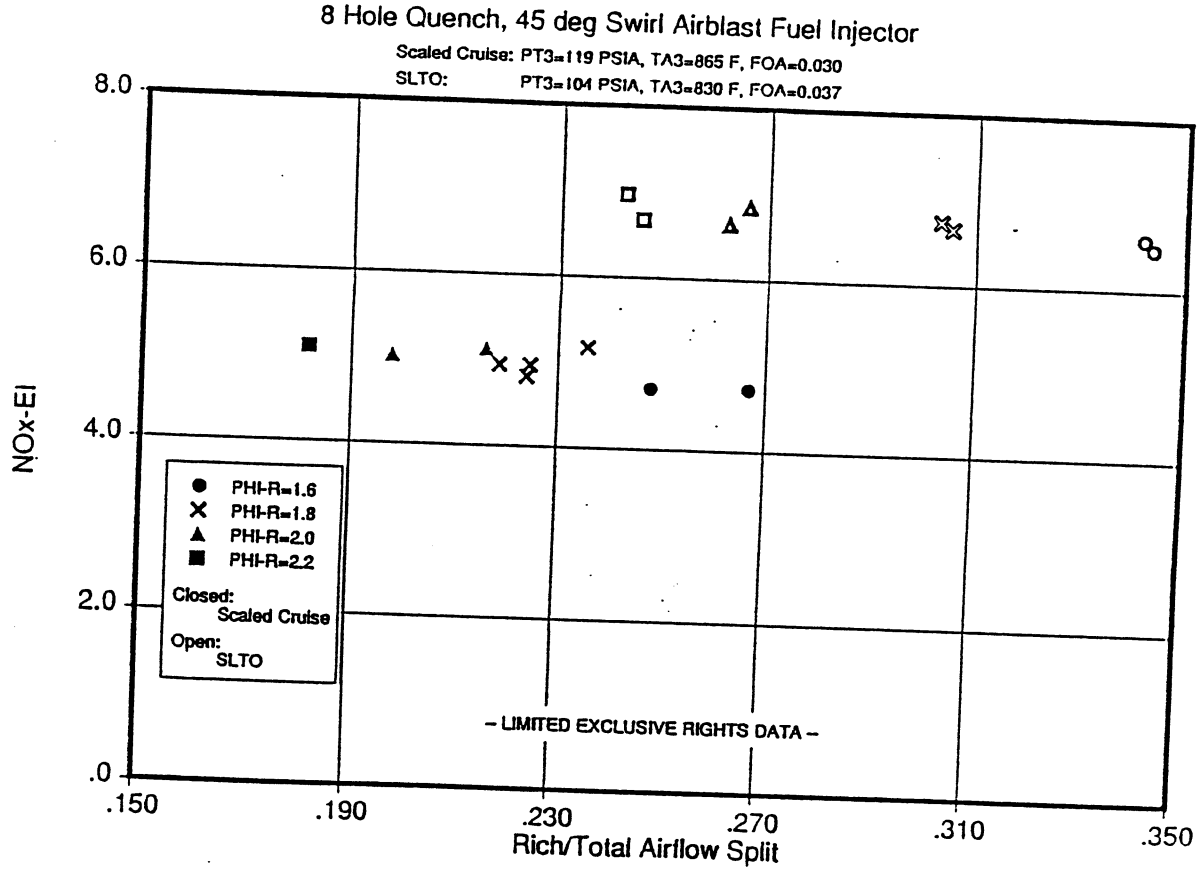

Figure 7-5. Effect of Varying ϕ_{RB} on NO_x EI

Using the NIC, the spatial unmixedness was determined and plotted in Figure 7-6. From prior numerical results, the J of 36 case was perceived to produce the optimum mixing configuration. The spatial unmixedness curves presented in Figure 7-6 do not necessarily support this earlier conclusion, as the curves show the J of 70 case has the lowest unmixedness. For the J of 70 configuration, the initial mixing takes place much faster than the J of 36 and J of 15 cases. Farther downstream the J of 70 and J of 36 cases have similar unmixedness levels.

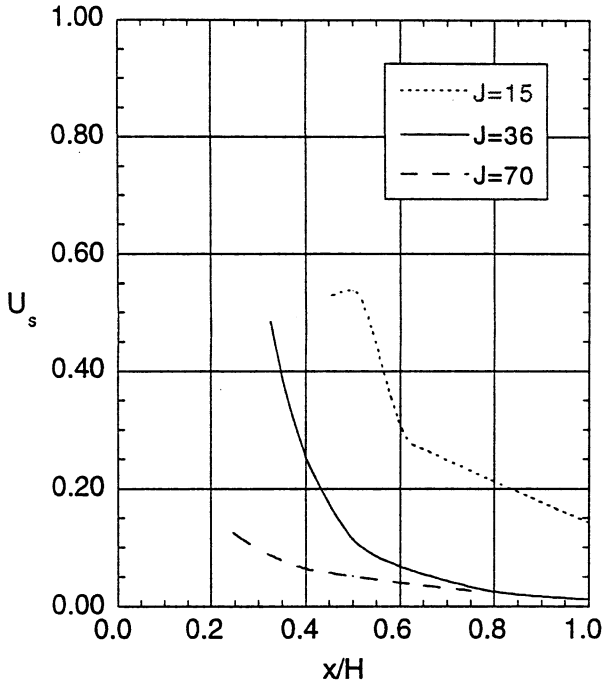

Figure 7-6. Spatial Unmixedness Comparison for UTRC Data

Figure 7-7 shows NIC results for accumulated NO production as function of x/H for flow conditions 1 ($\phi_{lean\text{-}burn}$ = 0.55). At x/H of 0.75, the accumulated NO production values for the three configurations are 85 kg/sec for J of 15, 130 kg/sec for J of 36, and 170 kg/sec for J of 70. For the range x/H=0.2 to x/H=1.0, the J of 15 curve has the lowest overall NO production rate. This result seems to be in disagreement with the unmixedness trends. Note that the NO_x levels are continuing to increase as x/H increases, indicating NO_x will continue to be produced in the lean-burn section. Indeed, since the residence time in the lean-burn section is about six times that in the quick-mix section, cumulative NO_x levels of 1200 kg/sec would be expected for all three configurations. This implies jet mixing is not very important for $\phi_{lean\text{-}burn}$ of 0.55 since the majority of NO_x is formed aft of the mixing process and is controlled by the overall exit equivalence ratio.

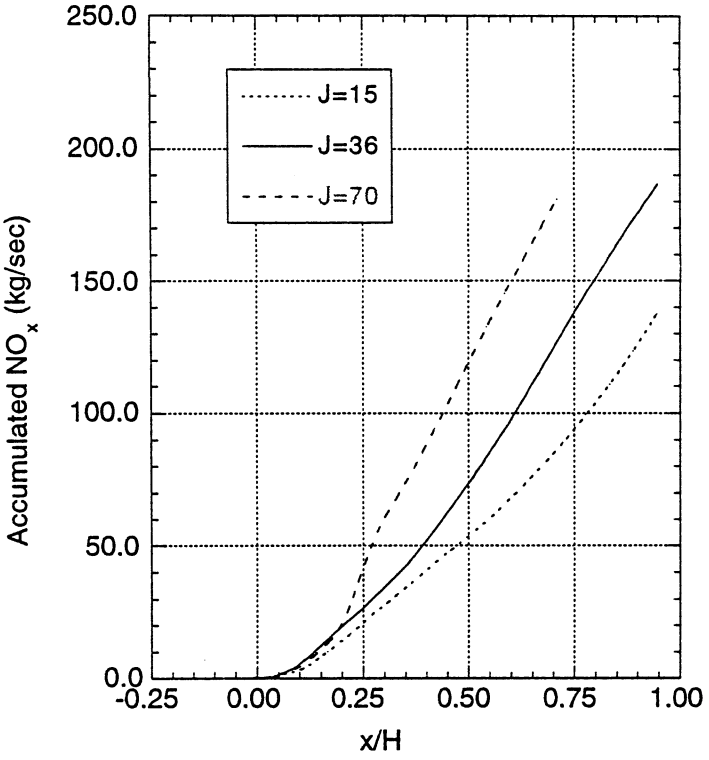

Figure 7-7. Accumulated NO_x for Overall Equivalence Ratio of 0.55

Figure 7-8 shows the accumulated NO_x production values for supersonic cruise condition ($\phi_{lean\text{-}burn}$ = 0.425). The J of 70 and J of 36 cases show little NO_x formation downstream of x/H of 0.75 (i.e., the curves are leveling off at x/H of 0.75). This implies there will be little NO_x being formed by these configurations in the lean-burn section. For the J of 15 case, the NO_x production curve maintains a steep slope at x/H of 0.75, signifying ongoing NO_x formation. At x/H of 0.75, the J of 70 case forms the least amount of NO_x. This result is in agreement with unmixedness trends. For $\phi_{lean\text{-}burn}$ of 0.425, the process of jet mixing controls NO_x production because little or no NO_x is formed aft of the mixer.

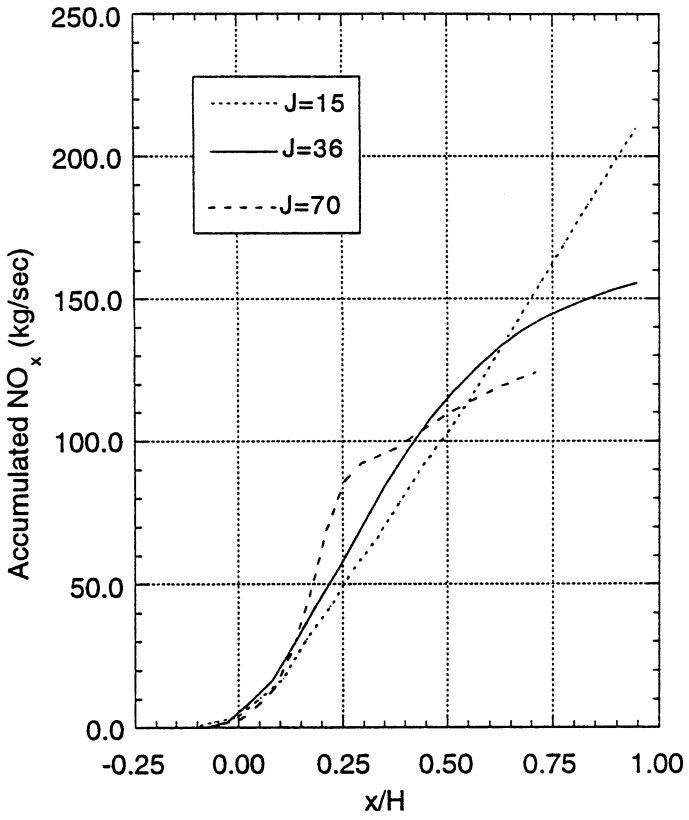

Figure 7-8. Accumulated NO_x for Overall Equivalence Ratio of 0.425 (Supersonic Cruise Condition)

In addition to NO production rates, another important criteria in the evaluation of the RQL mixing configurations is CO oxidation. Specifically, in order to achieve high combustion efficiency, CO must be oxidized before exiting the combustor. The NIC code uses a fast CO chemistry assumption. This assumption suggests that any remaining CO present in the flowfield is the direct result of lack of mixing. The fast chemistry assumption is substantiated by the results of a plug flow analysis shown in Figure 7-9. This analysis was performed using LSENS[66], a NASA Lewis kinetics package. The analysis shows that for $\phi > 0.4$ and temperatures exceeding 2750 °F, the

CO oxidation occurs very rapidly. If one was to assume that 99.5% combustion efficiency is considered acceptable, a corresponding CO EI level of 5 above exit equilibrium levels must be achieved. For flow conditions 1, a 99.5% combustion efficiency corresponds to a CO EI of 9.3, while for flow conditions 2, a CO EI of 5.5.

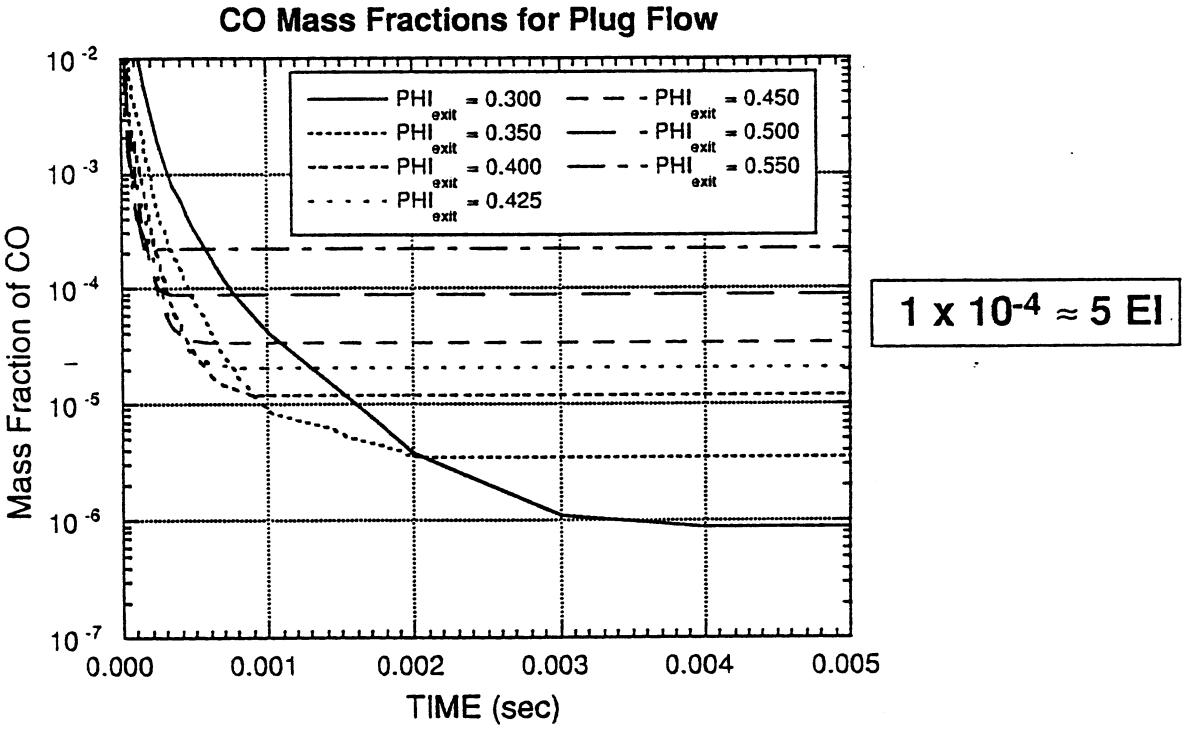

Figure 7-9. LSENS CO Mass Fraction of Plug Flow Analysis

Figures 7-10 and 7-11 show the CO emission indices as a function of x/H for the two flow conditions. For flow conditions 1 ($\phi_{lean\text{-}burn}$ = 0.55), it does not appear that any of the three cases will achieve the desired efficiency by x/H=1.0. Hence, the lean-burn section is needed to achieve combustion efficiency of 99.5%.

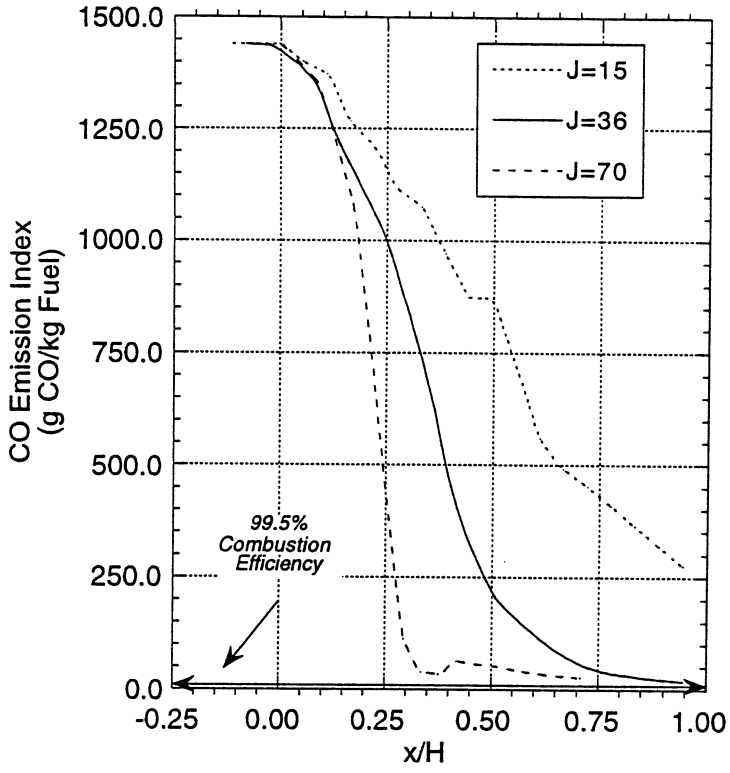

Figure 7-10. CO Emission Index of Overall Equivalence Ratio of 0.55

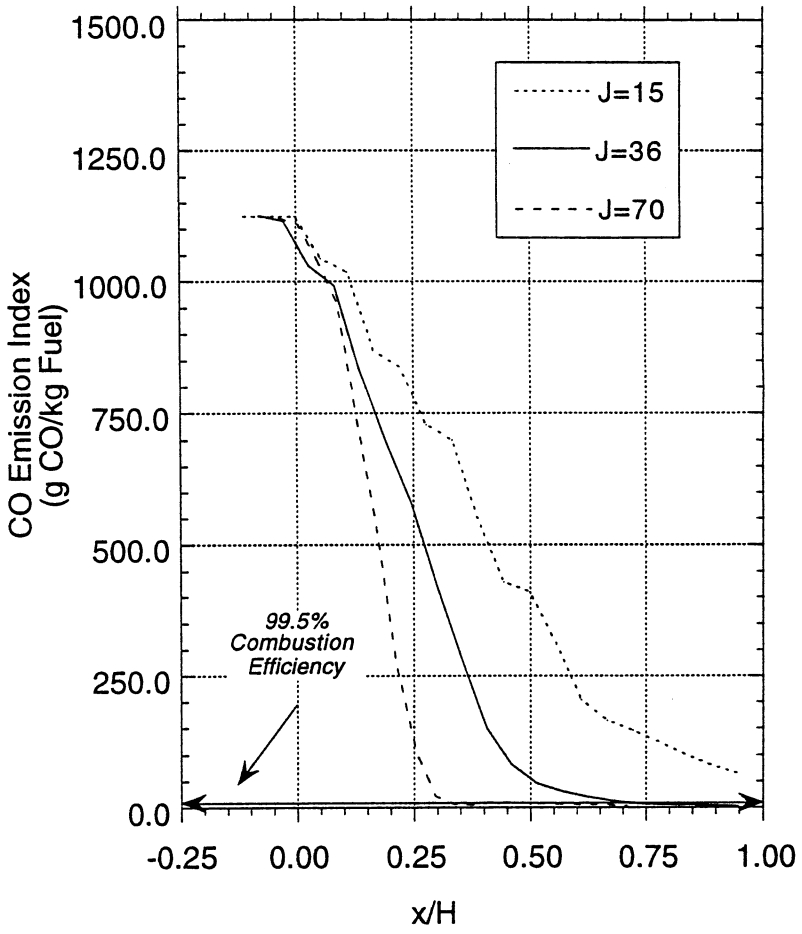

Figure 7-11. CO Emission Index for Overall Equivalence Ratio of 0.425 (Supersonic Cruise Condition)

For supersonic cruise condition ($\phi_{lean\text{-}burn}$ of 0.425), the J of 70 and J of 36 cases both reach the desired combustor efficiency before x/H=1.0. The J of 70 case oxidizes the CO rapidly and reaches an efficiency of 99.5% by x/H=0.50. The J of 36 case reaches 99.5% efficiency by x/H of 0.75. For J of 15, a large amount of unreacted CO still exists in the flowfield, at x/H of 1.0. This is the reason why NO_x is still increasing at x/H of 1.0 (as seen in Figure 7-8).

Figure 7-12, 7-13, and 7-14 show a qualitative look at the local NO production rate for the three cases. The figures show NO production rate contours at 1) axial plane through the slot centerline, 2) top lateral plane, and 3) the axial plane located between the slot centerline. As shown in Figure 7-13, the over-penetrated case has the greatest NO potential to be formed along the walls downstream of the orifices. With a decrease in the jet penetration, the local NO production is concentrated in the jet/mainstream shear layer for the J=36 case (Figure 7-12). Further reducing the jet penetration shows NO production being formed along the duct centerline for the J=15 case (Figure 7-14).

7.3 Effect of Design Variables on the Production of NOx

Using a set of isothermal mixing data, the NIC code was used to address possible effects of initial conditions and geometry on the production of NO_x. Isothermal experimental mass fraction data provided by UTRC were used. As described in the previous section, Section 7.2, the experimental mass fraction data sets represented an optimum and two off-optimum mixing designs for inline orifices.

The positive NO_x slopes seen in Figures 7-7 and 7-8 suggest the possible ongoing NO_x production occurring in the lean burn section. To investigate the role of the Lean-Burn section in NO_x production, a NIC analysis modification was required. To simulate the flow through the lean burn section, the NIC data set was modified to include a fully mixed out plane at x/H=5.0. Shown in Figure 7-15 is a schematic of this modification. Figure 7-16 shows the results of NO_x EI for the Quick-Mix and Lean-Burn section. For the J of 36 and 70 cases, the lean-burn section plays a very small role in additional NO_x production. This is shown by the slightly positive NO_x EI slopes of the corresponding curves. On the other hand, the J of 15 case exhibits ongoing NO_x production until x/H=3.0 where the curve begins to level off. Thus the under-penetrated case, J of 15, has approximately 2 1/2 times more NO_x than of the other two cases.

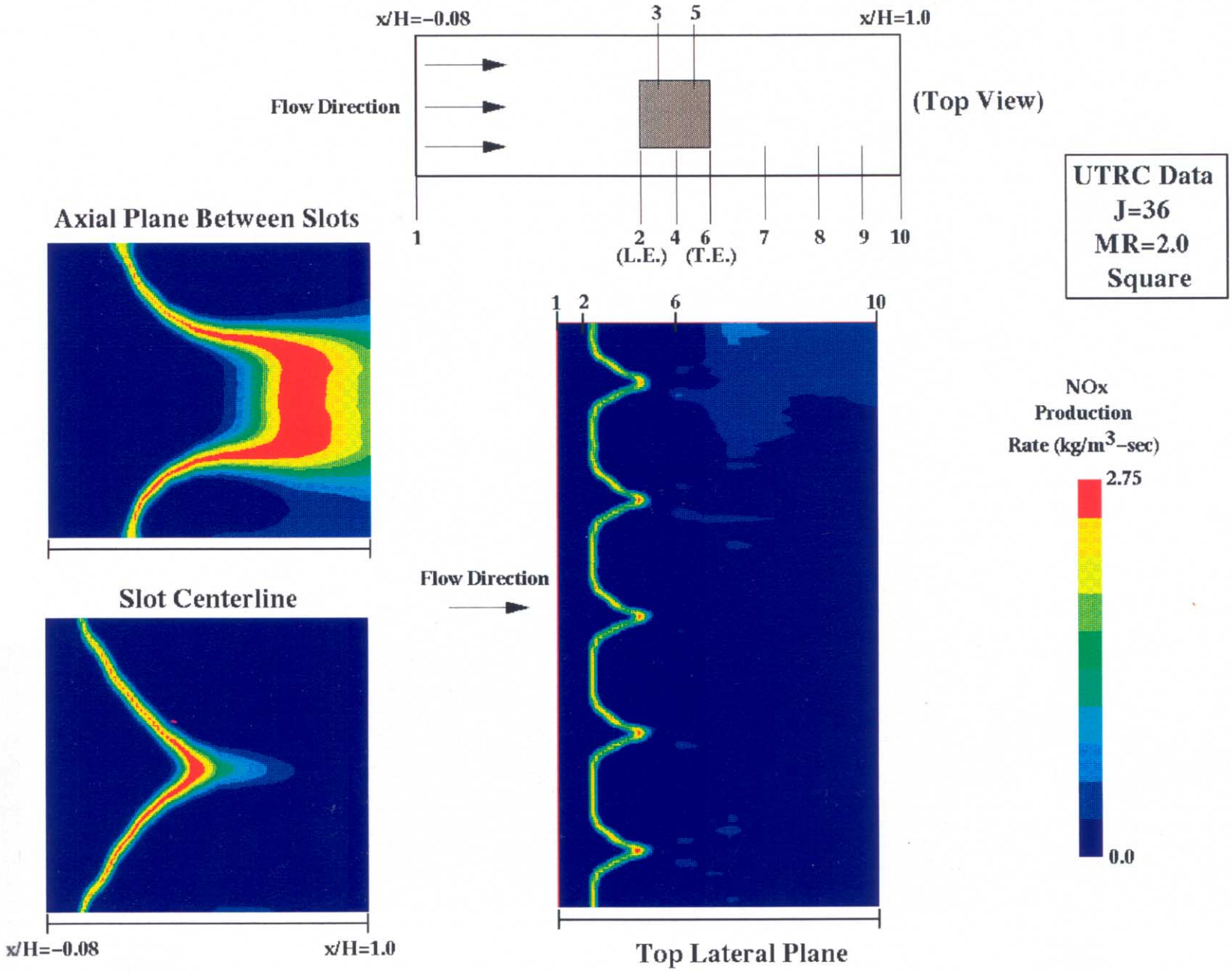

Figure 7-12. Local NO Production Rate Contours for Case 1 (S/H=0.425, J of 36, MR=2.0)

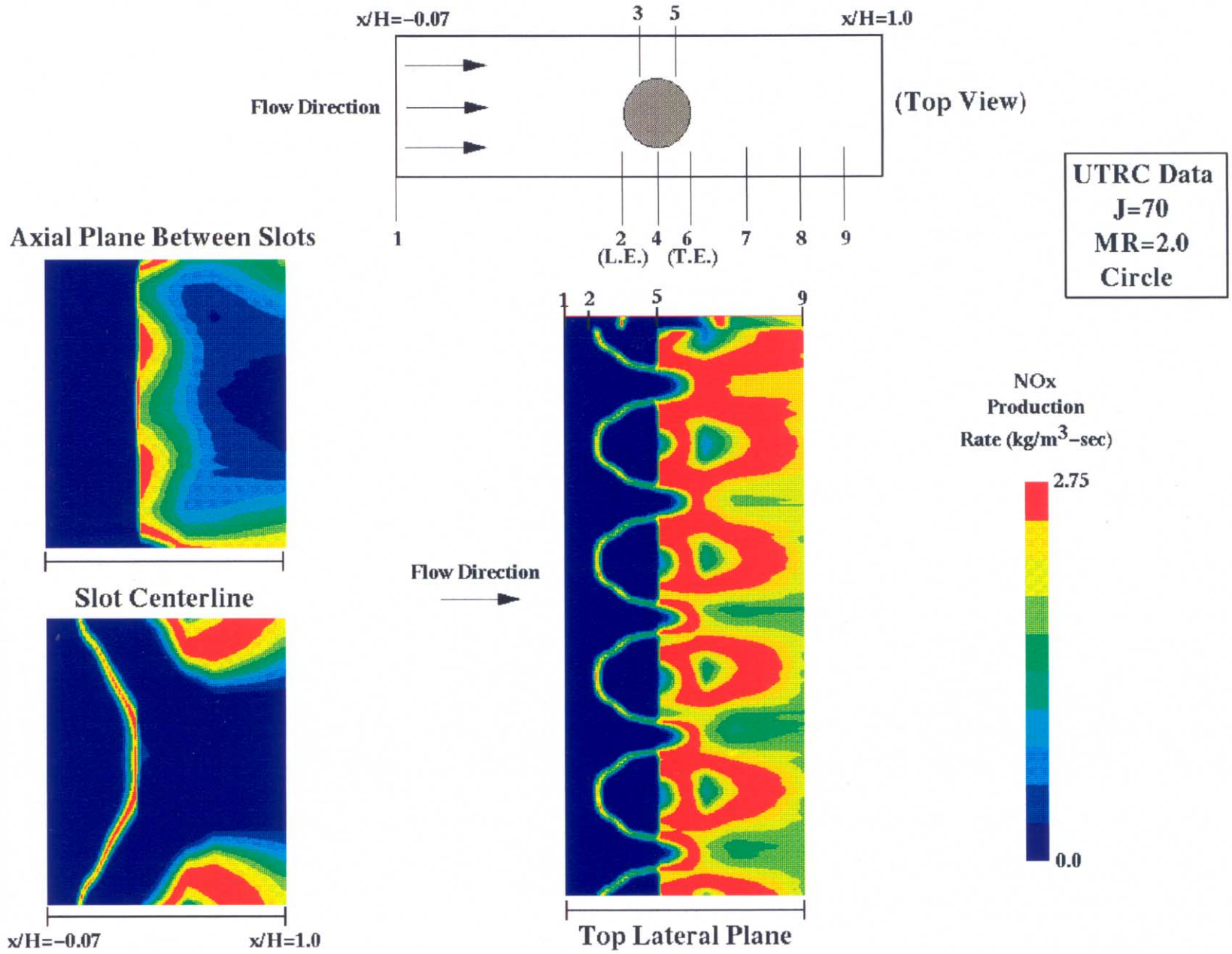

Figure 7-13. Local NO Production Rate Contours for Case 2 (S/H=0.425, J of 70, MR=2.0)

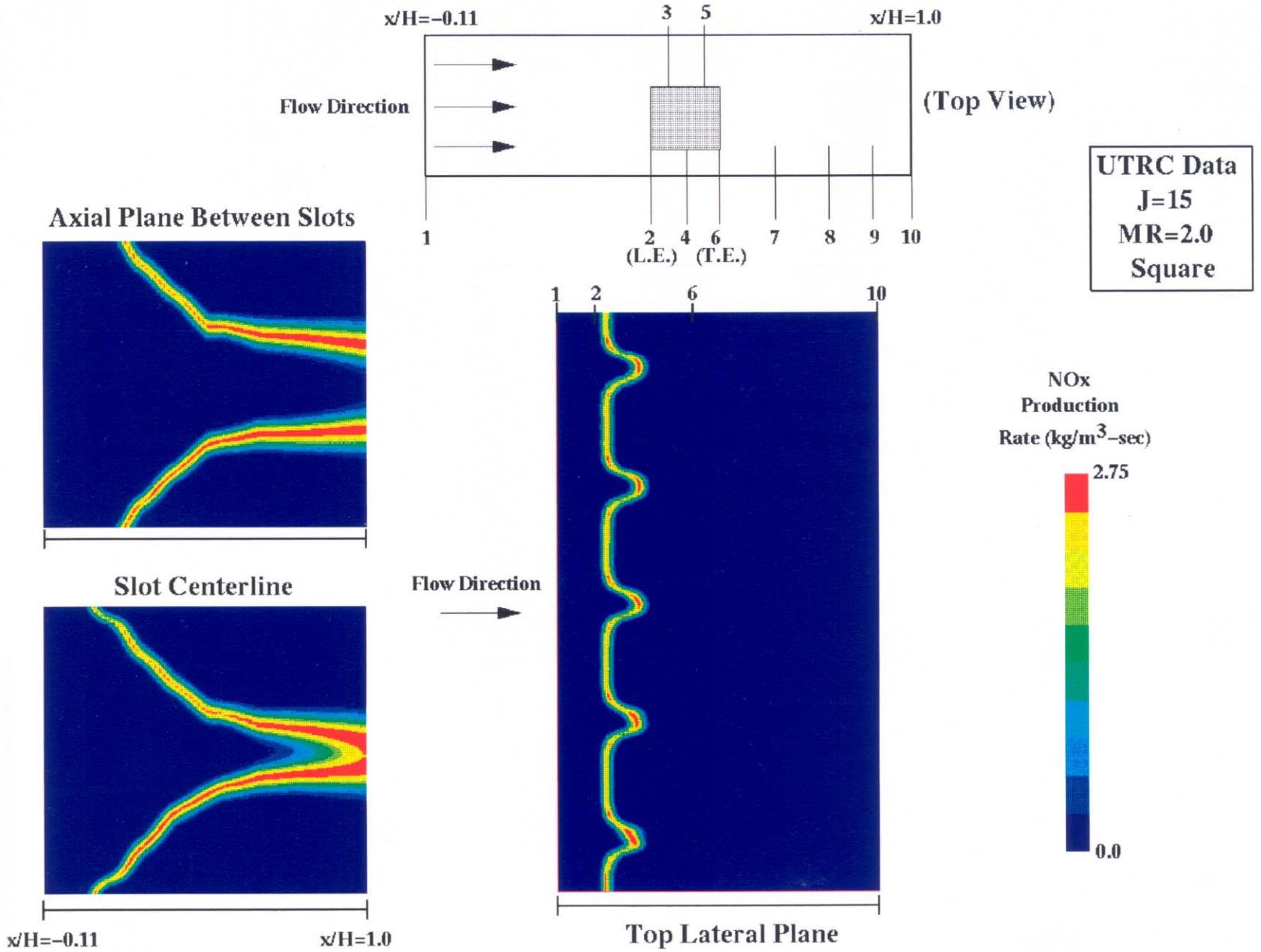

Figure 7-14. Local NO Production Rate Contours for Case 3 (S/H=0.425, J of 15, MR=2.0)

Figure 7-15. Lean-Burn Section Modification (Mixed-Out Data Set Added at x/H=5.0)

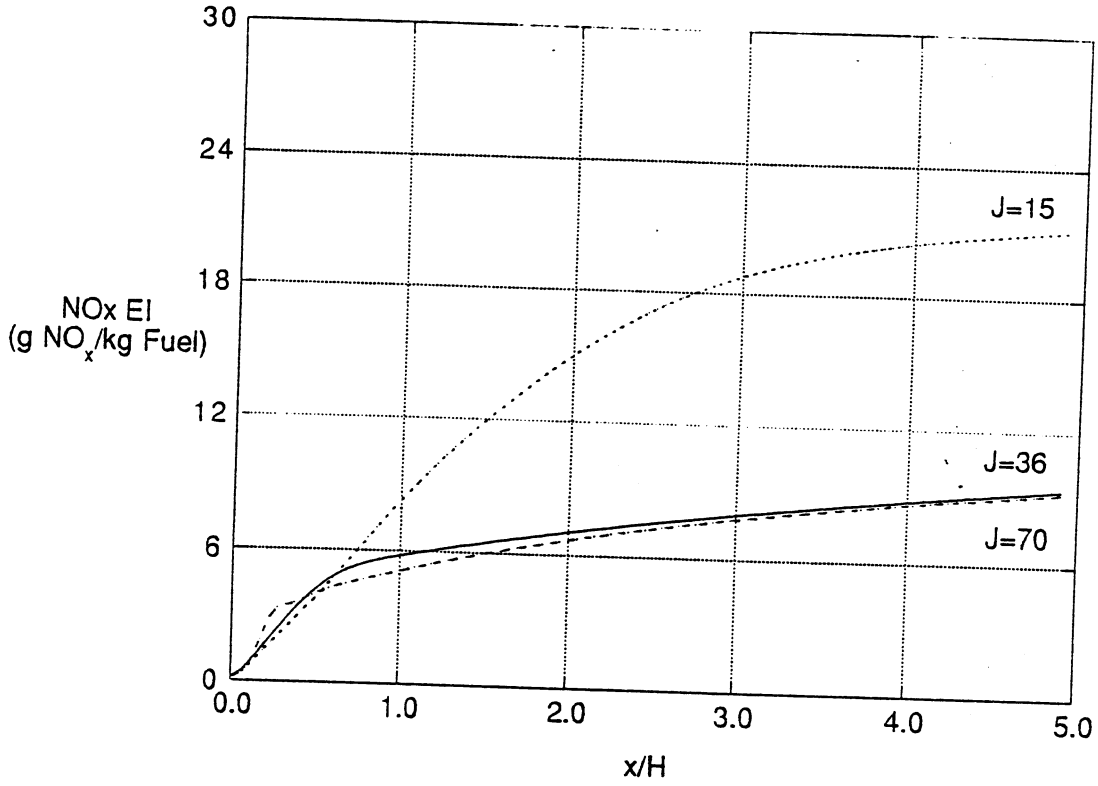

Figure 7-16. NIC NO_x EI Results for QM and Lean Burn Sections

Figure 7-17 shows the effect of varying the Quick-Mix (QM) velocity. The variation in velocity can be accomplished by reducing and increasing the QM height. Shown in Figure 7-17 are the NO_x EI curves for the baseline velocity of 35 m/sec and two others, 20 and 50 m/sec. The NIC velocity analysis was performed incorporating both the QM and Lean-Burn sections. The curves illustrate that increasing the QM velocity results in a linear reduction in the NO_x. These findings are similar to the results shown by Smith et al.[33] In this analysis the effect of varying the Quick-Mix (QM) velocity was achieved by reducing the neckdown diameter.

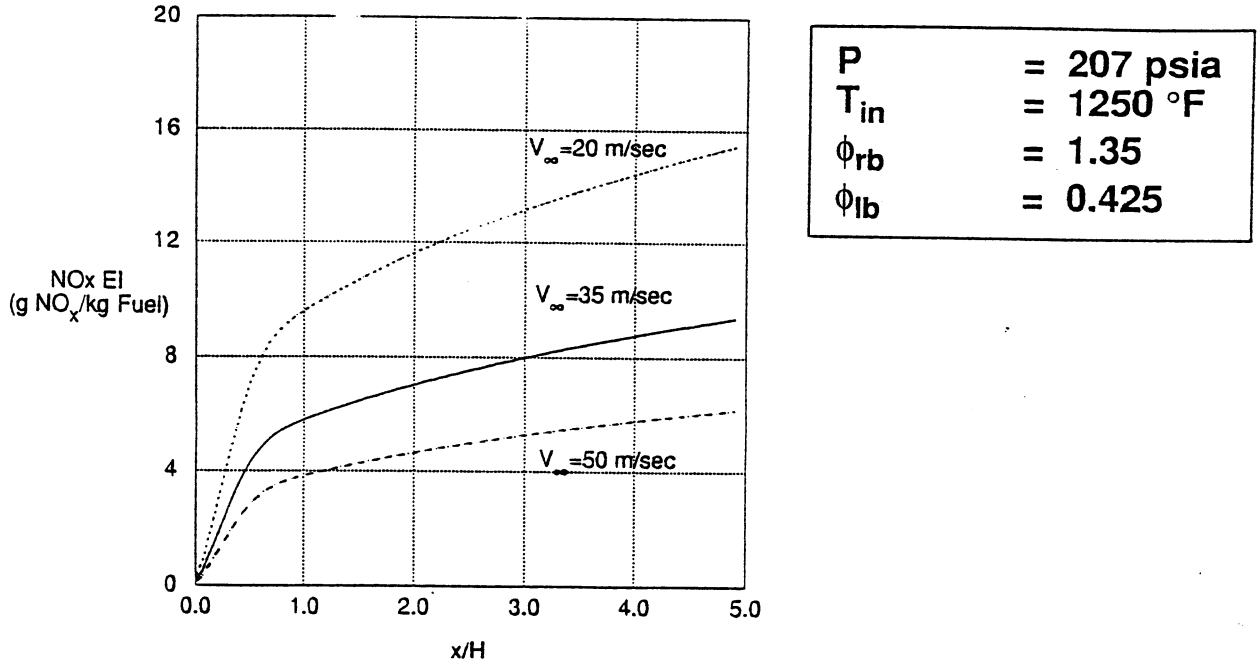

Figure 7-17. Effect of QM Velocity Variation on NO_x EI

The NIC was also used to determine the effect of inlet temperature. Shown in Figure 7-18 is the comparison of the NIC predictions with previously discussed Rosfjord's experimental flame tube data.[65] As seen from the graph, the NIC predictions and experimental data exhibit similar trends. For the assumptions employed in NIC, this result is very good.

7.4 Application of the NIC; Comparison of Optimum Staggered and Inline Geometries

7.4.1 Approach

A good practical application of the NO_x Inference code would be to determine the emission characteristics of two mixing concepts that produce similar downstream mixing levels, but had different paths to reach them. Two such mixing concepts are optimum two-sided inline and staggered orifices in a rectangular geometry. Shown in Figure 7-19 are curves for unmixedness for optimum inline and staggered configurations, calculated from 3D CFD isothermal analysis.

	NIC	Rosfjord's Data
P	207 psia	~130 psia
ϕ_{rb}	1.35	1.8
ϕ_{lb}	0.425	0.42
V_∞	35 m/sec	35 m/sec
J	36	25
τ_{lb}	3.0 msec	3.0 msec

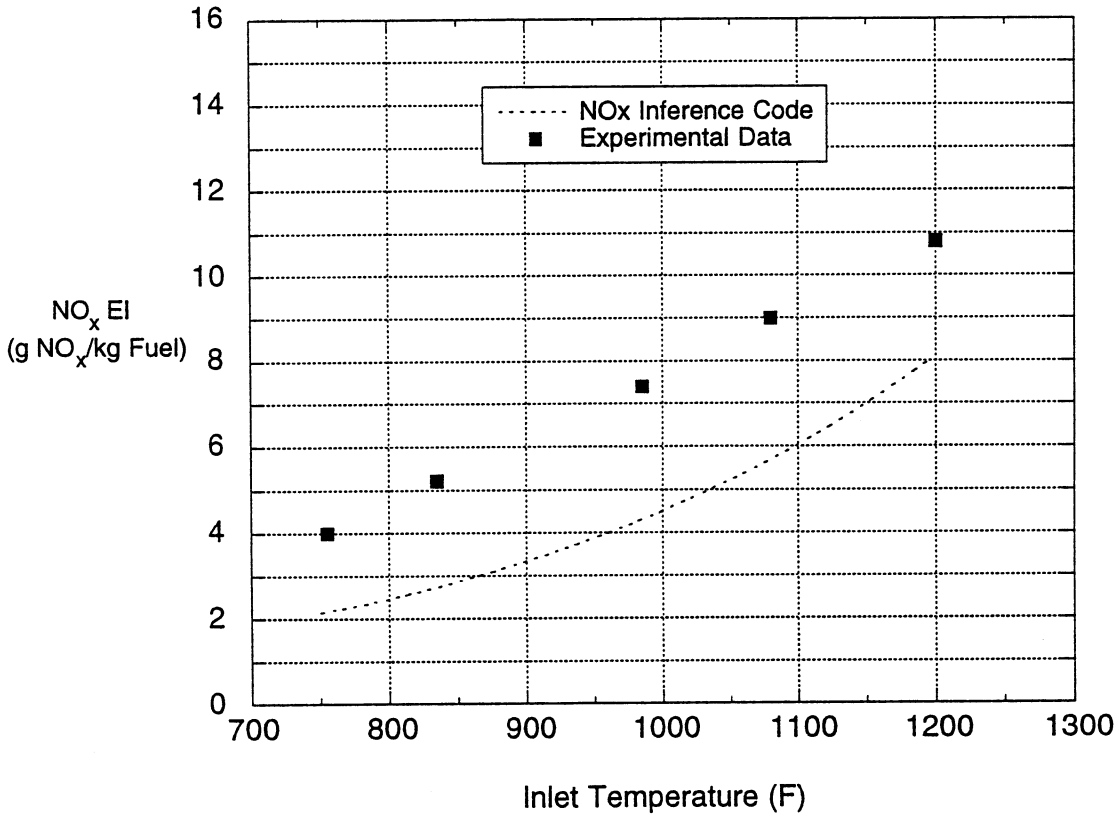

Figure 7-18. Comparison of Inlet Temperature Effects for NIC and Experimental Data

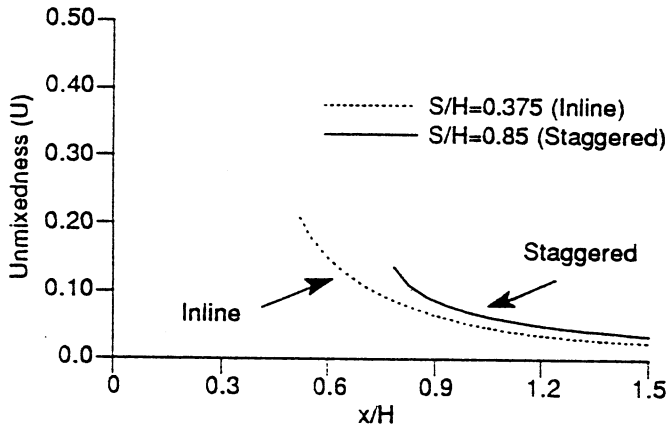

Figure 7-19. Effect of Lateral Arrangement on Unmixedness, J=36

For this analysis a set of experimental data for an optimized staggered and inline geometry would be necessary for comparison. Unfortunately there were insufficient experimental data planes available for such an analysis. The next best alternative was to use existing isothermal 3D CFD results to represent an experimental data set. The case chosen for analysis was originally completed for the work presented in AIAA-96-2762. The geometry shown in Figure 7-20 represents optimized inline and staggered configurations. The optimized spacing-to-duct height ratio for the inline case was 0.375 while the staggered case required an S/H of 0.85. The momentum-flux ratio used in this case was J=36.

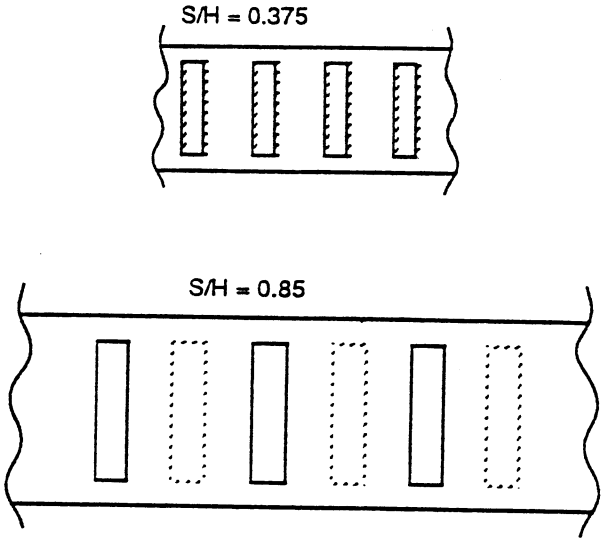

Figure 7-20. Slot Configuration at Optimum S/H

To create the appropriate data sets, 10 selected planes were extracted from the CFD output for both geometries. The data consisted of jet mass fraction for each computational cell in each of the selected planes. Using this data set, the NO_x Inference Code interpolated the 10 selected planes into 100 planes and then performed the emissions calculations. The conditions for this analysis are similar to HSCT operating parameters and those that have used previously (see Table 7-2, Supersonic Cruise).

7.4.2 Results

Shown in Figure 7-19 is the unmixedness comparison for the staggered and inline configurations. From the graph it can be seen that the inline configuration has better initial mixing. (Note the curves start at the trailing edge of the orifice; x/H=0.0 is the leading edge.) This can be attributed to the inline orifices being substantially shorter (smaller) than the staggered orifices. Farther downstream both configurations mix out to about the same level. The question to be answered is which configuration is better in terms of NO_x emissions.

Figure 7-21 shows the NO_x EI as a function of axial location. The graph clearly shows that the NO_x EI levels for the inline case are superior to that of the staggered case. Both configurations produce NO_x at about the same rate initially as evidenced by the similar slopes of the curves, but the inline configuration levels off faster. The leveling off of the NO_x EI curve is an indication of near complete mixing. The larger orifices associated with the staggered configuration leads to a slower mixing rate. The slower mixing rate translates into higher NO_x levels due to the longer residence times needed to complete the quenching of the hot mainstream flow.

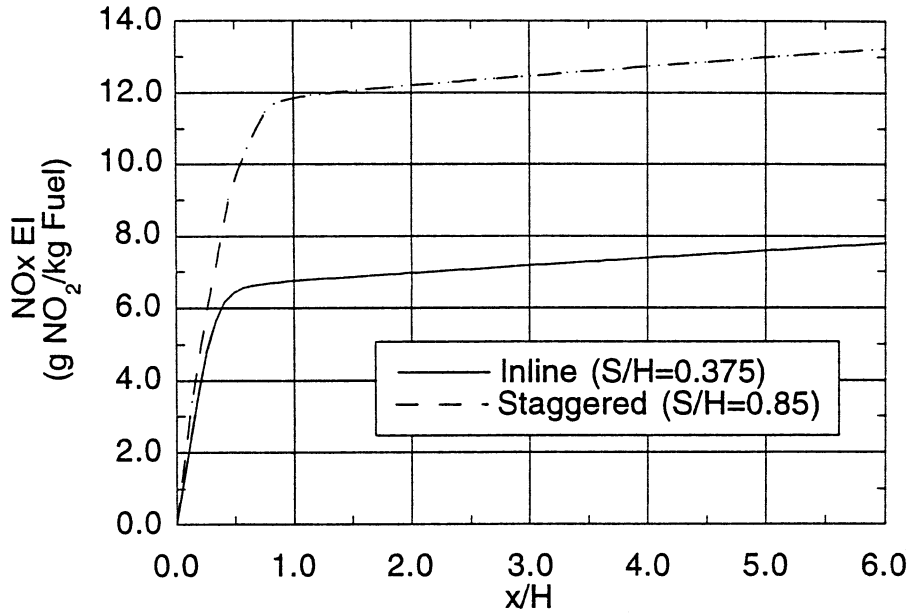

Figure 7-21. Comparison of NO_x EI for Optimum Inline and Staggered Configuration (MR=2.0, J=36)

Figure 7-22 illustrates the CO EI as a function of axial location. Based on the NO_x Inference code assumption of fast CO chemistry, any CO existing in the flowfield is the result of poor mixing. A horizontal line is drawn to illustrate the region where the CO EI corresponds to a combustion efficiency of 99.5%. For this comparison both cases meet the criteria of 99.5% combustion efficiency, though it is clear that the inline case reaches this level much faster than the staggered case (inline x/H~0.5; staggered x/H~0.75). For the staggered configuration, regions of unreacted CO still exist until x/H of 0.75 explaining the continuing formation of NO_x. The CO EI curves again illustrate that the inline case mixes out much faster than the staggered case.

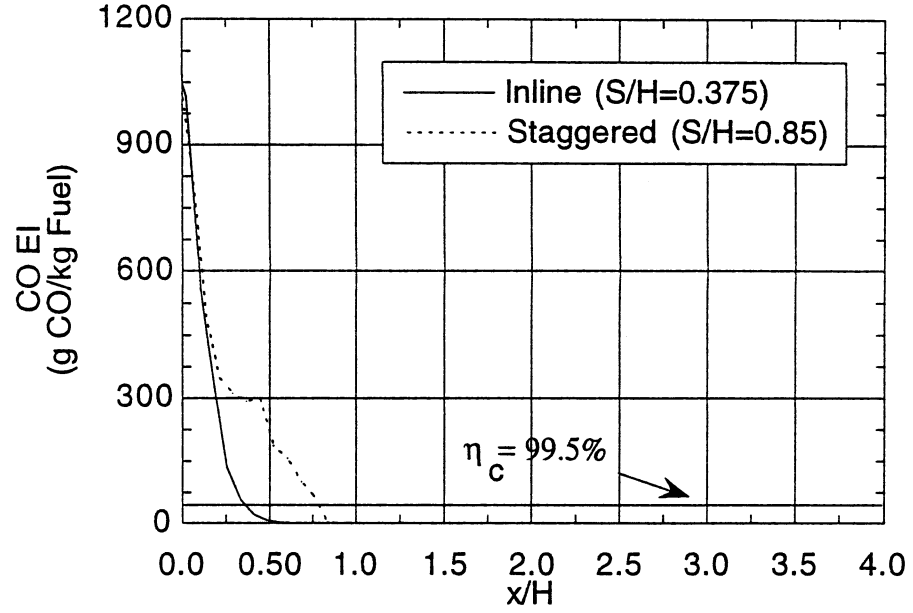

Figure 7-22. Comparison of CO EI for Optimized Inline and Staggered Configuration (MR=2.0, J=36)

8.0 CONCLUSIONS

The following major conclusions can be drawn from this project.

a. Jet penetration is of utmost importance when trying to optimize a configuration in terms of mixing. Optimum jet penetration occurs when the jets penetrate to 1/4 duct height for two-sided injection in rectangular or annular geometries, and to mid-radius (area based) for can geometries.

b. Various orifices (holes, slots, rounded slots) optimized for jet penetration provide little difference is overall mixing.

c. Increasing the momentum-flux ratio improves the overall mixing if the configuration is optimized for jet penetration.

d. Holdeman's correlation constants for optimum mixing must be increased by a factor of two for mass-flow ratios present in RQL combustors. This is true only for rectangular/annular geometries, but not for can geometries.

e. Increasing the orifice blockage through decreasing the orifice aspect ratio has little effect on mixing until orifice blockage approaches 90% or greater.

f. NO_x production is dominant in the jet shear layers and regions near stoichiometric temperatures.

g. Reduction of the mainstream flow area by necking down the passage at the quick-mix section provides NO_x reduction by reducing the residence time in the mixing process.

h. The NO_x Inference Code (NIC), though not as reliable as experimental reacting data or full reacting CFD analysis, can be a viable tool for predicting NO_x emissions from isothermal experimental data, and helping to screen mixing configurations for lowest NO_x potential.

i. Rectangular or annular geometries will produce lower NO_x emissions than can geometries for optimized jet configurations.

j. Increasing the pressure drop across the orifices will reduce NO_x emissions if the jet penetration is optimized.

9.0 REFERENCES

1. Shaw, R.J., "Engine Technology Challenges for a 21st Century High Speed Civil Transport," *AIAA Tenth International Symposium on Air Breathing Engines*, September 1-6, 1991 (Also NASA TM 104363).
2. Mosier, S. A. and Pierce, R. M., "Advanced Combustion Systems for Stationary Gas Turbine Engines," Vol. 1, EPA Contract 68-02-2136, 1980.
3. Crocker, D.S. and Smith, C.E., "Numerical Investigation of Enhanced Dilution Zone Mixing in a Reverse Flow Gas Turbine Combustor," ASME 93-GT-129, 1993.
4. Holdeman, J.D., "Mixing of Multiple Jets with a Confined Subsonic Crossflow," Progress in Energy and Combustion Sciences, Vol. 19, pp. 31-70, 1993. (See also NASA TM 104412, 1991 and AIAA 91-2458, 1991.)
5. Bain, D.B., Smith, C.E., and Holdeman, J.D., "CFD Mixing Analysis of Jets Injected from Straight and Slanted Slots into Confined Crossflow in Rectangular Ducts," AIAA 92-3087, June 1992 (Also NASA TM 105699).
6. Bain, D.B., Smith, C.E., and Holdeman, J.D., "CFD Assessment of Orifice Aspect Ratio and Mass Flow Ratio on Jet Mixing in Rectangular Ducts," AIAA Paper 94-0218, January 1994 (Also NASA TM 106477).
7. Bain, D.B., Smith, C.E., and Holdeman, J.D., "CFD Mixing Analysis of Axially Opposed Rows of Jets Injected in Confined Crossflow," Journal of Propulsion and Power, Vol. 11, No. 5, p. 885-893, September-October 1995 (See also AIAA Paper 93-2044 and NASA TM 106179).
8. Bain, D.B., Smith, C.E. and Holdeman, J.D., "Jet Mixing and Emission Characteristics of Transverse Jets in Annular and Cylindrical Confined Crossflow," AIAA-95-2995, July 1995 (Also NASA TM 106975).
9. Bain, D.B., Smith, C.E. and Holdeman, J.D., "Flow Coupling Effects in Jet-In-Crossflow Flowfields," AIAA-96-2762, July 1996 (Also NASA TM 107257).
10. Doerr, Th., Blomeyer, M., and Henneke, D.K., "Optimization of Multiple Jets Mixing with a Confined Crossflow," ASME Paper 95-GT-313, 1995.
11. Doerr, Th., Blomeyer, M., and Henneke, D.K., "Experimental Investigation of Optimum Jet Mixing Configurations for RQL-Combustors," 12th ISABE, Melborne, Aus., 1995.
12. Doerr, Th. and Hennecke, D.K., "The Mixing Process in the Quenching Zone of the Rich-Lean Combustion Concept," *AGARD 81st Symposium on Fuels*

and Combustion Technology for Advanced Aircraft Engines, Colleferro, NR Rome, Italy, May 10-14, 1993.

13. Hatch, M.S., Sowa, W.A., Samuelsen, G.S. and Holdeman, J.D. (1995), "Jet Mixing into a Heated Cross Flow in a Cylindrical Duct: Influence of Geometry and Flow Variations," Journal of Propulsion and Power, Vol. 11, No. 3, May-June 1995, pp. 393-402 (see also AIAA-92-0773 & NASA TM 105390).
14. Hatch, M.S., Sowa, W.A., Samuelsen, G.S., and Holdeman, J.D. (1995b), "Influence of Geometry and Flow Variation on NO Formation in the Quick Mixer of a Staged Combustor," To be published in Journal of Engineering for Gas Turbines and Power, (see also NASA TM 105639).
15. Holdeman, J.D., Liscinsky, D.S., Oechsle, V.L., Samuelsen, G.S. and Smith, C.E., "Mixing of Multiple Jets with a Confined Subsonic Crossflow in a Cylindrical Duct," Accepted for publication in Journal of Engineering for Gas Turbines and Power, 1996 (Also ASME Paper-GT-482 & NASA TM 107185).
16. Kroll, J.T., Sowa, W.A., Samuelsen, G.S., and Holdeman, J.D., "Optimization of Circular Orifice Jets Mixing into a Heated Crossflow in a Cylindrical Duct," AIAA Paper 93-0249 (also NASA TM 105934), 1993.
17. Holdeman, J.D. and Walker, R.E., "Mixing of a Row of Jets with a Confined Crossflow," AIAA Journal, Vol. 15, No. 2, pp. 243ff (see also AIAA-76-48 & NASA TM 71821), 1977.
18. Leong, M.Y., Samuelsen, G.S., and Holdeman, J.D., "Jet Mixing in a Reacting Cylindrical Crossflow," AIAA Paper 95-3109 (also NASA TM 106975), 1995.
19. Liscinsky, D.S., True, B., and Holdeman, J.D., "An Experimental Study of Crossflow Jet Mixing in Rectangular Ducts," AIAA-93-2037, June 1993 (Also TM 106152).
20. Liscinsky, D.S., True, B., and Holdeman, J.D., "Mixing Characteristics of Directly Opposed Rows of Jets Injected Normal to a Crossflow in a Rectangular Ducts," AIAA Paper 94-0217, January 1994 (Also NASA TM 106477).
21. Liscinsky, D.S., True, B., and Holdeman, J.D., "Crossflow Mixing of Noncircular Jets," Journal of Propulsion and Power, Vol. 12, No. 2, pp. 225-230, January-February 1996 (See also AIAA Paper 95-0732 and NASA TM 106865).
22. Liscinsky, D.S., True, B., Vranos, A., and Holdeman, J.D., "Experimental Study of Cross-Stream Mixing in a Rectangular Duct," AIAA 92-3090, June 1992

(Also NASA TM 106194).

23. Liscinsky, D.S., Vranos, A., and Lohmann, R.P., "Experimental Study of Cross-Stream Mixing in Cylindrical and Rectangular Ducts," NASA CR 187141, 1993.
24. Liscinsky, D.S., Vranos, A., and Lohmann, R.P., "Experimental Study of Crossflow Mixing in Cylindrical and Rectangular Ducts," NASA CR 187141, March 1993.
25. Oechsle, V.L., "Mixing and NOx Emission Calculation of Confined Reacting Jet Flows in a Cylindrical Duct," Allison Engine Company, Indianapolis, IN, August 1995 (Allison LER report HSR005 prepared under NASA Contract NAS 3-25950, Task Order 1).
26. Oechsle, V.L. and Conner, C.H., "Mixing and NOx Emission Calculation of Confined Reacting Jet Flows in Cylindrical and Annular Ducts," Allison Engine Company, Indianapolis, IN, April 1995 (Allison LER report HSR021 prepared under NASA Control NAS 3-25950, Task Order 1).
27. Oechsle, V.L., Mongia, H.C., and Holdeman, J.D., "A Parametric Numerical Study of Mixing in a Cylindrical Duct," AIAA Paper 92-3088 (also NASA TM 105695), 1992.
28. Oechsle, V.L., Mongia, H.C., and Holdeman, J.D., "An Analytical Study of Jet Mixing in a Cylindrical Duct," AIAA Paper 93-2043 (also NASA TM 106181), 1993.
29. Oechsle, V.L., Mongia, H.C., and Holdeman, J.D., "Comparison of the Mixing Calculations of Reacting and Non-reacting Flows in a Cylindrical Duct," AIAA Paper 94-0865 (also NASA TM 106435), 1994.
30. Oechsle, V.L. and Holdeman, J.D., "Numerical Mixing Calculations of Confined Reacting Jet Flows in a Cylindrical Duct," AIAA Paper 95-0733 (also NASA TM 106736), 1995.
31. Pierce, R.M., Smith, C.E., and Hinton, B.S., "Advanced Combustion Systems for Stationary Gas Turbine Engines," Vol. III, EPA Contract 68-02-2136, 1980.
32. Smith, C.E., "Mixing Characteristics of Dilution Jets in Small Gas Turbine Combustors," AIAA 90-2728, 1990.
33. Smith, C.E., Talpallikar, M.V. and Holdeman, J.D., "A CFD Study of Jet Mixing in Reduced Flow Areas for Lower Combustor Emissions," AIAA 91-2460, June 1991 (Also NASA TM 104411).
34. Smith, C.E., Talpallikar, M.V., and Holdeman, J.D., "Jet Mixing in Reduced Flow Areas for Lower Emission Combustors," AIAA Paper 91-2460 (also

NASA TM 104411), 1991.

35. Sowa, W.A., Kroll, J.T., Samuelsen, G.S., and Holdeman, J.D., "Optimization of Orifice Geometry for Crossflow Mixing in a Cylindrical Duct," AIAA Paper 94-0219 (also NASA TM 106436), 1994.
36. Hatch, M.S., Sowa, W.A. and Samuelsen, G.S., "Influence of Geometric and Flow Variation on Jet Mixing and NO Formation in a Model Staged Combustor with Eight Orifices," NASA Contractor Report 194473, June 1996.
37. Srinivasan, R., Myers, G., Coleman, E., and White, C., "Dilution Jet Mixing Program," Phase III Report, NASA CR-174884, September 1985.
38. Talpallikar, M.V., Smith, C.E., and Lai, M.-C., "Rapid Mix Concepts for Low Emission Combustors in Gas Turbine Engines," NASA CR 185292, 1990.
39. Talpallikar, M.V., Smith, C.E., Lai, M.-C., and Holdeman, J.D., "CFD Analysis of Jet Mixing in Low NOx Flametube Combustors," Journal of Engineering for Gas Turbines and Power, April 1992, pp. 416-424 (see also ASME Paper 91-GT-217, NASA TM 104466), 1992.
40. Vranos, A., Liscinsky, D.S., True, B., and Holdeman, J.D., "Experimental Study of Cross-Stream Mixing in a Cylindrical Duct," AIAA Paper 91-2459 (also NASA TM 105180), 1991.
41. Zhu, G. and Lai, M.-C., "A Parametric Study of Penetration and Mixing of Radial Jets in Necked-Down Cylindrical Cross-Flow," Journal of Propulsion and Power, Vol. 11, No. 2, March-April 1995, pp. 252-260 (see also AIAA-92-3091), 1995.
42. Chen, Y.S. and Kim, S.W., "Computation of Turbulent Flows Using an Extended k–ε Turbulence Closure Model," NASA CR-179204, 1987.
43. Chien, K.Y., "Predictions of Channel and Boundary-Layer Flows with a Low-Reynolds Number-Turbulence Model," AIAA Journal, Vol. 23, No. 2, 1985.
44. Przekwas, A.J., et al., "REFLEQS-3D: A Computer Program for Turbulent Flows With and Without Chemical Reaction, Volume 1: User's Manual," CFDRC Report GR-89-4, January 1990.
45. Smith, C.E., Ratcliff, M.L., Przekwas, A.J., Habchi, S.D., and Singhal, A.K., "Modeling of Turbulent Combustion in Liquid Rocket Engine Components," NASA MSFC Contract NAS8-37619, SBIR Phase I Final Report, CFDRC Report 4045/1, 1988.
46. Launder, B.E. and Spalding, D.B., "The Numerical Computation of Turbulent Flows," *Computer Methods in Applied Mechanics and Engineering*, Vol. 3,

pp. 269-289, 1974.

47. Owens, S.F. "CFD-ACE: Command Language Reference Manual," CFD Research Corporation, Huntsville, AL, CFDRC Report GR-92-6, 1992.
48. CFD-GEOM User Manual, Version 1.3, March 1995.
49. Walatka, P.P., Buning, P.G., Pierce, L., and Elson, P.A., "PLOT3D User's Manual," NASA TM 101067, 1990.
50. Harrand, V.J., "CFD-VIEW: A 3D Computer Graphics Software; Volume 1: Technical Manual and Volume 2: Users Manual," August 1992.
51. CFD-POST User Manual, Version 1.06, July 1994.
52. Danckwertz, P.V., "The Definition and Measurement of Some Characteristics of Mixtures," *Appl. Sci. Res.*, Sec. A., Vol. 3, pp. 279-296, 1952.
53. Holdeman, J.D., Srinivasan, R., Reynolds, R., and White, C. , "Studies of the Effects of Curvature on Dilution Jet Mixing," Journal of Propulsion and Power, Vol. 8, No. 1, pp. 209-218 (see also AIAA-87-1953 (NASA TM 84878) & AIAA-88-3180 (NASA TM 100896)), 1992.
54. Holdeman, J.D., Walker, R.E., and Kors, D.L., "Mixing of Multiple Dilution Jets with a Hot Primary Airstream for Gas Turbine Applications," AIAA-73-1249 (also NASA TM 71426), 1973.
55. Lichtarowicz, S., Duggins, R.K., and Markland, E., "Discharge Coefficients for Incompressible Non-Cavitating Flow Through Long Orifices," Journal Mechanical Engineering Science, Vol. 7, No. 2, pp. 210-219, 1965.
56. McGuirk, J.J. and Baker, S.J., "Multi-Jet Annulus/ Core-Flow Mixing-Experiments and Calculations," ASME 92-GT-111, 1992.
57. McGuirk, J.J. and Spencer, A., "CFD Modeling of Annulus/Port Flows," ASME 93-GT-185, 1993.
58. Stevens, S.J. and Carrotte, J.F. "Experimental Studies of Combustor Aerodynamics, Part I: Mean Flowfields," J. of Propulsion and Power, Vol. 6, No. 3, pp. 297-304, May-June 1990 (See also AIAA Paper 87-1827, The Influence of Dilution Hole Aerodynamics on the Temperature Distribution in a Combustor Dilution Zone).
59. Stevens, S.J. and Carrotte, J.F. "Experimental Studies of Combustor Dilution Zone Aerodynamics, Part II: Jet Development," J. of Propulsion and Power, Vol. 6, No. 4, pp. 503-511, July-August 1990 (See also AIAA Paper 88-3274).
60. Carrotte, J. F. and Stevens, S.J., "The Influence of Dilution Hole Geometry on Jet Mixing," J. of Engineering for Gas Turbines and Power, Vol. 112, No. 1, pp.

73-75, January 1990 (See also ASME Paper 89-GT-292).

61. Nickerson, G.R., Coats, D.E., Dang, A.L., Dunn, S.S., and Kehtarnavaz, H., "Two-Dimensional Kinetics (TDK) Nozzle Performance Computer Program Volume II - Programming Manual," Marshall Space Flight Center, NAS8-36863, March 1989.
62. Bartok, W. and Sarofim, A.F., Fossil Fuel Combustion, New York, p. 233, 1991.
63. Nicol, D.G., Steele, R.C., Marinov, N.M., and Malte, P.C., "The Importance of the Nitrous Oxide Pathway to NO_x in Lean-Pre-Mixed Combustion," ASME Paper 93-GT-342, ASME Transactions, Cincinnati, May 1993.
64. Anderson, D., "Effects of Equivalence Ratio and Dwell Time on Exhaust Emissions from an Experimental Premixing Prevaporizing Burner," NASA TMX-71592, March 1975.
65. Rosfjord, T.J. and Padgent, F.C., "Experimental Assessment of the Emissions Control Potential of a Rich/Quench/Lean Combustor for High Speed Civil Transport Aircraft Engine," United Technologies Research Center, E. Hartford, CT, April 1996 (Pratt & Whitney LER report HSR032 prepared under Contract NAS 3-25952, Task Order 3).
66. Radhakrishnan, K. and Bittker, D.A., LSENS, A General Chemical Kinetics and Sensitivity Analysis Code for Gas-Phase Reactions: User's Guide, NASA Technical Memorandum 105851, January 1993.

Appendix A

NASA Technical Memorandum 105699

NASA Technical Memorandum 105699
AIAA–92–3087

CFD Mixing Analysis of Jets Injected From Straight and Slanted Slots Into Confined Crossflow in Rectangular Ducts

D.B. Bain and C.E. Smith
CFD Research Corporation
Huntsville, Alabama

and

J.D. Holdeman
Lewis Research Center
Cleveland, Ohio

Prepared for the
28th Joint Propulsion Conference and Exhibit
cosponsored by the AIAA, SAE, ASME, and ASEE
Nashville, Tennessee, July 6–8, 1992

NASA

CFD MIXING ANALYSIS OF JETS INJECTED FROM STRAIGHT AND SLANTED SLOTS INTO CONFINED CROSSFLOW IN RECTANGULAR DUCTS

D. B. Bain* and C. E. Smith**
CFD Research Corporation
3325-D Triana Blvd.
Huntsville, Alabama 35805

J. D. Holdeman†
National Aeronautics and Space Administration
Lewis Research Center
21000 Brookpark Road
Cleveland, Ohio 44135

Abstract

A CFD study was performed to analyze the mixing potential of opposed rows of staggered jets injected into confined crossflow in a rectangular duct. Three jet configurations were numerically tested: 1) straight (0°) slots, 2) perpendicular slanted (45°) slots angled in opposite directions on top and bottom walls, and 3) parallel slanted (45°) slots angled in the same direction on top and bottom walls. All three configurations were tested at slot spacing-to-duct height ratios (S/H) of 0.5, 0.75, and 1.0; a jet-to-mainstream momentum flux ratio (J) of 100; and a jet-to-mainstream mass flow ratio of 0.383. Each configuration had its best mixing performance at S/H of 0.75. Asymmetric flow patterns were expected and predicted for all slanted slot configurations. The parallel slanted slot configuration was the best overall configuration at x/H of 1.0 for S/H of 0.75.

1. Introduction

The technology demonstration of low NO_x combustors applicable to commercial aircraft is a subject of ongoing research[1]. One combustor concept currently being evaluated experimentally is the Rich-burn/Quick-mix/Lean-burn (RQL) combustor, originally conceived and developed for industrial combustors[2,3]. A key design technology required for successful demonstration of the RQL is a method of rapidly mixing bypass air with rich-burn gases. To identify improved mixing schemes, a number of recent studies have been performed[4,5,6,7]. The current investigation is focused on jet mixing in rectangular cross-sectional geometries in order to identify orifice configurations with the most potential for annular combustors.

In past studies (see Holdeman[8]) applicable to conventional gas turbine dilution zones, it was shown that the rate of mixing and penetration of a row of jets in crossflow is governed mainly by the jet-to-mainstream momentum flux ratio (J) and hole spacing-to-duct height ratio (S/H). One-sided injection (from one wall only) and two-sided injection (from top and bottom walls) were studied. Optimum mixing configurations were identified as shown in Table 1[8]. Of the configurations studied, two-sided, opposed (in

---

* Project Engineer
Member, AIAA

** Manager, Application Projects
Member AIAA

† Senior Research Engineer
Senior Member, AIAA

the same axial plane), staggered (alternate between top and bottom walls in lateral direction) holes were suggested to be the best mixing configuration if the jets penetrated past each other. However, this conclusion was based on relatively few two-sided experimental tests, and it is still unclear if opposed, staggered holes are really better than opposed, inline holes.

In can geometries, air injection through 45° slanted slots is thought to enhance mixing by introducing swirl into the mixing zone that enhances lateral spreading, albeit at a reduction in jet penetration. It was shown by Novick and Troth[9] that slanted slots were better mixers than holes and straight slots for a select few configurations. However, a systematic study, either experimentally or numerically, has not been performed to show that the slanted slot configuration is a better mixing configuration than the straight slot configuration.

This investigation examined the mixing effectiveness of opposed, staggered jets injected through straight (0°) slots and slanted (45°) slots into a rectangular crossflow. Three different configurations were studied:

1. straight slots as a baseline;
2. perpendicular slanted (45°) slots (angled in opposite directions on top and bottom walls); and
3. parallel slanted (45°) slots (angled in the same direction on top and bottom walls).

Note that the orifice centerlines were staggered between top and bottom walls for all configurations studied. Also, note that there are no counterpart configurations in cylindrical geometries.

2. CFD Code

The approach in this study was to perform 3-D numerical calculations on a generic geometry section. A CFD code named REFLEQS[10,11] was used to perform the computations. The basic capabilities/methodologies in REFLEQS include:

1. Solution of two- and three-dimensional Navier-Stokes equations for incompressible and compressible flows;
2. Cartesian, polar, and non-orthogonal body-fitted coordinates;
3. Porosity-resistivity techniques for flows with internal blockages;
4. Fully implicit and strongly conservative formulation;
5. Three differencing schemes: upwind, hybrid, and central differencing with damping terms;
6. Standard, extended, and low Reynolds number k-ε turbulence models, and the multiple-scale turbulence model of Chen;
7. Instantaneous, one-step and two-step combustion models;
8. Modified form of Stone's strongly implicit solver; and
9. Pressure-based solution algorithms including SIMPLE and a variant of SIMPLEC.

3. Validation Case for Slanted Slot Jet Mixing

One slanted slot validation case was selected from the Dilution Jet Mixing Program[8,12]. The selected case consisted of jets injected through single-sided 45° slanted slots into a rectangular crossflow. The geometry and flow conditions are described in Figure 1.

Grid

The numerical computations were performed with the grid shown in Figure 2. Only one slot was modeled to conserve computational time. The grid consisted of 47,488 cells, 53 in the axial (x) direction, 28 in the vertical (y) direction, and 32 in the lateral (z) direction. The origin of the coordinate system in the axial direction is located at the slot center. The slot had an aspect ratio of 2.6 and was modelled using 128 cells. In the axial direction, the calculation domain began one duct height upstream (4 inches, 0.1016 m) and extended 3 duct heights downstream (12 inches, 0.3048 m) of the slot's leading edge.

Numerics

The following conservation equations were solved: u momentum, v momentum, w momentum,

mass (pressure correction), total enthalpy (h), turbulent kinetic energy (k), and turbulent energy dissipation (ε). The convective fluxes were calculated using upwind differencing, and the diffusive fluxes were calculated using central differencing. The standard k-ε turbulence model was employed and conventional wall functions were used. Thermal properties (specific heat and laminar viscosity) of air were calculated as a function of temperature. A turbulent Prandtl number of 0.9 was assumed. A uniform velocity profile was assumed for both mainstream and jet flows. The inlet turbulence levels were determined by analyzing the flow from upstream screens to the test section. The inlet mainstream and jet turbulence levels were:

MAINSTREAM	JET
$u/U = 0.20$	$v/V = 0.20$
$\ell_t = 0.05\ H$	$\ell_t = 0.05\ D$

where
- u = rms of U velocity fluctuation
- v = rms of V velocity fluctuation
- U = averaged velocity in X direction
- V = averaged velocity in Y direction
- H = duct height
- D = equivalent hole diameter
- ℓ_t = turbulent length scale.

The top and bottom walls were treated as no-slip boundaries and the lateral boundaries were treated as cyclic (meaning properties leaving a cell on one boundary enter the corresponding cell on the other boundary). A fixed pressure exit boundary was specified.

Convergence

All error residuals were reduced at least 5 orders of magnitude, and continuity was conserved in each axial plane to the fifth decimal. Convergence was relatively smooth requiring about 450 iterations. A converged solution required approximately 0.75 CPU hours on a CRAY-YMP computer.

Results

The flow vectors at x/H = 0.0, 0.5, 1.0, and 2.0 are shown in Figure 3. It can be seen that the mainstream flow is forced to the upper wall. As the mainstream flow passes by the jet, the jet acts like a stator vane, forcing the mainstream flow to turn. The turning of the mainstream puts an equal, but opposite, turning force on the jet. Thus, at x/H of 2.0, the mainstream flow is moving from right to left on the top wall, while the jet flow is moving from left to right on the bottom wall. A slip line separates the two flows.

Temperature isotherms for the numerical analysis and experimental measurements are shown in Figure 4. The results are shown for two axial (yz) planes, x/H = 0.25 and x/H = 0.50. Overall, good agreement is seen. The jet penetration coincides well with the experimental data. As is commonly seen with CFD codes, the downstream mixing is underpredicted, although not as severely underpredicted as shown in Reference 8. Also, the numerical results show a lag in the lateral shift of the vortex as the flow moves downstream. Overall, in an engineering sense, it was shown that the CFD code could model the slanted slot quite well, thus providing the framework for numerical experiments to be explained in the sections that follow.

4. Numerical Test Configuration and Flow Conditions

A schematic of the test configuration is shown in Figure 5. The height of the mixing section was 4 inches (0.1016 m), and the width was 12 inches (0.3048 m). The mainstream flow entered the calculation domain one duct height upstream (x/H = −1.0) of the slots and continued downstream, making the total axial length 28 inches (0.7112 m). The model consisted of top and bottom wall jet injection into a cold mainstream flow.

Ten different slot configurations were analyzed as shown in Figure 6 and Table 2. As S/H was varied from 0.5 to 1.0, the slot dimensions changed to maintain constant jet-to-mainstream mass flow ratio. The slots were straight (long dimension in direction of mainstream) or slanted 45° to the mainstream flow direction. Note the rows on the top and bottom walls are in the same axial plane, but that the orifices are staggered in the lateral direction. For slanted slots, the slots

were either parallel to each other on top and bottom walls, or perpendicular to each other on top and bottom walls.

The flow conditions of the mainstream and jets were:

MAINSTREAM		JETS	
U_∞	= 5 m/s	V_j	= 50 m/s
T_∞	= 300°K	T_j	= 300°K
u/U_∞	= 0.20	v/V_j	= 0.20
ℓ_t	= 0.2 H	ℓ_t	= 0.2 D

$P = 1 \times 10^5$ Pa
$J = 100$
$m_j/m_\infty = 0.383$

where ∞ = mainstream flow conditions
j = jet conditions
D = equivalent hole diameter.

The turbulent length scales for the mainstream and jets were varied between five and twenty percent of their characteristic dimensions without any appreciable difference in the calculations.

5. Details of Numerical Calculations

Grid

The grid used for the numerical mixing model is presented in Figure 7. The grid consisted of 145,600 cells, 65 cells in the axial (x) direction, 28 cells in the vertical (y) direction, and 80 cells in the lateral (z) direction. The slot had an aspect ratio of four-to-one and was composed of 144 (24 x 6) cells. In the axial direction, the grid distribution in the slot region was uniform. The grid upstream and downstream of the slot region was expanded/contracted so that the cell adjacent to the slot region matched the cell size in the slot region. The cells in the vertical direction were all of uniform size. In the lateral direction, six zones were used, and the grid distribution in the slot regions was uniform.

Note that the lateral boundaries are located at the midplanes between jet centerlines. Most of the analyses presented in this paper were performed using this lateral arrangement. However, in some cases to be discussed later, two other lateral arrangements were used. First, geometrically symmetric configurations (straight slots) were run with the lateral domain between the jet centerline on the top wall and the jet centerline on the bottom wall. Second, in some checkcases, the lateral boundaries were placed between jet centerlines on the same wall.

Numerics

The same numerics and models were employed as discussed in the validation case.

Convergence

Similar convergence criteria was used as in the validation case. Due to the significant increase in grid size, the required CRAY-YMP computer time per case increased to approximately 4 CPU hours.

6. Data Postprocessing

To quantify mixing effectiveness, the area-averaged standard deviation of jet flow was calculated in each axial plane. The area-averaged standard deviation (σ) of jet flow is defined as

$$\sigma = \sqrt{\frac{1}{A_{TOT}} \sum_i A_i (f_i - f_{avg})^2}$$

where

A_{TOT} = total flow area in each axial plane
A_i = flow area of cell i
f_i = jet mass fraction in cell i
$f_{avg} = \theta^8_{EB} = \dfrac{\dot{m}_j}{\dot{m}_j + \dot{m}_\infty}$

The area-averaged standard deviation of jet flow was selected as the parameter of interest in order to compare numerical results with experimental results. Mass-averaged standard deviations were also calculated in this study, and they gave essentially the same results as the area-averaged numbers. For the sake of clarity,

only area-averaged standard deviations are reported in this paper.

Unmixedness[6] is defined as σ/f_{avg}. Relative unmixedness[6] (which bounds unmixedness between 0 and 1) is defined as:

$$\chi = \frac{\sigma/f_{avg}}{F}$$

where

$$F = \sqrt{\frac{1 - f_{avg}}{f_{avg}}} = \left(\frac{\dot{m}_j}{\dot{m}_\infty}\right)^{-1/2}$$

For this study, F is 1.62.

7. Results

Straight Slots

For straight slots, two different sets of solutions were obtained. In the first set of solutions, lateral symmetry boundaries were imposed to account for the slot geometry being symmetric. The lateral domain went from jet centerline on the top wall to jet centerline on the bottom wall, and symmetry conditions were imposed on the lateral (xy) boundaries. The second set of solutions for straight slots was obtained by analyzing one full cyclic pattern, going from midplane to midplane between slots (in the lateral direction) and including one slot on the top wall and one slot on the bottom wall. Cyclic boundary conditions were assumed on the lateral (xy) boundaries. With this assumption, the flow is permitted to exit and enter the lateral boundaries. This simulates an annular combustor with walls having infinite radius of curvature.

Solutions with Symmetric Lateral Boundaries: The numerical results for the lateral symmetric boundary cases are shown in Figure 8. Figure 8 presents jet mass fraction color concentration maps for three S/H ratios (0.5, 0.75, and 1.0) and four x/H ratios (0.0, 0.25, 0.50 and 1.0). The origin of the axial (x/H) planes was located at the center of the slots. In terms of NO_x production, it is more appropriate to represent the downstream distances as a function of the orifices' leading edge. An alternate coordinate system in terms of x′ was established that had its origin at the orifice leading edge. Both x/H and x′/H distances are shown in the figure. The jet mass fraction color bar has an arrow signifying the overall jet mass fraction at equilibrium (0.277).

The multiple cycles shown in Figure 8 were generated graphically. For each S/H case, the same cross-sectional flow area is shown, encompassing twelve jets for S/H of 0.5, eight jets for S/H of 0.75, and six jets for S/H of 1.0.

For S/H of 0.5, the jets do not fully penetrate to the opposite wall. The mainstream flow is forced to the walls, and the jet flow occupies the center of the duct. For S/H of 0.75 and 1.0, the jets penetrate to the opposite wall, as evidenced by backflow on the walls (see x/H = 0.0). For S/H of 1.0, the mainstream flow passes between jets in the center of the duct.

A qualitative comparison of mixing effectiveness can be made by close examination of Figure 8. By comparing the color patterns at x/H of 0.25, 0.50, and 1.0, it can be seen that the best mixing occurs at S/H = 0.75. A more quantitative comparison of mixing is presented in Figure 12, where relative unmixedness is plotted as a function of x/H. The configurations with S/H of 0.5 and 0.75 are clearly superior to S/H of 1.0. While both configurations have nearly identical unmixedness values (≈ 0.042) at x/H of 1.0, it can be seen that S/H of 0.75 is mixed better at all x/H upstream of 1.0. It is hypothesized that the integrated area under the unmixedness curve is probably a good indicator of overall mixing effectiveness, hence S/H of 0.75 is probably better in terms of reducing NO_x emissions. Further reacting CFD analysis will have to be performed to verify this hypothesis.

Solutions with Cyclic Lateral Boundaries: Figure 9 displays the results for the cyclic cases. For S/H of 0.5, the flowfield is symmetric about the lateral planes through the jet centerlines, having a flow pattern identical to the symmetric boundary case discussed previously. However, for S/H of 0.75 and 1.0, the flowfield is quite different from the symmetric boundary cases. The

flow asymmetry causes the jets to pair-up, allowing little opening for the mainstream to pass through the paired jets, but more opening for the mainstream to pass between jet pairs. It is interesting to note that for S/H of 0.75 the flow flipped in one direction, while for S/H of 1.0, the flow flipped in the opposite direction. Thus, it appears either flipped solution is attainable and stable.

Qualitatively, it appears from Figure 9 that the best mixing occurs for S/H of 0.75. Figure 13 presents the unmixedness results for the cyclic boundary cases. As with the symmetric boundary cases, the best mixing occurs for S/H of 0.75 for the cyclic cases.

In rectangular rig tests, flow symmetry has always been measured. It is hypothesized that sidewalls force the symmetric flow patterns by suppressing flow in the lateral direction at the walls. In annular combustors, the flowfield may resemble the flow solutions attained with cyclic boundaries. Future numerical tests modelling multiple jets with and without sidewalls will be executed to verify this hypothesis.

Check Cases: In hindsight, to eliminate any effects caused by other factors, a common lateral domain should have been used for both sets of solutions. The lateral domain should have extended from jet centerline to jet centerline on one wall, and symmetric and cyclic lateral boundaries should have been imposed on the same grid. To check the computed flow results in Figures 8 and 9, two repeat cases (S/H of 0.75) were performed with the lateral arrangement from jet centerline-to-jet centerline on the top wall. In one case, symmetric lateral boundaries were imposed, and for the other case, cyclic lateral boundaries were imposed. The computed flow patterns were exactly the same as the computed results in Figures 8 and 9. Thus, the results presented in this paper are consistent with the imposed lateral boundary conditions.

Perpendicular Slanted Slots

For the perpendicular slanted slots, the geometry is asymmetric, and hence this configuration must be modelled using cyclic lateral boundary conditions. The jet mass fraction concentration maps for perpendicular slanted slots are presented in Figure 10. The jets from perpendicular slanted slots penetrate less than those from straight slots. The jets penetrate to the opposite walls only for S/H of 1.0, and only a small amount of backflow is evident for S/H of 1.0. The jets pair up as would be expected based on the geometry. For the perpendicular slanted slots, the flow is asymmetric for all S/H, including S/H of 0.5. Physically, the asymmetry is caused by the induced swirl of the mainstream flow as it passes the angled jets (see earlier validation case).

For S/H of 0.5, the jets do not penetrate past each other. Thus, the jet flow is concentrated in the center of the duct, and the mainstream flow is concentrated on the walls. For S/H of 0.75, the mainstream flow passes between the paired jets and appears to be the most mixed at the displayed axial locations. For S/H of 1.0, it is obvious that the gap between paired jets is too large, and needs to be reduced to improve mixedness.

Whereas the jet pairing appears to be arbitrary for straight slots (depending on which way the flow flipped), the jet pairing is defined by the geometric configuration for perpendicular slanted slots. The slots' midpoints are uniformly spaced, making the leading edges of the slots unevenly spaced (see Figure 6). Hence, the jets will pair-up according to which slots have their leading edges closest together. To eliminate the jet pairing and, hopefully, improve jet mixing, the slot spacing can be modified.

An alternate slot spacing with S/H of 1.0 was analyzed to show the feasibility of improving jet mixing for perpendicular slanted slots (see Figure 6 for spacing). For the alternate spacing, the slots' leading edges were equally spaced. The results are shown in Figure 11. It can be seen that the alternate slot spacing forces the bottom jets to penetrate about halfway between the top jets. The even lateral distribution of the jets' leading edges better distributes the mainstream flow between jets.

Comparison of unmixedness results for the perpendicular slanted slots is shown in Figure 14 for the S/H parametrics. It can be seen that the best spacing is S/H of 0.75. Figure 15 shows the effect of the alternate slot spacing to eliminate jet pairing. It can be seen that a more uniform lateral distribution of the jets' leading edges does, indeed, improve jet mixing for S/H of 1.0.

Parallel Slanted Slots

Figure 16 shows the jet mass fraction concentrations for the parallel slanted slot configuration. Except for S/H of 1.0, the parallel slanted slots penetrated less than the straight slots. For S/H of 1.0, the jets originating from the bottom wall penetrate to the opposite wall and exhibit significant backflow, almost identical to the straight slot cases at S/H of 1.0. However, the jets originating from the top wall penetrate significantly less than the bottom wall jets, and significantly less than the straight slot cases.

Flow asymmetry was predicted in this case also. However, in contrast to the previous cases, the parallel slanted slots produced a flowfield on the top wall completely different than the flowfield on the bottom wall. The cause of the phenomena is still being investigated. It should be noted that the flowfield flipped one way for S/H of 0.75, and the other way for S/H of 1.0. By starting with the restart file from the converged solution for S/H of 1.0, a different (*i.e.*, opposite direction) flipped solution could be obtained for S/H of 0.75. Thus, as was shown with straight slots, either flipped solution is attainable and stable.

For S/H of 0.5, the parallel slanted slot jets only penetrate to mid-duct, thus forcing the mainstream flow to the walls and resulting in poor mixing. For S/H of 0.75, the jets penetrate slightly past each other, and appear to mix out quite well. For S/H of 1.0, the bottom jets overpenetrate, and jet pairing produces a large gap for mainstream flow to pass through. Figure 17 shows the unmixedness levels for each spacing. The effect of S/H is much more pronounced for parallel slanted slots compared to perpendicular slanted slots. S/H of 0.75 is the best spacing for this configuration, the same as for straight slots and perpendicular slots.

A comparison between all configurations is presented in Figure 18 for S/H of 0.75. At x/H of 1.0, the best mixed configuration is the parallel slanted slot configuration, followed in order by straight slots (symmetric lateral boundaries), straight slots (cyclic lateral boundaries), and perpendicular slanted slots. If overall mixedness (lowest NO_x) is based on the integrated area under the unmixedness curves, the parallel slanted slots and straight slots (symmetric lateral boundaries) are nearly equal, and the straight slots (cyclic lateral boundaries) and perpendicular slanted slots are much inferior. It should be mentioned that alternate spacings for perpendicular slanted slots to more uniformly distribute the jets laterally should improve its mixing performance, but it is unlikely to improve its performance better than the parallel slanted slots.

8. Conclusions

A CFD parametric study was performed on opposed rows of staggered jets mixing in a confined rectangular crossflow. Three configurations were analyzed: 1) straight (0°) slots, 2) perpendicular slanted (45°) slots, and 3) parallel slanted (45°) slots. For a jet-to-mainstream momentum flux ratio (J) of 100, all three configurations produced their best mixing at a slot spacing-to-duct ratio (S/H) of 0.75 (compared to S/H of 0.5 and 1.0). The parallel slanted slots produced the best overall mixing at x/H of 1.0, having an unmixedness value of 0.037, compared to 0.050 for perpendicular slanted slots, 0.047 for cyclic boundary straight slots, and 0.042 for symmetric boundary straight slots. Asymmetric flow patterns were predicted for most configurations when cyclic lateral boundaries were assumed. Such flow patterns are expected to occur in annular combustors, but rectangular rigs with sidewalls may force symmetric flow patterns and/or contaminate the mid-duct measurements. Future study of the ramifications of asymmetric/symmetric flow patterns in rectangular geometries is warranted.

9. Acknowledgements

The authors wish to thank NASA Lewis Research Center for funding this work under NASA Contract NAS3-25967, and for the use of NAS Computer time. Valuable discussions and assistance were provided by Mr. Milind Talpallikar, Dr. Vincent Harrand, and Dr. Scott Crocker of CFD Research Corporation. Our thanks also are extended to Ms. Kathy W. Rhoades for preparing this typescript.

10. References

1. R. J. Shaw, "Engine Technology Challenges for a 21st Century High Speed Civil Transport," AIAA Tenth International Symposium on Air Breathing Engines, September 1-6, 1991 (Also NASA TM 104363).
2. S. A. Mosier and R. M. Pierce, "Advanced Combustion Systems for Stationary Gas Turbine Engines," Vol. I, EPA Contract 68-02-2136, 1980.
3. R. M. Pierce, C. E. Smith, and B. S. Hinton, "Advanced Combustion Systems for Stationary Gas Turbine Engines," Vol. III, EPA Contract 68-02-2136, 1980.
4. M. V. Talpallikar, C. E. Smith, M. C. Lai, and J. D. Holdeman, "CFD Analysis of Jet Mixing in Low NO_x Flametube Combustors," ASME Paper 91-GT-217, to be published in ASME Transactions, Journal of Engineering for Gas Turbines and Power, 1992 (Also NASA TM 104466).
5. C. E. Smith, M. V. Talpallikar, and J. D. Holdeman, "A CFD Study of Jet Mixing in Reduced Flow Areas for Lower Combustor Emissions," AIAA Paper 91-2460, June, 1991, (Also NASA TM 104411) .
6. A. Vranos, D. S. Liscinsky, B. True, and J. D. Holdeman, "Experimental Study of Cross-Stream Mixing in a Cylindrical Duct," AIAA Paper 91-2459, June, 1991 (Also NASA TM 105180).
7. M. S. Hatch, W. A. Sowa, G. S. Samuelsen, and J.D. Holdeman, "Jet Mixing Into a Heated Cross Flow in a Cylindrical Duct: Influence of Geometry and Flow Variations," AIAA Paper 92-0773, January, 1992 (Also NASA TM 105390).
8. J. D. Holdeman, "Mixing of Multiple Jets with a Confined Subsonic Crossflow," AIAA Paper AIAA-91-2458, 1991 (Also NASA TM 104412).
9. A. S. Novick and D. L. Troth, "Low NO_x Heavy Fuel Combustor Concept," NASA CR-165367, 1981.
10. A. J. Przekwas, *et al.*, "REFLEQS-3D: A Computer Program for Turbulent Flows With and Without Chemical Reaction, Volume 1: User's Manual," CFDRC Report GR-89-4, January 1990.
11. C. E. Smith, M. L. Ratcliff, A. J. Przekwas, S. D. Habchi, and A. K. Singhal, "Modeling of Turbulent Combustion in Liquid Rocket Engine Components," NASA MSFC Contract NAS8-37619, SBIR Phase I Final Report, CFDRC Report 4045/1, 1988.
12. R. Srinivasan, G. Myers, E. Coleman, and C. White, "Dilution Jet Mixing Program," Phase III Report, NASA CR-174884, September 1985.

Table 1. Spacing and Momentum-Flux Ratio Relationships

Configuration	$C = (S/H)\ \sqrt{(J)}$
Single-side injection:	
Under-penetration	<1.25
Optimum	2.5
Over-penetration	>5.0
Opposed rows of jets:	
In-line optimum	1.25
Staggered optimum	5.0

Table 2. Specifications of Configurations

Configuration	S/H	Slant Angle	S_1/H	S_2/H	L/W	A_j/A_∞	Blockage	Slot Leading Edge (X/H)	Slot Trailing Edge (X/H)
Straight	0.5	0°	0.25	0.25	4	0.0189	9.7%	-0.10	0.10
Straight	0.75		0.375	0.375			7.9%	-0.12	0.12
Straight	1.0		0.5	0.5			6.9%	-0.14	0.14
Parallel Slanted	0.5	45°	0.25	0.25			34.3%	-0.06	0.06
Parallel Slanted	0.75		0.375	0.375			28.0%	-0.08	0.08
Parallel Slanted	1.0		0.5	0.5			24.3%	-0.09	0.09
Perpendicular Slanted	0.5		0.25	0.25			34.3%	-0.06	0.06
Perpendicular Slanted	0.75		0.375	0.375			28.0%	-0.08	0.08
Perpendicular Slanted	1.0		0.5	0.5			24.3%	-0.09	0.09
Perpendicular Slanted	1.0		0.60	0.40			24.3%	-0.09	0.09

where

S = Slot Spacing = $S_1 + S_2$
H = Duct Height
S_1 = Slot Spacing Parameter (see Figure 6)
S_2 = Slot Spacing Parameter (see Figure 6)
L = Slot Length (Long Dimension)
W = Slot Width (Short Dimension)
A_j = Jet Flow Area
A_∞ = Mainstream Flow Area

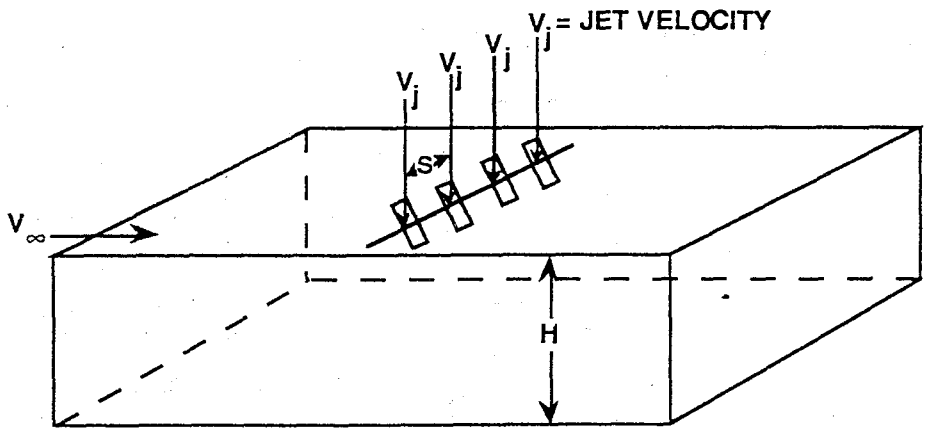

S = Hole Spacing
D = Equivalent Hole Diameter
H = Test Section Height
V_j = Jet Velocity (m/s)
T_j = Jet Tempeature (°K)
V_∞ = Mainstream Velocity (m/s)
T_∞ = Mainstream Tempeature (°K)
J = Jet-to-Mainstream Momentum Flux Ratio $\left[\left(\rho_j V_j^2\right)/\left(\rho_\infty V_\infty^2\right)\right]$
MFR = Mass Flow Ratio $(\Sigma \dot{m}_j/\dot{m}_\infty)$

ORIFICE CONFIGURATION	EQUIVALENT DIA (CM)	S / H	S / D	H / D	V_j	T_j	V_∞	T_∞	J	MFR
Single Row 45° Slots	2.54	0.5	2.0	4.0	60.5	314.5	17.2	675.5	27.1	0.50

Figure 1. Validation Case from Reference 12

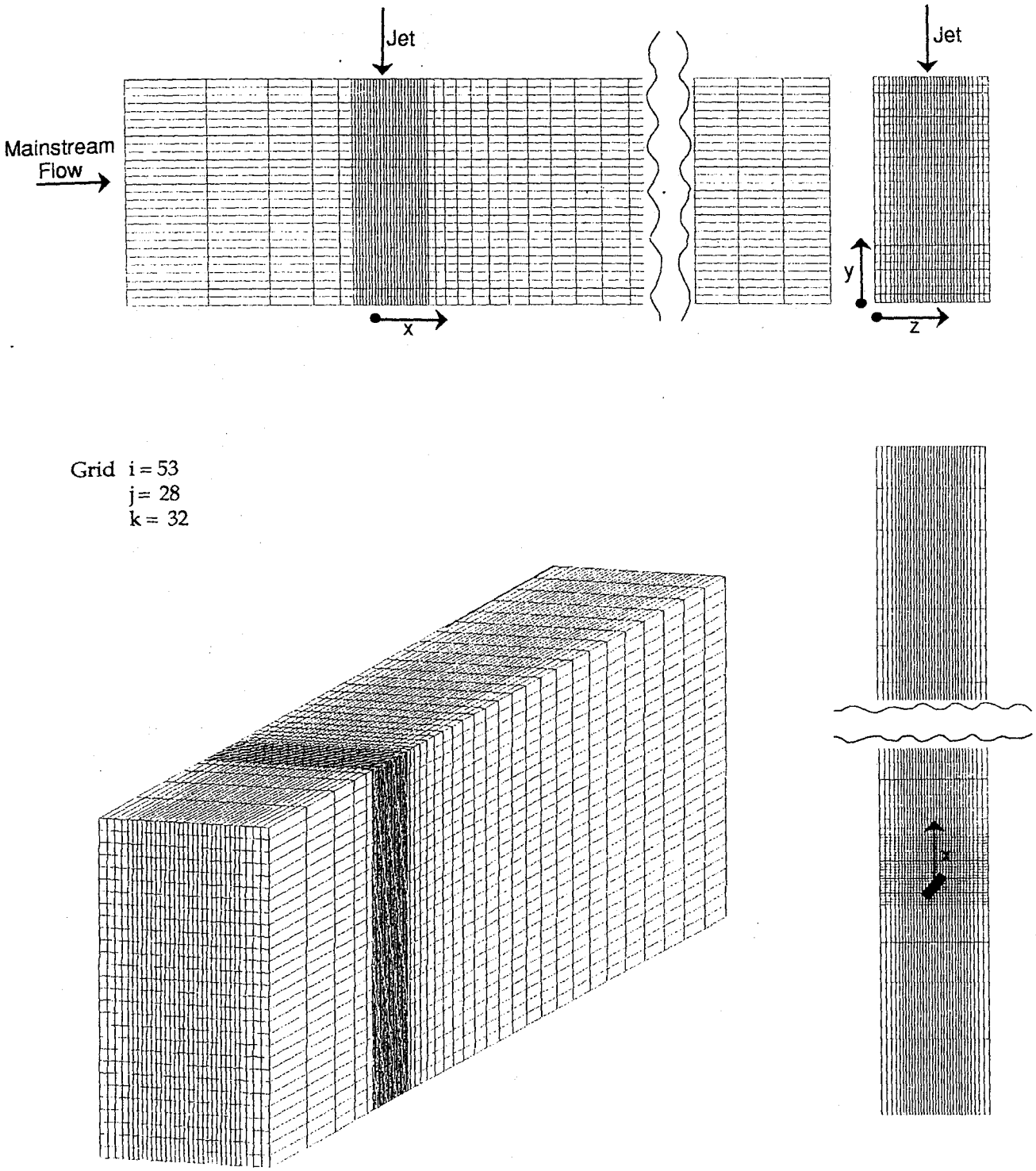

Figure 2. Grid used for Code Validation

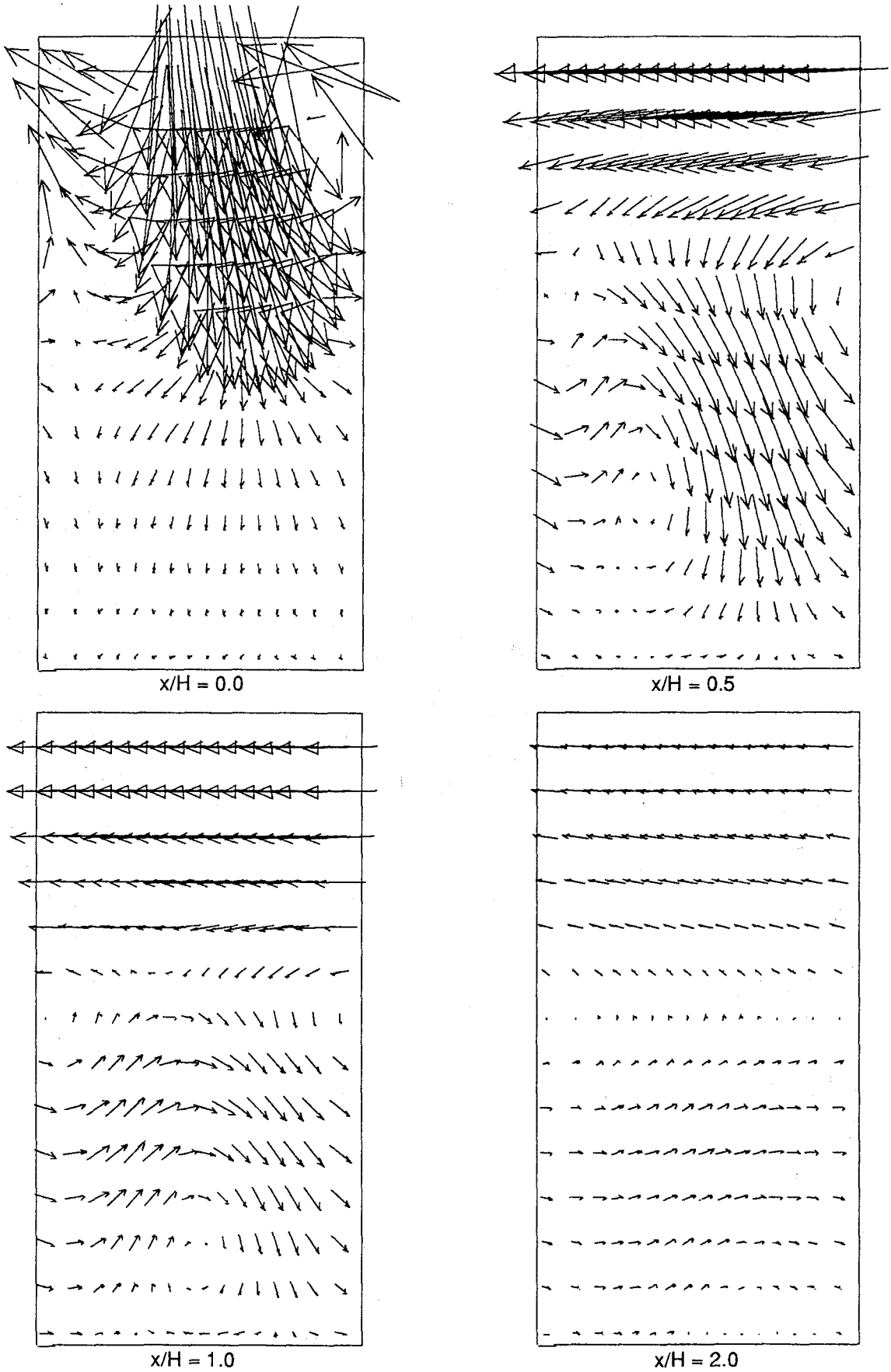

Figure 3. Validation Case: Velocity Vectors

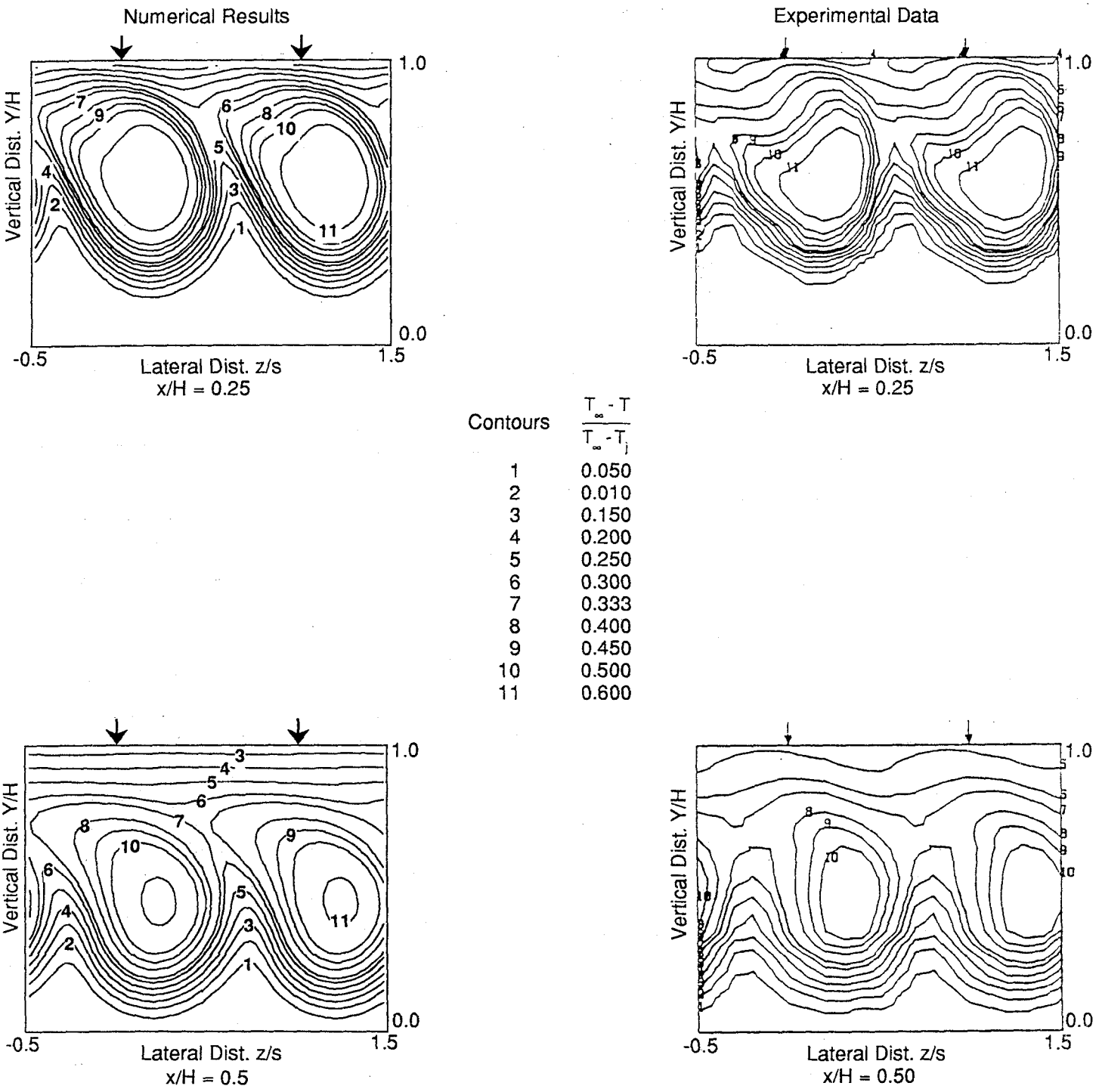

Contours	$\frac{T_\infty - T}{T_\infty - T_j}$
1	0.050
2	0.010
3	0.150
4	0.200
5	0.250
6	0.300
7	0.333
8	0.400
9	0.450
10	0.500
11	0.600

Figure 4. Comparison of Temperature Isotherms between Experimental Results and REFLEQS Calculations

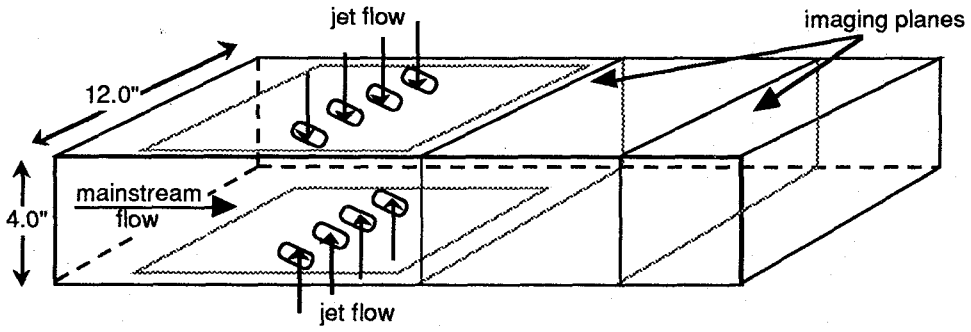

Figure 5. Schematic of Numerical Test Configuration

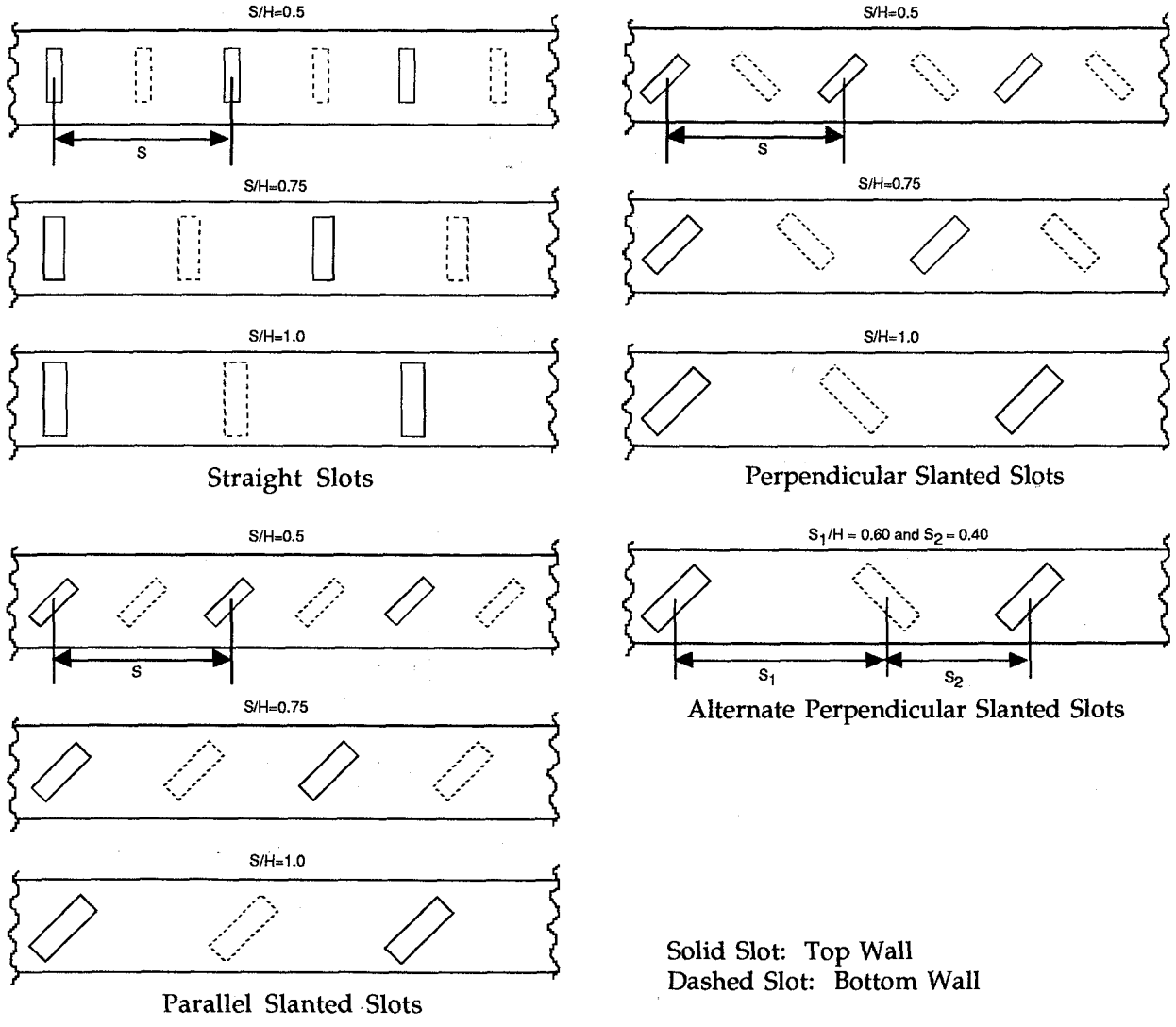

Figure 6. Slot Configurations Analyzed

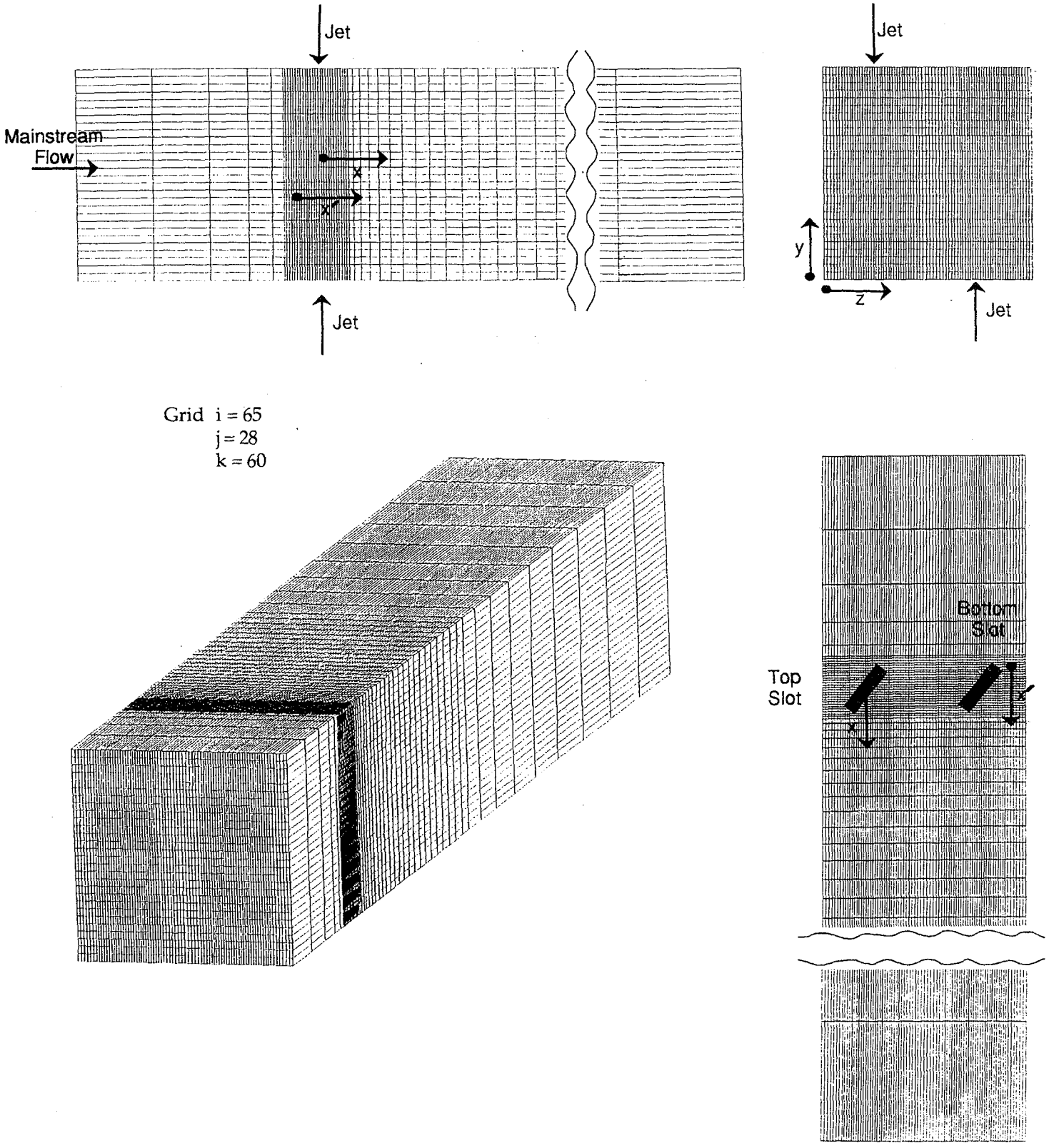

Figure 7. Grid Employed in Parametric Studies

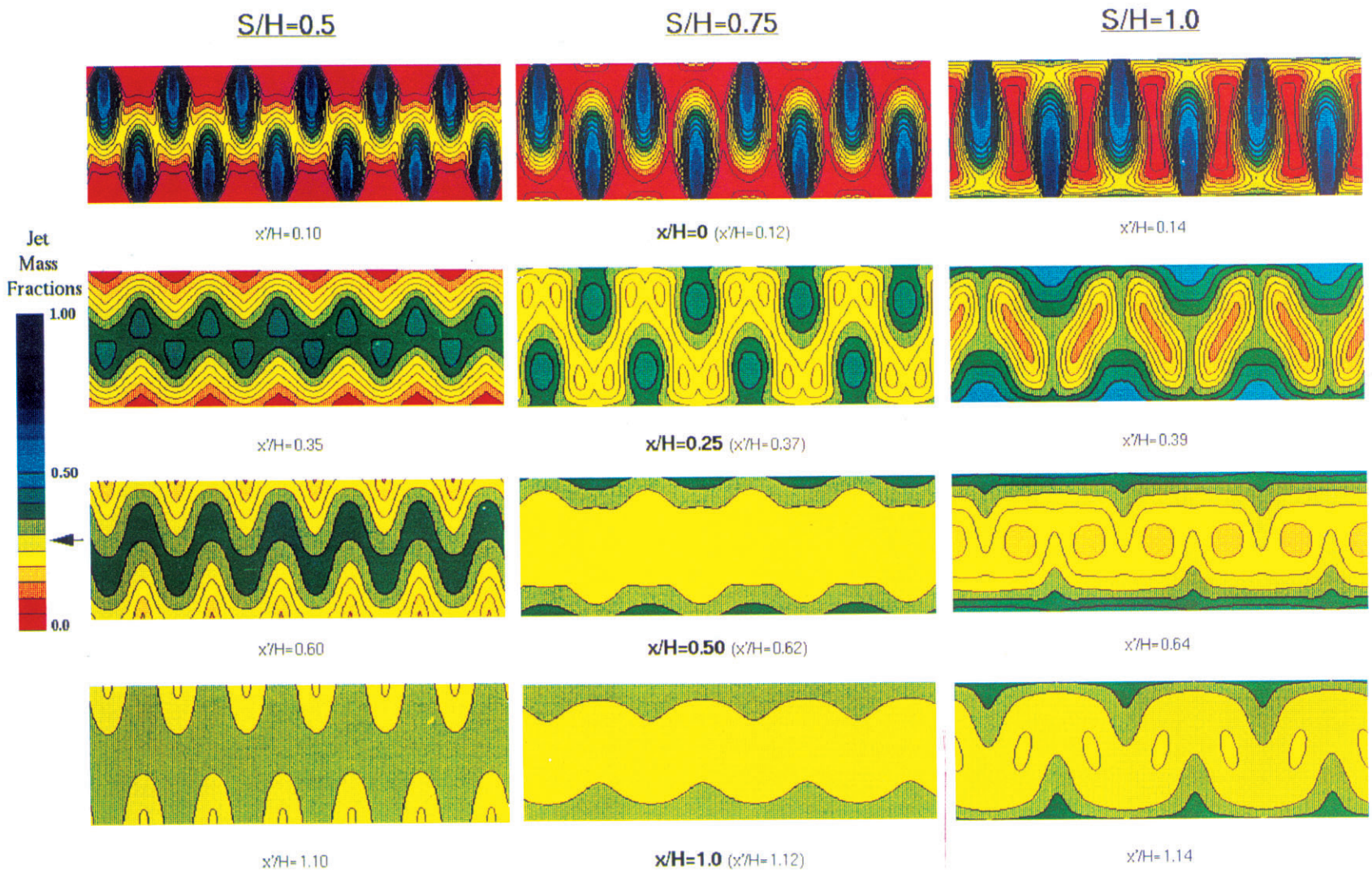

Figure 8. Jet Mass Fraction Color Maps for Straight Slots: Momentum Flux Ratio of 100, Mass Flow Ratio of 0.383 (Symmetric Boundaries)

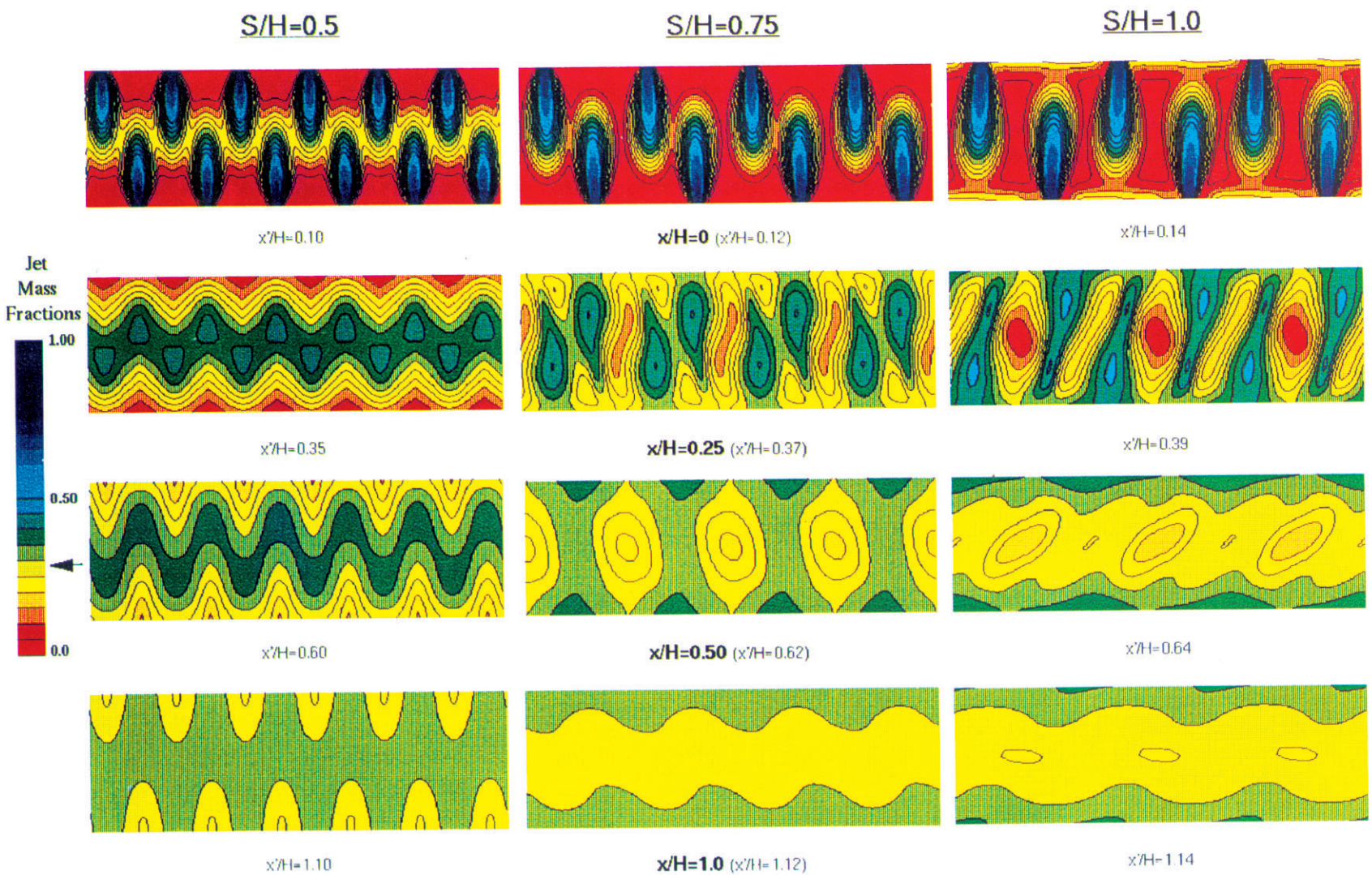

Figure 9. Jet Mass Fraction Color Maps for Straight Slots: Momentum Flux Ratio of 100, Mass Flow Ratio of 0.383 (Cyclic Boundaries)

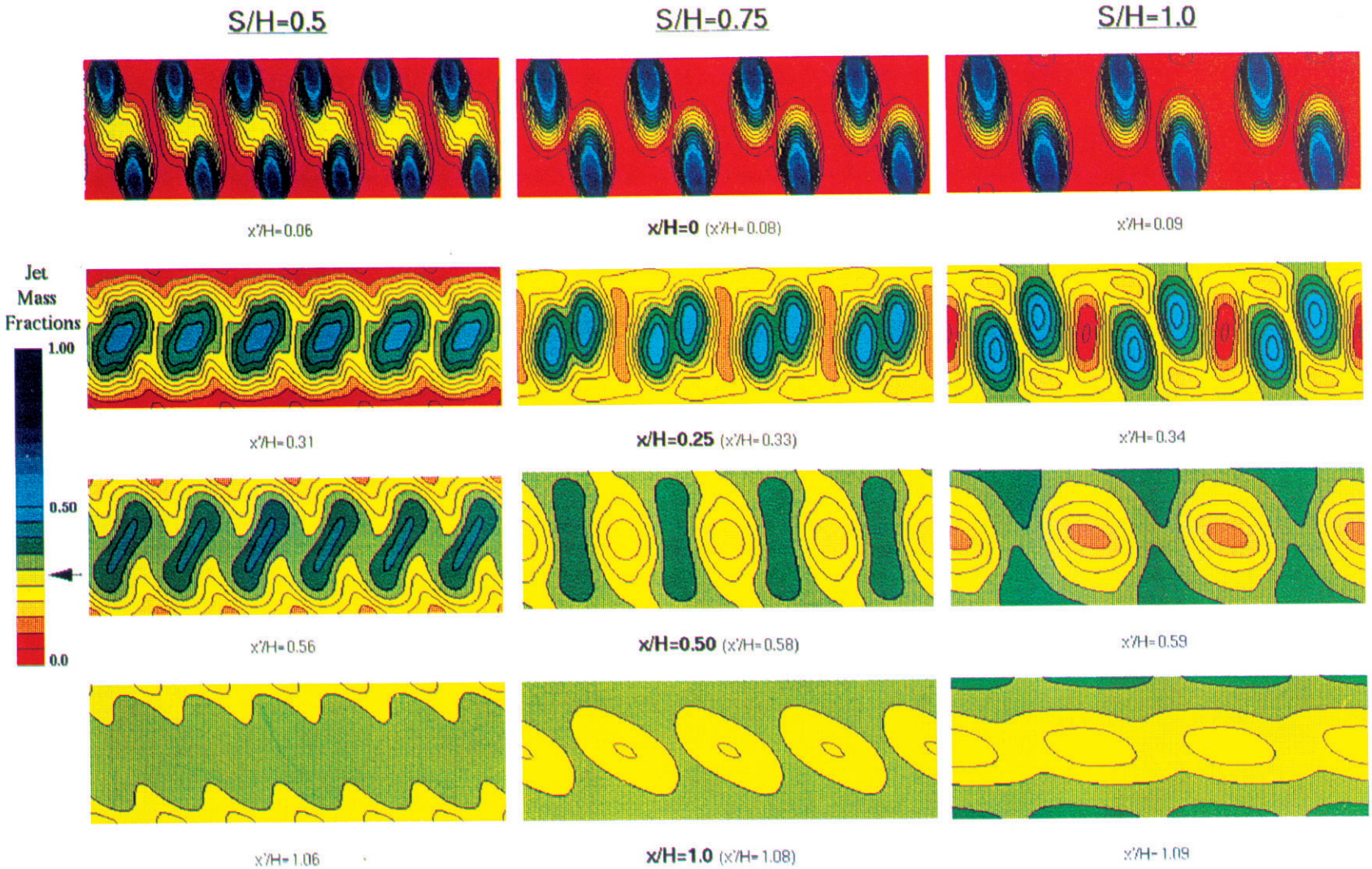

Figure 10. Jet Mass Fraction Color Maps for Perpendicular Slanted Slots: Momentum Flux Ratio of 100, Mass Flow Ratio of 0.383 (Cyclic Boundaries)

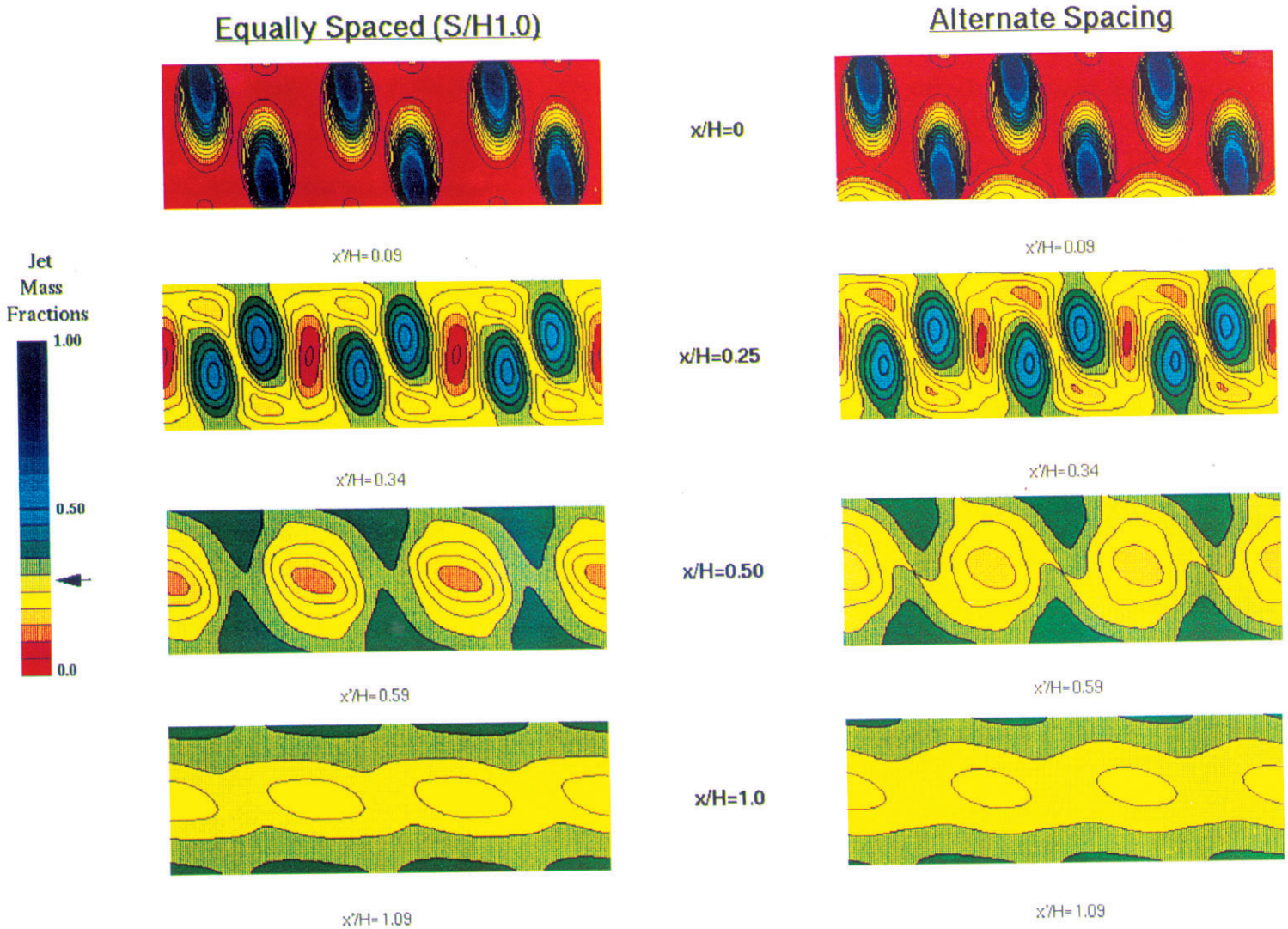

Figure 11. Jet Mass Fraction Color Maps for Modified Perpendicular Slanted Slots: Momentum Flux Ratio of 100, Mass Flow Ratio of 0.383 (Cyclic Boundaries)

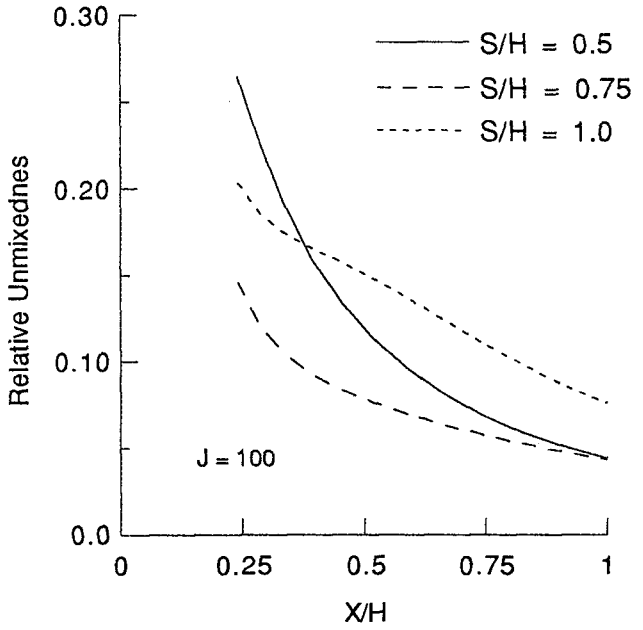

Figure 12. Unmixedness Comparison for Straight Slots (Symmetric Boundaries)

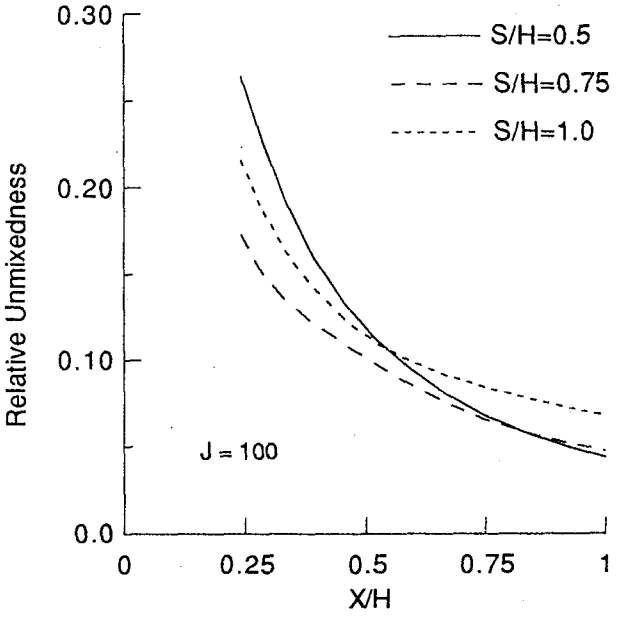

Figure 13. Unmixedness Comparison for Straight Slots (Cyclic Boundaries)

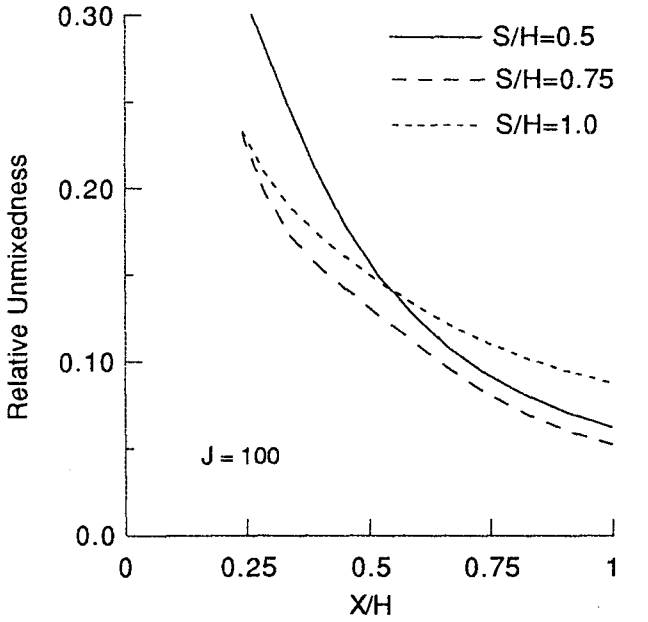

Figure 14. Unmixedness Comparison for Perpendicular Slanted Slots

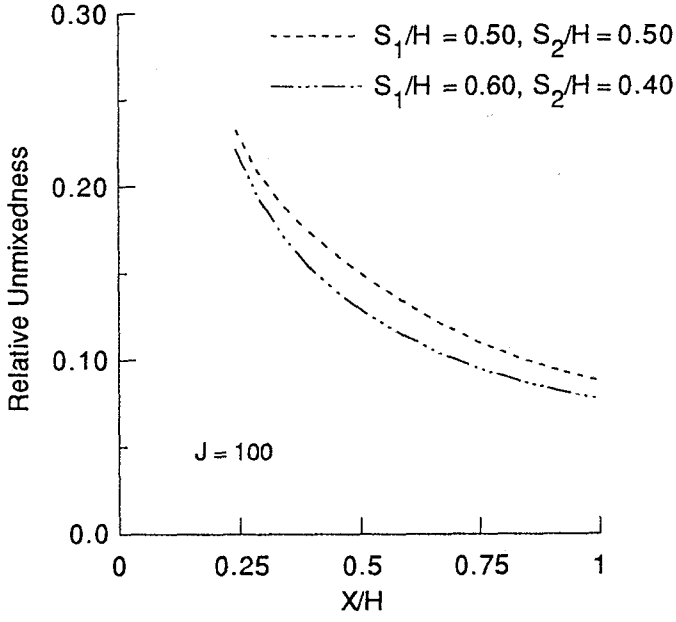

Figure 15. Unmixedness Comparison for Perpendicular Slanted Slots with Different Slot Spacings (S/H = 1)

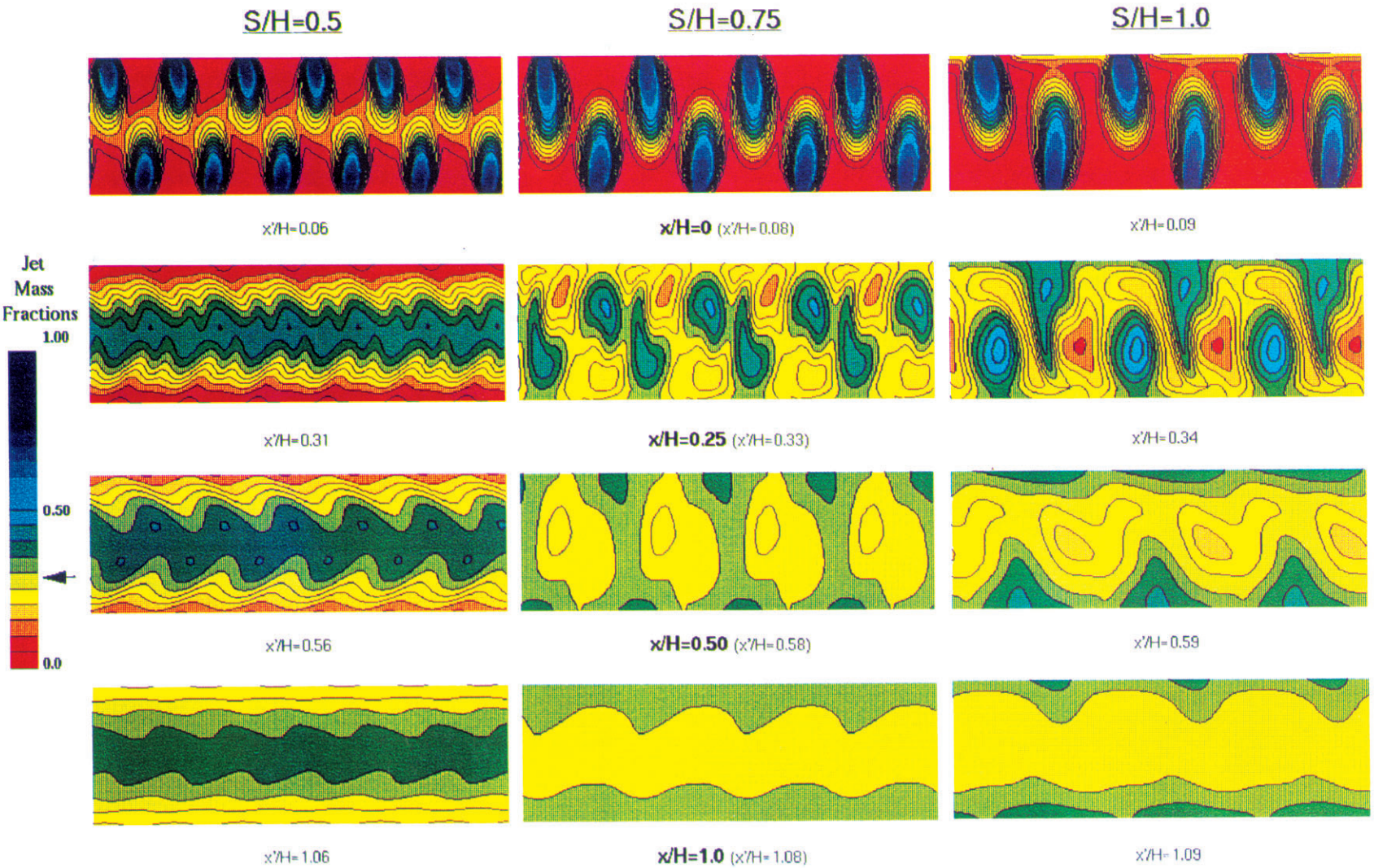

Figure 16. Jet Mass Fraction Color Maps for Parallel Slanted Slots: Momentum Flux Ratio of 100, Mass Flow Ratio of 0.383 (Cyclic Boundaries)

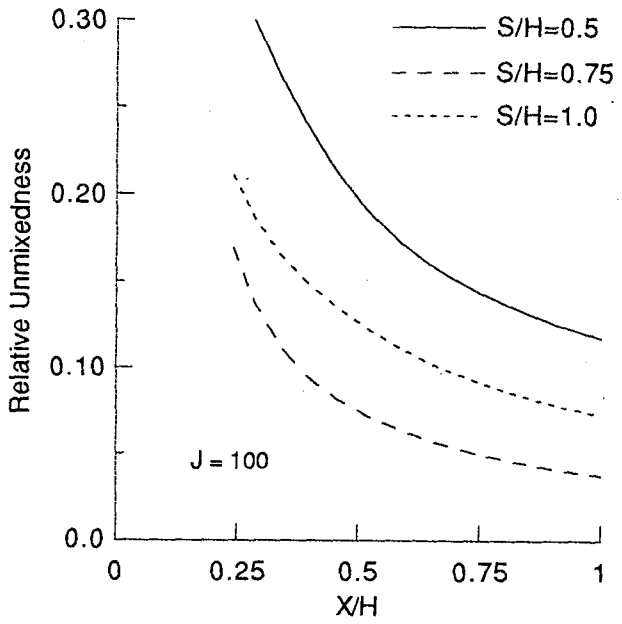

Figure 17. Unmixedness Comparison for Parallel Slanted Slots

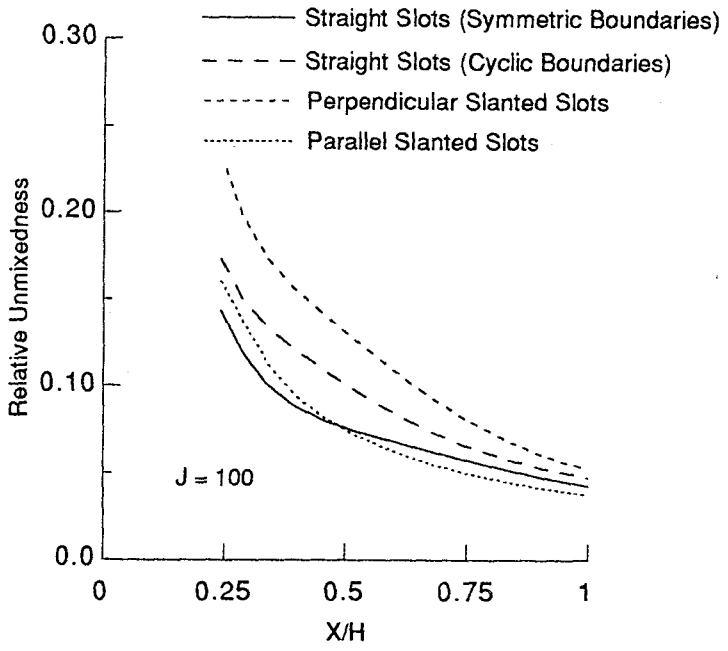

Figure 18. Unmixedness Comparison for the Different Slot Configurations (S/H of 0.75)

REPORT DOCUMENTATION PAGE

Form Approved
OMB No. 0704-0188

1. AGENCY USE ONLY (*Leave blank*)	2. REPORT DATE	3. REPORT TYPE AND DATES COVERED
	July 1992	Technical Memorandum

4. TITLE AND SUBTITLE

CFD Mixing Analysis of Jets Injected From Straight and Slanted Slots Into Confined Crossflow in Rectangular Ducts

5. FUNDING NUMBERS

WU–537–02–20–00

6. AUTHOR(S)

D.B. Bain, C.E. Smith, and J.D. Holdeman

7. PERFORMING ORGANIZATION NAME(S) AND ADDRESS(ES)

National Aeronautics and Space Administration
Lewis Research Center
Cleveland, Ohio 44135–3191

8. PERFORMING ORGANIZATION REPORT NUMBER

E–7087

9. SPONSORING/MONITORING AGENCY NAME(S) AND ADDRESS(ES)

National Aeronautics and Space Administration
Washington, DC 20546–0001

10. SPONSORING/MONITORING AGENCY REPORT NUMBER

NASA TM–105699
AIAA–92–3087

11. SUPPLEMENTARY NOTES

Prepared for the 28th Joint Propulsion Conference and Exhibit cosponsored by the AIAA, SAE, ASME, and ASEE, Nashville, Tennessee, July 6–8, 1992. D.B. Bain and C.E. Smith, CFD Research Corporation, 3325–D Triana Blvd., Huntsville, Alabama, 35805, and J.D. Holdeman, NASA Lewis Research Center, Cleveland, Ohio 44135. Responsible person, J.D. Holdeman, (216) 433–5846.

12a. DISTRIBUTION/AVAILABILITY STATEMENT

Unclassified - Unlimited
Subject Category: 07

Available electronically at http://gltrs.grc.nasa.gov/GLTRS
This publication is available from the NASA Center for AeroSpace Information, (301) 621–0390.

12b. DISTRIBUTION CODE

13. ABSTRACT ***(Maximum 200 words)***

A CFD study was performed to analyze the mixing potential of opposed rows of staggered jets injected into confined crossflow in a rectangular duct. Three jet configurations were numerically tested: (1) straight (0°) slots, (2) perpendicular slanted (45°) slots angled in opposite directions on top and bottom walls, and 3) parallel slanted (45°) slots angled in the same direction on top and bottom walls. All three configurations were tested at slot spacing-to-duct height ratios (S/H) of 0.5, 0.75, and 1.0; a jet-to-mainstream momentum flux ratio (J) of 100; and a jet-to-mainstream mass flow ratio of 0.383. Each configuration had its best mixing performance at S/H of 0.75. Asymmetric flow patterns were expected and predicted for all slanted slot configurations. The parallel slanted slot configuration was the best overall configuration at x/H of 1.0 for S/H of 0.75.

14. SUBJECT TERMS

Dilution; Jet mixing flow; Gas turbine; Combustion chamber; Emissions

15. NUMBER OF PAGES

30

16. PRICE CODE

A03

17. SECURITY CLASSIFICATION OF REPORT	18. SECURITY CLASSIFICATION OF THIS PAGE	19. SECURITY CLASSIFICATION OF ABSTRACT	20. LIMITATION OF ABSTRACT
Unclassified	Unclassified	Unclassified	

Appendix B

NASA Technical Memorandum 106179

NASA Technical Memorandum 106179
AIAA–93–2044

CFD Mixing Analysis of Axially Opposed Rows of Jets Injected Into Confined Crossflow

D.B. Bain and C.E. Smith
CFD Research Corporation
Huntsville, Alabama

and

J.D. Holdeman
Lewis Research Center
Cleveland, Ohio

Prepared for the
29th Joint Propulsion Conference and Exhibit
cosponsored by the AIAA, SAE, ASME, and ASEE
Monterey, California, June 28–30, 1993

NASA

CFD MIXING ANALYSIS OF AXIALLY OPPOSED ROWS OF JETS INJECTED INTO CONFINED CROSSFLOW

D. B. Bain* and C. E. Smith**
CFD Research Corporation
Huntsville, Alabama

J. D. Holdeman***
NASA Lewis Research Corporation
Cleveland, Ohio

Abstract

A CFD parametric study was performed to analyze axially opposed rows of jets mixing with crossflow in a rectangular duct. Isothermal analysis was conducted to determine the influence of lateral geometric arrangement on mixing. Two lateral arrangements were analyzed: 1) inline (jets' centerlines aligned with each other on top and bottom walls), and 2) staggered (jets' centerlines offset with each other on top and bottom walls). For a jet-to-mainstream mass flow ratio (MR) of 2.0, design parameters were systematically varied for jet-to-mainstream momentum-flux ratios (J) between 16 and 64 and orifice spacing-to-duct height ratios (S/H) between 0.125 and 1.5.

Comparisons were made between geometries optimized for S/H at a specified J. Inline configurations had a unique spacing for best mixing at a specified J. In contrast, staggered configurations had two "good mixing" spacings for each J, one corresponding to optimum inline spacing and the other corresponding to optimum non-impinging jet spacing. The inline configurations, due to their smaller orifice size at optimum S/H, produced better initial mixing characteristics. At downstream locations (*e.g.* x/H of 1.5), the optimum non-impinging staggered configuration produced better mixing than the optimum inline configuration for J of 64; the opposite results were observed for J of 16. Increasing J resulted in better mixing characteristics if each configuration was optimized with respect to orifice spacing. Mixing performance was shown to be similar to results from previous dilution jet mixing investigations (MR < 0.5).

Nomenclature

C	$(S/H)\sqrt{J}$ (see Eq. 1)
C_{avg}	$m_j/(m_j+m_\infty) = \theta_{EB}$
H	Duct Height
J	Momentum-Flux Ratio $(\rho_j V_j^2)/(\rho_\infty U_\infty^2)$
L	Orifice Length (long dimension)
L/W	Orifice Aspect Ratio (SAR in previous reports)
m_j	Mass Flow of Jets
m_∞	Mass Flow of Mainstream Flow
MR	Mass Flow Ratio m_j/m_∞
P	Pressure (N/m^2)
S	Orifice Spacing

* Project Engineer, Member AIAA
** Vice President/Engineering, Member AIAA
*** Senior Research Engineer, Associate Fellow AIAA

S/H	Orifice Spacing-to-Duct Height Ratio
T	Temperature (K)
U_∞	Mainstream Flow Velocity (m/s)
U	Unmixedness (see Eq. 2)
u	rms of Axial Velocity Fluctuation
v	rms of Vertical Velocity Fluctuation
W	Orifice Width (short dimension)
x	Axial Coordinate, x=0 at leading edge of the orifice
x/H	Axial Distance-to-Duct Height Ratio
V_j	Jet Velocity (m/s)
y	Vertical Coordinate
z	Lateral Coordinate
μ_T	Turbulent Viscosity (kg/m·sec)
ρ_j	Density of Jet
ρ_∞	Density of Mainstream

1. Introduction

The technology demonstration of low NO_x combustors applicable to commercial aircraft is a subject of ongoing research.[1] One combustor concept currently being evaluated both numerically and experimentally is the Rich-burn/Quick-mix/Lean-burn (RQL) combustor. The RQL combustor utilizes staged burning.[2] In this concept, the rich-burn zone is designed to operate at equivalence ratios greater than 1. The combustion products from the rich-burn section enter the quick mix section where mixing takes place with bypass air. The combustion process is then completed in the lean-burn region.

A key design technology required for successful demonstration of the RQL concept is a method of rapidly mixing bypass air with rich-burn gases to suppress the formation of harmful emissions. Recent studies have been performed that focus on identifying improved mixing concepts.[3-13] The current investigation focuses on jet mixing in rectangular cross-sectional ducts.

2. Background

The mixing of jets in a confined crossflow has been important in gas turbine combustion applications for many years. Perhaps foremost in importance is the jet mixing that occurs in the combustor dilution zone. In conventional annular gas turbine combustors, the dilution zone is the aft zone in which air dilutes combustion products before entering the turbine. The dilution jets should effectively penetrate and mix with combustion gases, thereby establishing a temperature profile acceptable to the turbine. The typical range of jet-to-mainstream mass flow ratio (MR) is 0.25 to 0.50.

RQL jet mixing applications offer some sharp contrasts to conventional dilution zone mixing. First, the mass flow ratio is approximately 2.0. Such a large MR results in larger orifices, potentially creating jet blockage effects that can substantially affect mixing. Because round orifices may not be practical due to blockage and structural concerns, slots may be needed. Second, low pollutant levels are the drivers for "good" mixing in RQL applications, in contrast to temperature profile and "hot spots" for dilution zone applications.

Significant research has been performed for dilution zone mixing.[14] This research has identified two design variables that control jet penetration and mixing characteristics: 1) jet-to-mainstream momentum-flux ratio (J) and 2) orifice spacing-to-duct height ratio (S/H). Single-sided (from one wall only) injection was extensively studied while two-sided (from top and bottom walls) injection was studied to a lesser extent. Optimum mixing relationships were determined to be a function of $(S/H)\sqrt{J}$ for the range of conditions tested and analyzed.

$$C = (S/H)\sqrt{J} \qquad (1)$$

For one-sided injection, optimum mixing was obtained when C was about 2.5.

Two-sided injection with an inline lateral arrangement was shown to be similar to one-sided injection if the duct was considered sliced in half, yielding a constant of proportionality that is one-half of the corresponding value for one-sided injection. Thus a C of 1.25 would be expected for optimum mixing of opposed rows of jets with centerlines inline.

For two-sided injection with a staggered lateral arrangement, very little data, either experimentally or numerically, have been generated. Holdeman[14] has suggested staggered holes produce optimum mixing if the jets penetrate past each other. He determined (from the few tests conducted) that best mixing was obtained when alternate jets for optimum one-sided injection were moved to the opposite wall. Thus the correlation constant would be expected to be 5.0 for opposed rows of jets with centerlines staggered.

A basic question often arises concerning which lateral arrangement produces superior mixing: inline or staggered. This fundamental question has never truly been answered. Indeed, even combustor designers differ in their opinion, as evidenced by conventional dilution zones with both types of lateral alignments. As an added complication in this RQL application, past results may not be directly applicable due to the mass flow ratio (0.50 for conventional dilution zone vs 2.0 for RQL). This study sought to address the lateral arrangement issue by a systematic computational investigation. A complete description of the cases studied and their results are discussed below.

3. CFD Code

The approach in this study was to perform 3-D numerical calculations on a generic geometry section. The CFD code named REFLEQS[15] was used to perform the computations. The basic capabilities/methodologies in REFLEQS include:

1. Solution of two- and three-dimensional, time-accurate or steady-state Navier-Stokes equations for incompressible and compressible flows;
2. Cartesian, polar, and non-orthogonal body-fitted coordinates;
3. Porosity-resistivity techniques for flows with internal blockages;
4. Fully implicit and strongly conservative formulation;
5. Three differencing schemes: upwind, hybrid, and central differencing with damping terms;
6. Standard, extended, and low Reynolds number k-ε turbulence models, and the multiple-scale turbulence model of Chen;
7. Instantaneous, one-step and two-step combustion models;
8. Modified form of Stone's strongly implicit solver; and
9. Pressure-based solution algorithms including SIMPLE and a variant of SIMPLEC.

4. Details of Numerical Calculations

A schematic of the numerical model is shown in Figure 1. The height of the mixing section was 4 inches (0.1016 m.). The mainstream flow entered the calculation domain one duct height upstream (x/H of -1.0) of the leading edge of the orifices, and continued downstream to x/H of 7.0. The model consisted of jet injection from top and bottom walls into mainstream flow. All of the orifices were straight slots with an aspect ratio of 4:1, with the long dimension of the slot in the direction of the mainstream flow.

Two orifice arrangements were modeled: staggered and inline. For the staggered cases, the lateral calculation domain extended from midplane to midplane between top and bottom jet centerlines, and modeled one jet on the top wall and one jet on the bottom wall. Periodic boundary conditions were imposed along the lateral boundaries. For the inline cases, the lateral domain extended from midplane to midplane between the jets' centerlines. Again periodic lateral boundary conditions

were imposed. It should be noted that the staggered configurations consisted of twice the lateral domain of the inline configurations.

Six parametrics consisting of 44 cases were analyzed as shown in Table 1. The case sequence for each parametric consisted of fixing J (at 16, 36, or 64) and lateral arrangement (inline or staggered), and then parametrically changing S/H to optimize mixing. For each parametric, the slot geometry producing optimum mixedness is shown in Figure 2.

The flow conditions of the mainstream and jets were

Mainstream		Jets	
U_∞	= 10 m/s	V_j	= 40 m/s*
			60 m/s*
			80 m/s*
T_∞	= 300 K	T_j	= 300 K
u/U_∞	= 0.20	v/V_j	= 0.20
μ_T	= 1×10^{-2} kg/m•sec	μ_T	= 1×10^{-2} kg/m•sec

$P = 1 \times 10^5$ N/m^2

J = 16, 36, 64

$m_j/m_\infty = 2.0$

* V_j varies according to specified J.

The turbulent length scales of the jets were varied to maintain a constant inlet turbulent viscosity.

Grids

A typical staggered case consisted of 80,000 cells, 64 cells in the axial (x) direction, 28 cells in the vertical (y) direction, and 44 cells in the lateral (z) direction. The slots were composed of 144 (24 x 6) evenly distributed cells. The grid upstream and downstream of the slot region was expanded/contracted so that each cell adjacent to the slot region matched the cell size in the slot region. The cells in the vertical direction were all of uniform size. Note that the grid size for the inline cases were typically half the size for the staggered cases.

In earlier works[8], a much finer grid (≈145,000 cells) was used in the numerical calculations. Since that paper, a grid density study has been performed and it was determined that such fine grids are not needed for engineering calculations. Thus, the number of cells was reduced for computational efficiency in this study.

Numerics

The following conservation equations were solved: u momentum, v momentum, w momentum, mass (pressure correction), turbulent kinetic energy (k), and turbulent energy dissipation (ε). The convective fluxes were calculated using upwind differencing, and the diffusive fluxes were calculated using central differencing. The standard k-ε turbulence model was employed and conventional wall functions were used.

Convergence

All error residuals were reduced at least 6 orders of magnitude, and continuity was conserved in each axial plane to the fifth decimal. Convergence was relatively smooth requiring about 600 iterations. A converged solution required approximately 4.0 CPU hours on a CRAY-YMP computer.

5. Data Postprocessing

In order to quantify the mixing effectiveness, the area-averaged spatial concentration variance of jet flow was calculated in each axial plane. The use of area-averaged quantities, rather than mass-averaged quantities, was chosen to be consistent with concurrent experimental measurements and allow one-to-one comparison. The area-averaged unmixedness (U) is defined[16] as

$$U = C_{var} / [C_{avg}(1-C_{avg})] \qquad (2)$$

where

$C_{var} = (1/A_{TOT}) \sum_i A_i (C_i - C_{avg})^2$

A_{TOT} = total flow area in each axial plane

A_i = flow area of cell *i*

C_i = jet mass fraction in cell *i*

$C_{avg} = m_j / (m_j + m_\infty) = \theta_{EB}$

For this study, C_{avg} is 0.667.

The use of C_{avg} in determining U is only correct downstream of the slots' trailing edge. Upstream of the slots' trailing edge, the injection of jet mass flow makes the use of C_{avg} incorrect. Therefore, the unmixedness values shown plotted in this paper always begin one computational cell aft of the slots' trailing edge.

6. Results and Discussion

Figure 3 displays the results for the inline and staggered configurations for a J of 16, 36, and 64. The optimum S/H ratio for each parametric is identified by the boldest curve. Discussion of these results is presented below.

Effect of S/H on Jet Penetration

A qualitative view of how S/H affects jet penetration and corresponding mixing levels is shown in Figures 4, 5, and 6. These figures show the jet mass fraction concentrations for inline slots at J of 16, 36, and 64. The views presented are lateral slices taken through the slot centerline. S/H variations are presented to illustrate the effect of S/H on jet penetration. For discussion, the cases for J of 36 (*i.e.* Figure 5) present the essential features of jet penetration into crossflow. At the smaller S/H, the jets are underpenetrated, allowing the approach flow to pass through the center of the duct. As S/H increases, the jets penetrate farther into the duct, beginning to pinch off the approach flow along the duct centerline. At the largest S/H, the jets have clearly over-penetrated, blocking off most of the approach flow in the center of the duct and forcing more of the approach flow to go between the jets. S/H of 0.375 gives the optimum penetration which agrees well with the optimum S/H in terms of unmixedness (as shown in Figure 3). In general terms, inline jets that penetrate to about 1/4 duct height produce optimum mixing.

Similar lateral slices showing jet penetration for staggered slots at J of 16, 36, and 64 are shown in Figures 7, 8, and 9. The lateral planes in these figures are through the centerline of the top jets, and the corresponding plane through the bottom jet would be the mirror image of that shown. In contrast to optimum inline configurations, optimum staggered jets penetrate completely across the duct and do not collide with each other. As will be discussed later, another "good mixing" orifice spacing is obtained for staggered configurations if staggered jets are configured at optimum inline spacing. In this case, the staggered jets penetrate to 1/4 duct height, just like the optimum inline jets. To differenciate between these two "good mixing" modes for staggered jets, the term "non-impinging staggered configuration" will refer to jets that penetrate across the duct.

Effect of J

The effect of J on unmixedness is shown in Figure 10 for inline slots, and in Figure 11 for non-impinging staggered slots. Each curve represents the optimum S/H for a specified J. Both lateral arrangements, staggered and inline, exhibited an initial mixing advantage gained by increasing J from 16 to 64. The improved initial mixing is caused by the slots being geometrically smaller as J increases from 16 to 64. Downstream mixing (*i.e.* x/H of 1.5) is seen to be similar for inline geometry as J varies, but substantial improvement is seen when J is increased for non-impinging staggered configurations.

The jet mass fraction concentrations for inline and staggered slots are shown in Figure 12. The location of the axial section is x/H of 0.75. Using the criteria of

better mixing being indicated by fewer concentration levels, the cases for J of 64 are more thoroughly mixed than the J cases of 16 or 36. The enhancement in mixing by an increase in J is not unexpected due to a higher pressure drop experienced as J is increased.

Effect of Lateral Arrangement on Mixing

The effect of lateral arrangement on unmixedness is shown in Figures 13, 14, and 15 for J of 16, 36, and 64, respectively. Only the curves corresponding to optimum S/H are presented. In each figure, it can be seen that the inline slots have better initial mixing. This is due to the inline orifices being substantially smaller than staggered orifices. At locations farther downstream (*i.e.* x/H of 1.5), inline is better than staggered at J of 16, but inline is worse than staggered at J of 64. Indeed, the best mixing case of all cases studied is the staggered case shown in Figure 15 for J of 64. The unmixedness values for the best mixing case was 0.02 at x/H of 1.5.

A more qualitative comparison of mixing illustrating the effect of lateral arrangement is presented in Figures 16, 17, and 18. These figures present jet mass color concentration maps for the optimum inline and non-impinging staggered configurations at three momentum-flux ratios (J of 16, 36, and 64, respectively). The multiple cycles shown in these figures were generated graphically to maintain the same cross-sectional area for each case. It can be seen that the inline slots produce better initial mixing than the staggered slots at x/H of 0.75.

For completeness, a single-sided injection case was examined to determine the impact of two-sided vs one-sided injection. Figure 19 shows the jet mass fraction concentrations for the two-sided and single-sided injection cases at their optimum S/H. It would be expected (based on previous dilution jet studies[14]) that optimum staggered two-sided injection would have:

1) an S/H that is four times the S/H of inline two-sided injection; and
2) two times the S/H of single-sided injection.

Numerically, the ratios were found to be 2.3 and 1.4, respectively. Based on previous research, optimum mixing was reached if the jets penetrated one-quarter of the way into the duct for inline slots, penetrated past each other for staggered slots, and penetrated to the duct centerline for single-sided injection. Figure 19 illustrates that the numerical results in this study coincide well with the previous research. In terms of unmixedness, the two-sided injection cases show a significant advantage over the single-sided cases, as seen in Figure 20.

When experimental mixing tests are performed, only a limited number of orifice configurations can be tested. Typically, inline arrangements are first tested, followed by a lateral movement of one wall to produce staggered arrangements. If an inline arrangement at a given J is optimized (in terms of S/H), the corresponding staggered case obtained by laterally moving one wall will produce nearly identical mixing (see Figure 21). The converse is not true; *i.e.*, if a non-impinging staggered arrangement at a given J is optimized, the corresponding inline case will produce inferior mixing (see Figure 21).

Figures 22 and 23 show the unmixedness comparisons of inline and non-impinging staggered configurations at the same S/H. In Figure 22 it is evident that running the inline configuration at optimum non-impinging staggered spacing (S/H of 0.85) produces poorer mixing characteristics than the optimum staggered case. In contrast, there is no difference seen (see Figure 23) between inline and staggered results at the optimum inline spacing (S/H of 0.375). Staggered configurations thus have two minimum values of unmixedness, as shown in Figure 24 for J of 36. One minimum value corresponds to the optimum S/H arrangement for non-impinging jets (S/H of 0.85), and the other minimum value

corresponds to jets not being able to penetrate by each other (S/H of 0.375). Inline configurations have only a unique minimum unmixedness value (at S/H of 0.375) as shown in Figure 25.

Comparison to Empirical Calculations for Optimum Mixing

Shown in Table 2 are the empirically and numerically determined constants for optimum mixing for the cases studied. For the inline cases, the numerical constant is about 75% higher than the empirical constant. Most of this difference may be attributed to the effect of mass flow ratio, since the empirical constants were based on experiments with mass flow ratios less than 0.50, while the numerical constants were determined with a mass flow ratio of 2.0. (In other CFD studies not reported here, the numerical constant was only 30% higher than the empirical constant for a mass flow ratio of 0.5). Note that the jet blockage (at the wall) was about 33% for all J values. The constant blockage for all J values is expected due to geometry considerations if blockage is not important in the mixing process.

For the staggered cases, the numerical constants vary from 25% low for J of 16 to 36% high for J of 64. This agreement is considered adequate from an engineering design viewpoint, but there is probably a secondary effect (*e.g.* grid density, inlet turbulence boundary conditions, *etc.*) that is causing the disagreement.

7. Conclusions

A CFD parametric mixing study was performed on axially opposed rows of staggered and inline jets injected into confined rectangular crossflow. The analysis was performed at jet-to-mainstream momentum-flux ratios (J) of 16, 36, and 64, orifice spacing-to-duct height ratios (S/H) of 0.125 to 1.5, and a jet-to-mainstream mass flow ratio (MR) of 2.0. Based on the numerical results, the following conclusions can be drawn:

1. Inline configurations have better initial mixing than non-impinging staggered configurations at their respective optimum S/H.
2. In terms of overall downstream mixing, (*i.e.* at x/H of 1.5), the optimum inline configuration is better than the optimum staggered configuration for J of 16, but the opposite is true for J of 64.
3. Increasing J improves initial mixing at optimum S/H. Increasing J improves downstream mixing (*i.e.* x/H of 1.5) for staggered configurations, but has neglible effect for inline configurations.
4. Mixing performance is similar to results from previous dilution jet mixing investigations with jet-to-mainstream mass flow ratios less than 0.50.

8. Acknowledgement

This work was supported by NASA Contract NAS3-25967, and NAS computer time was provided by NASA Lewis Research Center. Valuable discussions and assistance were provided by Mr. Milind Talpallikar. Our thanks are also extended to Ms. Kathy W. Rhoades for preparing this typescript.

9. References

1. R. J. Shaw, "Engine Technology Challenges for a 21st Century High Speed Civil Transport," AIAA Tenth International Symposium on Air Breathing Engines, September 1-6, 1991 (Also NASA TM 104363).
2. S. A. Mosier and R. M. Pierce, "Advanced Combustion Systems for Stationary Gas Turbine Engines," Vol. I, EPA Contract 68-02-2136, 1980.
3. C. E. Smith, "Mixing Characteristics of Dilution Jets in Small Gas Turbine Combustors," AIAA 90-2728, 1990.
4. C. E. Smith, M. V. Talpallikar, and J. D. Holdeman, "A CFD Study of Jet Mixing in

Reduced Flow Areas for Lower Combustor Emissions," AIAA 91-2460, June, 1991 (Also NASA TM 104411).

5. A. Vranos, D. S. Liscinsky, B. True, and J. D. Holdeman, "Experimental Study of Cross-Stream Mixing in a Cylindrical Duct," AIAA 91-2459, June, 1991 (Also NASA TM 105180).
6. M. V. Talpallikar, C. E. Smith, M. C. Lai, and J. D. Holdeman, "CFD Analysis of Jet Mixing in Low NO_x Flametube Combustors," ASME Paper 91-GT-217, Vol. 114, pp. 416-424, ASME Transactions, Journal of Engineering for Gas Turbines and Power, 1992 (Also NASA TM 104466).
7. M. S. Hatch, W. A. Sowa, G. S. Samuelsen, and J.D. Holdeman, "Jet Mixing Into a Heated Cross Flow in a Cylindrical Duct: Influence of Geometry and Flow Variations," AIAA 92-0773, January 1992 (Also NASA TM 105390).
8. D. B. Bain, C. E. Smith, and J. D. Holdeman, "CFD Mixing Analysis of Jets Injected from Straight and Slanted Slots into Confined Crossflow in Rectangular Ducts," AIAA 92-3087, Nashville, TN, July 6-8, 1992 (Also NASA TM 105699)
9. D. S. Liscinsky, B. True, A. Vranos, and J. D. Holdeman, "Experimental Study of Cross-Stream Mixing in a Rectangular Duct," AIAA 92-3090, Nashville, TN, July 6-8, 1992 (Also NASA TM 106194).
10. V. L. Oechsle, H. C. Mongia, and J. D. Holdeman, "A Parametric Numerical Study of Mixing in a Cylindrical Duct," AIAA 92-3088, Nashville, TN, July 6-8, 1992 (Also NASA TM 105695).
11. G. Zhu and M.-C. Lai, "A Parametric Study of Penetration and Mixing of Radial Jets in Necked-Down Cylindrical Crossflow," AIAA 92-3091, Nashville, TN, July 6-8, 1992.
12. J. T. Kroll, W. A. Sowa, G. S. Samuelsen, and J. D. Holdeman, "Optimization of Circular Orifice Jets Mixing into a Heated Crossflow in a Cylindricxal Duct," AIAA 93-0249, Reno, Nevada, January 11-14, 1993.
13. D. S. Liscinsky, A. Vranos, and R. P. Lohman, "Experimental Study of Crossflow Mixing in Cylindrical and Rectangular Ducts," NASA CR 187141, March 1993.
14. J. D. Holdeman, "Mixing of Multiple Jets with a Confined Subsonic Crossflow," AIAA 91-2458, 1991 (Also NASA TM 104412).
15. A. J. Przekwas, S. D. Habchi, H. Q. Yang, R. K. Avva, M. V. Talpallikar, and A. Krishnan, "REFLEQS-3D: A Computer Program for Turbulent Flows With and Without Chemical Reaction, Volume 1: User's Manual," CFDRC Report GR-89-4, January 1990.
16. P. V. Danckwertz, "The Definition and Measurement of Some Characteristics of Mixtures," *Appl. Sci. Res.*, Sec. A, Vol. 3, pp. 279-296, 1952.

TABLE 1. NUMERICAL CASES ANALYZED

Parametric	Case	Configuration	Slot Aspect Ratio	Momentum Flux Ratio (J)	Mass Flow Ratio (MR)	S/H	Trailing Edge x/H	Jet Blockage at Wall
Parametric 1	Case 1	Inline	4:1	36	2.0	0.125	0.29	57.7%
	Case 2					0.20	0.36	45.6
	Case 3					0.228	0.39	42.8
	Case 4					0.25	0.41	40.8
	Case 5					0.275	0.43	38.9
	Case 6					0.325	0.47	35.8
	Case 7					**0.375**	**0.50**	**33.3**
	Case 8					0.425	0.53	31.3
	Case 9					0.50	0.58	28.9
	Case 10					0.75	0.71	23.6
	Case 11					0.85	0.75	22.1
Parametric 2	Case 12	Staggered	4:1	36	2.0	0.375	0.50	33.3
	Case 13					0.75	0.71	23.6
	Case 14					**0.85**	**0.75**	**22.1**
	Case 15					1.0	0.81	20.4
	Case 16					1.25	0.91	18.3
	Case 17					1.50	1.00	16.7
Parametric 3	Case 18	Inline	4:1	16	2.0	0.325	0.57	43.8
	Case 19					0.375	0.61	40.8
	Case 20					0.425	0.65	38.4
	Case 21					**0.50**	**0.70**	**35.4**
	Case 22					0.55	0.74	33.7
	Case 23					0.60	0.77	32.3
	Case 24					1.00	1.00	25.0
Parametric 4	Case 25	Staggered	4:1	16	2.0	0.50	0.70	35.4
	Case 26					0.85	0.92	27.1
	Case 27					**1.0**	**1.0**	**25.0**
	Case 28					1.25	1.12	22.4
	Case 29					1.30	1.14	21.9
	Case 30					1.50	1.22	20.4
Parametric 5	Case 31	Inline	4:1	64	2.0	0.125	0.25	50.0
	Case 32					0.20	0.32	39.5
	Case 33					0.25	0.35	35.4
	Case 34					0.275	0.37	33.7
	Case 35					**0.285**	**0.38**	**33.1**
	Case 36					0.30	0.39	32.3
	Case 37					0.325	0.40	31.0
	Case 38					0.85	0.65	19.2
arametric 6	Case 39	Staggered	4:1	64	2.0	0.285	0.38	33.1
	Case 40					0.50	0.50	25.0
	Case 41					0.65	0.57	21.9
	Case 42					0.75	0.61	20.4
	Case 43					**0.85**	**0.65**	**19.2**
	Case 44					1.00	0.71	17.7

old font represents optimum mixing configuration.

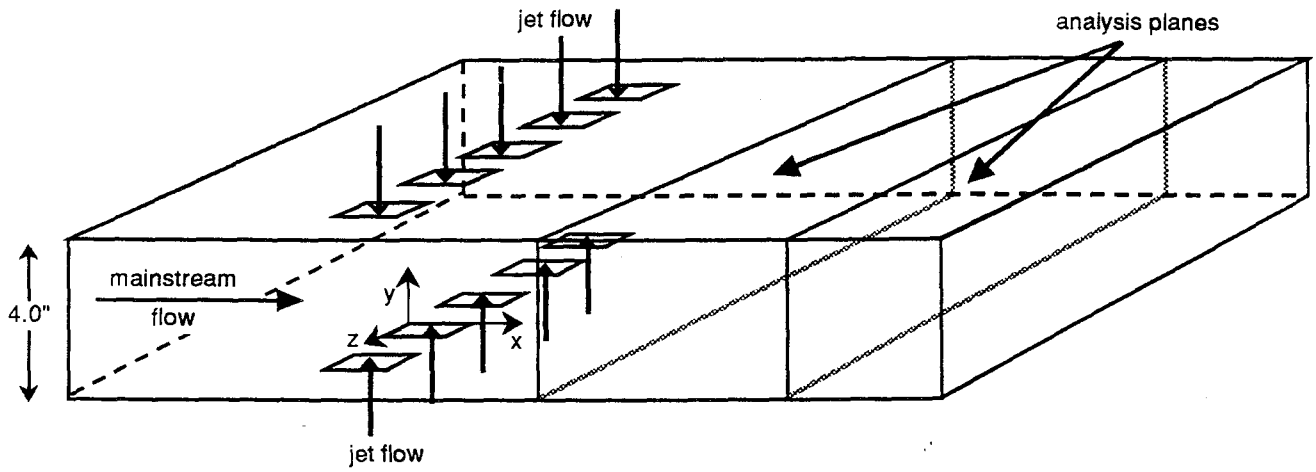

Figure 1. Schematic of Numerical Mixing Model

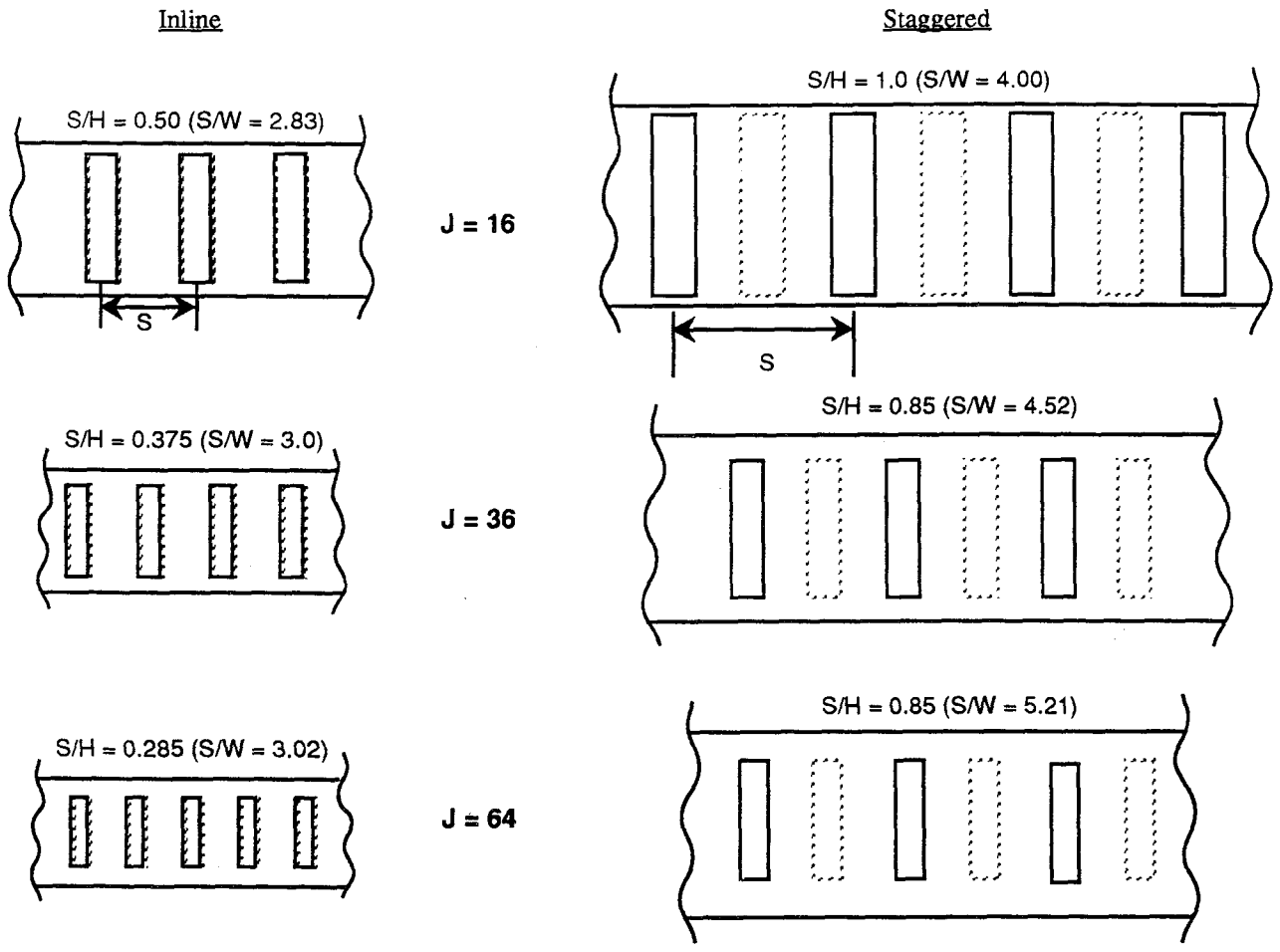

Figure 2. Slot Configurations At Optimum S/H

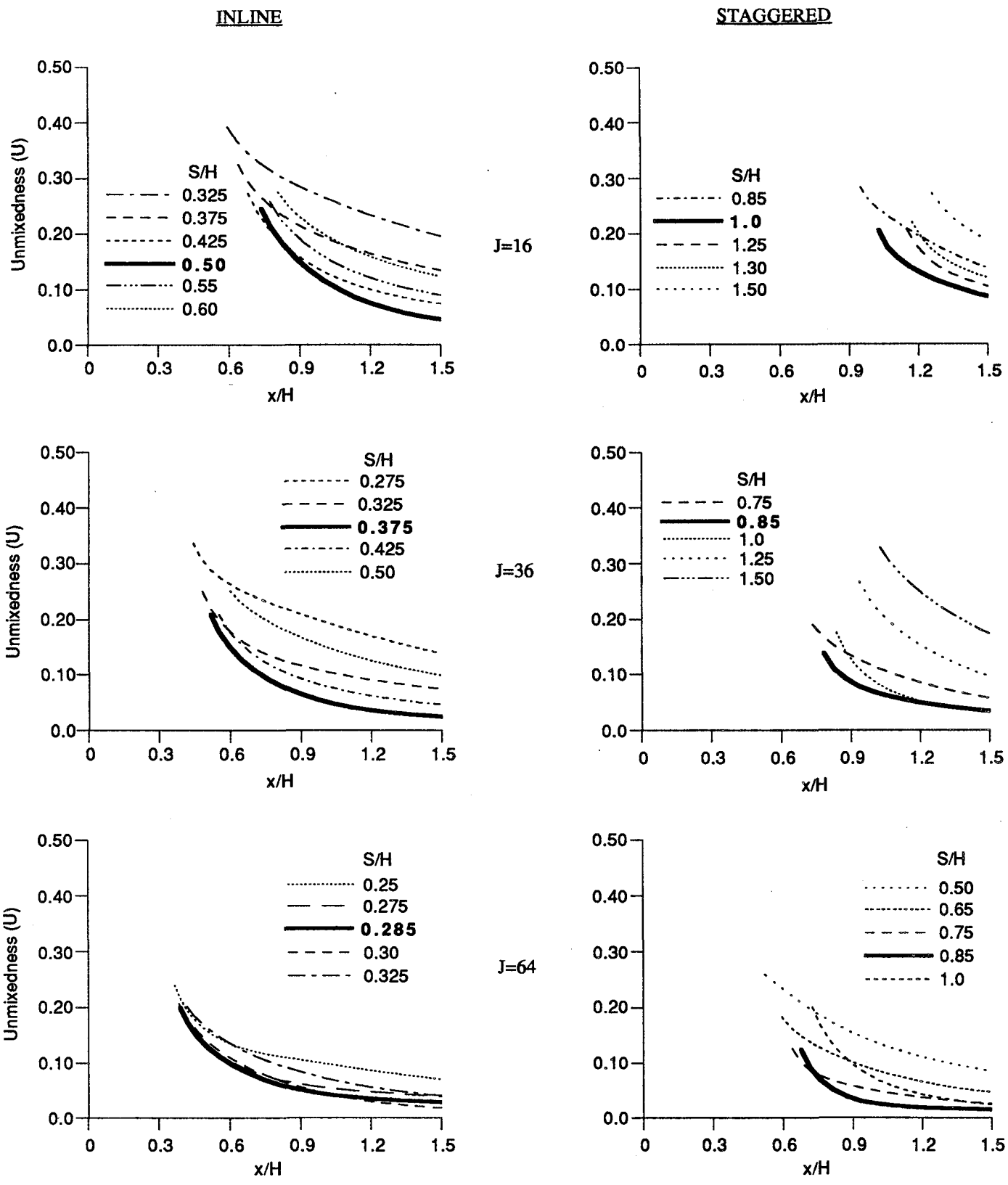

Figure 3. Computational Results of Parametrics 1-6

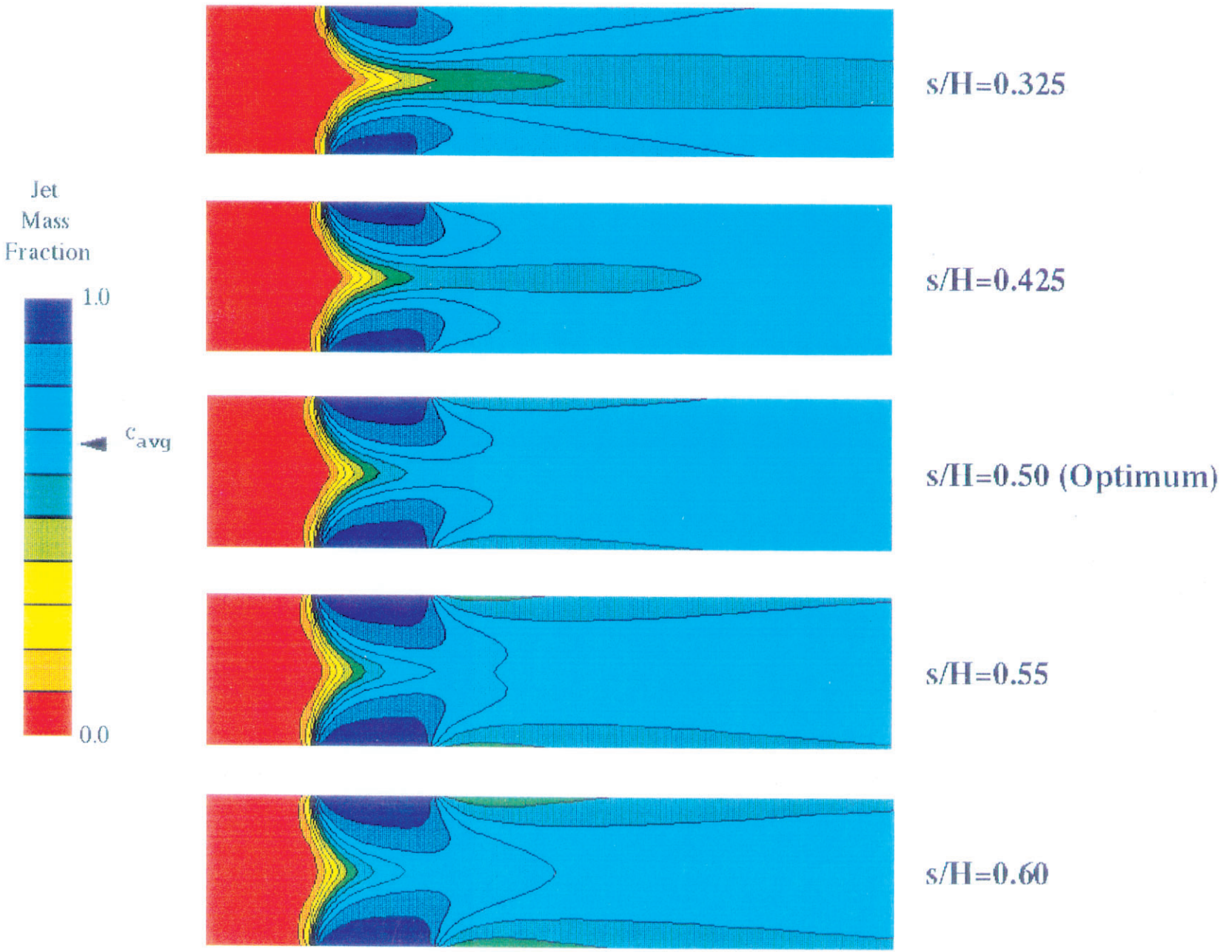

Figure 4. Effect of Jet Penetration on Mixing for Inline Slots: Momentum-Flux Ratio 16, Mass Flow Ratio 2.0

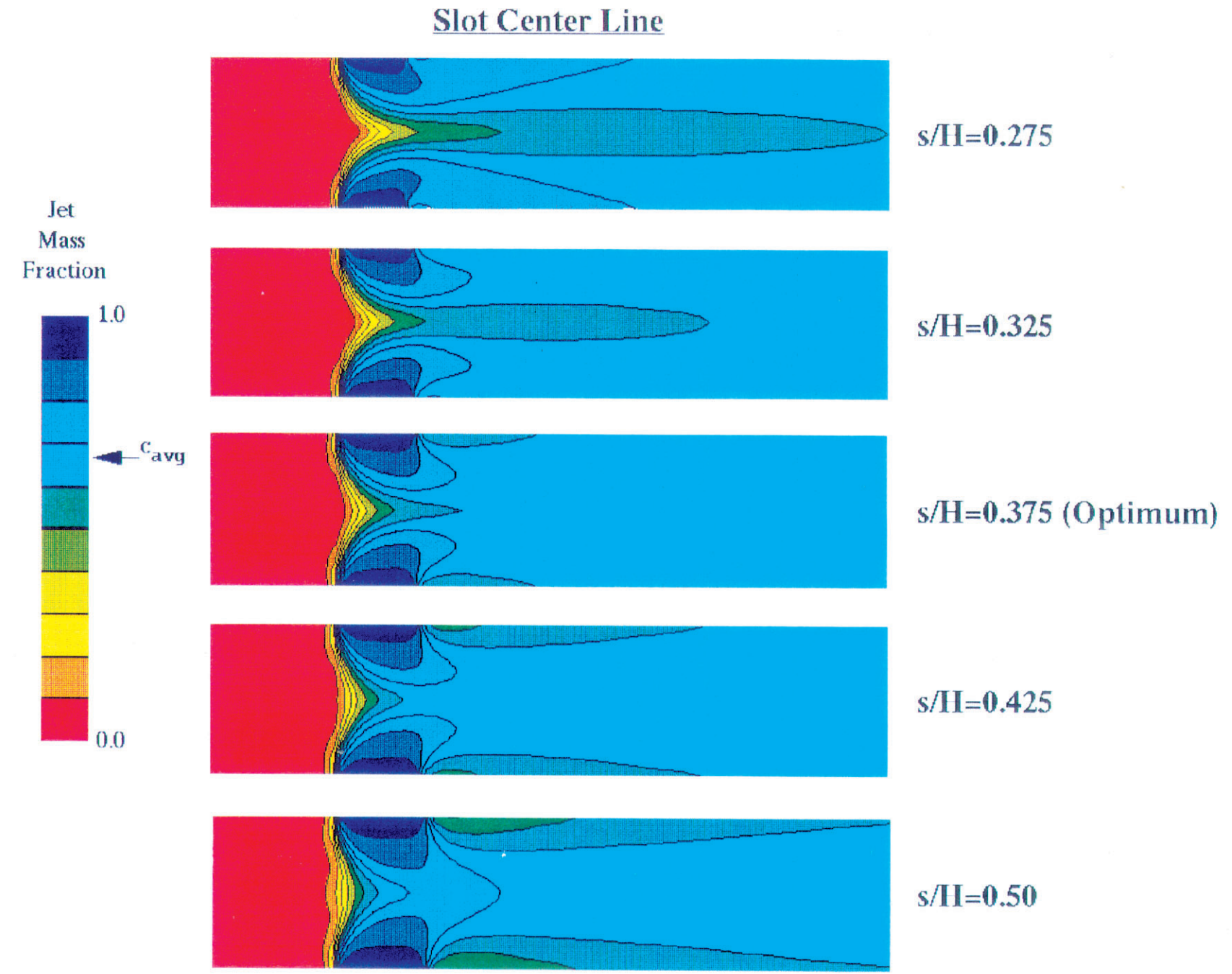

Figure 5. Effect of Jet Penetration on Mixing for Inline Slots: Momentum-Flux Ratio 36, Mass Flow Ratio 2.0

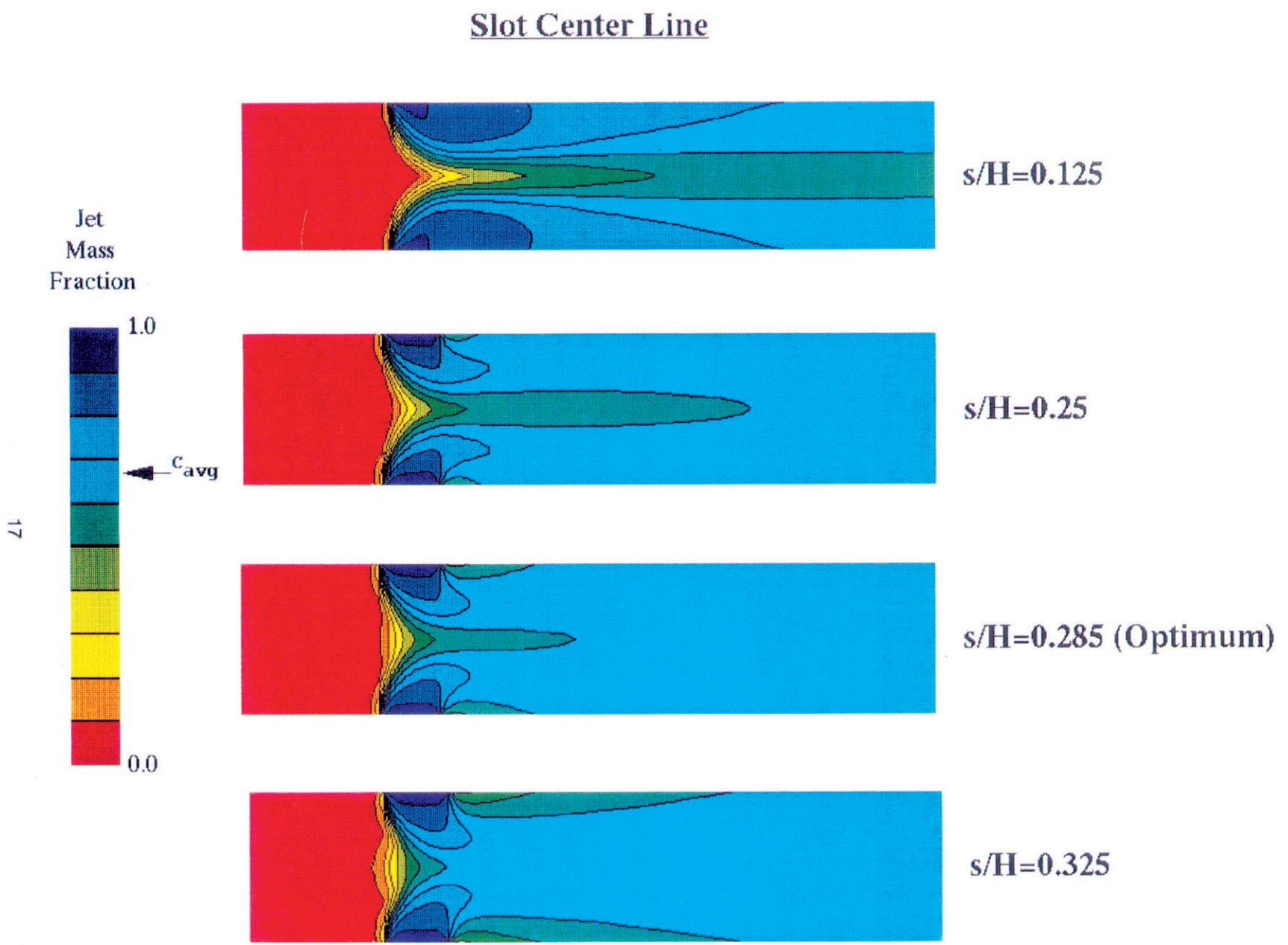

Figure 6. Effect of Jet Penetration on Mixing for Inline Slots: Momentum-Flux Ratio 64, Mass Flow Ratio 2.0

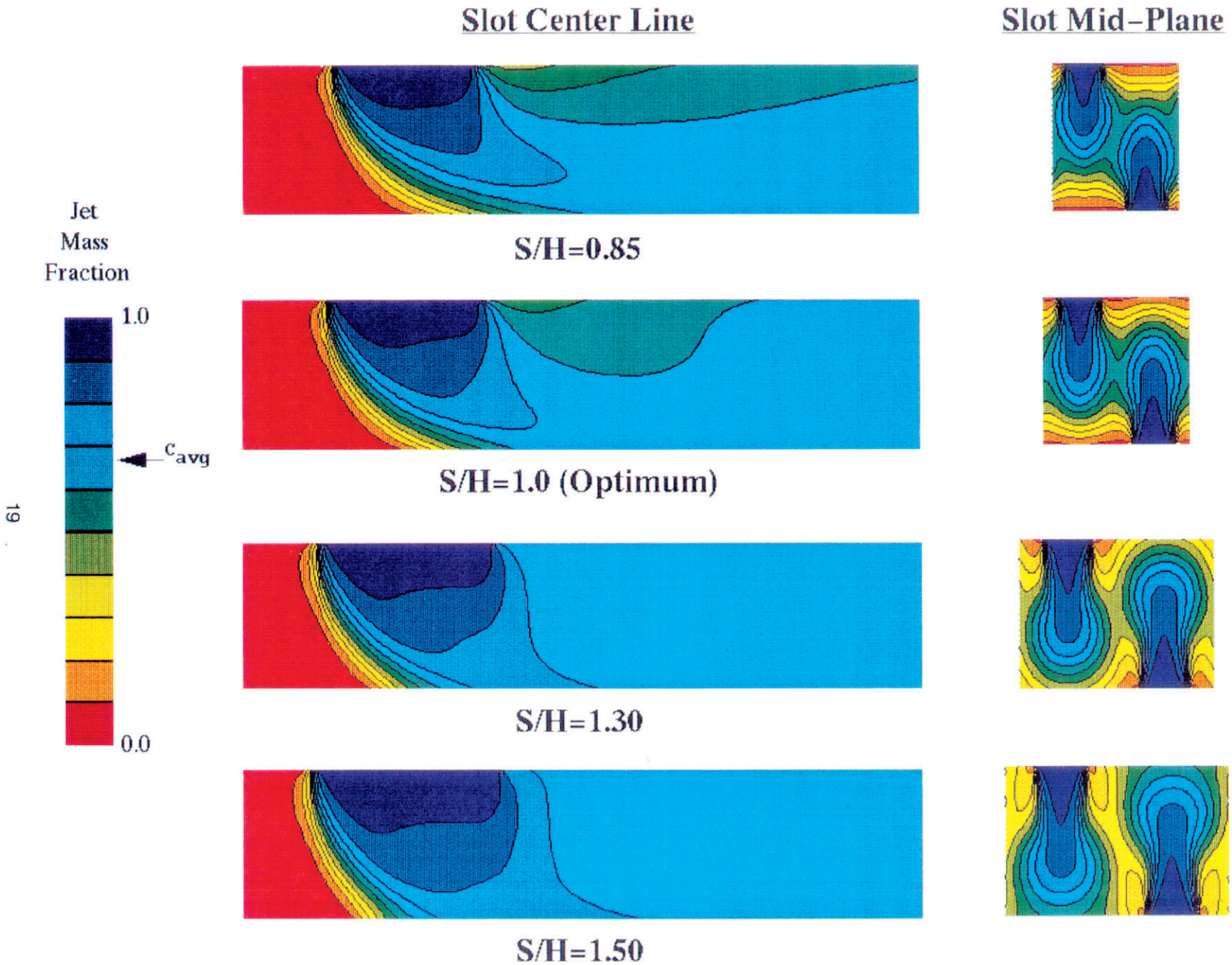

Figure 7. Effect of Jet Penetration on Mixing for Staggered Slots: Momentum-Flux Ratio 16, Mass Flow Ratio 2.0

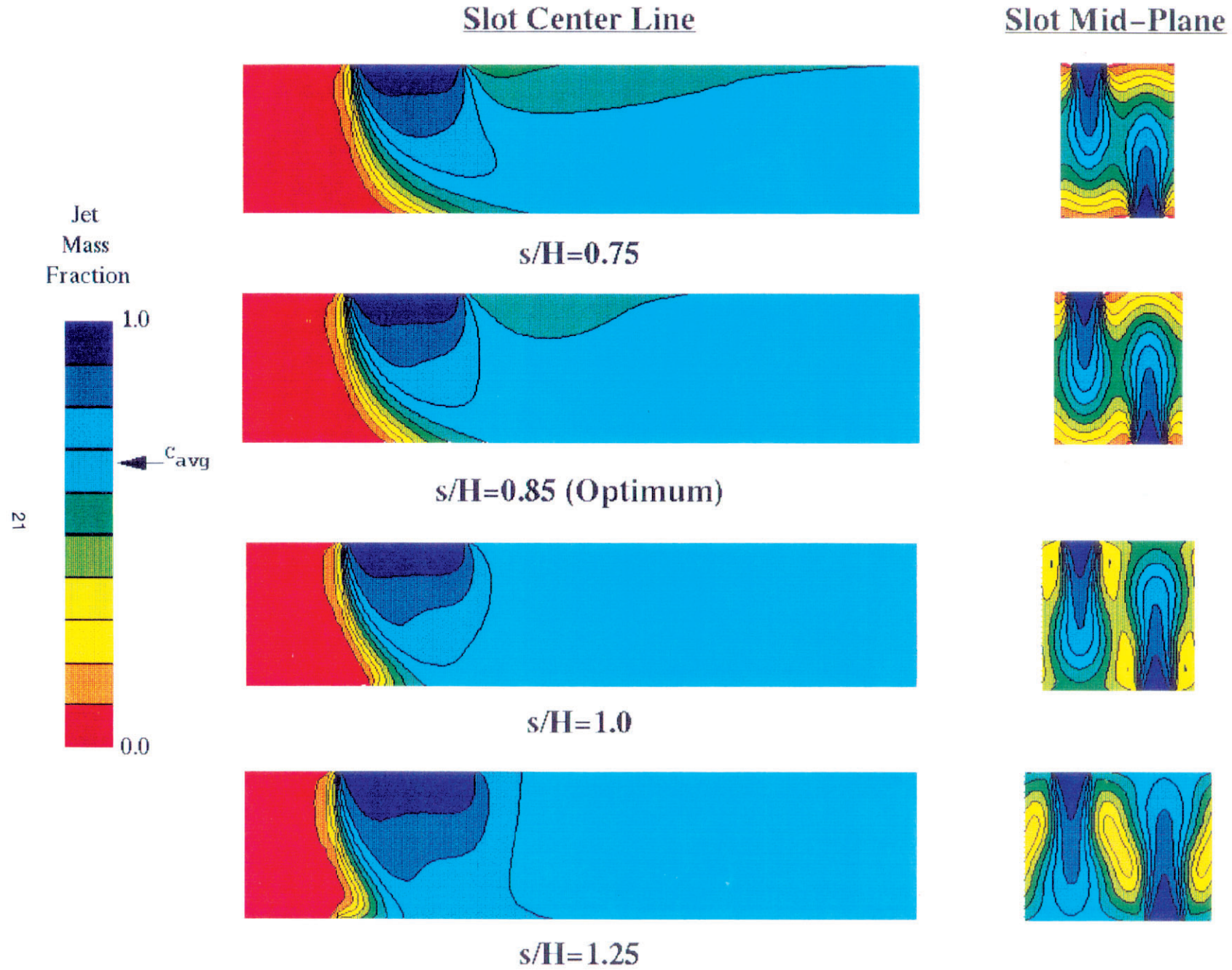

Figure 8. Effect of Jet Penetration on Mixing for Staggered Slots: Momentum-Flux Ratio 36, Mass Flow Ratio 2.0

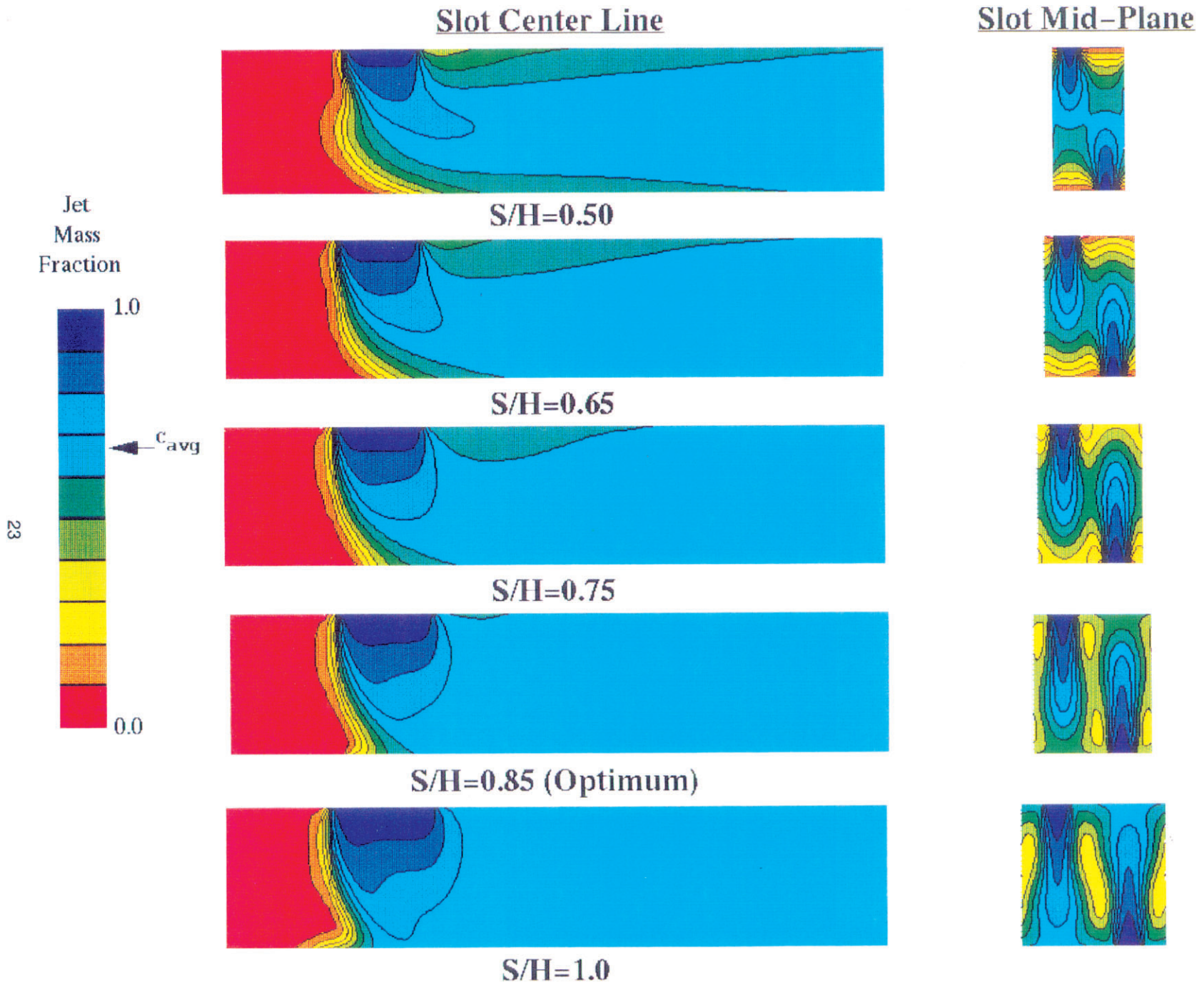

Figure 9. Effect of Jet Penetration on Mixing for Staggered Slots: Momentum-Flux Ratio 64, Mass Flow Ratio 2.0

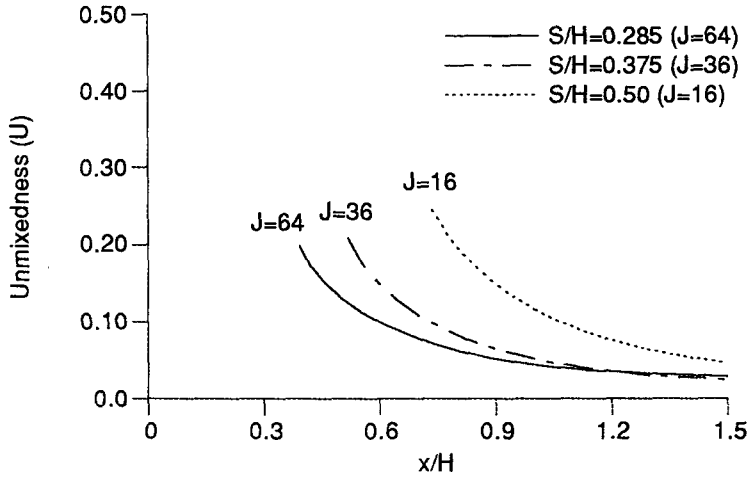

Figure 10. Effect of J on Unmixedness for Inline Slots: Mass Flow Ratio of 2.0

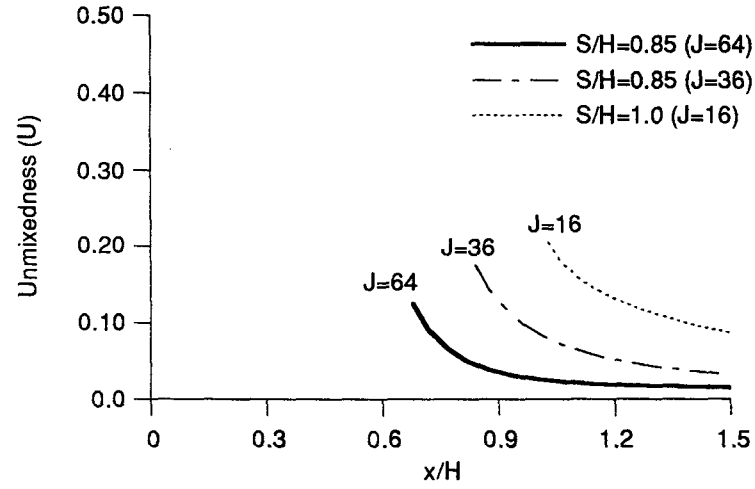

Figure 11. Effect of J on Unmixedness for Staggered Slots: Mass Flow Ratio of 2.0

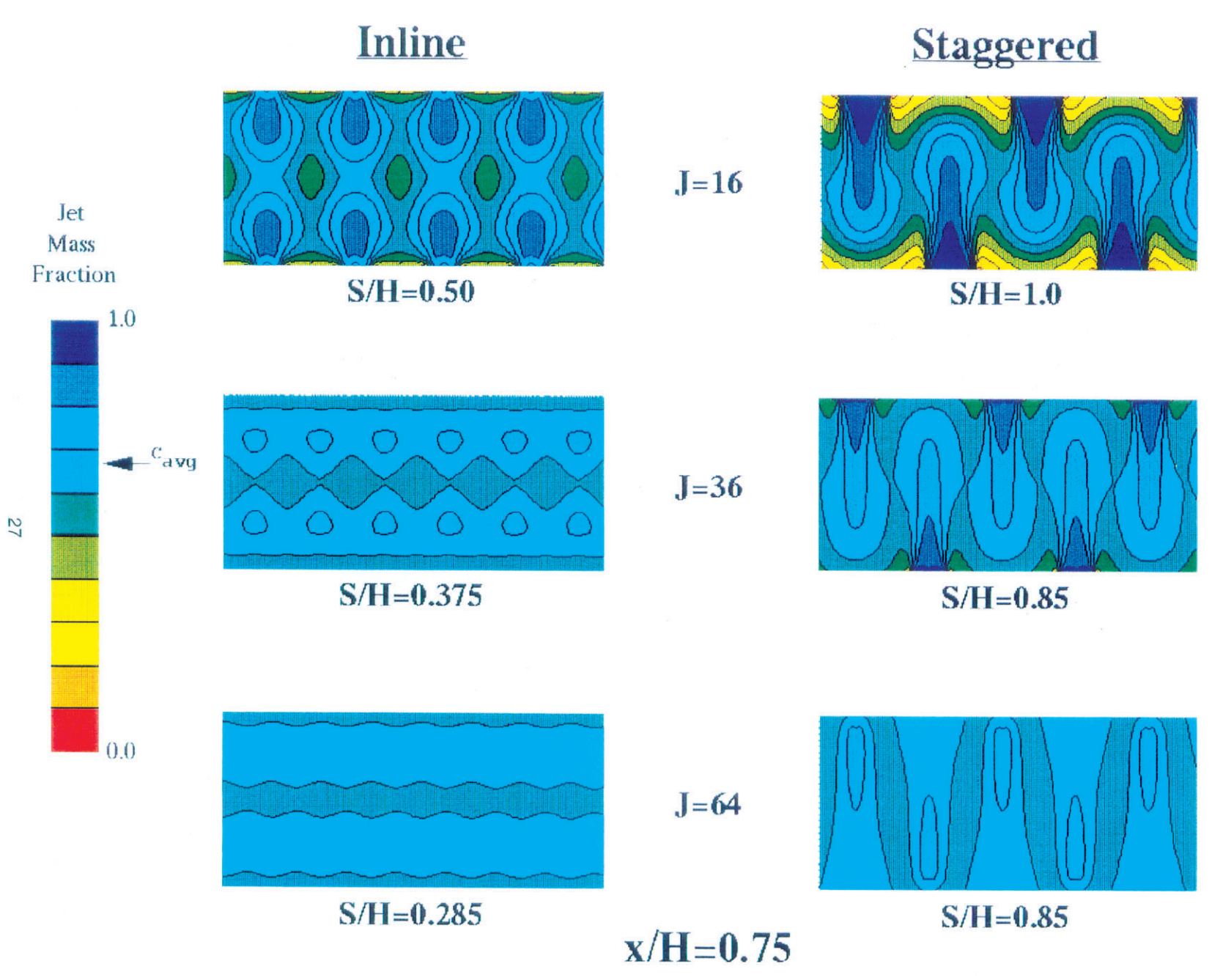

Figure 12. Effect of J Variation on Mixing for Inline and Staggered Slots: Mass Flow Ratio 2.0

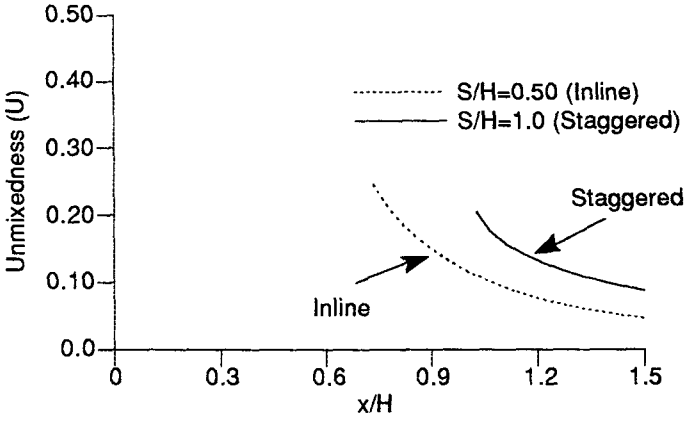

Figure 13. Effect of Lateral Arrangement on Unmixedness, J=16

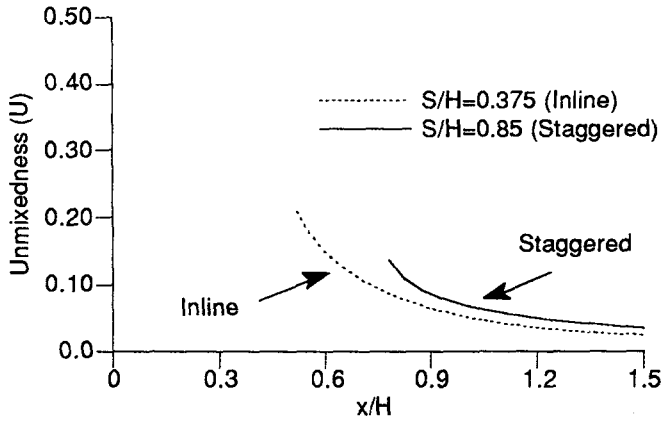

Figure 14. Effect of Lateral Arrangement on Unmixedness, J=36

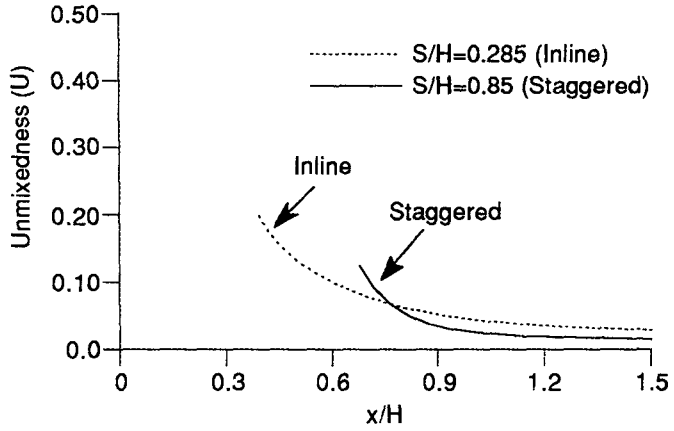

Figure 15. Effect of Lateral Arrangement on Unmixedness, J=64

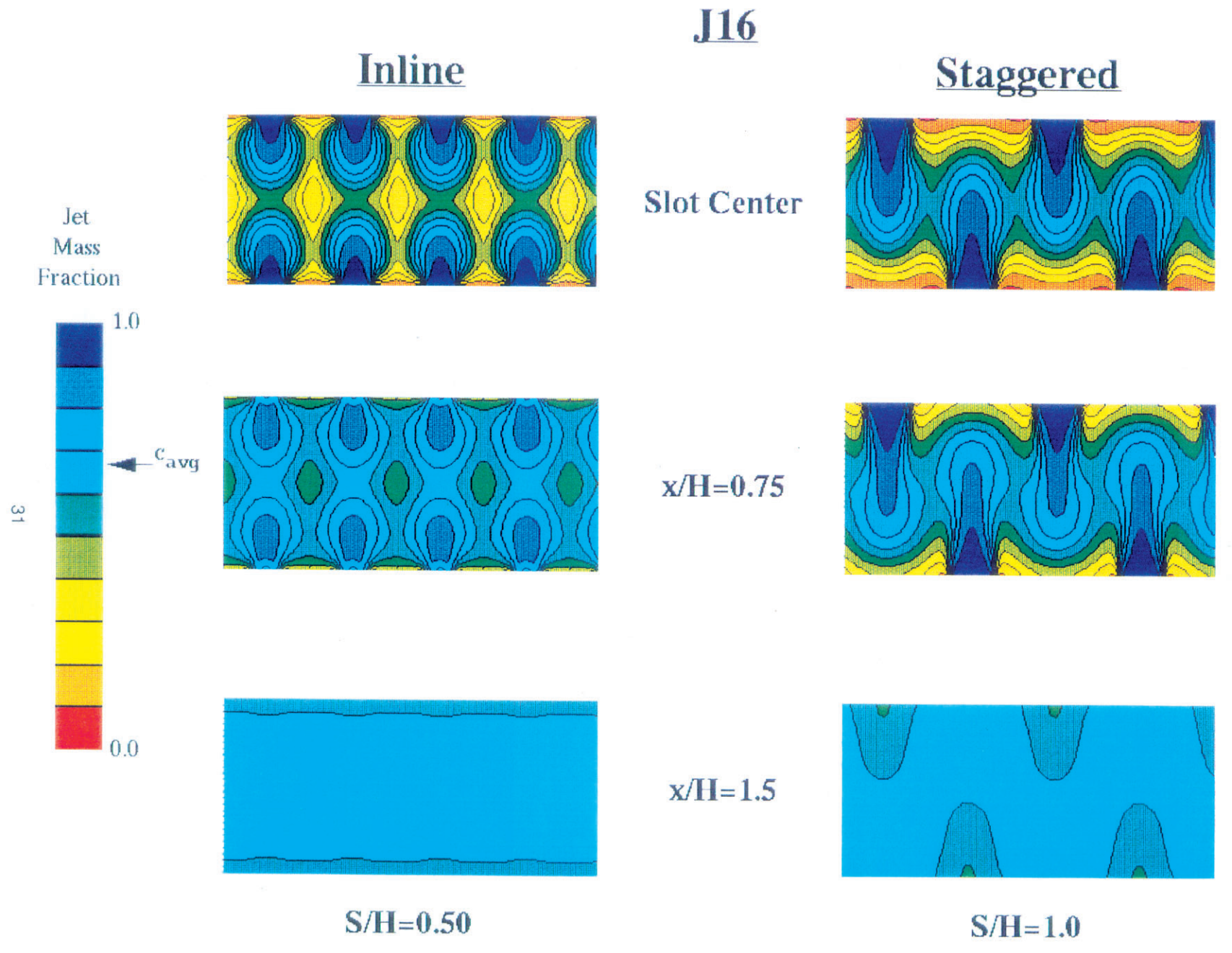

Figure 16. Effect of Lateral Arrangement on Mixing: J = 16, MR = 2.0

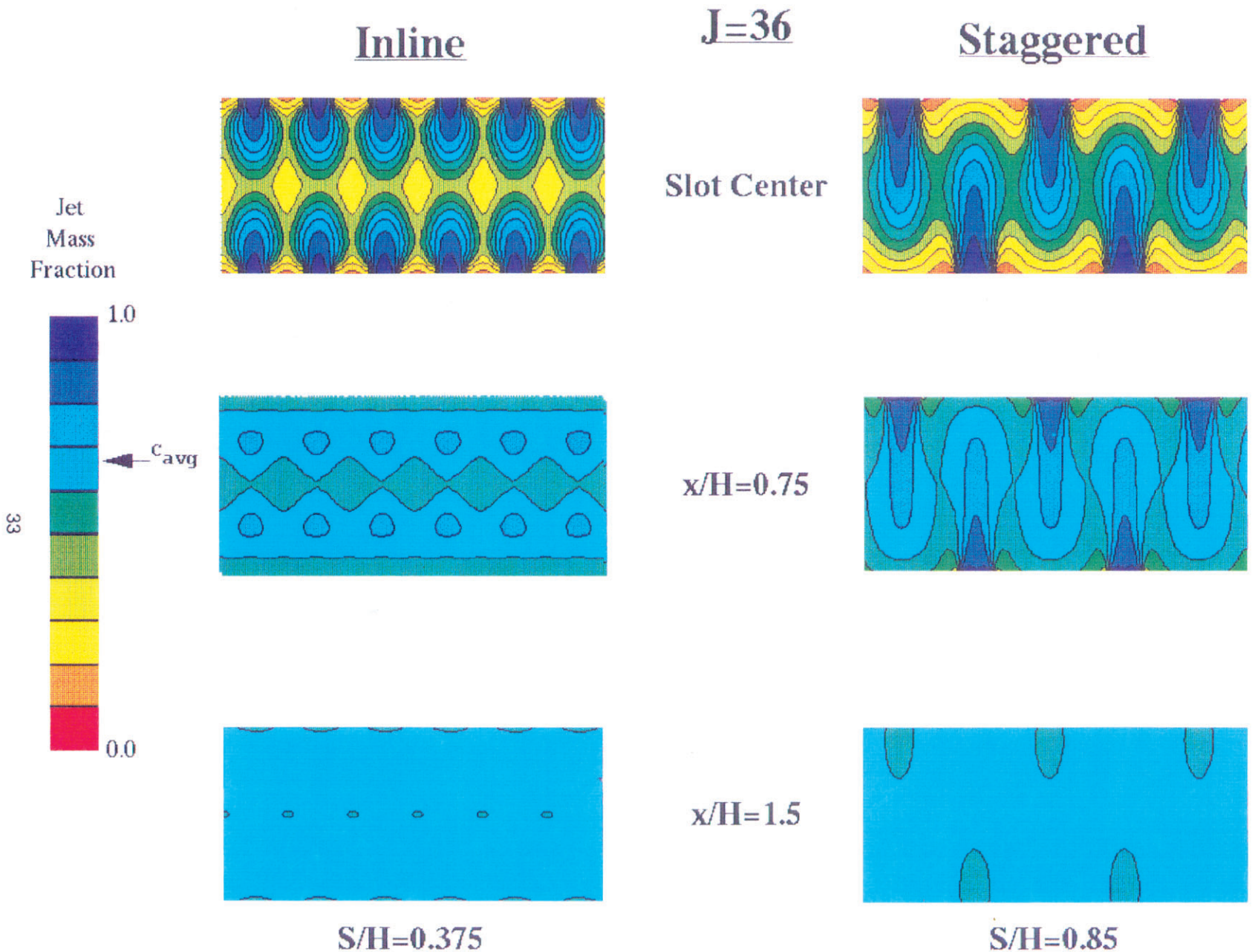

Figure 17. Effect of Lateral Arrangement on Mixing: J = 36, MR = 2.0

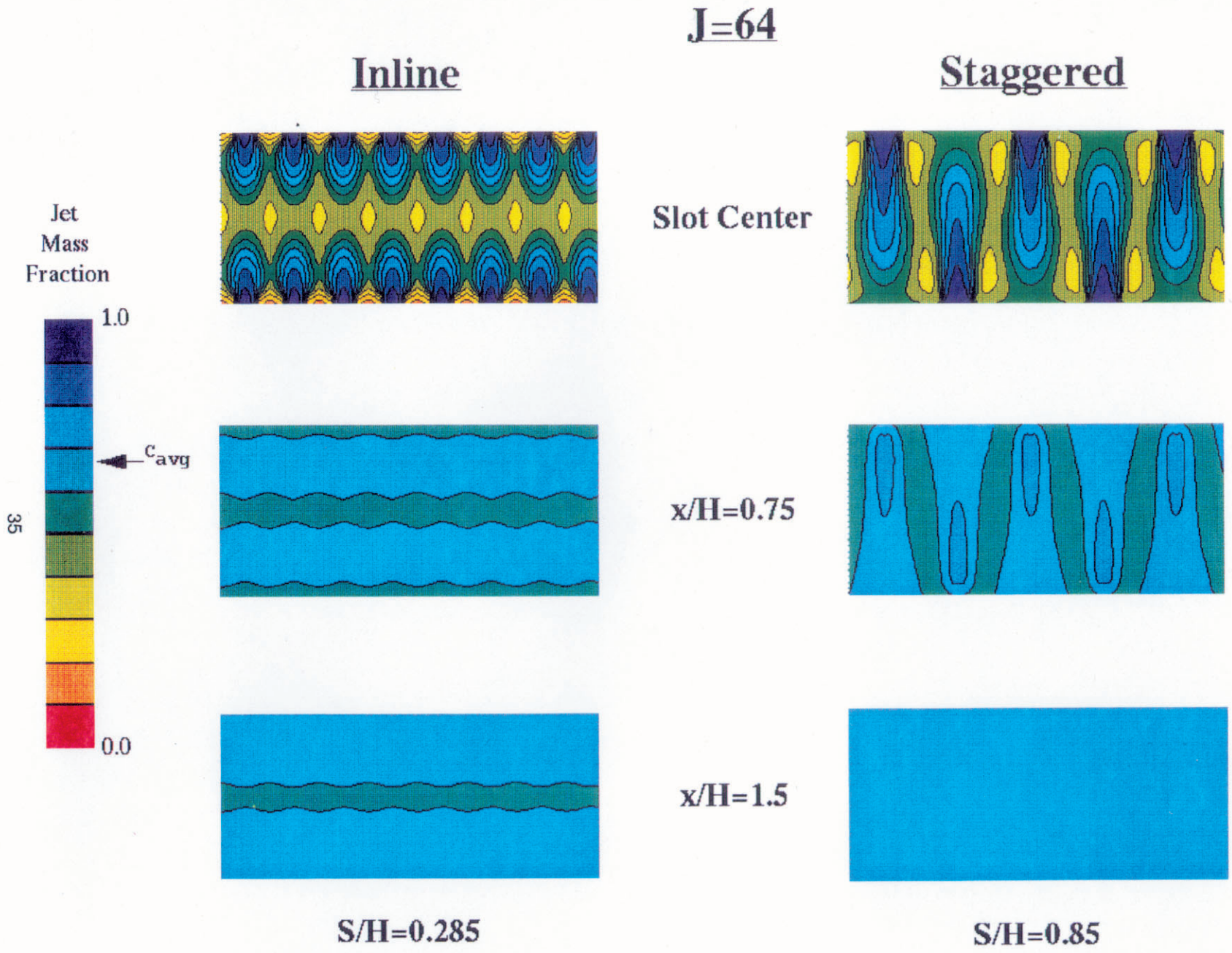

Figure 18. Effect of Lateral Arrangement on Mixing: J = 64, MR = 2.0

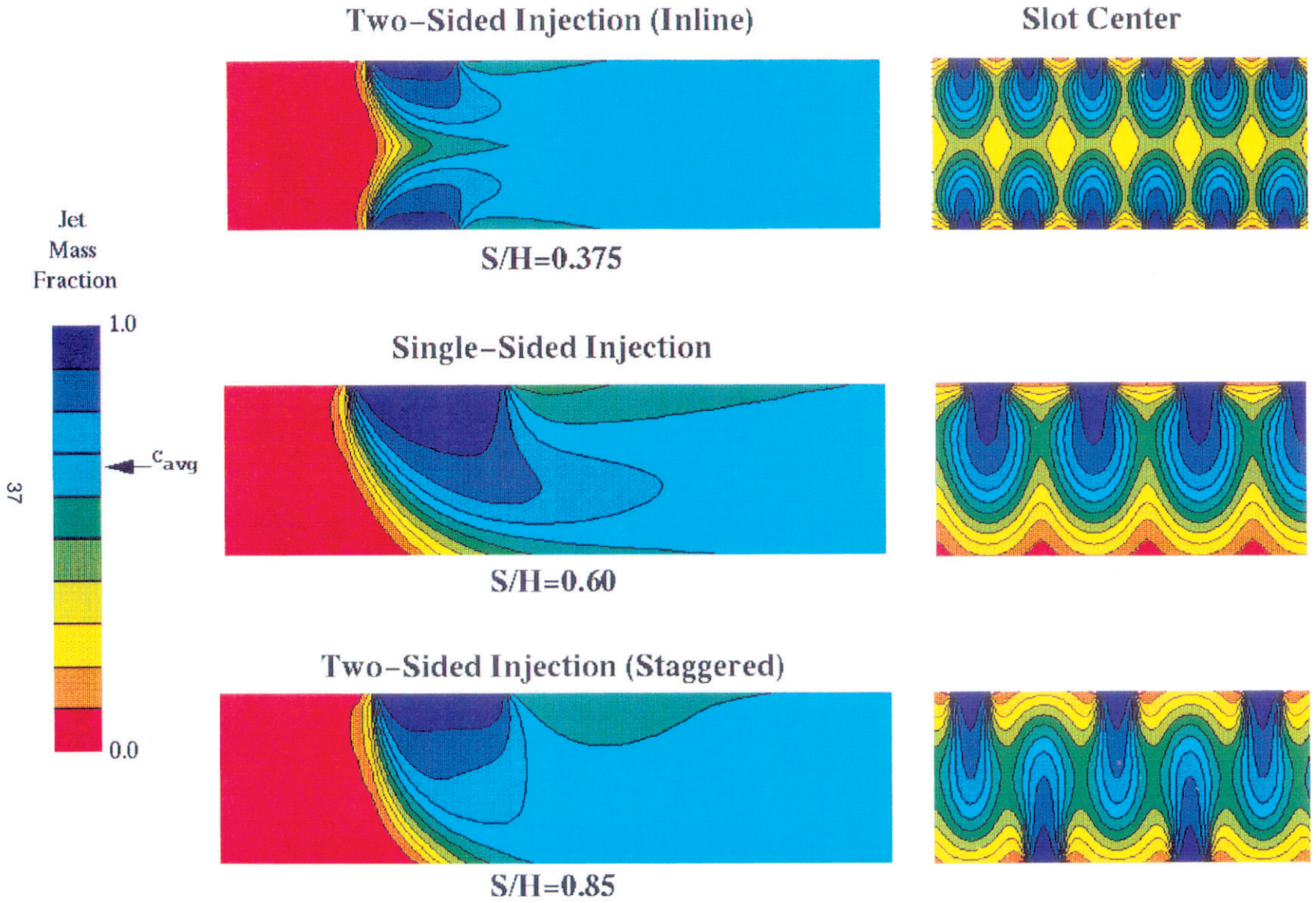

Figure 19. Comparison of Two-Sided and Single-Sided Injection at Optimum S/H: Momentum-Flux Ratio 36, MR = 2.0

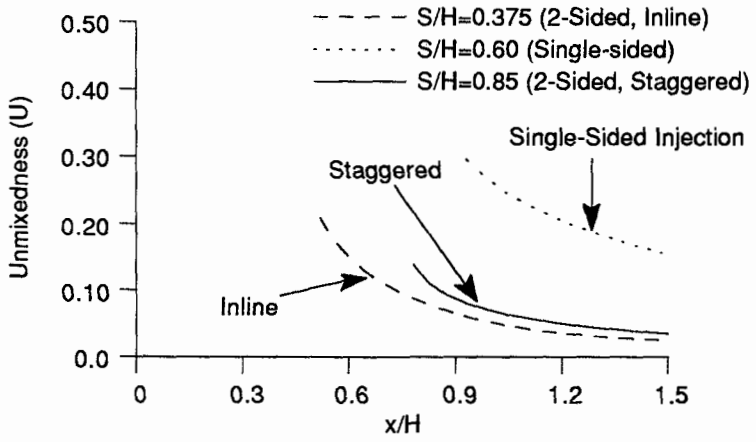

Figure 20. Unmixedness Curves for Two-Sided vs. Single-Sided Injection; Momentum-Flux Ratio 36, Mass Flow Ratio 2.0

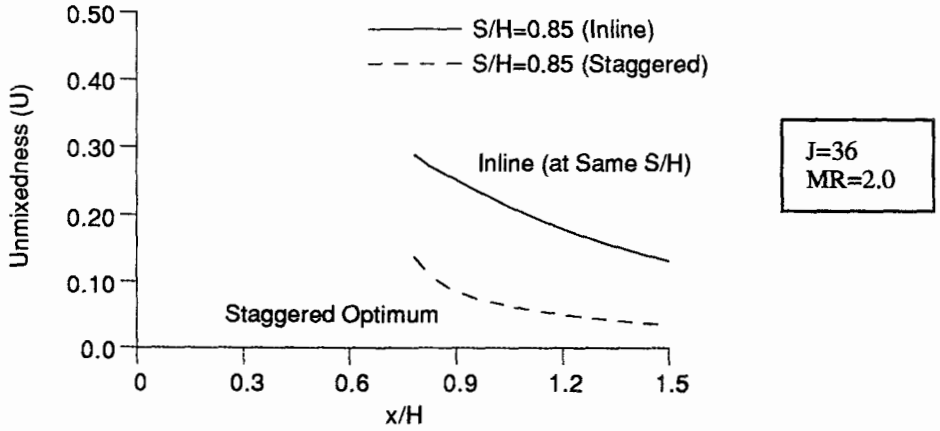

Figure 22. Unmixedness Comparison of Inline and Staggered Configurations at Staggered Optimum S/H

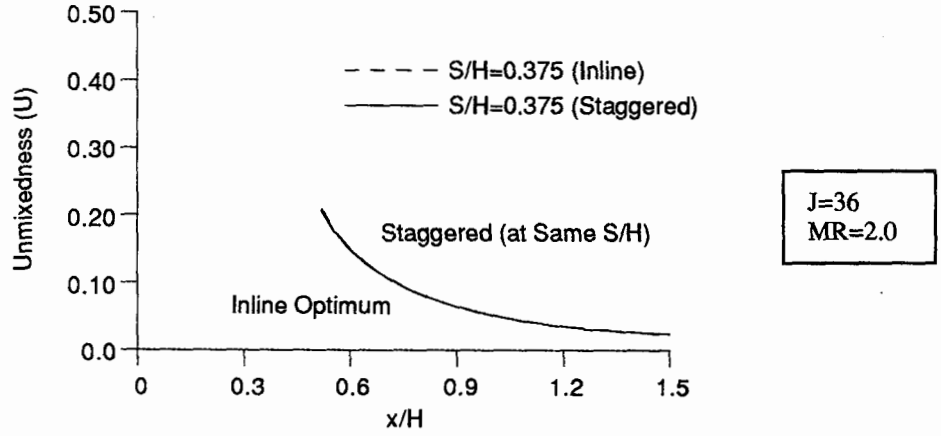

Figure 23. Unmixedness Comparison of Inline and Staggered Configurations at Inline Optimum S/H

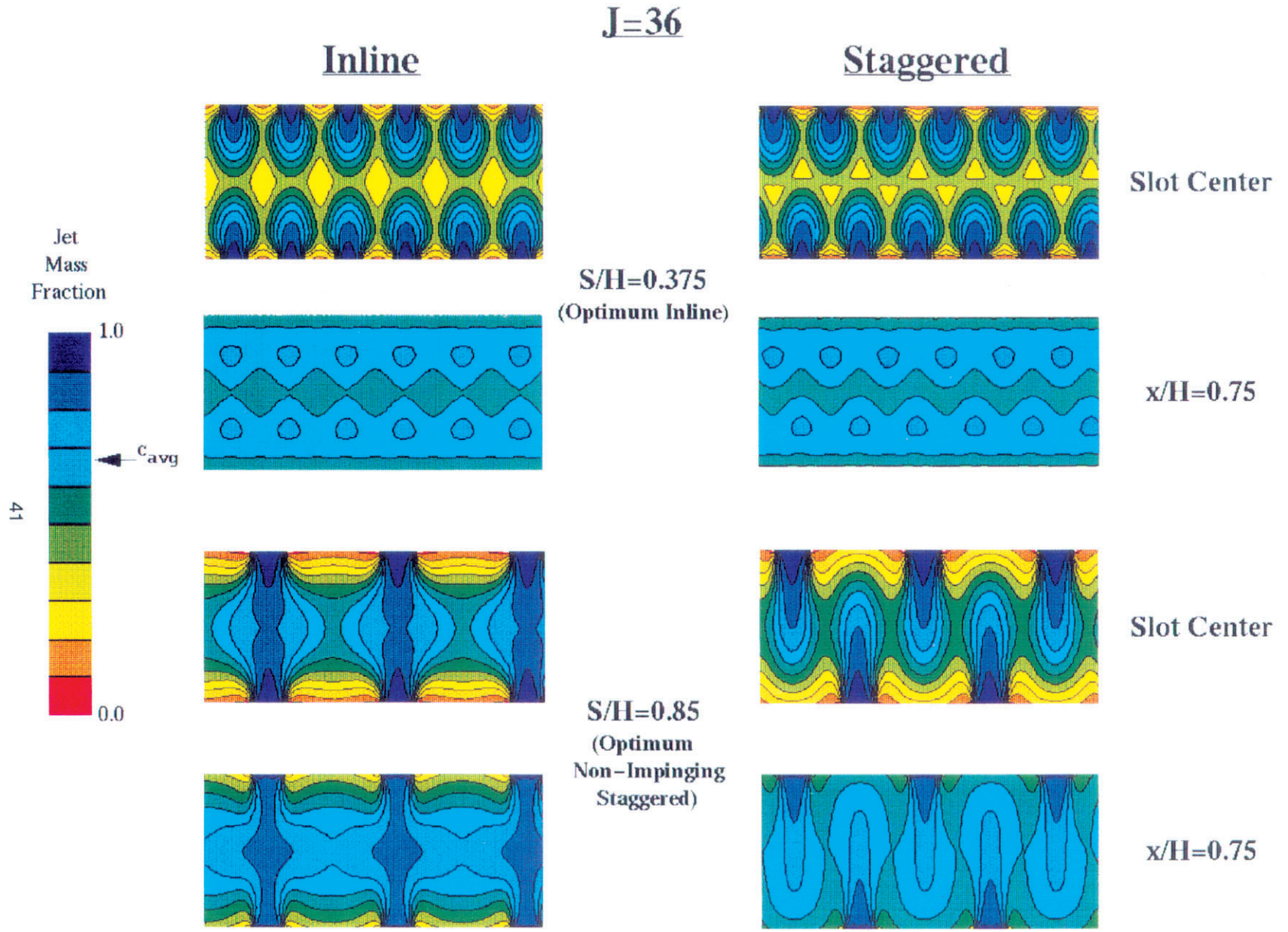

Figure 21. Comparison of Inline and Non-Impinging Staggered Slots at Optimum S/H: Momentum-Flux Ratio 36, MR = 2.0

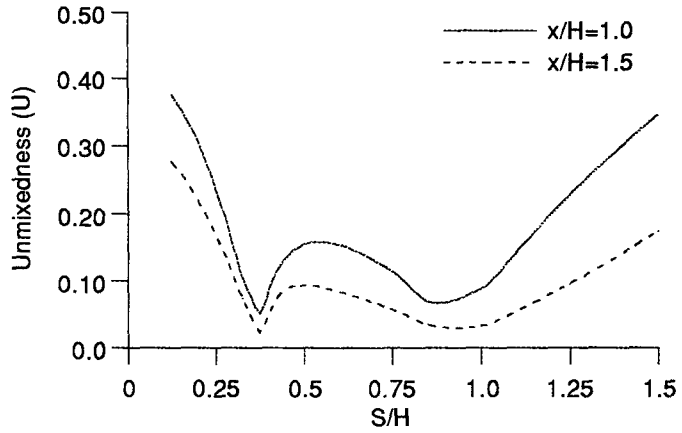

Figure 24. Staggered Cases Produce Double-Valued Function of Unmixedness Versus S/H (Parametric 2, J=36)

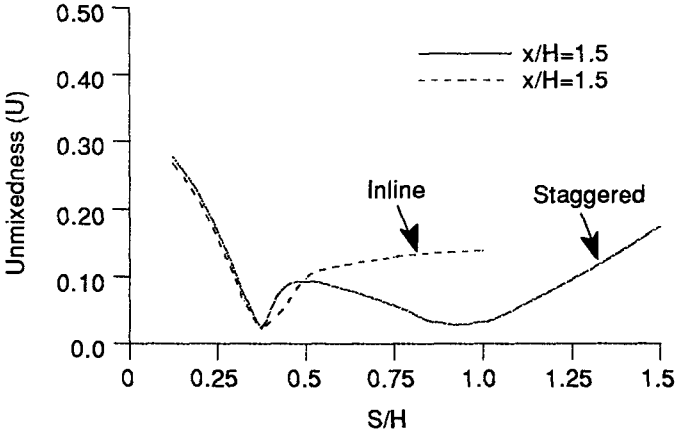

Figure 25. Unmixedness Comparison of Inline and Staggered Slots for S/H Variation at x/H=1.5 (J=36)

Table 2. Empircal and Numerical Determined Constants at Optimum S/H

Geometry	Lateral Arrangement	m_j/m_∞	J	S/H	C=S/H • √J		Blockage
					Empirical	Numerical	
Two-Sided	Inline	2.0	16	0.50	1.25	2.0	35%
	Inline		36	0.375		2.25	33%
	Inline		64	0.285		2.28	33%
	Staggered		16	1.0	5.0	4.0	25%
	Staggered		36	0.85		5.1	22%
	Staggered		64	0.85		6.8	19%
Single-Sided			36	0.60	2.5	3.6	37%

REPORT DOCUMENTATION PAGE

Form Approved
OMB No. 0704-0188

1. AGENCY USE ONLY (*Leave blank*)	2. REPORT DATE	3. REPORT TYPE AND DATES COVERED
	May 1993	Technical Memorandum

4. TITLE AND SUBTITLE

CFD Mixing Analysis of Axially Opposed Rows of Jets Injected Into Confined Crossflow

5. FUNDING NUMBERS

WU–537–02–21–00

6. AUTHOR(S)

D.B. Bain, C.E. Smith, and J.D. Holdeman

7. PERFORMING ORGANIZATION NAME(S) AND ADDRESS(ES)

National Aeronautics and Space Administration
Lewis Research Center
Cleveland, Ohio 44135–3191

8. PERFORMING ORGANIZATION REPORT NUMBER

E–7884

9. SPONSORING/MONITORING AGENCY NAME(S) AND ADDRESS(ES)

National Aeronautics and Space Administration
Washington, DC 20546–0001

10. SPONSORING/MONITORING AGENCY REPORT NUMBER

NASA TM–106179
AIAA–93–2044

11. SUPPLEMENTARY NOTES

Prepared for the 29th Joint Propulsion Conference and Exhibit cosponsored by the AIAA, SAE, ASME, and ASEE, Monterey, California, June 28–30, 1993. D.B. Bain and C.E. Smith, CFD Research Corporation, Huntsville, Alabama 35805; and J.D. Holdeman, NASA Lewis Research Center. Responsible person, J.D. Holdeman, (216) 433–5846.

12a. DISTRIBUTION/AVAILABILITY STATEMENT

Unclassified - Unlimited
Subject Category: 07

Available electronically at http://gltrs.grc.nasa.gov/GLTRS
This publication is available from the NASA Center for AeroSpace Information, (301) 621–0390.

12b. DISTRIBUTION CODE

13. ABSTRACT ***(Maximum 200 words)***

A CFD parametric study was performed to analyze axially opposed rows of jets mixing with crossflow in a rectangular duct. Isothermal analysis was conducted to determine the influence of lateral geometric arrangement on mixing. Two lateral arrangements were analyzed: 1) inline (jets' centerlines aligned with each other on top and bottom walls), and 2) staggered (jets' centerlines offset with each other on top and bottom walls). For a jet-to-mainstream mass flow ratio (MR) of 2.0, design parameters were systematically varied for jet-to-mainstream momentum-flux ratios (J) between 16 and 64 and orifice spacing-to-duct height ratios (S/H) between 0.125 and 1.5. Comparisons were made between geometries optimized for S/H at a specified J. Inline configurations had a unique spacing for best mixing at a specified J. In contrast, staggered configurations had two "good mixing" spacings for each J, one corresponding to optimum inline spacing and the other corresponding to optimum non-impinging jet spacing. The inline configurations, due to their smaller orifice size at optimum S/H, produced better initial mixing characteristics. At downstream locations (e.g., x/H of 1.5), the optimum non-impinging staggered configuration produced better mixing than the optimum inline configuration for J of 64; the opposite results were observed for J of 16. Increasing J resulted in better mixing characteristics if each configuration was optimized with respect to orifice spacing. Mixing performance was shown to be similar to results from previous dilution jet mixing investigations (MR < 0.5).

14. SUBJECT TERMS

Dilution; Jet mixing flow; Gas turbine; Combustion chamber; Emissions

15. NUMBER OF PAGES

44

16. PRICE CODE

A03

17. SECURITY CLASSIFICATION OF REPORT	18. SECURITY CLASSIFICATION OF THIS PAGE	19. SECURITY CLASSIFICATION OF ABSTRACT	20. LIMITATION OF ABSTRACT
Unclassified	Unclassified	Unclassified	

Appendix C

NASA Technical Memorandum 106434

NASA Technical Memorandum 106434
AIAA–94–0218

CFD Assessment of Orifice Aspect Ratio and Mass Flow Ratio on Jet Mixing in Rectangular Ducts

D.B. Bain and C.E. Smith
CFD Research Corporation
Huntsville, Alabama

and

J.D. Holdeman
Lewis Research Center
Cleveland, Ohio

Prepared for the
32nd Aerospace Sciences Meeting and Exhibit
sponsored by the American Institute of Aeronautics and Astronautics
Reno, Nevada, January 10–13, 1994

NASA

CFD Assessment of Orifice Aspect Ratio and Mass Flow Ratio on Jet Mixing in Rectangular Ducts

D. B. Bain* and C. E. Smith**
CFD Research Corporation
Huntsville, Alabama

J. D. Holdeman***
NASA Lewis Research Center
Cleveland, Ohio

Abstract

Isothermal CFD analysis was performed on axially opposed rows of jets mixing with crossflow in a rectangular duct. Laterally, the jets' centerlines were aligned with each other on the top and bottom walls. The focus of this study was to characterize the effects of orifice aspect ratio and jet-to-mainstream mass flow ratio on jet penetration and mixing. Orifice aspect ratios (L/W) of 4-to-1, 2-to-1, and 1-to-1, along with circular holes, were parametrically analyzed. Likewise, jet-to-mainstream mass flow ratios (MR) of 2.0, 0.5, and 0.25 were systematically investigated. The jet-to-mainstream momentum-flux ratio (J) was maintained at 36 for all cases, and the orifice spacing-to-duct height (S/H) was varied until optimum mixing was attained for each configuration.

The numerical results showed that orifice aspect ratio (and likewise orifice blockage) had little effect on jet penetration and mixing. Based on mixing characteristics alone, the 4-to-1 slot was comparable to the circular orifice. The 4-to-1 slot has a smaller jet wake which may be advantageous for reducing emissions. However, the axial length of a 4-to-1 slot may be prohibitively long for practical application, especially for MR of 2.0. The jet-to-mainstream mass flow ratio had a more significant effect on jet penetration and mixing. For a 4-to-1 aspect ratio orifice, the design correlating parameter for optimum mixing [$C = (S/H)\sqrt{J}$] varied from 2.25 for a mass flow ratio of 2.0 to 1.5 for a mass flow ratio of 0.25.

Nomenclature

C	$(S/H)\sqrt{J}$ (see Eq. 1)
C_{avg}	$m_j/(m_j + m_\infty) = \theta_{EB}$
H	Duct Height
J	Momentum-Flux Ratio $(\rho_j V_j^2)/(\rho_\infty U_\infty^2)$
L	Orifice Length (long dimension)
L/W	Orifice Aspect Ratio (SAR in previous reports)
m_j	Mass Flow of Jets
m_∞	Mass Flow of Mainstream
MR	Mass Flow Ratio m_j/m_∞
P	Pressure (N/m^2)
S	Orifice Spacing
S/H	Orifice Spacing-to-Duct Height Ratio
T	Temperature (K)
U_∞	Mainstream Flow Velocity (m/s)
U	Unmixedness (see Eq. 2)
u	rms of Axial Velocity Fluctuation

* Project Engineer, Member AIAA
** Vice President/Engineering, Member AIAA
*** Senior Research Engineer, Associate Fellow AIAA

v	rms of Vertical Velocity Fluctuation
W	Orifice Width (short dimension)
x	Axial Coordinate, x=0 at leading edge of the orifice
x/H	Axial Distance-to-Duct Height Ratio
V_j	Jet Velocity (m/s)
y	Vertical Coordinate
z	Lateral Coordinate
μ_T	Turbulent Viscosity (kg/m·sec)
ρ_j	Density of Jet
ρ_∞	Density of Mainstream

1. Introduction

In recent years increased public awareness on issues such as global warming and upper atmosphere ozone depletion have sparked a growing concern over the environment. Despite the ever tightening emissions regulations, the vast majority of upper atmosphere pollutants still originate from combustion systems. To meet the increasing stringent air quality standards, low emission combustors must be developed.

One such concept being evaluated both experimentally and numerically is the Rich-burn/Quick-mix/Lean-burn (RQL) combustor[1]. This combustor utilizes staged burning in which the primary zone is designed to operate fuel rich at equivalence ratios exceeding one.[2] The combustion products high in carbon monoxide concentration enter the quick-mix section where mixing is initiated with bypass air. The combustion process is then completed in the lean-burn region.

In order to make the RQL combustor a viable combustor concept for low emissions, rapid and uniform mixing must take place in the quick-mix section. Recent studies have been performed that focus on identifying improved mixing concepts.[3-17]

2. Background

The mixing of jets in a confined crossflow has proven to have far reaching practical applications and has spurred a variety of research studies over the last quarter of a century. In gas turbine combustors, jet mixing is particularly important in the combustor dilution zone. The dilution zone is the aft zone where the products of combustion are mixed with air to produce a temperature profile acceptable to the turbine.[18-20]

Dilution zone mixing studies[18] have identified two significant design parameters that influence the mixing pattern: 1) jet-to-mainstream momentum-flux ratio (J) and 2) orifice spacing-to-duct height ratio (S/H). Optimum mixing relationships were determined to be a function of the product of S/H and square root of J for the range of conditions tested and analyzed:

$$C = (S/H)\sqrt{J} \qquad (1)$$

One-sided injection (from the top wall only) and two-sided injection (from both the top and bottom walls) were studied. The optimum mixing constants were identified as shown in Table 1. For two-sided, axially opposed rows of jets with jets' centerlines aligned, optimum mixing was obtained when C was 1.25. The best mixing occurred when the dilution jets penetrated to about one-quarter duct height.

In contrast to conventional dilution zones, the quick-mix section of RQL combustors has a larger jet-to-mainstream mass flow ratio (MR$\geq$ 2.0 vs. $\leq$ 0.5). Such a large MR for RQL combustors might necessitate the use of slots rather than holes in the combustor liner. It is unclear whether orifice aspect ratio affects jet mixing, especially at large mass flow ratios. It is also unclear if design correlations developed for MR < 0.5 are applicable to large MR ($\geq$ 2.0). This study sought to address these issues by a systematic computational investigation. A complete description of the cases studied and their results are discussed below.

3. CFD Code

The approach in this study was to perform 3-D numerical calculations on a generic geometry section.

The CFD code named CFD-ACE[21] was used to perform the computations. The basic capabilities/methodologies in CFD-ACE include:

(1) co-located, fully implicit and strongly conservative finite volume formulation;
(2) solution of two- and three-dimensional Navier-Stokes equations for incompressible and compressible flows;
(3) non-orthogonal curvilinear coordinates;
(4) multi-domain grid topology;
(5) upwind, central (with damping), second order upwind and Osher-Chakravarthy differencing schemes;
(6) standard[22], extended[23], and low Reynolds number[24] K-ε turbulence models;
(7) instantaneous, one-step, and two-step heat release and emission combustion models;
(8) spray models including trajectory, vaporization, etc.; and
(9) pressure-based solution algorithms including SIMPLE and a variant of SIMPLEC.

4. Details of Numerical Calculations

A schematic of the computational model is shown in Figure 1. The height of the mixing section was 4 inches (0.1016 m). The mainstream flow entered the calculation domain one duct height upstream (x/H of -1.0) of the leading edge of the orifices, and continued downstream to x/H of 7.0. The model consisted of jet injection from top and bottom walls into mainstream flow. Three slot orifices were analyzed, having aspect ratios of 4-to-1, 2-to-1, and 1-to-1. A circular orifice was also analyzed for completeness. The slots were aligned with the long dimension in the direction of the mainstream flow.

The rows of orifices located on the top and bottom walls were in the same axial plane and inline in the lateral direction. The lateral calculation domain extended from midplane to midplane between the jets' centerlines. Periodic boundary conditions were imposed on the lateral boundaries.

Six parametrics consisting of 31 cases were analyzed as shown in Table 2. The case sequence for each parametric consisted of holding J, MR, and L/W constant, and then parametrically changing S/H to optimize mixing. As S/H was varied, the slot dimensions changed to maintain a constant jet-to-mainstream mass flow ratio. For each parametric, the slot geometry producing optimum mixedness is shown in Figure 2. Parametrics 1, 2, and 3 show the effect of MR. A 4-to-1 slot orifice was held constant in parametrics 1, 2, and 3. Parametrics 1, 4, 5, and 6 show the effect of orifice aspect ratio. The mass flow ratio was held constant at 2.0 for parametrics 1, 4, 5, and 6.

The flow conditions of the mainstream and jets were

Mainstream		Jets	
U_∞	= 10 m/s	V_j	= 60 m/s
T_∞	= 300 K	T_j	= 300 K
u/U_∞	= 0.20	v/V_j	= 0.20
μ_T	= 1 x 10^{-2} kg/m•sec	μ_T	= 1 x 10^{-2} kg/m•sec

$P = 1 \times 10^5$ N/m^2
$J = 36$
$m_j/m_\infty = 2.0, 0.50, 0.25$

The turbulent length scales of the jets were varied to maintain a constant inlet turbulent viscosity.

Grids

A typical case consisted of 60,000 cells, 64 cells in the axial (x) direction, 28 cells in the vertical (y) direction, and 34 cells in the lateral (z) direction. The slots were composed of uniformly distributed cells; 192 cells (24 x 8) for the 4:1 slot, 384 cells (24 x 16) for the 2:1 slot, and 528 cells (24 x 24) for the 1:1 slot. The circle was generated using boundary fitted coordinates and was

composed of 576 cells. The grid upstream and downstream of the orifice region was expanded/contracted so that each cell adjacent to the slot region matched the cell size in the slot region. The cells in the vertical direction were all of uniform size.

Numerics

The following conservation equations were solved: u momentum, v momentum, w momentum, mass (pressure correction), turbulent kinetic energy (k), and turbulent energy dissipation (ε). The convective fluxes were calculated using upwind differencing, and the diffusive fluxes were calculated using central differencing. The standard k-ε turbulence model was employed and conventional wall functions were used.

Convergence

All error residuals were reduced at least 6 orders of magnitude, and continuity was conserved in each axial plane to the fifth decimal. Convergence was relatively smooth requiring about 600 iterations. A converged solution required approximately 4.0 CPU hours on a CRAY-YMP computer.

5. Data Postprocessing

Graphics postprocessing was performed using NASA PLOT3D software.[25] The only exception was Figure 11 which was processed using CFD-VIEW.[26,27]

In order to quantify the mixing effectiveness, the mass-averaged spatial concentration variance of jet flow (C_{var}) was calculated in each axial plane. The mass-averaged unmixedness (U) is defined[28] as

$$U = C_{var} / [C_{avg}(1 - C_{avg})] \qquad (2)$$

where

C_{var} = $(1/m_{TOT}) \sum_i m_i (C_i - C_{avg})^2$

m_{TOT} = total mass flow in each axial plane

m_i = mass flow of cell *i*

C_i = jet mass fraction in cell *i*

C_{avg} = $m_j / (m_j + m_\infty) = \theta_{EB}$[17] (downstream of orifice)

Calculating the unmixedness parameter can be broken down into two parts: 1) in the orifice (jet injection) region, and 2) aft of the trailing edge of the orifice. Downstream of the orifice all of the jet flow has been added and C_{avg} is a constant value as defined above. In the orifice region, C_{avg} is calculated in each axial plane based on the amount of jet mass in that plane. The unmixedness curves show a sharp spike (just downstream of x/H of 0) where the jet flow first enters the domain and then gradually drops as the jet flow begins to mix with the mainstream flow.

6. Results and Discussion

Figure 3 presents the unmixedness results for all of the parametrics. The optimum mixing curve for each parametric is illustrated by the bold line. Note that the inflection points in the unmixedness curves identify the location of the trailing edge of the orifice. Discussion of the results follows.

Effect of Jet-to-Mainstream Mass Flow Ratio

The effect of MR on jet penetration is presented in Figure 4. Plotted are the jet mass fraction color concentrations in a lateral plane through the orifice centerline. S/H is held constant (0.275) in the figure. The color bar distribution was the same for all three MR cases in Figure 4. Each color bar has an arrow signifying the overall jet mass fraction at equilibrium. It is hard to discern differences in jet penetration with this color bar since mixed-out (equilibrium) values of mass fraction vary significantly between MR cases. An alternate way to compare jet penetration is to alter the color bar distribution such that the color at mixed-out conditions is maintained for each MR case. Figure 5 is similar to Figure 4 but with the revised color bar for each MR case.

For the MR of 2.0 case, the jets are somewhat underpenetrated, allowing too much of the approach

flow to pass through the center of the duct. In contrast, for MR of 0.25, the jets are somewhat overpenetrated as evidenced by more mainstream flow being forced between the jets. For MR of 0.50, the jets have penetrated to 1/4 duct height and an equal balance of mainstream flow has passed through the center of the duct and between the jets. Thus, a significant effect of MR on jet penetration is seen.

Figure 6 presents unmixedness results for each MR at the optimum S/H. Note that the optimum S/H is 0.375 for MR of 2.0, while the optimum S/H is 0.25 for MR of 0.25. Such a variation in optimum S/H shows there is significant effect of MR on unmixedness. In the orifice region, a large difference is seen between the different MR due to the large variation in orifice geometric size. Although the MR of 2.0 case exhibits the lowest value of unmixedness at the orifice leading edge, it has the highest value of unmixedness at x/H between 0.3 and 0.5 because of the slot's length. For x/H>0.7, the MR of 2.0 case exhibits slightly better mixing than the other two MR cases.

Figure 7 presents the jet mass fraction contours in a lateral plane through the orifice centerline for each mass flow ratio. Figure 7 is similar to Figure 5 except the results are shown at optimum S/H instead of constant S/H. Figure 8 presents the jet mass fraction contours for each mass flow ratio in an axial plane (x/H of 0.5). Optimum S/H cases are shown. At this axial location, the jets for the MR of 2.0 case are still entering the flowfield. For the other two MR cases, it can be seen there is equal balance of mainstream flow in the center of the duct and along the ducts' walls.

Aspect Ratio Analysis

The effect of aspect ratio variation on jet penetration is seen in Figure 9. Note that all cases have MR of 2.0. Presented are jet mass fraction concentrations in a lateral plane taken through the orifice centerline. S/H was held constant (0.425) in the figure. For each aspect ratio case, the jets penetrate approximately one-quarter of the duct height. There are some subtle differences between each aspect ratio case, the most recognizable being the difference between the square orifice (aspect ratio of 1-to-1) and the other orifices. The square orifice appears to penetrate slightly less than the other orifices as evidenced by less mainstream flow in the wakes of the jets (less green behind jets). However, in general, aspect ratio has little effect on jet penetration.

Figure 10 provides insight into why the square jet has slightly less penetration than the other orifices. Figure 10 presents the jet mass fraction concentrations in a vertical plane next to the top wall. Compared to the 4-to-1 and 2-to-1 slot orifices, the square orifice presents significantly more blockage to the mainstream flow. The blockage of the square orifice is 63% as compared to 44% and 31% for the 2-to-1 and 4-to-1 slot orifices. If the orifice aspect ratio is further decreased, the mainstream flow would be almost totally blocked from passing between jets. Thus, the slight decrease in jet penetration for the square orifice case is probably caused by jet blockage effects. It is interesting to note that the circle orifice, although having larger frontal area (and jet blockage, 71%), has less blockage effect on the mainstream flow than the square orifice. A possible cause of the reduced blockage effect of the circle is discussed in the next paragraph. It is interesting to note that Liscinsky[15] has experimentally shown there is minimal effect of jet blockage for circle orifices having geometric blockages less than 75%.

The effect of slot aspect ratio on jet wakes is illustrated in Figure 11. Figure 11 presents velocity vectors in the vertical plane next to the top wall. Near the wall the jet acts like a bluff body to the mainstream flow. The mainstream flow accelerates around the jet before separating and forming a wake behind the jet. As the base area of the orifice increases, the size of the wake recirculation zone increases. Thus, the square orifice has a wake width approximately twice that of the 4-to-1 slot. The wake width of the circle orifice is less than the wake width of the square orifice because the mainstream flow stays attached around the circular jet before separating. Such flow attachment may be the

cause of slightly greater jet penetration of the circle compared to the square orifice. Wake sizes may have an impact on emissions in quick-mix strategies.

The effect on aspect ratio on unmixedness is illustrated in Figure 12. The unmixedness curves are presented at optimum S/H. In the orifice region there are sizable differences in the mixing between aspect ratios. The 4:1 slot had the best initial mixing followed by the 2:1, 1:1 and circle cases. Aft of the orifices' trailing edges, the different aspect ratio curves essentially yield the same level of unmixedness.

At x/H of 0.5, Figure 12 shows that the 4:1 slot is the most unmixed, while the 2:1 slot is the least unmixed, and the 1:1 slot and circle orifices are somewhere in between. Figure 13 gives insight into why the 4:1 slot is the most unmixed. Figure 13 shows the jet mass concentration contours of all four orifice shapes in an axial plane at x/H of 0.5. It can be seen that the 4:1 jets are still entering the flowfield at x/H of 0.5, resulting in a high degree of unmixedness. The most mixed appears to be the 2:1 slots and circle orifices.

Figure 14 shows a direct comparison of unmixedness for the 4-to-1 slot and circle cases. The optimum S/H for the slot is 0.375 while for the circle it is 0.425, almost the same. Aft of the slot trailing edge (x/H>0.5), the mixing levels of both orifices are identical. In the orifice region, there are some differences between orifices. At the orifice leading edge, the slot has less unmixedness than the circle, but aft of the circle trailing edge and upstream of the slot trailing edge, the circle case has less unmixedness than the slot case. From an overall unmixedness viewpoint, the circle and slot appear to be similar.

Design Correlation Constant for Optimum Mixing

Shown in Table 3 is a comparison of the design correlation constants $[(S/H)\sqrt{J}]$ for optimum mixing. The constants are presented based on the numerical results of this study as well as based on previous experimental tests reported in the literature for low MR (<0.5). For MR of 2.0, the numerically determined constant was significantly higher than for the MR of 0.25 case (2.25 vs. 1.50). The design constant based on previous experiments was 1.25 for MR less than 0.5. Thus, there appears to be a significant mass flow ratio effect.

The constants were determined to be 2.25 for the 4:1 and 2:1 cases and 2.55 for the 1:1 and circle cases. The design constant of 2.55 for circles is in agreement with recent isothermal experiments by Liscinsky.[15] Thus, in an engineering sense, the design constants were nearly the same for the four different orifice configurations. This result is consistent with the unmixedness and jet penetration results signifying little effect of aspect ratio.

7. Conclusions

A CFD parametric mixing study was performed on axially opposed rows of inline jets injected into a confined rectangular crossflow. Design variables systematically investigated were orifice aspect ratio (4-to-1, 2-to-1, 1-to-1, and circle) and jet-to-mainstream mass flow ratio (2.0, 0.5, and 0.25). A constant jet-to-mainstream momentum-flux ratio (J) of 36 was maintained for all simulations. Based on the numerical analysis, the following conclusions can be drawn:

1. Slot aspect ratio had little effect on jet penetration and mixing.
2. Circle and slot orifices had similar mixing characteristics.
3. The jet wake recirculation zone increased in size as slot aspect ratio decreased, as expected.
4. Jet-to-mainstream mass flow ratio influenced jet penetration and mixing. The design correlation constant $[C = (S/H)\sqrt{J}]$ varied from 2.25 at a MR of 2.0 to 1.5 for a MR of 0.25. Previous experimental results had reported a design correlation constant of 1.25 for MR less than 0.5.

8. Acknowledgement

This work was supported by NASA Contract NAS3-25967, and NAS computer time was provided by NASA Lewis Research Center. Valuable discussions and assistance were provided by Mr. Milind Talpallikar and Dr. Vincent Harrand. Our thanks are also extended to Ms. Kathy W. Rhoades for preparing this typescript.

9. References

1. R. J. Shaw, "Engine Technology Challenges for a 21st Century High Speed Civil Transport," *AIAA Tenth International Symposium on Air Breathing Engines*, September 1-6, 1991 (Also NASA TM 104363).
2. S. A. Mosier and R. M. Pierce, "Advanced Combustion Systems for Stationary Gas Turbine Engines," Vol. 1, EPA Contract 68-02-2136, 1980.
3. C. E. Smith, M. V. Talpallikar, and J. D. Holdeman, "A CFD Study of Jet Mixing in Reduced Flow Areas for Lower Combustor Emissions," AIAA 91-2460, June, 1991 (Also NASA TM 104411).
4. A. Vranos, D. S. Liscinsky, B. True, and J. D. Holdeman, "Experimental Study of Cross-Stream Mixing in a Cylindrical Duct," AIAA 91-2459, June, 1991 (Also NASA TM 105180).
5. M. V. Talpallikar, C. E. Smith, M. C. Lai, and J. D. Holdeman, "CFD Analysis of Jet Mixing in Low NO_x Flametube Combustors," ASME Paper 91-GT-217, Vol. 114, pp. 416-424, ASME Transactions, *Journal of Engineering for Gas Turbines and Power*, 1992 (Also NASA TM 104466).
6. G. W. Howe, Z. Li, T. I.-P. Shih, and H. L. Nguyen, "Simulation of Mixing in the Quick Quench Region of a Rich Burn-Quick Quench-Lean Burn Combustor," AIAA 91-0410, 1991.
7. M. S. Hatch, W. A. Sowa, G. S. Samuelsen, and J.D. Holdeman, "Jet Mixing Into a Heated Cross Flow in a Cylindrical Duct: Influence of Geometry and Flow Variations," AIAA 92-0773, January 1992 (Also NASA TM 105390).
8. D. B. Bain, C. E. Smith, and J. D. Holdeman, "CFD Mixing Analysis of Jets Injected from Straight and Slanted Slots into Confined Crossflow in Rectangular Ducts," AIAA 92-3087, Nashville, TN, July 6-8, 1992 (Also NASA TM 105699).
9. D. S. Liscinsky, B. True, A. Vranos, and J. D. Holdeman, "Experimental Study of Cross-Stream Mixing in a Rectangular Duct," AIAA 92-3090, Nashville, TN, July 6-8, 1992 (Also NASA TM 106194).
10. V. L. Oechsle, H. C. Mongia, and J. D. Holdeman, "A Parametric Numerical Study of Mixing in a Cylindrical Duct," AIAA 92-3088, Nashville, TN, July 6-8, 1992 (Also NASA TM 105695).
11. G. Zhu and M.-C. Lai, "A Parametric Study of Penetration and Mixing of Radial Jets in Necked-Down Cylindrical Crossflow," AIAA 92-3091, Nashville, TN, July 6-8, 1992.
12. J. T. Kroll, W. A. Sowa, G. S. Samuelsen, and J. D. Holdeman, "Optimization of Circular Orifice Jets Mixing into a Heated Crossflow in a Cylindrical Duct," AIAA 93-0249, Reno, Nevada, January 11-14, 1993 (Also NASA TM 105984).
13. D. S. Liscinsky, A. Vranos, and R. P. Lohmann, "Experimental Study of Crossflow Mixing in Cylindrical and Rectangular Ducts," NASA CR 187141, March 1993.
14. Th. Doerr and D. K. Hennecke, "The Mixing Process in the Quenching Zone of the Rich-Lean Combustion Concept," *AGARD 81st Symposium on Fuels and Combustion Technology for Advanced Aircraft Engines*, Colleferro, NR Rome, Italy, May 10-14, 1993.
15. D. S. Liscinsky, B. True, and J. D. Holdeman, "An Experimental Study of Crossflow Jet Mixing in Rectangular Ducts," AIAA-93-2037, Monterey, CA, June 28-30, 1993.

16. D. B. Bain, C. E. Smith, and J. D. Holdeman, "CFD Mixing Analysis of Axially Opposed Rows of Jets Injected in Confined Crossflow," AIAA 93-2044, Monterey, CA, 1993 (Also NASA TM 106179).
17. V. L. Oechsle, H. C. Mongia, and J. D. Holdeman, "An Analytical Study of Jet Mixing in a Cylindrical Duct", AIAA 93-2043, Monterey, CA, June 28-30, 1993 (Also NASA TM 106181).
18. J. D. Holdeman, "Mixing of Multiple Jets with a Confined Subsonic Crossflow," *Progress in Energy and Combustion Sciences*, Vol. 19, pp. 31-70, 1993. (also NASA TM 104412, 1991 and AIAA 91-2458, 1991).
19. J. D. Holdeman, R. Srinivasan, R. Reynolds, and C. D. White, "Studies of the Effects of Curvature on Dilution Jet Mixing, *Journal Propulsion and Power*, Vol. 8, No. 1, p. 209, 1992. (Also, AIAA Paper 87-1953; NASA TM –89878 and AIAA Paper 88-3180; NASA TM–00896).
20. D. S. Crocker and C. E. Smith, "Numerical Investigation of Enhanced Dilution Zone Mixing in a Reverse Flow Gas Turbine Combustor," ASME 93-GT-129, 1993.
21. S. F. Owens, "CFD-ACE: Command Language Reference Manual," CFD Research Corporation, Huntsville, AL, CFDRC Report GR-92-6, 1992.
22. B. E. Launder and D. B. Spalding, "The Numerical Computation of Turbulent Flows," *Computer Methods in Applied Mechanics and Engineering*, Vol. 3, pp. 269-289, 1974.
23. Y. S. Chen and S. W. Kim, "Computation of Turbulent Flows Using an Extended k–ε Turbulence Closure Model," NASA CR-179204, 1987.
24. K. Y. Chien, "Predictions of Channel and Boundary-Layer Flows with a Low-Reynolds Number-Turbulence Model," *AIAA Journal*, Vol. 23, No. 2, 1985.
25. P. P. Walatka, P. G. Buning, L. Pierce, and P. A. Elson, "PLOT3D User's Manual", NASA TM 101067, 1990.
26. V. J. Harrand, "CFD VIEW: A 3D Computer Graphics Software; Volume 1: Technical Manual," August 1992.
27. V. J. Harrand, "CFD VIEW: A 3D Computer Graphics Software; Volume 2: User's Manual," August 1, 1992.
28. P. V. Danckwertz, "The Definition and Measurement of Some Characteristics of Mixtures," *Appl. Sci. Res.*, Sec. A, Vol. 3, pp. 279-296, 1952.

Table 1. Spacing and Momentum-Flux Ratio Relationships

Configuration	$C = (S/H)\sqrt{(J)}$
Single-side injection:	
Under-penetration	<1.25
Optimum	2.5
Over-penetration	>5.0
Opposed rows of jets:	
In-line optimum	1.25
Staggered optimum	5.0

Table 2. Numerical Cases Analyzed

Parametric	Case	Orifice Aspect Ratio	Momentum Flux Ratio	Mass Flow Ratio (m_j/m_m)	S/H	Trailing Edge X/H	Jet Blockage at Wall
Parametric 1	Case 1	4:1	J=36	2.0	0.125	0.29	57.7
	Case 2	↓	↓	↓	0.20	0.36	45.6
	Case 3				0.228	0.39	42.8
	Case 4				0.25	0.41	40.8
	Case 5				0.275	0.43	38.9
	Case 6				0.325	0.47	35.8
	Case 7				0.375*	0.50	33.3
	Case 8				0.425	0.53	31.3
	Case 9				0.50	0.58	28.9
	Case 10				0.75	0.71	23.6
	Case 11				1.0	0.82	20.4
Parametric 2	Case 12	4:1	J=36	0.50	0.125	0.14	28.9
	Case 13	↓	↓	↓	0.20	0.18	22.8
	Case 14				0.250	0.20	20.4
	Case 15				0.275*	0.21	19.5
	Case 16				0.325	0.23	17.9
Parametric 3	Case 17	4:1	J=36	0.25	0.20	0.13	16.1
	Case 18	↓	↓	↓	0.25*	0.14	14.4
	Case 19				0.275	0.15	13.8
Parametric 4	Case 20	2:1	J=36	2.0	0.30	0.32	52.7
	Case 21	↓	↓	↓	0.375*	0.35	47.1
	Case 22				0.425	0.38	44.3
	Case 23				0.45	0.39	43.0
	Case 24				0.50	0.41	40.8
Parametric 5	Case 25	1:1	J=36	2.0	0.325	0.23	71.6
	Case 26	↓	↓	↓	0.375	0.25	66.7
	Case 27				0.425*	0.27	62.6
	Case 28				0.50	0.29	57.7
Parametric 6	Case 29	Circle-BFC	J=36	2.0	0.375	0.28	75.2
	Case 30	↓	↓	↓	0.425*	0.30	70.7
	Case 31				0.50	0.33	65.1

* represents Optimum Mixing Configuration

Table 3. Experimentally[18] and Numerically Determined Constants at Optimum S/H

Geometry	Lateral Arrangement	m_j/m_∞	Aspect Ratio	J	S/H	$C = (S/H)\sqrt{J}$	
						Experimental	Numerical
Two-Sided	Inline	2.0	4:1	36	0.375	1.25	2.25
		0.5			0.275		1.65
		0.25			0.25		1.50
		2.0	2:1		0.375		2.25
			1:1		0.425		2.55
			Circle		0.425		2.55

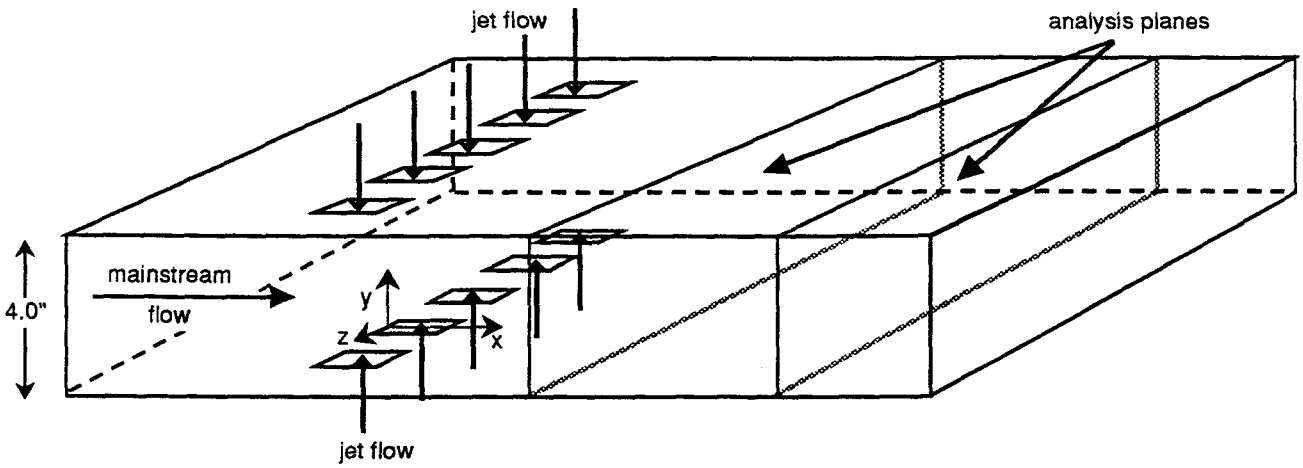

Figure 1. Schematic of Numerical Mixing Model

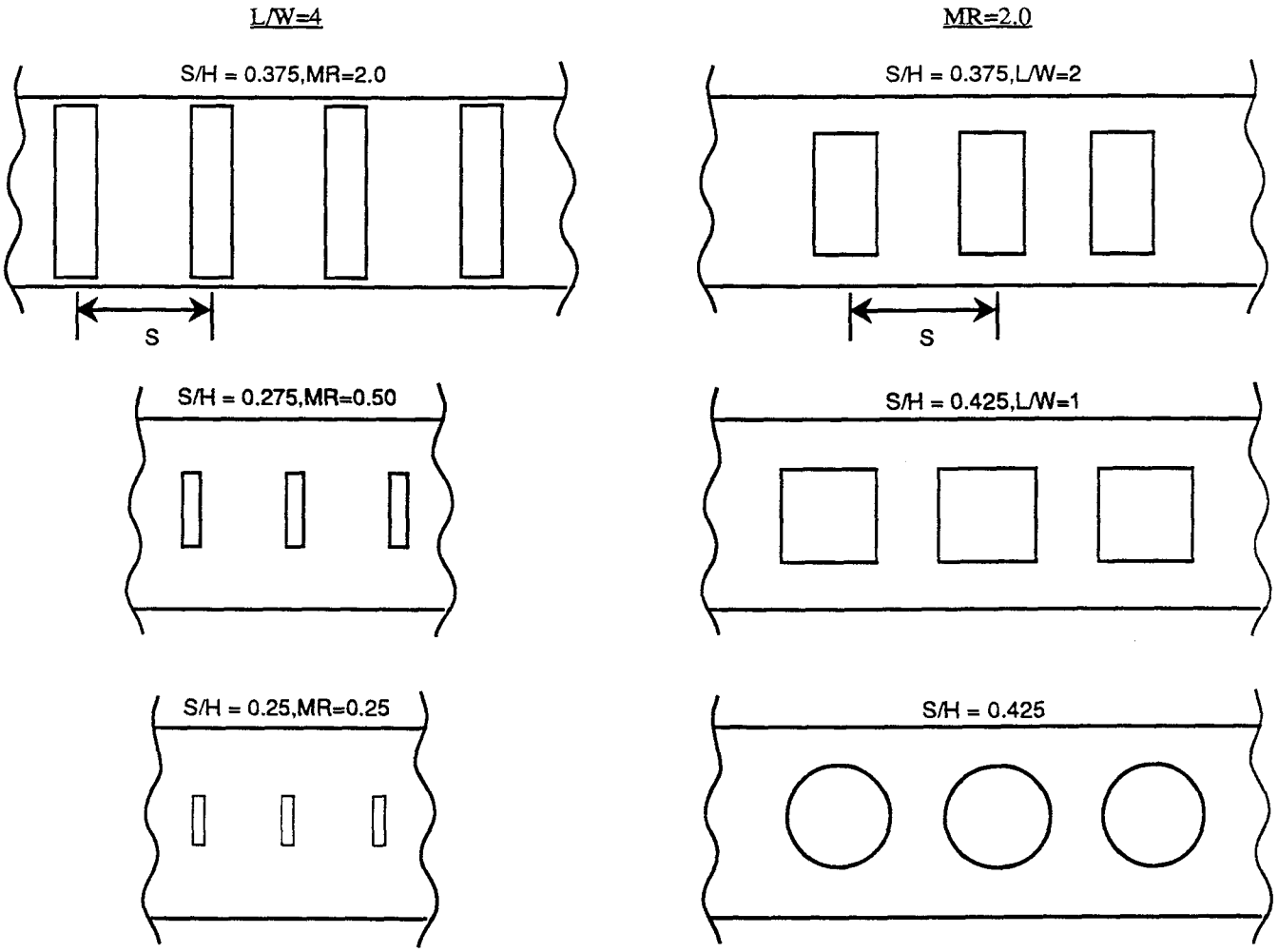

Figure 2. Slot Configurations At Optimum S/H

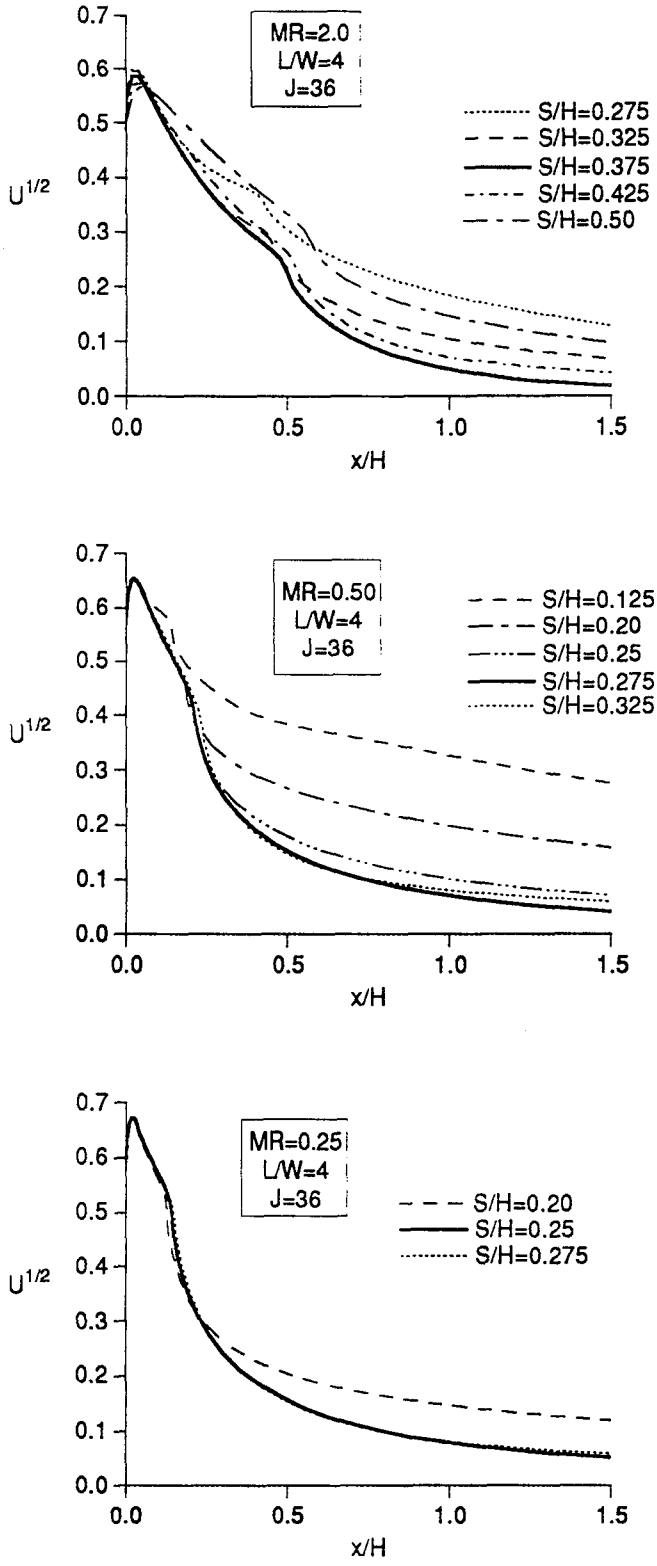

Figure 3. Computational Results of Parametrics 1-3

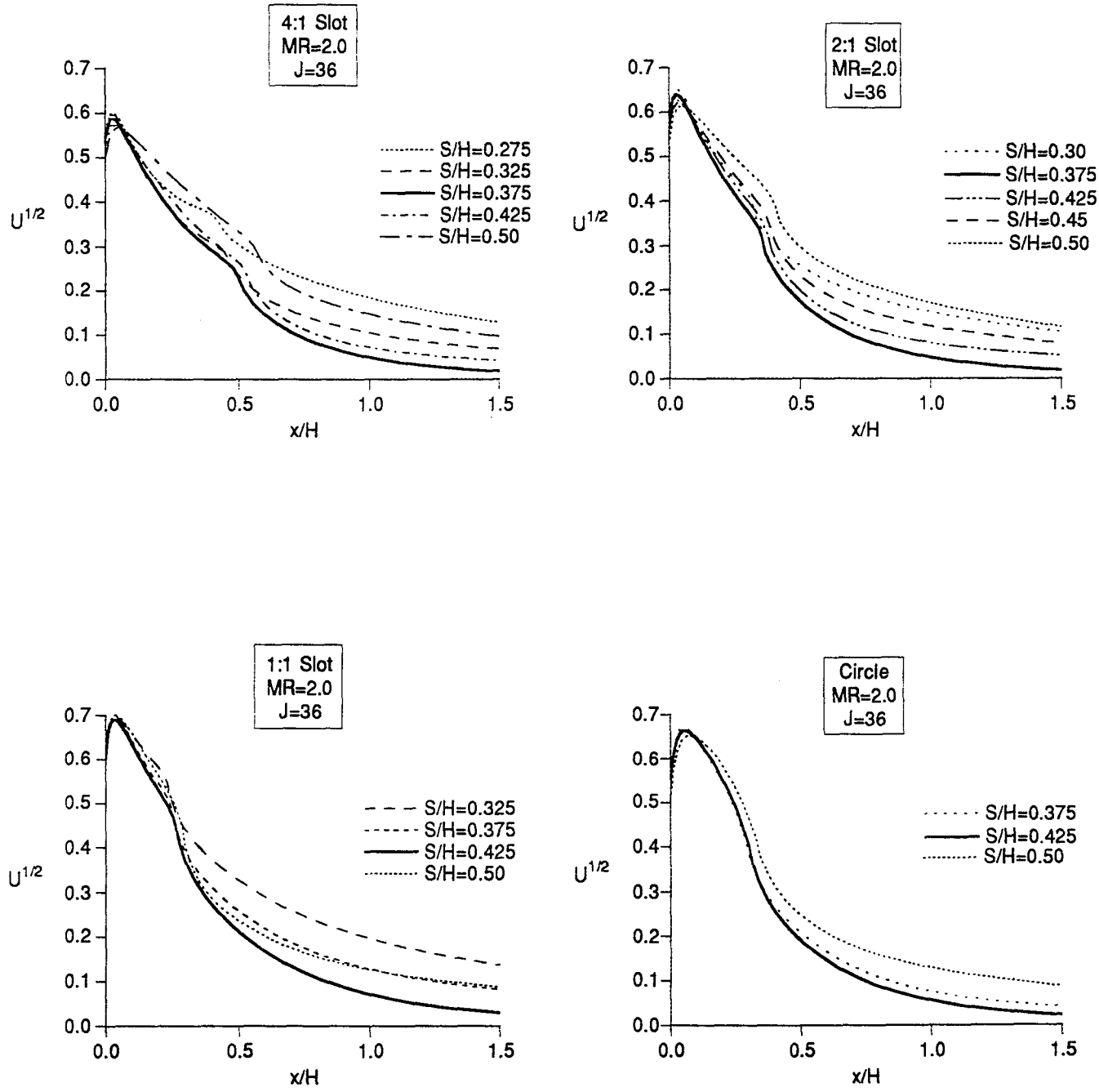

Figure 3. Computational Results of Parametrics 1, 4, 5, and 6 (cont'd)

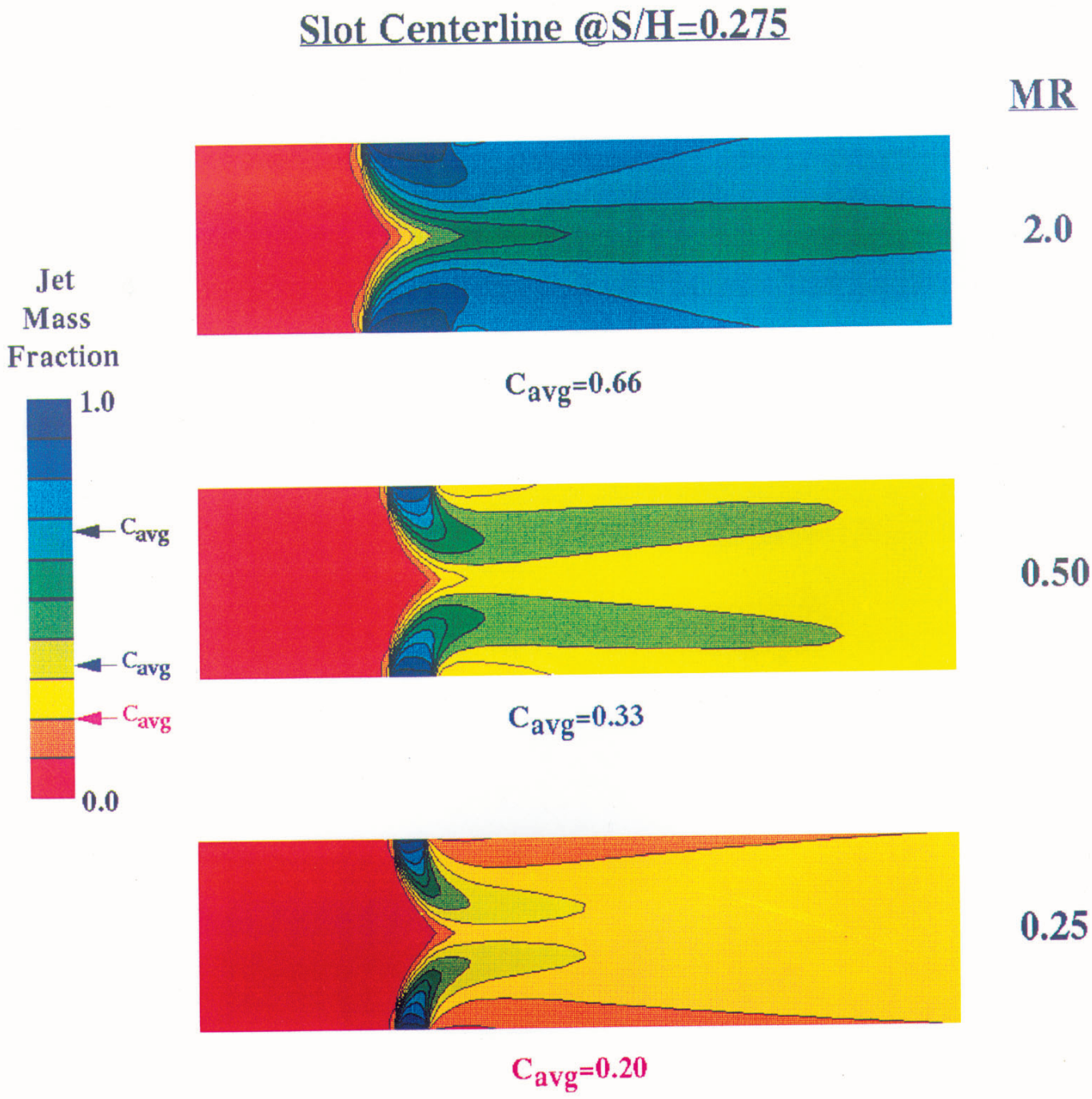

Figure 4. Effect of Jet-to-Mainstream Mass Flow Variation on Jet Penetration: J=36, L/W=4 (Uniform Color Bar Distribution)

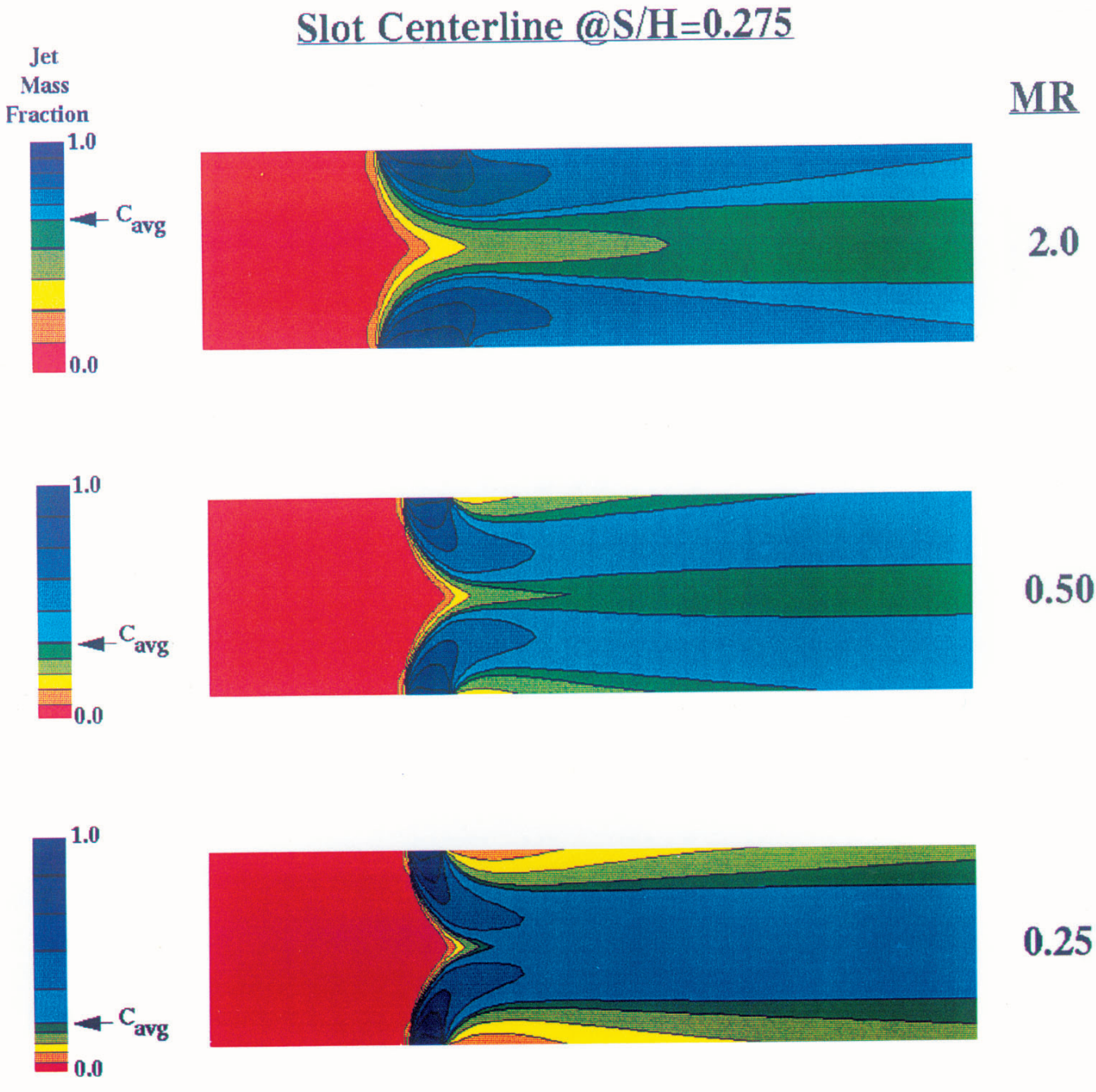

Figure 5. Effect of Jet-to-Mainstream Mass Flow Variation on Jet Penetration: J=36, L/W=4 (Non-uniform Color Bar Distribution)

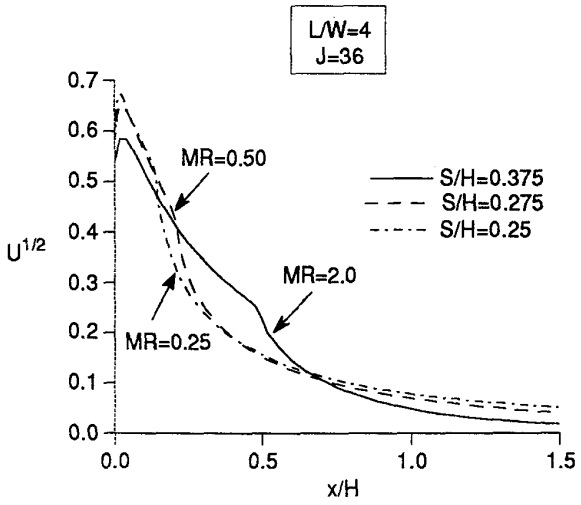

Figure 6. Effect of Jet-to-Mainstream Mass Flow Ratio on Unmixedness at Optimum S/H

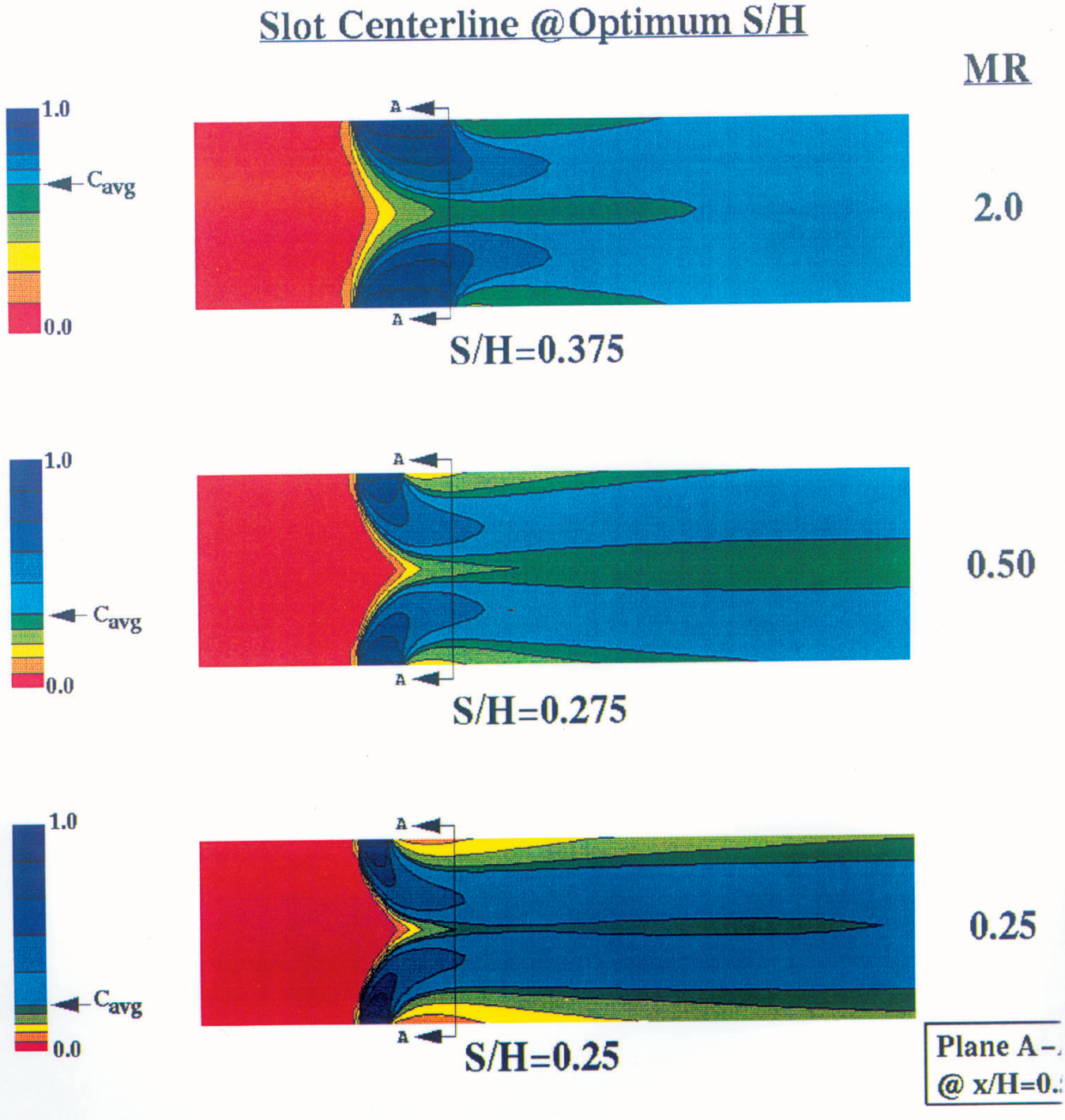

Figure 7. Effect of Jet-to-Mainstream Mass Flow Variation on Jet Penetration at Optimum S/H: J=36, L/W=4

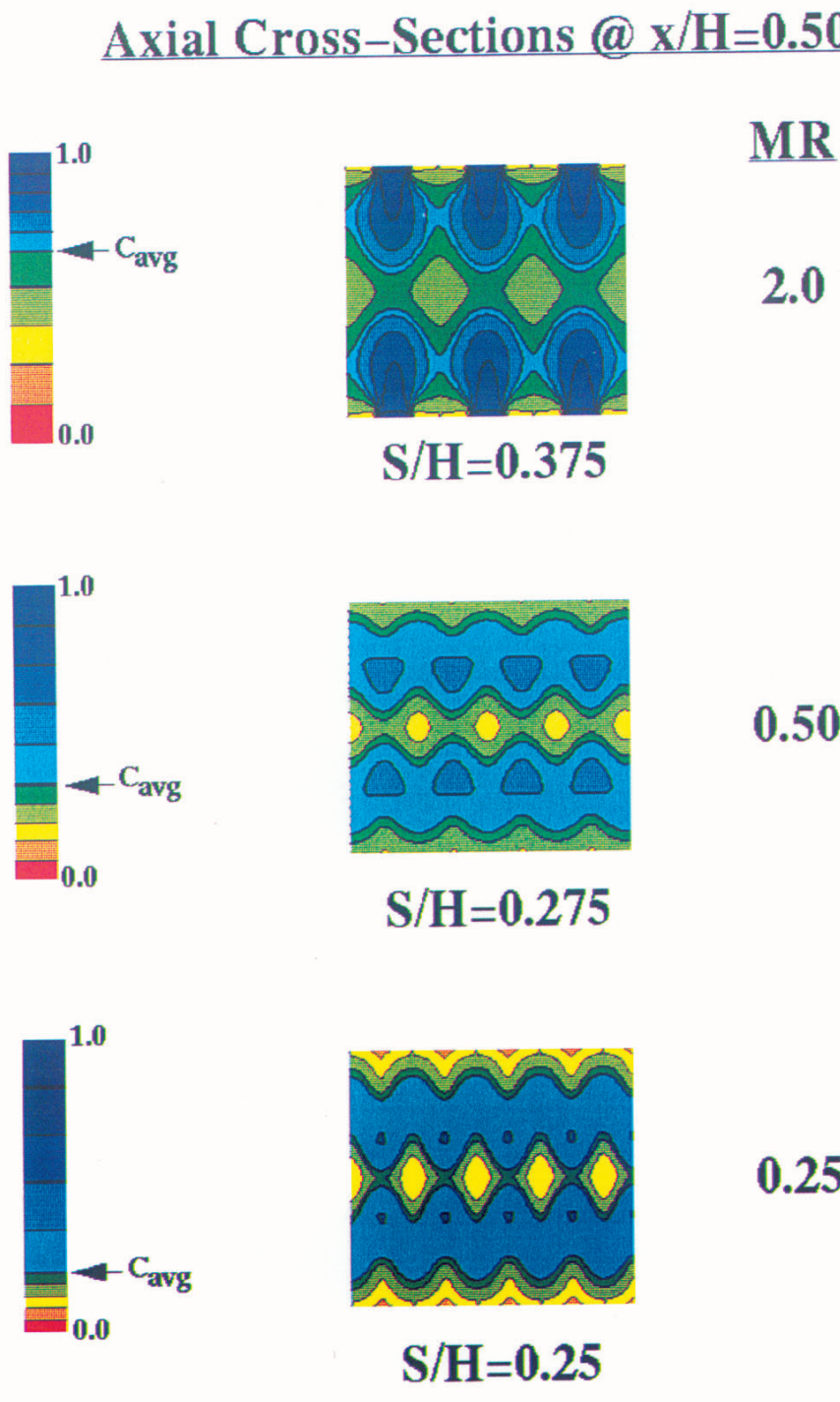

Figure 8. Effect of Jet-to-Mainstream Mass Flow Ratio on Jet Penetration: MR=2.0, J=36

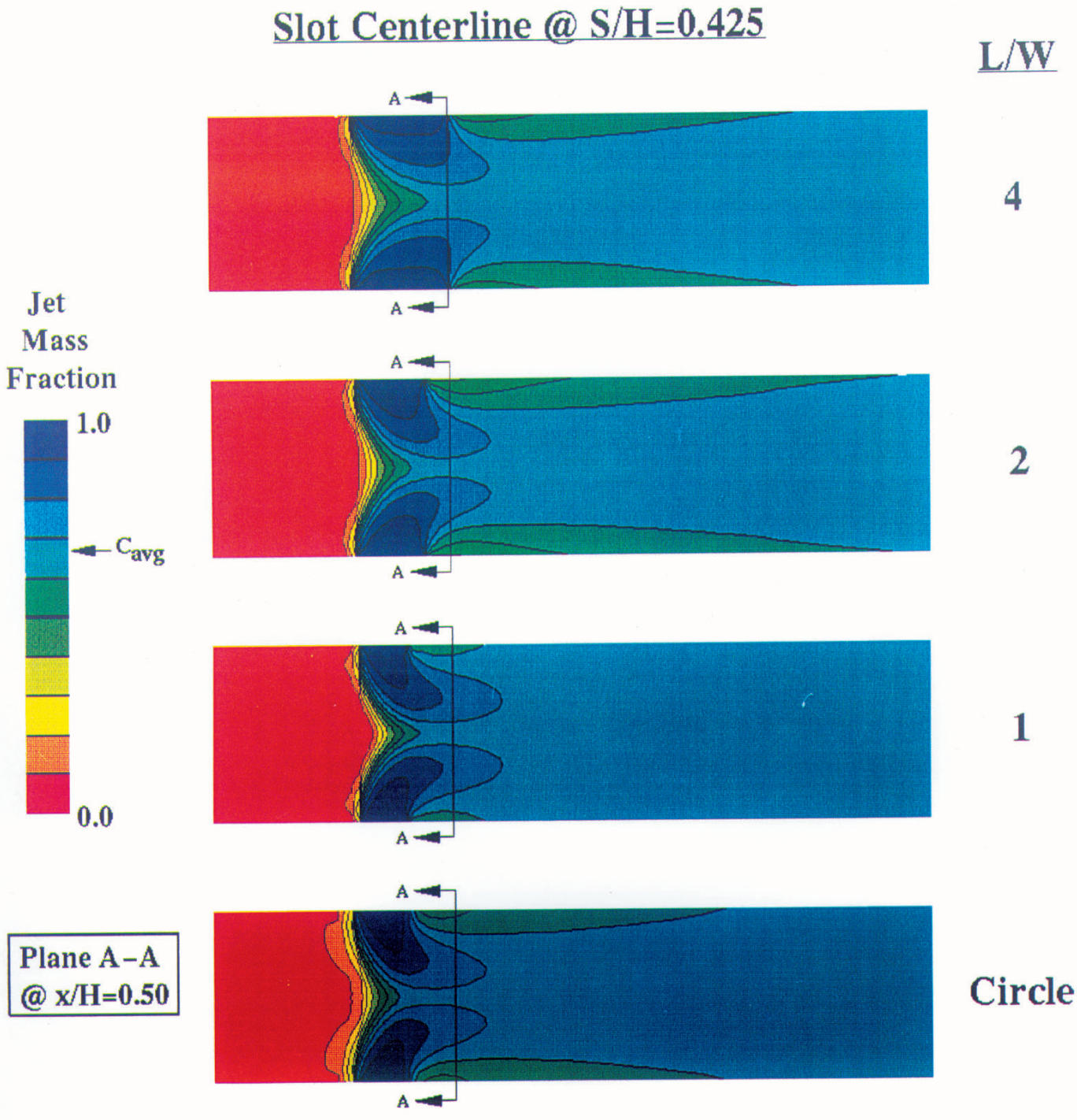

Figure 9. Effect of Aspect Ratio on Jet Penetration: MR=2.0, J=36

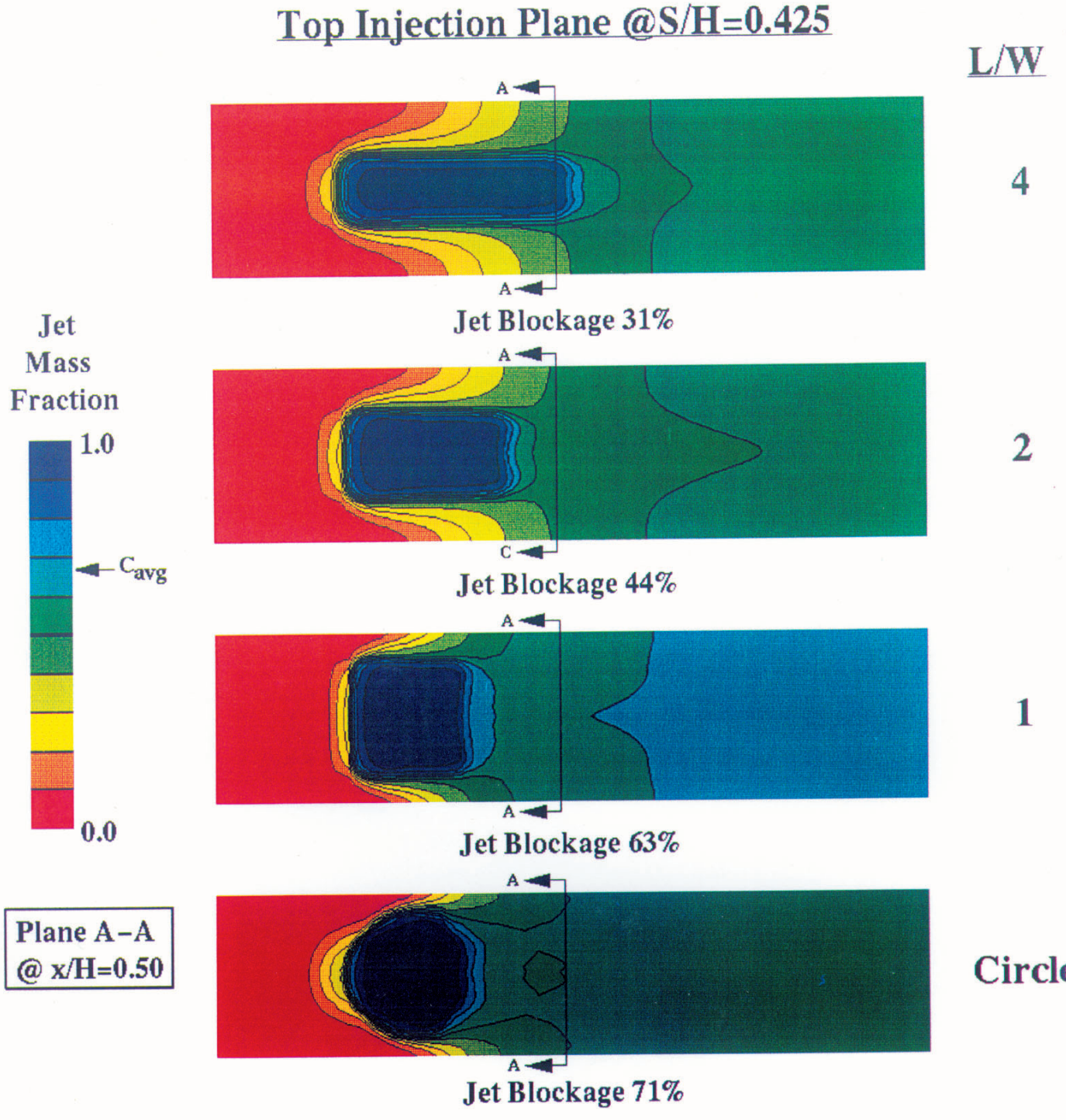

Figure 10. Effect of Aspect Ratio on Flow Characteristics at Top Wall: MR=2.0, J=36

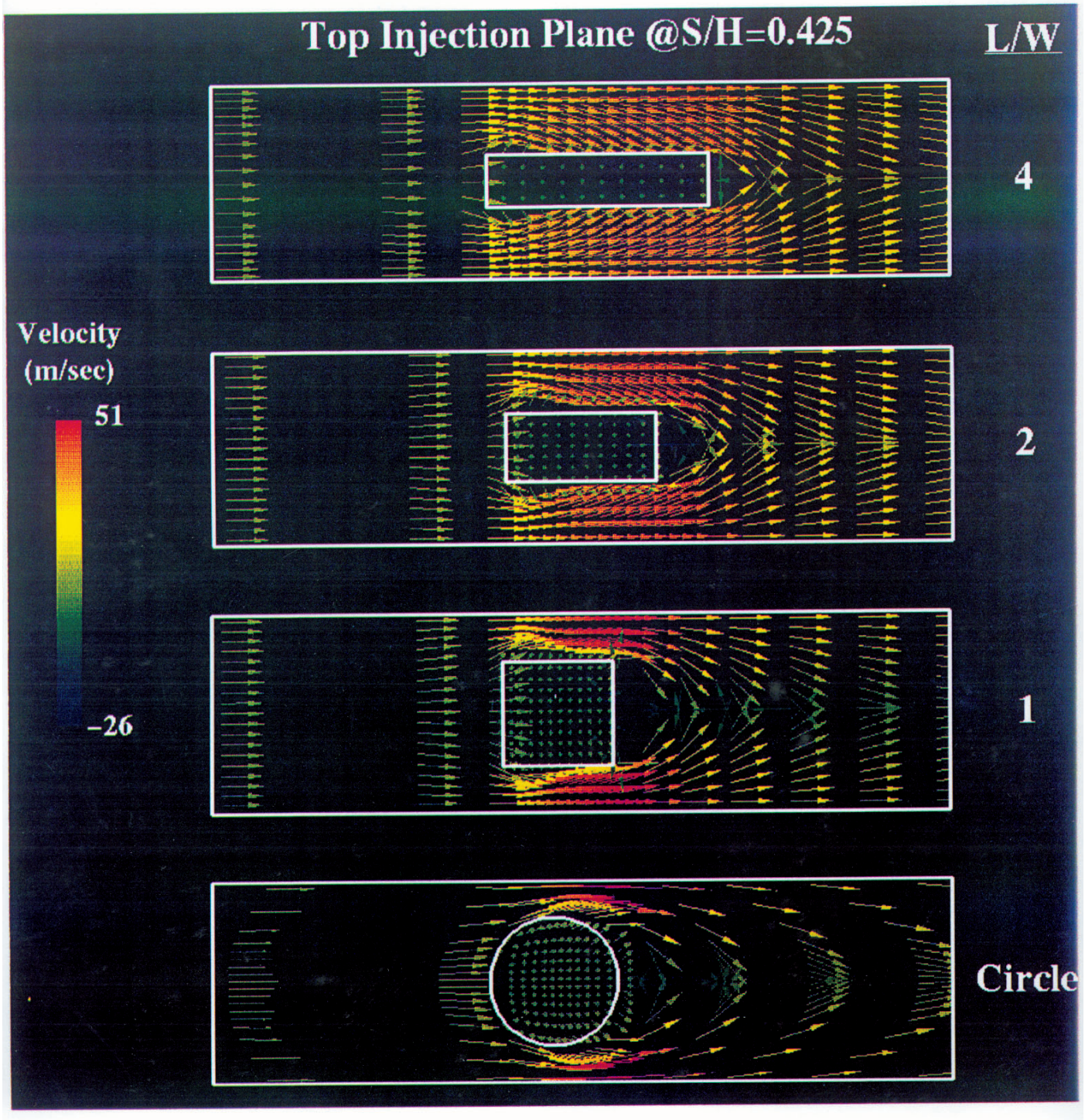

Figure 11. Effect of Aspect Ratio on Jet Wakes: MR=2.0, J=36 (Every 2nd Vector Shown)

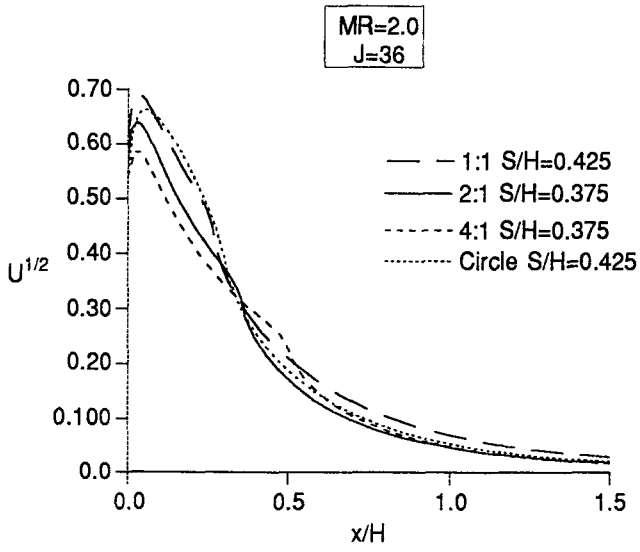

Figure 12. Effect of Aspect Ratio on Unmixedness

Axial Cross-Sections @ x/H=0.50

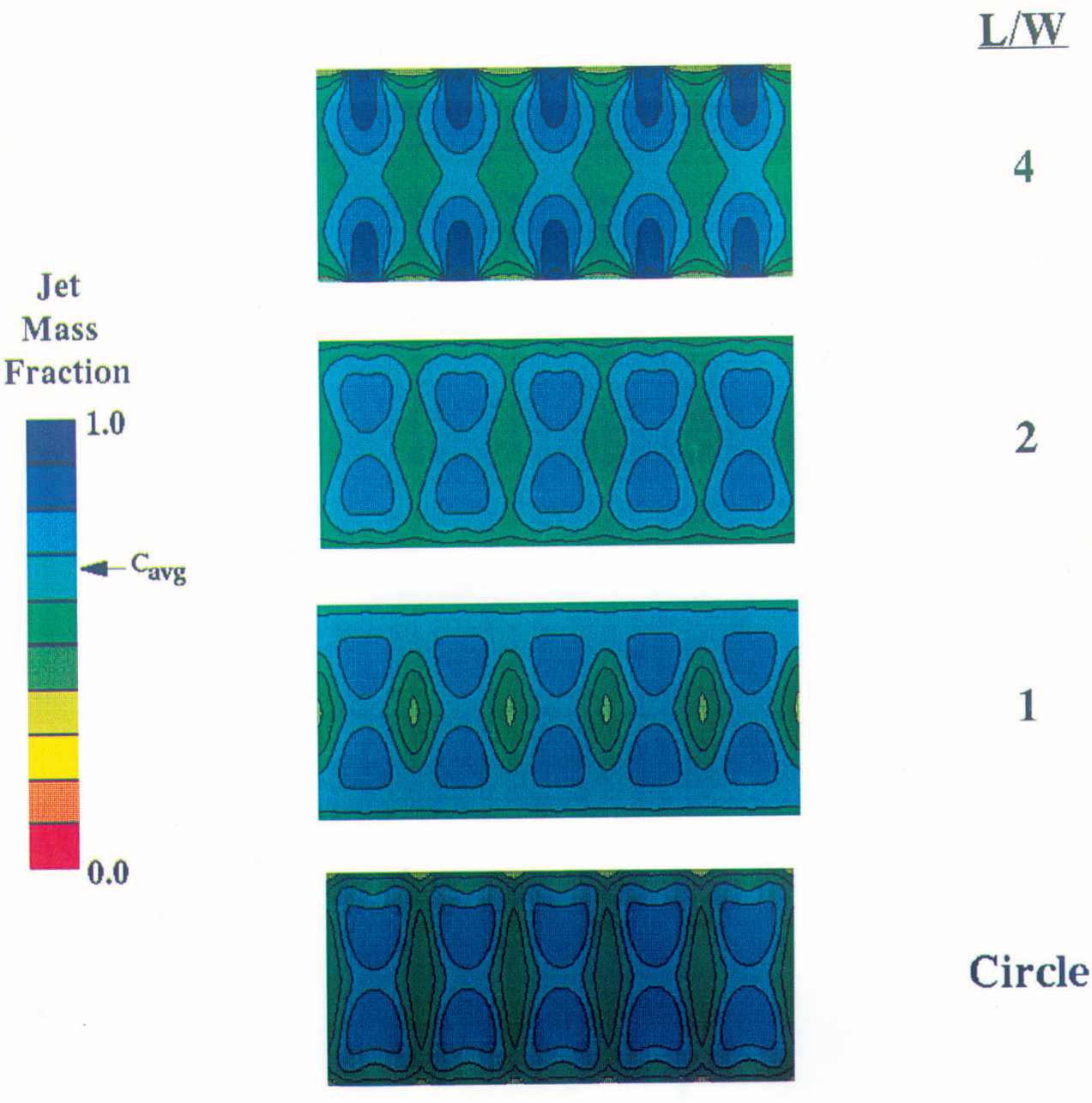

Figure 13. Effect of Aspect Ratio on Jet Penetration: MR=2.0, J=36

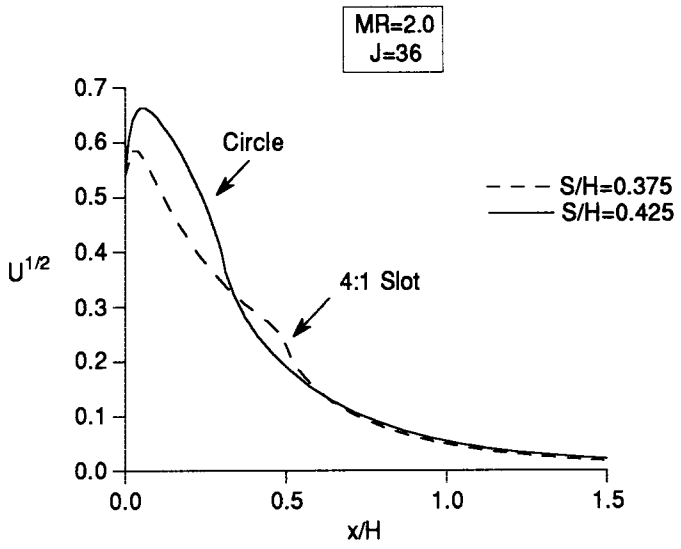

Figure 14. Unmixedness Comparison of 4:1 Slot and Circle at Optimum S/H

REPORT DOCUMENTATION PAGE

Form Approved
OMB No. 0704-0188

1. AGENCY USE ONLY (*Leave blank*)	2. REPORT DATE	3. REPORT TYPE AND DATES COVERED
	January 1994	Technical Memorandum

4. TITLE AND SUBTITLE

CFD Assessment of Orifice Aspect Ratio and Mass Flow Ration on Jet Mixing in Rectangular Ducts

5. FUNDING NUMBERS

WU–537–02–21–00

6. AUTHOR(S)

D.B. Bain, C.E. Smith, and J.D. Holdeman

7. PERFORMING ORGANIZATION NAME(S) AND ADDRESS(ES)

National Aeronautics and Space Administration
Lewis Research Center
Cleveland, Ohio 44135–3191

8. PERFORMING ORGANIZATION REPORT NUMBER

E–8276

9. SPONSORING/MONITORING AGENCY NAME(S) AND ADDRESS(ES)

National Aeronautics and Space Administration
Washington, DC 20546–0001

10. SPONSORING/MONITORING AGENCY REPORT NUMBER

NASA TM–106434
AIAA–94–0218

11. SUPPLEMENTARY NOTES

Prepared for the 32nd Aerospace Sciences Meeting and Exhibit, sponsored by the American Institue of Aeronautics and Astronautics, Reno, Nevada, January 10–13, 1994. D.B. Bain and C.E. Smith, CFD Research Corporation, Huntsville, Alabama, (work funded by NASA contract NAS3–25967); J.D. Holdeman, NASA Lewis Research Center. Responsible person, J.D. Holdeman, (216) 433–5846.

12a. DISTRIBUTION/AVAILABILITY STATEMENT

Unclassified - Unlimited
Subject Category: 07

Available electronically at http://gltrs.grc.nasa.gov/GLTRS

This publication is available from the NASA Center for AeroSpace Information, (301) 621–0390.

12b. DISTRIBUTION CODE

13. ABSTRACT ***(Maximum 200 words)***

Isothermal CFD analysis was performed on axially opposed rows of jets mixing with crossflow in a rectangular duct. Laterally, the jets' centerlines were aligned with each other on the top and bottom walls. The focus of this study was to characterize the effects of orifice aspect ratio and jet-to-mainstream mass flow ratio on jet penetration and mixing. Orifice aspect ratios (L/W) of 4–to–1, 2–to–1, and 1–to–1, along with circular holes, were parametrically analyzed. Likewise, jet-to-mainstream mass flow ratios (MR) of 2.0, 0.5, and 0.25 were systematically investigated. The jet-to-mainstream momentum-flux ratio (J) was maintained at 36 for all cases, and the orifice spacing-to-duct height (S/H) was varied until optimum mixing was attained for each configuration. The numerical results showed that orifice aspect ratio (and likewise orifice blockage) had little effect on jet penetration and mixing. Based on mixing characteristics alone, the 4–to–1 slot was comparable to the circular orifice. The 4–to–1 slot has a smaller jet wake which may be advantageous for reducing emissions. However, the axial length of a 4–to–l slot may be prohibitively long for practical application, especially for MR of 2.0. The jet-to-mainstream mass flow ratio had a more significant effect on jet penetration and mixing. For a 4–to–1 aspect ratio orifice, the design correlating parameter for optimum mixing [$C = (S/H)\sqrt{}$] varied from 2.25 for a mass flow ratio of 2.0 to 1.5 for a mass flow ratio of 0.25.

14. SUBJECT TERMS

Dilution; Jet mixing flow; Gas turbine; Combustion chamber; Emissions

15. NUMBER OF PAGES

37

16. PRICE CODE

A03

17. SECURITY CLASSIFICATION OF REPORT	18. SECURITY CLASSIFICATION OF THIS PAGE	19. SECURITY CLASSIFICATION OF ABSTRACT	20. LIMITATION OF ABSTRACT
Unclassified	Unclassified	Unclassified	

Appendix D

NASA Technical Memorandum 104466

NASA Technical Memorandum 104466
ASME-91-GT-217

CFD Analysis of Jet Mixing in Low NO_x Flametube Combustors

M.V. Talpallikar and C.E. Smith
CFD Research Corporation
Huntsville, Alabama

M.C. Lai
Wayne State University
Detroit, Michigan

and

J.D. Holdeman
Lewis Research Center
Cleveland, Ohio

Prepared for the
36th International Gas Turbine and Aeroengine Congress and Exposition
sponsored by the American Society of Mechanical Engineers
Orlando, Florida, June 3-6, 1991

NASA

CFD ANALYSIS OF JET MIXING IN LOW NO_x FLAMETUBE COMBUSTORS

M. V. Talpallikar and C. E. Smith
CFD Research Corporation
Huntsville, AL 35805

M. C. Lai
Wayne State University
Detroit, MI 48202

J. D. Holdeman
NASA Lewis Research Center
Cleveland, OH 44135

ABSTRACT

The Rich-burn/Quick-mix/Lean-burn (RQL) combustor has been identified as a potential gas turbine combustor concept to reduce NO_x emissions in High Speed Civil Transport (HSCT) aircraft. To demonstrate reduced NO_x levels, cylindrical flametube versions of RQL combustors are being tested at NASA Lewis Research Center. A critical technology needed for the RQL combustor is a method of quickly mixing by-pass combustion air with rich-burn gases.

In this study, jet mixing in a cylindrical quick-mix section was numerically analyzed. The quick-mix configuration was five inches in diameter and employed twelve radial-inflow slots. The numerical analyses were performed with an advanced, validated 3-D Computational Fluid Dynamics (CFD) code named REFLEQS. Parametric variation of jet-to-mainstream momentum flux ratio (J) and slot aspect ratio was investigated. Both non-reacting and reacting analyses were performed.

Results showed mixing and NO_x emissions to be highly sensitive to J and slot aspect ratio. Lowest NO_x emissions occurred when the dilution jet penetrated to approximately mid-radius. The viability of using 3-D CFD analyses for optimizing jet mixing was demonstrated.

NOMENCLATURE

A	Pre-exponential Factor
D	Diameter of Quick-Mix Section
D_h	Hydraulic Diameter
EI	Emission Index
E/R	Activation Energy/Gas Constant
J	Jet-to-Mainstream Momentum Flux Ratio
m_i	Mass Flow in Each Cell i
m_j	Jet Mass Flow
m_∞	Mainstream Mass Flow
σ_T	Mass Weighted Standard Deviation of Temperature
n	Optimum Number of Slots
NO_x	Oxides of Nitrogen
T_{avg}	Mass-Weighted Average Temperature
T_i	Temperature in Each Cell i
u'	RMS of U Velocity
U	Averaged Axial Velocity
v'	RMS of V Velocity
V	Averaged Radial Velocity

INTRODUCTION

In order to meet the growing need for faster transportation, High-Speed Civil Transport (HSCT) aircraft and associated propulsion systems have been under study in recent years. One major concern that has surfaced concerning HSCT engines is their impact on deteriorating the earth's ozone layer. Using current technology, a fleet of HSCT aircraft would produce large amounts of oxides of nitrogen (NO_x) while cruising in the stratosphere. Such high levels of NO_x, through a series of well known reactions, would drastically reduce ozone levels. In order to reduce NO_x emissions, technology must be developed to design advanced, low emission combustors.

One combustor concept that has been identified as a leading candidate to reduce NO_x emissions is the Rich-burn/Quick-mix/Lean-burn (RQL) combustor. Originally conceived and developed for industrial combustors (Mosier and Pierce, 1980 and Pierce *et al.* , 1980), the RQL concept utilizes staged burning, as shown in Figure 1. Combustion is initiated in a fuel rich zone at equivalence ratios between 1.2 and 1.8, thereby reducing NO_x formation by depleting the available oxygen. Bypass combustion air is introduced in a quick-mix section and lean combustion occurs downstream at an overall equivalence ratio between 0.5 and 0.7. The quick-mix section usually has a smaller geometric cross-section area than the rich burn zone in order to prevent backflow and enhance mixing.

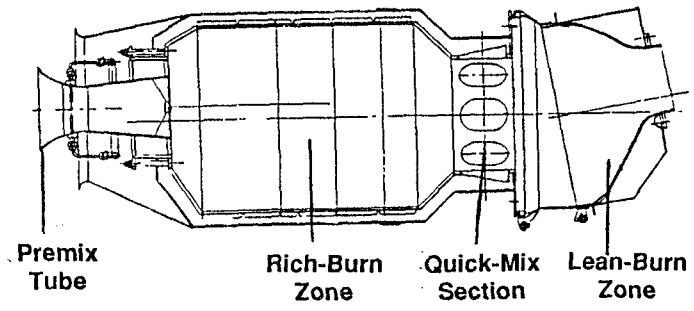

Fig. 1. Industrial Rich-burn/Quick-mix/ Lean-burn (RQL) Combustor (Pierce *et al.* , 1980)

Perhaps the single most important issue of the RQL concept is the design of the quick-mix section. For previous laboratory combustors,

Tacina (1990) has shown RQL NO_x levels to be higher than lean, premixed combustor NO_x levels. The higher NO_x emissions for RQL was attributed to stoichiometric burning in the quick-mix section, thus emphasizing the need for optimized rapid mix concepts. Indeed, Nguyen *et al.* (1989) have shown that if instantaneous mixing is assumed in the quick-mix section, low NO_x emission index can be obtained at HSCT cruise flight conditions. Hence, one challenge of the RQL concept is to identify quick-mix sections with rapid mixing.

This study sought to investigate the influence of jet-to-mainstream momentum flux ratio (J) and slot aspect ratio (SAR) on mixing effectiveness in a RQL flametube combustor to be tested at NASA Lewis Research Center (LeRC). Conventionally, dilution air in can combustors has been introduced through radial inflow holes. According to Holdeman's correlation (Holdeman *et al.*, 1987), optimum mixing occurs when the following expression is satisfied:

$$n = \pi \frac{\sqrt{2J}}{C} \tag{1}$$

where

- n = optimum number of holes
- C = experimentally derived constant ~2.5
- J = jet-to-mainstream momentum flux ratio ($\rho_j V_j^2 / \rho_\infty V_\infty^2$).

Unfortunately, this correlation was developed for circular holed dilution jet mixing and jet mass flow-to-mainstream mass flow ratios (m_j/m_∞) of approximately 0.5. The RQL combustor requires m_j/m_∞ of 2.0, thus necessitating slots instead of holes around the can's perimeter. The design of slots for optimum mixing needs further investigation, and was the focus of this study.

CFD CODE

The approach in this study was to perform 3-D numerical computations on a cylindrical quick-mix section. The goal of the study was to provide improved understanding of slot injection and mixing. An advanced CFD code, REFLEQS, was used to perform the computations. REFLEQS was developed by CFD Research Corporation (Przekwas *et al.*, 1990 and Smith *et al.*, 1988) to analyze turbulent, reacting flows. The basic capabilities/methodologies in REFLEQS include:

1. solution of two and three-dimensional Navier-Stokes equations for incompressible and compressible flows;
2. cartesian, polar, and non-orthogonal body-fitted coordinates;
3. porosity-resistivity technique for flows with internal blockages;
4. fully implicit and strongly conservative formulation;
5. three differencing schemes: upwind, hybrid, and central differencing with damping terms;
6. standard (Launder and Spalding, 1974) and extended (Chen and Kim, 1987) k-ε turbulence models, the two-scale turbulence model of Kim and Chen (1988), and the low-Reynolds number k-ε model of Chien (1985);
7. instantaneous, one-step, and two-step combustion models;
8. modified form of Stone's Strongly Implicit Solver; and
9. pressure-based solution algorithms including SIMPLE and a variant of SIMPLEC.

REFLEQS has undergone a considerable amount of systematic quantitative validation for both incompressible and compressible flows. Over 30 validation cases have been performed to date, and good-to-excellent agreement between benchmark data and predictions has been shown (Smith *et al.*, 1989; Ratcliff and Smith, 1989; and Avva *et al.*, 1990). The good agreement gives confidence in the numerical results of this study.

HEAT RELEASE MODEL

After reviewing the time scales for heat release at cruise-type conditions in RQL mixers, it was determined reaction rates were much faster than mixing rates. Hence, the combustion process was considered mixing controlled, and instantaneous reaction rates for heat release were assumed.

When rich burn gases (composed of equilibrium concentration of CO, CO_2, H_2, H_2O and N_2) were mixed with air, they were assumed to react according to the equation:

$$0.0570\,CO + 0.0197\,CO_2 + 0.0383\,H_2 + 0.0680\,H_2O + 0.1371\,N_2$$

$$+ 0.1047\,O_2 + 0.3953\,N_2$$

$$\rightarrow 0.0767\,CO_2 + 0.1063\,H_2O + 0.7123\,N_2 + 0.0565\,O_2 \tag{2}$$

Accordingly, any CO concentration that remained in the mixer exit was the result of unmixedness.

NO_x MODEL

It was assumed that the NO_x reactions did not contribute to the overall heat release in the combustor, thus allowing the NO_x reactions to be "decoupled" from the heat release reactions. NO_x was calculated as a passive scalar after the computation of the reacting flowfield.

A simple Zeldovich reaction scheme was used to model the NO_x formation. According to the mechanism, *NO* formation can be described by:

$$N_2 + O \leftrightarrow NO + N \tag{3}$$

and

$$O_2 + N \leftrightarrow NO + O. \tag{4}$$

The first reaction is much slower than the second one and hence controls the rate of *NO* formation. If the concentration of *NO* is much smaller than the corresponding equilibrium value, the rate equation for *NO* can be written as:

$$\frac{d(NO)}{dt} = K\,[N_2]\,[O] \tag{5}$$

Approximating the concentrations of N_2 and O by the local equilibrium values, the rate equation is given by

$$\frac{d\,(NO)}{dt} = A\,e^{-\left(\frac{E}{RT}\right)}[N_2][O_2]^{\frac{1}{2}} \tag{6}$$

From Quan *et al.*, (1972), the rate constants were determined to be:

$$A = 5.74 \times 10^4 \frac{1}{sec}\sqrt{\frac{moles}{m^3}} \tag{7}$$

$$\frac{E}{R} = 6.7 \times 10^{11}\,^\circ K \tag{8}$$

The NO_x model was calibrated against the experimental results of Anderson (1975), who used a premixed, prevaporized laboratory combustor. The REFLEQS test case consisted of premixed propane and air reacting in a straight channel and instantaneous heat release. The rate constants had to be modified to give good agreement with Anderson's data. The final constants used in this study were:

$$A = 3.3 \times 10^4 \frac{1}{sec}\sqrt{\frac{moles}{m^3}} \tag{9}$$

$$\frac{E}{R} = 1.03 \times 10^{14}\,^\circ K \tag{10}$$

Figure 2 shows the computed results compared to Anderson's data of Emission Index (EI) as a function of adiabatic flame temperature.

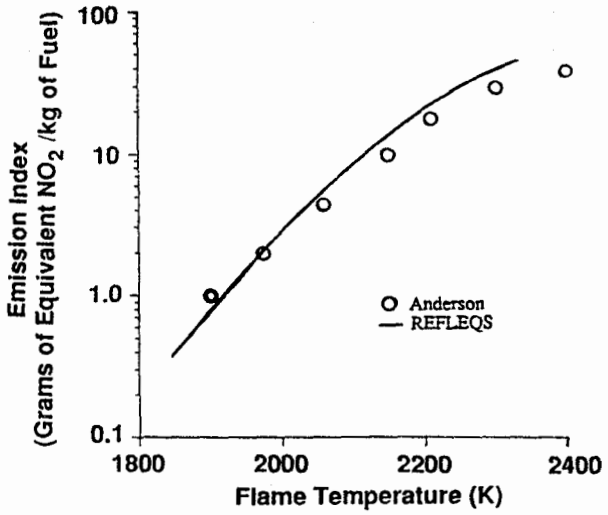

Fig. 2. Calibration of NO_x Model in REFLEQS

DETAILS OF NUMERICAL MODEL

A geometry compatible with the NASA LeRC flametube combustor was selected for analysis. The geometry, numerical grid, numerical details, boundary conditions, grid independence, and convergence criteria are discussed below.

Geometry

The geometry of the numerical model consisted of three components: an inlet pipe, converging section and a quick-mix section (see Figure 3). The inlet pipe was 0.152 m (6.0 in.) in diameter and 0.076 m (3.0 in.) in length. The inlet pipe converged into the quick-mix section which was 0.127 m (5.0 in.) in diameter (D). The length of the quick-mix section was 0.333 m (13.0 in.). In reality, the length of actual quick-mix section hardware is approximately 6 inches, but the computational domain is extended for better understanding of NO_x formation and to eliminate flowfield contamination by exit boundary conditions.

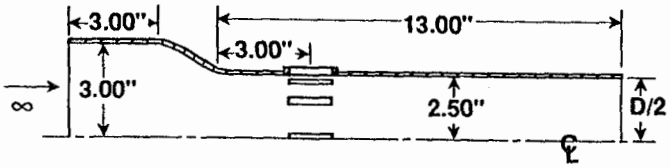

Fig. 3. Schematic of Quick-Mix Geometry

Twelve slots were located symmetrically around the perimeter of the quick-mix section. The axial location of the slot centerline was 0.076 m (3.0 in.) from the inlet of the quick-mix section. The baseline slots were rectangular in shape with an aspect ratio of four and aligned in the streamwise direction. Three variations in slot aspect ratio (SAR) were tested: 1, 4 and 16.

Due to geometric symmetry, only one slot was modeled with planes of symmetry set up halfway between adjacent slots. This allowed greater grid resolution and reduction of computer turnaround time. The rθ domain was reduced to a pie section with a central angle of thirty degrees.

Grid

A baseline grid of 9,216 cells (32x16x18 in x, r, θ directions) was selected and used for modeling the mixer. The grid is shown in Figure 4. Note that the origin of the coordinate system is located at the center of the slot. The axial grid spacing is dense near the slot, and gets coarser upstream and downstream of the slot. The grid in the radial direction was non-uniform with greater density near the combustor wall (power expansion of 1.2). The grid in the transverse direction was uniform in the slot, and slowly expanding away from the slot. The baseline slot was represented by a 6x6 mesh. As will be discussed in grid independence studies, this rather coarse grid is not grid-independent, but it does capture all of the relevant flow features. For comparative studies, it was felt sufficient.

Numerical Details

The numerical details of the calculations included:

1. Whole field solution of u-momentum, v-momentum, w-momentum, pressure correction, turbulent kinetic energy k, dissipation rate ϵ, total enthalpy, and mixture fraction;
2. Upwind Differencing for parametric studies of J and central differencing for parametric studies of SAR;
3. Variable Fluid Properties (*i.e.* temperature dependency of specific heat, laminar viscosity, *etc.*);
4. Adiabatic Walls;
5. Standard k-ϵ Model with wall functions;
6. Turbulent Prandtl number of 0.9;
7. Instantaneous heat-release model; and
8. Six active chemical species.

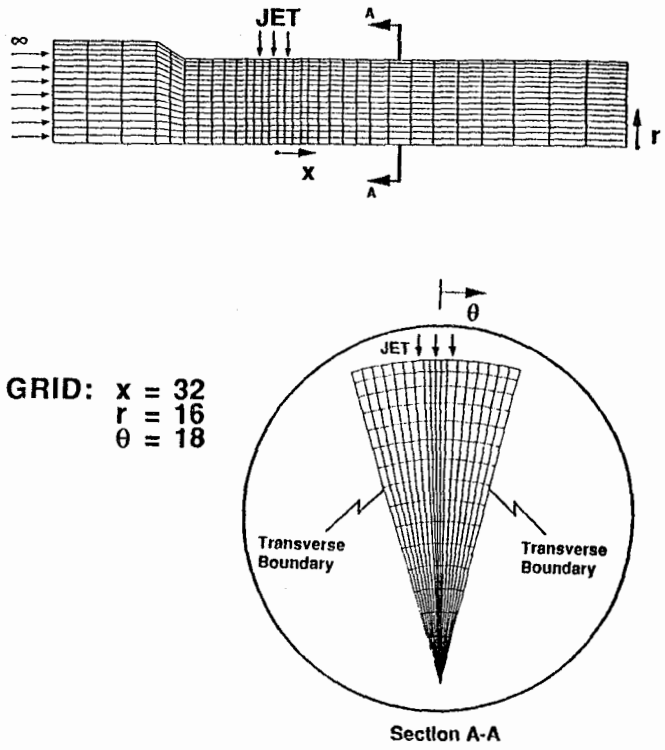

Fig. 4. Baseline Grid

Boundary Conditions

Mainstream Boundary. At the mainstream inlet boundary, propane and air are assumed to have completely reacted at an equivalence ratio (ϕ) of 1.6. The species and temperature of the reaction products were taken from the JANNAF-standard rocket code named One Dimensional Equilibrium (ODE) (Nickerson *et al.* , 1989).

Velocity and pressure were obtained from experimental test plans for the RQL flametube combustor. A uniform velocity profile was assumed with a turbulent intensity typical of primary zones in gas turbine combustors and a turbulent length scale corresponding to a turbulent viscosity 1000 times greater than laminar viscosity. The mainstream inlet conditions (at 6.0 in. diameter) were:

Axial velocity	= 35.5 m/s
Temperature	= 2221°K
Density	= 2.32 kg/m^3
Composition (mass fraction)	= 0.134 CO, 0.068 CO_2, 0.006 H_2, 0.096 H_2O, 0.696 N_2
Turbulent intensity (u′/U)	= 50%
Turbulent length scale (l_t/D_∞)	= 0.02

Since equilibrium NO_x levels are very low for ϕ of 1.6 (≈ 4 ppm), no NO_x was assumed in the mainstream inlet.

Jet Inlet. The composition at the dilution jet inlet was assumed to be air. A uniform velocity profile was assumed and turbulent properties were selected using the same logic as discussed for mainstream turbulence. The jet inlet flow conditions were:

Mass flux ratio (m_j/m_∞)	= 1.94
Jet temperature	= 811°K
Density	= 6.35 kg/m^3
Composition (mass fraction)	= 0.232 O_2, 0.768 N_2
Turbulent intensity (v′/V)	= 10%
Turbulent length scale (l_t/D_h)	= 0.13

The momentum flux ratio (J) was varied parametrically from 16 to 64 by variation of jet velocity from 120 m/s to 240 m/s. The jet velocity variation corresponded to liner pressure drops ($\Delta P/P$) of 3 to 12 percent. For each jet velocity, the slot flow area was modified to maintain constant jet flow.

Exit Boundary. The exit boundary condition was a zero gradient boundary condition.

Transverse Boundaries. The transverse boundaries were assumed to be symmetry planes. These boundaries were also tested for possible outflow by setting them to be periodic boundaries. No discernable difference was seen between cases with symmetric and periodic transverse boundaries.

Combustor Wall. The combustor wall was treated as a no-slip adiabatic wall (zero enthalpy gradient). Wall functions were used for the calculations of wall shear stress and near-wall turbulent quantities (k and ε).

Centerline. The computational boundary at the centerline was assumed to be a symmetry plane.

Grid Independence

Two different sizes of grids were run to test grid independence: 9,216 and 52,650 cells. The finer grid was obtained by increasing the grid density by ~75% in all three directions. Comparison of the two grids is shown in Figure 5.

Computational results from the two grids are presented in Figure 6 for a momentum flux ratio (J) of 32.0. The isotherms in an rx plane through the jet centerline are shown and compared. Qualitatively they exhibit similar features, although the jet penetrated a little further in the case of the fine grid. Isotherms are also shown for two axial planes: x/D = 0.0 and 2.0. The isotherms at x/D = 2.0 show slightly higher temperatures (~22°K) for the fine grid. Also, the cold region in the fine grid solution is located closer to the centerline, indicating greater penetration. However, overall the coarse grid solution is very similar to the fine grid solution.

Based on this grid-independence study, it appears the coarse grid captures the overall physics of the problem, and can be used to qualitatively compare quick-mix designs.

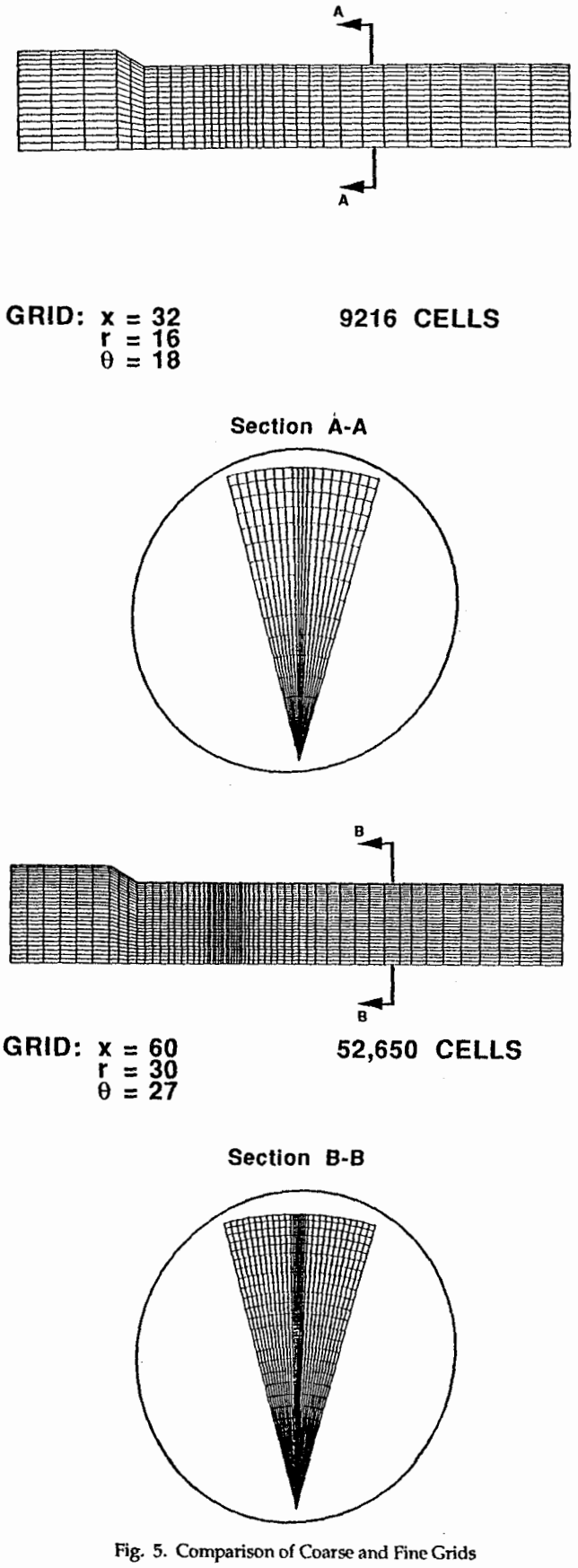

Fig. 5. Comparison of Coarse and Fine Grids

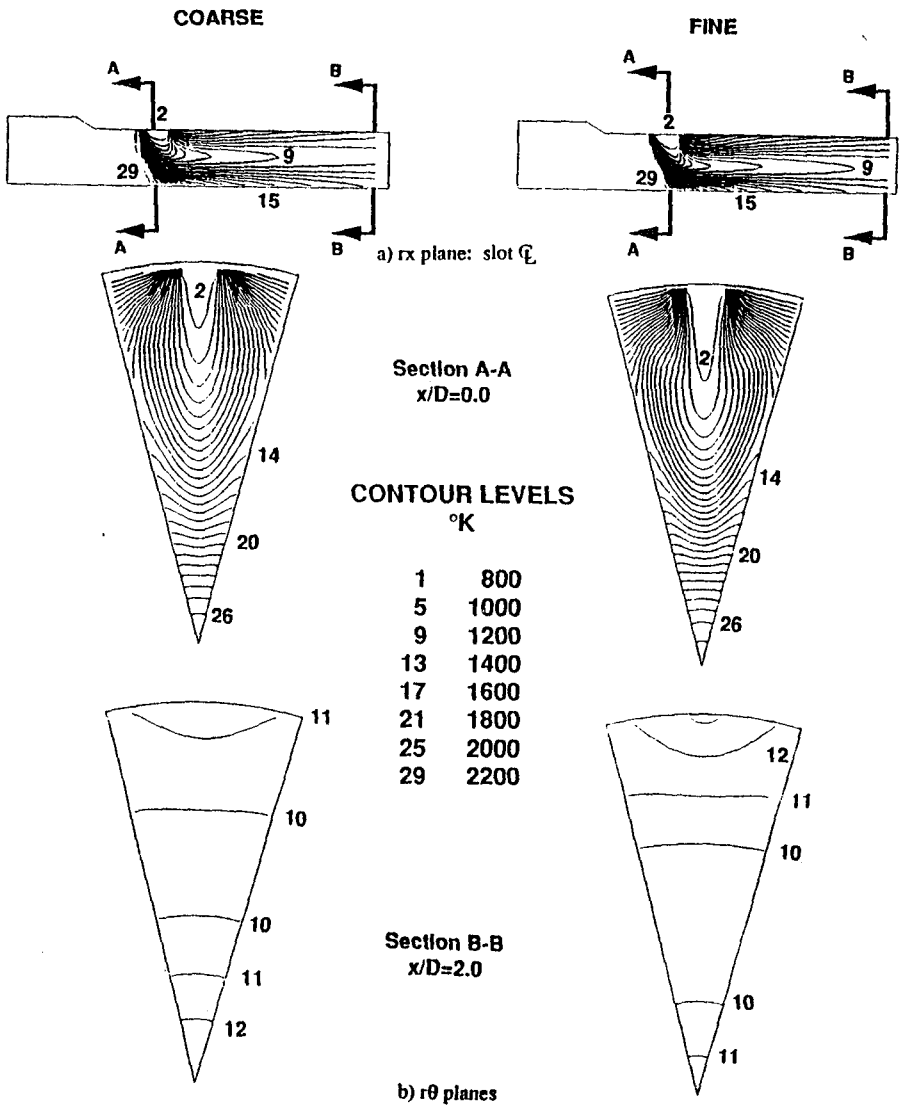

Fig. 6. Comparison of Isotherms for Coarse and Fine Grids: J=32

Convergence

The summations of all error residuals were reduced five orders of magnitude, and continuity was conserved in each axial plane. Typically, convergence required approximately 150 iterations as shown in the Figure 7. The relaxation on the velocity components (u and v only) was continuously varied during the run through a user specified input file. The repeated variation of relaxation allowed resolution of different scales of numerical error. This was found to speed up convergence by a factor of six compared to constant relaxation. Approximately 3 CPU hours were required on an Alliant FX/8 mini-supercomputer (operating on one computational element). Fine grid calculations took approximately 500 iterations and 40 CPU hours. For comparison, the ALLIANT computer speeds are ~20 times slower than a CRAY X-MP.

RESULTS

Parametric numerical tests were performed for jet-to-mainstream momentum flux ratios (J), for both non-reacting and reacting gases. Parametric variation of slot aspect ratio (SAR) was also studied. Discussion of the findings are reported below.

Variation of J: Non-Reacting Flow

Five jet-to-mainstream momentum flux ratios were parametrically tested: 16, 32, 40, 48, and 64. All other flow conditions were held constant, including mass flow ratio (jet-to-mainstream) at 1.94. To maintain a constant mass flow, the slot size was changed for each J. The slot aspect ratio was held constant at four, and was always centered at the same location. The same number of grid cells were used in all cases. However, since the slot size was changing, the grid density had to be slightly altered for each case. This variation is thought to have a minimal effect on the results discussed below.

Computed temperature contour maps are presented at x/D of 1.0, as shown in Figure 8. The radial location of the lowest temperatures indicates the penetration location of the cold jet. As expected, increased jet penetration can be seen for larger values of J. Best mixing seems to occur when the jet penetrates to approximately mid-radius. J of 32 and J of 40 appear to be optimum mixers. For comparison, the optimum J is 45.6 using Eq. (1).

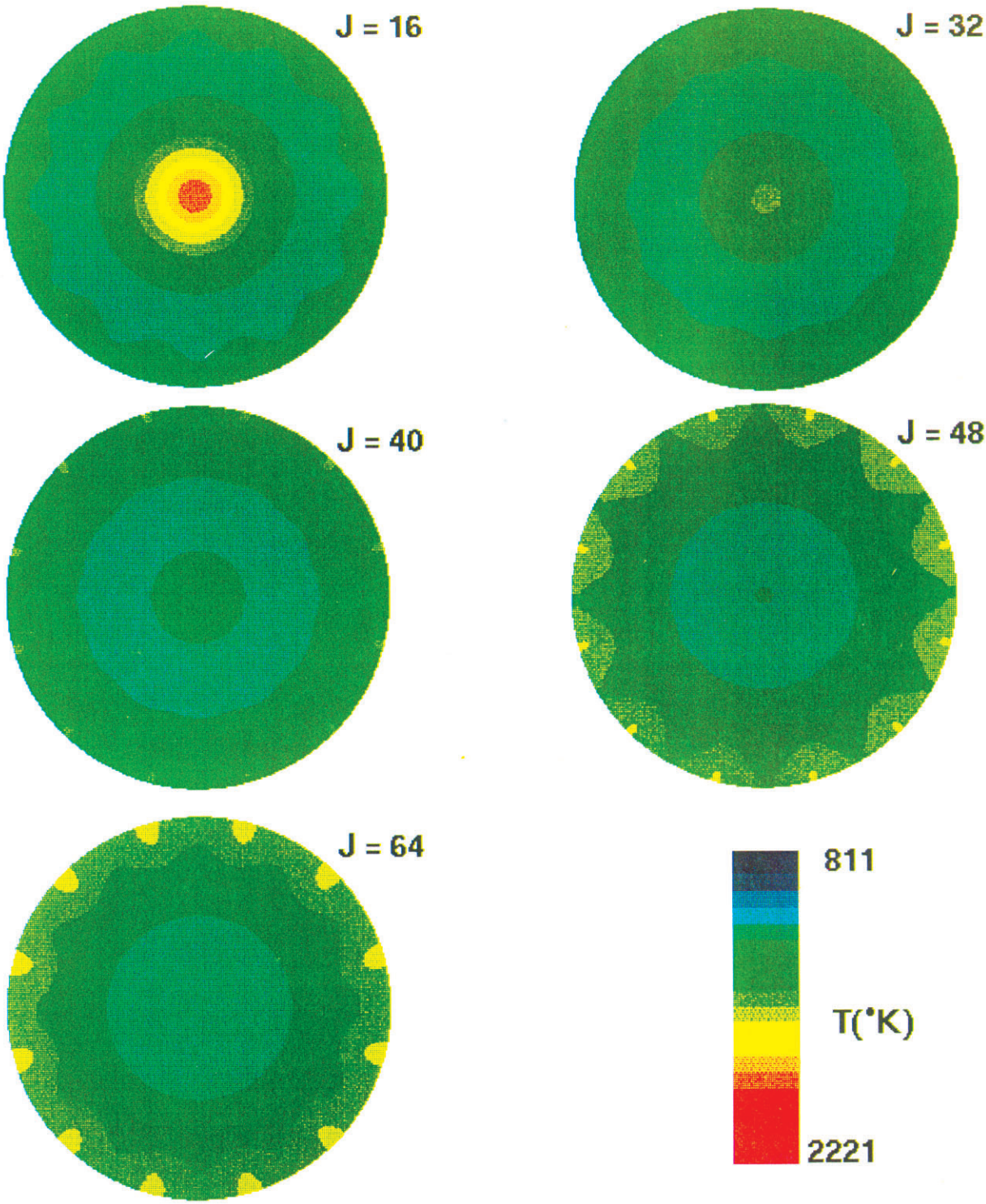

Fig 8. Temperature Contour Maps for Non-Reacting Conditions: x/D=1.0

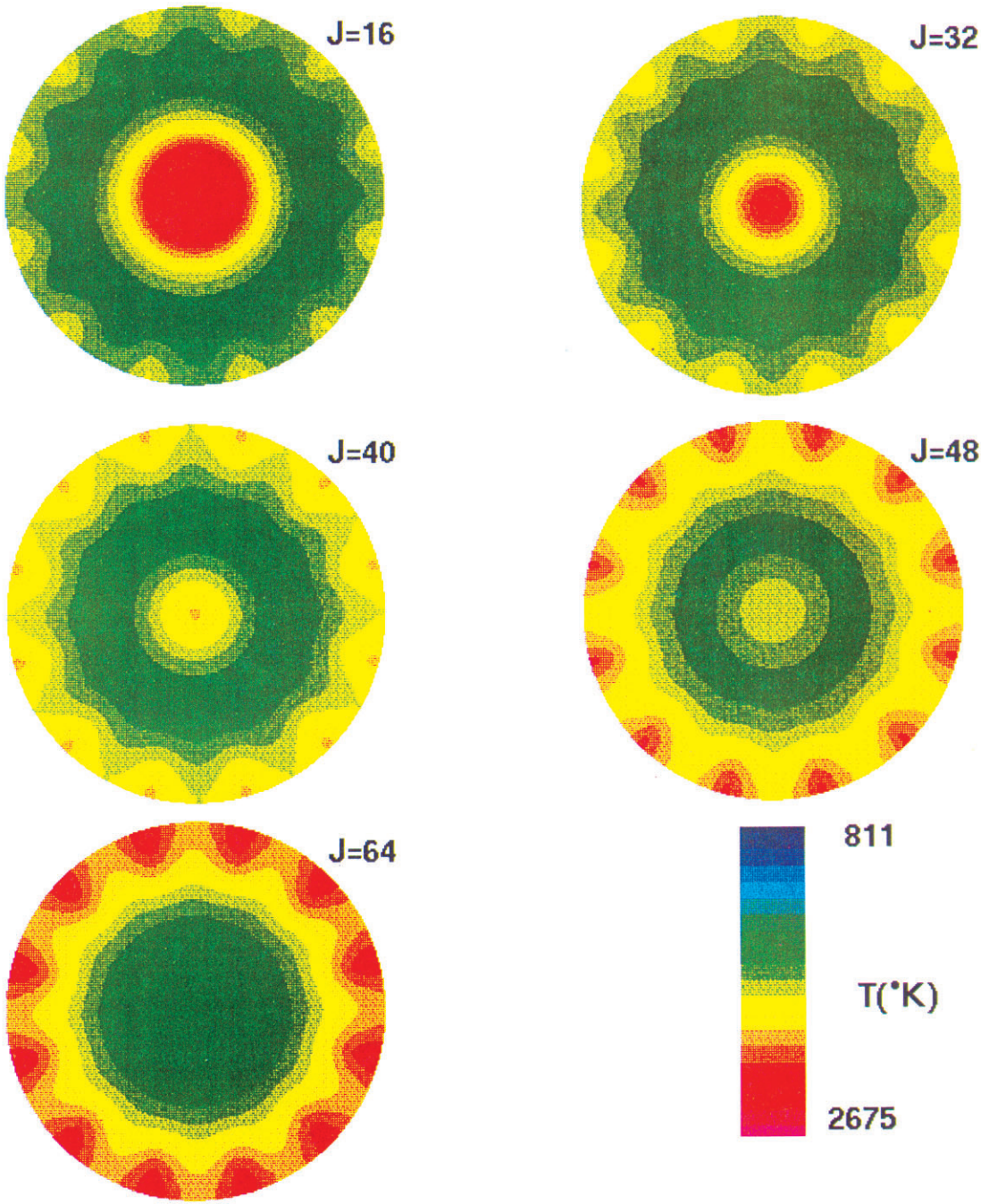

Fig 10. Temperature Contour Maps for Reacting Conditions: x/D=1.0

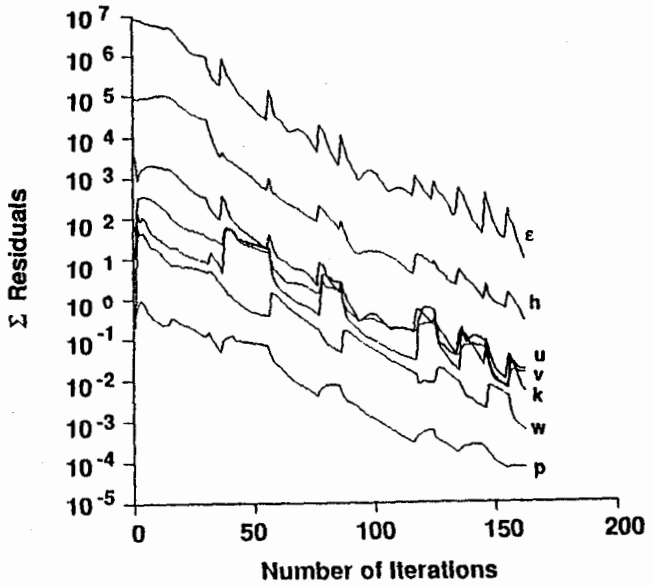

Fig. 7. Convergence History for a Typical Run

For a more quantitative comparison of mixing effectiveness, the mass-weighted standard deviation of temperature (σ_T) was calculated for each case. σ_T was defined as:

$$\sigma_T = \frac{\sqrt{\frac{\sum_i m_i (T_i - T_{avg})^2}{\sum_i m_i}}}{T_{avg}} \qquad (11)$$

In Figure 9, σ_T is presented versus J. It can be seen that J of 32 has the lowest σ_T at x/D = 2.0. Underpenetration is worse than overpenetration in terms of σ_T.

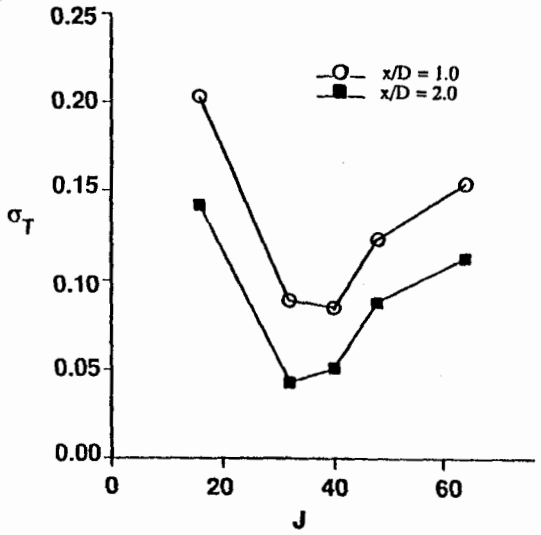

Fig. 9. Mixing Effectiveness: Non Reacting Flow

Variation of J: Reacting Flow

The same cases were analyzed as discussed above, except chemical reaction was turned on. Due to reaction, the overall mass-averaged exit temperature increased from 1301°K for non-reacting flows to 1790°K for reacting flows. Figure 10 shows temperature contour maps for the reacting cases one diameter downstream of the jet center. From this figure, it appears that J = 40 is the best mixer. This can be further elucidated by looking at the mixing effectiveness (σ_T) shown in Figure 11. Figure 11 shows J = 40 to be the best mixer at x/D = 1.0 and 2.0.

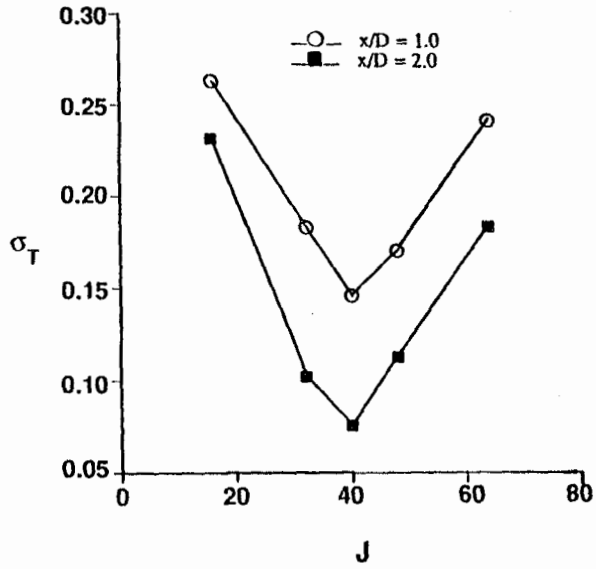

Fig. 11. Mixing Effectiveness: Reacting Flow

In addition to mixing effectiveness, another important criterion for evaluation of quick-mix sections is combustion efficiency. In particular, CO concentrations should be essentially eliminated from the combustor exit. The CO emission level in various axial planes downstream of the dilution jet is displayed in Figure 12. For all cases except J = 16, it can be seen that the CO species has been oxidized (to CO_2) by x/D = 0.25. For J = 16, unreacted CO remains in the flowfield even at x/D = 2.0. This is due to jet underpenetration, thus allowing rich burn gases (containing CO) on the centerline to pass through the quick-mix section without contact with dilution air.

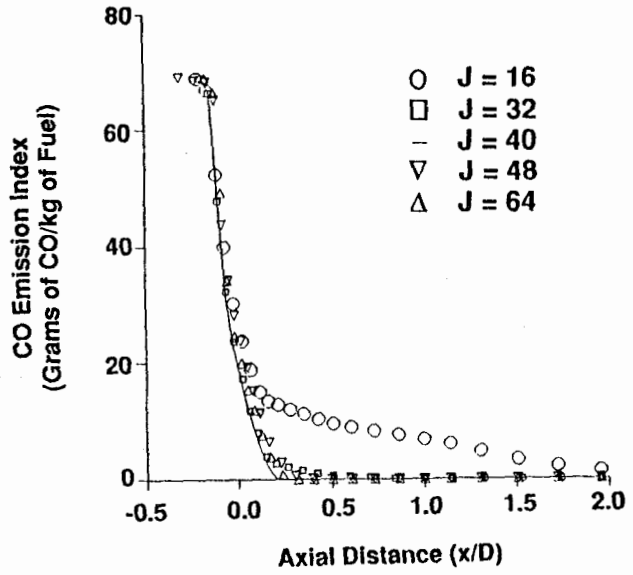

Fig. 12. Predicted CO Emissions

The NO_x results are presented in terms of Emission Index (EI) in Figure 13. For the optimum case (J_{opt}=40), EI is 2.9 at x/D = 2.0. Significant increase in EI is predicted as J is increased or decreased from the optimum value. For J greater than J_{opt}, jet overpenetration causes jet backflow on the centerline, resulting in higher NO_x emissions. For J less than J_{opt}, underpenetration of the jet results in reaction (and high temperatures) on the combustor centerline.

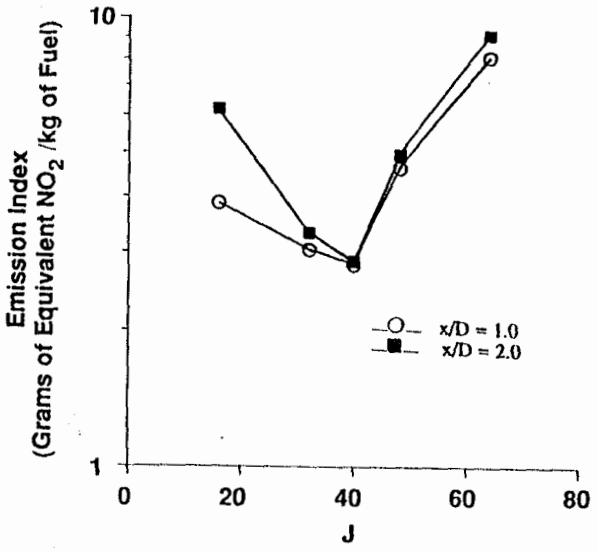

Fig. 13. Predicted NO_x Emission Index

Figure 14 shows NO_x concentrations convected out of each axial plane. Except for J = 16, all the cases show very little NO_x formation downstream of x/D = 1.0. This indicates that high temperature zones are no longer existent. For the J = 16 case, NO_x formation is increasing significantly downstream of x/D = 1.0, indicating high temperature and chemical reaction is still taking place.

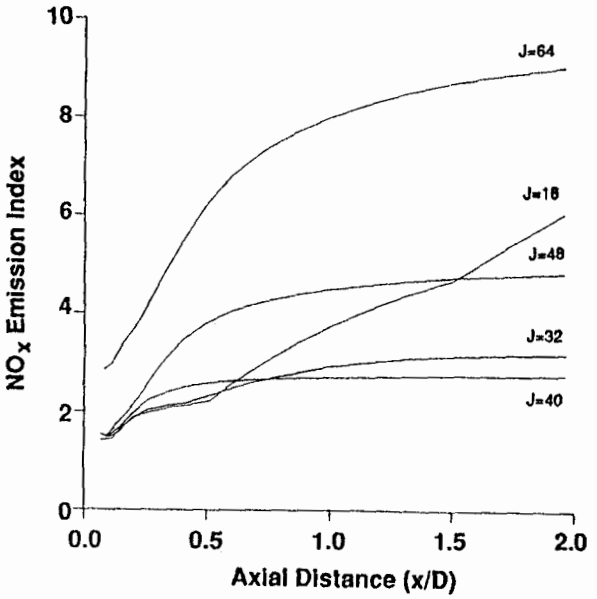

Fig. 14. History of NO_x Formation in Mixer

Variation of Slot Aspect Ratio

Three slot aspect ratios (SAR) were numerically analyzed: 1, 4 and 16. The long dimension was aligned in the mainstream flow direction. The numerical grid was slightly modified for each slot, and central differencing was employed for increased accuracy. The jet-to-mainstream momentum flux ratio and mass flow ratio was maintained constant at 32 and 1.94 respectively.

Isotherms in the rx plane through the jet centerline are shown in Figure 15. As SAR increased, jet penetration increased (as seen in Figure 15). This is due to reduced flow blockage as SAR is increased. Figure 16 shows the effect of SAR on NO_x emissions. For SAR of 1, predicted NO_x levels are less than those for SAR of 4, but chemical reaction and NO_x formation is still occurring at x/D of 1 due to jet underpenetration. This is evidenced by the steep slope of the NO_x curve at x/D of 1. A similar effect of delayed NO_x formation on the centerline caused by jet underpenetration was shown in Figure 14 for J of 16 and SAR of 4. Hence, the best SAR is 4, with jet overpenetration for SAR of 16 (and corresponding higher NO_x levels).

These results suggest the importance of SAR on NO_x emissions. As was shown earlier for J variation, the jet must penetrate to approximately mid-radius for optimum mixing, and hence lowest NO_x.

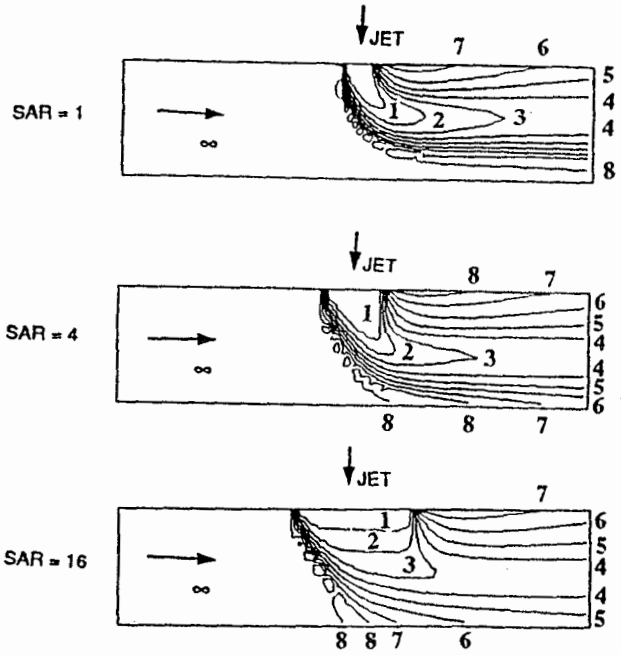

Fig. 15. Isotherms in rx Plane Through Jet Centerline: Effect of Slot Aspect Ratio (SAR)

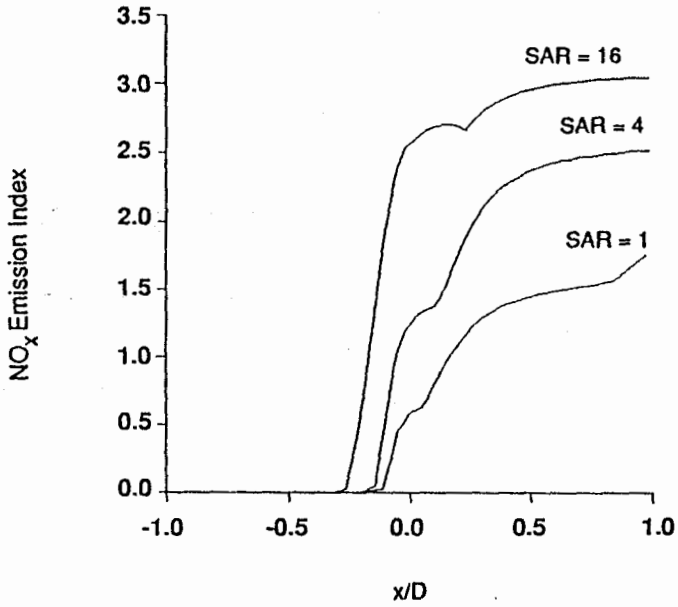

Fig. 16. Effect of Slot Aspect Ratio (SAR) on NO_x Emissions

CONCLUSIONS

The overall conclusions of this study were:

1. The viability of using 3-D CFD to model and screen quick-mix concepts of low emission combustors was successfully demonstrated.
2. A five-inch diameter quick-mix section compatible with the NASA LeRC Low Emission Combustor Program was numerically analyzed. The configuration consisted of twelve, radial-inflow slots uniformly distributed around the perimeter of the quick-mix section. Optimum mixing for non-reacting flow occurred for a jet-to-mainstream momentum flux ratio (J) between 32 and 40. For reacting flow, the NO_x emission index was shown to be highly sensitive to J, with the lowest value of 2.9 calculated for J of 40 (at x/D = 2.0).
3. The numerical results suggest that slot aspect ratio has a pronounced effect on jet penetration and mixing effectiveness. Conventional correlations for optimum mixing effectiveness for holes may not be applicable for slots.

ACKNOWLEDGEMENTS

The authors wish to thank NASA Lewis Research Center for funding this work under NASA Contract NAS3-25834. Our thanks also are extended to Drs. Laurence Keeton, H.Q. Yang, Andrzej Przekwas, Anantha Krishnan and Mr. Sami Habchi of CFD Research Corporation.

REFERENCES

Anderson, D., 1975, "Effect of Equivalence Ratios and Dwell Time on Exhaust Emissions from an Experimental Premixed Prevaporizing Burner," NASA TMX-71592.

Avva, R. K., Smith, C. E., and Singhal, A. K., 1990, "Comparative Study of High and Low Reynolds Number Versions of k- Models," AIAA-90-0246, 28*th Aerospace Sciences Meeting*.

Chen, Y. S., and Kim, S. W., 1987, "Computation of Turbulent Flows Using an Extended k-ε Turbulence Closure Model," NASA CR-179204.

Chien, K. Y., 1985, "Predictions of Channel and Boundary-Layer Flows with a Low-Reynolds-Turbulence Model," *AIAA Journal*, Vol. 23, No. 2.

Holdeman, J. D., Reynolds, R. and White, C., 1987, "A Numerical Study of the Effects of Curvature and Convergence on Dilution Jet Mixing," AIAA-87-1953, AIAA/SAE/ASME/ASEE 23*rd Joint Propulsion Conference*.

Kim, S. W., and Chen, C. P., 1988, "A Multiple Time Scale Turbulence Model Based on Variable Partitioning of Turbulent Kinetic Energy Spectrum," AIAA-88-1771.

Launder, B. E., and Spalding, D. B., 1974, "The Numerical Computation of Turbulent Flows," *Computer Methods in Applied Mechanics and Engineering*, Vol. 3, pp. 269-289.

Mosier, S. A., and Pierce, R. M., 1980, "Advanced Combustion Systems for Stationary Gas Turbine Engines," Vol. I, EPA Contract 68-02-2136.

Nguyen, H., Bittker, D., and Niedzwiecki, R., 1989, "Investigation of Low NO_x Staged Combustor Concept in High Speed Civil Transport Engines," AIAA-89-2942, AIAA/ASME/SAE/ASEE 25*th Joint Propulsion Conference*.

Nickerson, G. R., Coats, D. E., Dang, A. L., Dunn, S. S., and Kehtarnavaz, H., 1989, "Two-Dimensional Kinetics TDK Nozzle Performance Computer Program; Vol II: Programming Manual," NAS8-36863.

Pierce, R. M., Smith, C. E., and Hinton, B. S., 1980, "Advanced Combustion Systems for Stationary Gas Turbine Engines," Vol. III, EPA Contract 68-02-2136.

Przekwas, A. J., Habchi, S. D., Yang, H. Q., Avva, R. K., Talpallikar, M. V., and Krishnan, A., 1990, "REFLEQS-3D: A Computer Program for Turbulent Flows With and Without Chemical Reaction, Volume 1: User's Manual," CFD Research Corp., Huntsville, AL, CFDRC Report GR-89-4.

Quan, V., Marble, F. E., and Kliegel, J. R., 1972, "Nitric Oxide Formation in Turbulent Diffusion Flames," 14*th* Symposium on Combustion, pp. 851-860.

Ratcliff, M. L., and Smith, C. E., 1989, "REFLEQS-2D: A Computer Program for Turbulent Flow with and without Chemical Reaction; Volume 2: Validation Manual," CFD Research Corp., Huntsville, AL, CFDRC Report GR-88-4.

Smith, C. E., Ratcliff, M. L., Przekwas, A. J., Habchi, S. D., and Singhal, A. K., 1988, "Modeling of Turbulent Combustion in Liquid Rocket Engine Components," NASA MSFC Contract NAS8-37619, SBIR Phase I Final Report, CFDRC Report 4045/1.

Smith, C. E., Ratcliff, M. L., Przekwas, A. J., and Habchi, S. D., 1989, "Validation of an Advanced Turbulent Combustion Code: REFLEQS," 7*th* SSME CFD Workshop, NASA MSFC.

Tacina, R. R., 1990, "Low NO_x Potential Of Gas Turbine Engines," AIAA-90-0550, 28*th Aerospace Sciences Meeting*.

REPORT DOCUMENTATION PAGE

Form Approved
OMB No. 0704-0188

1. AGENCY USE ONLY (*Leave blank*)	2. REPORT DATE	3. REPORT TYPE AND DATES COVERED
	June 1991	Technical Memorandum

4. TITLE AND SUBTITLE

CFD Analysis of Jet Mixing in Low NO_x Flametube Combustors

5. FUNDING NUMBERS

WU–537–02–21–00

6. AUTHOR(S)

M.V. Talpallikar, C.E. Smith, M.C. Lai, and J.D. Holdeman

7. PERFORMING ORGANIZATION NAME(S) AND ADDRESS(ES)

National Aeronautics and Space Administration
Lewis Research Center
Cleveland, Ohio 44135–3191

8. PERFORMING ORGANIZATION REPORT NUMBER

E–6313

9. SPONSORING/MONITORING AGENCY NAME(S) AND ADDRESS(ES)

National Aeronautics and Space Administration
Washington, DC 20546–0001

10. SPONSORING/MONITORING AGENCY REPORT NUMBER

NASA TM–104466
ASME–91–GT–217

11. SUPPLEMENTARY NOTES

Prepared for the 36th International Gas Turbine and Aeroengine Congress and Exposition sponsored by the American Society of Mechanical Engineers, Orlando, Florida, June 3–6, 1991. M.V. Talpallikar and C.E. Smith, CFD Research Corporation, Huntsville, Alabama 35805 (work funded by NASA Contract NAS3–25834). M.C. Lai, Wayne State University, Detroit, Michigan 48202. J.D. Holdeman, NASA Lewis Research Center, (216) 433–5846.

12a. DISTRIBUTION/AVAILABILITY STATEMENT

Unclassified - Unlimited
Subject Category: 07

Available electronically at http://gltrs.grc.nasa.gov/GLTRS

This publication is available from the NASA Center for AeroSpace Information, (301) 621–0390.

12b. DISTRIBUTION CODE

13. ABSTRACT ***(Maximum 200 words)***

The Rich-burn/Quick-mix/Lean-burn (RQL) combustor has been identified as a potential gas turbine combustor concept to reduce NO_x emissions in High Speed Civil Transport (HSCT) aircraft. To demonstrate reduced NO_x levels, cylindrical flametube versions of RQL combustors are being tested at NASA Lewis Research Center. A critical technology needed for the RQL combustor is a method of quickly mixing by-pass combustion air with rich-burn gases. In this study, jet mixing in a cylindrical quick-mix section was numerically analyzed. The quick-mix configuration was five inches in diameter and employed twelve radial-inflow slots. The numerical analyses were performed with an advanced, validated 3-D Computational Fluid Dynamics (CFD) code named REFLEQS. Parametric variation of jet-to-mainstream momentum flux ratio (J) and slot aspect ratio was investigated. Both non-reacting and reacting analyses were performed. Results showed mixing and NO_x emissions to be highly sensitive to J and slot aspect ratio. Lowest NO_x emissions occurred when the dilution jet penetrated to approximately mid-radius. The viability of using 3-D CFD analyses for optimizing jet mixing was demonstrated.

14. SUBJECT TERMS	15. NUMBER OF PAGES
Dilution; Jet mixing flow; Gas turbines; Combustion chamber; Can; Emissions	14
	16. PRICE CODE: A03

17. SECURITY CLASSIFICATION OF REPORT	18. SECURITY CLASSIFICATION OF THIS PAGE	19. SECURITY CLASSIFICATION OF ABSTRACT	20. LIMITATION OF ABSTRACT
Unclassified	Unclassified	Unclassified	

Appendix E

NASA Technical Memorandum 104411

NASA Technical Memorandum 104411
AIAA-90-2460

A CFD Study of Jet Mixing in Reduced Flow Areas for Lower Combustor Emissions

C.E. Smith and M.V. Talpallikar
CFD Research Corporation
Huntsville, Alabama

and

J.D. Holdeman
Lewis Research Center
Cleveland, Ohio

Prepared for the
27th Joint Propulsion Conference
cosponsored by the AIAA, SAE, ASME, and ASEE
Sacramento, California, June 24-27, 1991

NASA

A CFD STUDY OF JET MIXING IN REDUCED FLOW AREAS FOR LOWER COMBUSTOR EMISSIONS

C. E. Smith*
M. V. Talpallikar**
CFD Research Corporation
Huntsville, AL 35805

J. D. Holdeman***
NASA Lewis Research Center
Cleveland, OH 44135

Abstract

The Rich-burn/Quick-mix/Lean-burn (RQL) combustor has the potential of significantly reducing NO_x emissions in combustion chambers of High Speed Civil Transport (HSCT) aircraft. Previous work on RQL combustors for industrial applications suggested the benefit of "necking down" the mixing section. In this study, a 3D numerical investigation was performed to study the effects of neckdown on NO_x emissions and to develop a correlation for optimum mixing designs in terms of neckdown area ratio. The results of the study showed that jet mixing in reduced flow areas does not enhance mixing, but does decrease residence time at high flame temperatures, thus reducing NO_x formation. By necking down the mixing flow area by four, a potential NO_x reduction of sixteen-to-one is possible for annular combustors. However, there is a penalty that accompanies the mixing neckdown: reduced pressure drop across the combustor swirler. At conventional combustor loading parameters, the pressure drop penalty does not appear to be excessive.

1. Introduction

The design of low NO_x combustors is a subject of ongoing research at NASA Lewis Research Center as applied to High Speed Civil Transport (HSCT) aircraft. One combustor design presently under study is the Rich-burn/Quick-mix/Lean-burn (RQL) combustor. Originally conceived and developed for industrial combustors[1-2], the RQL concept utilizes staged burning, as shown in Figure 1. Combustion is initiated in a fuel rich zone at equivalence ratios between 1.2 and 1.8, thereby reducing NO_x formation by depleting the available oxygen. Bypass air is introduced in a quick-mix section and lean combustion occurs downstream at equivalence ratios between 0.5 and 0.7. A key design technology required for the RQL combustor is a method of rapidly mixing bypass air with rich-burn gases. Rapid and uniform mixing is required for producing low amounts of NO_x while oxidizing CO produced in the rich-burn section.

Generic research on dilution jet mixing in gas turbine combustors has been performed in the past[3], and is applicable to RQL combustors. Good

* Manager, Application Projects
Member AIAA
** Project Engineer
Member AIAA
*** Senior Research Engineer
Member AIAA

engineering correlations were developed for optimum mixing of dilution jets in can, rectangular and annular geometries[4]. In search of improved mixing schemes, recent work has been performed on staggered dilution jets in rectangular geometries[5], asymmetric jets in can geometries[6], and slots in can geometries[7].

An important aspect of jet mixing that warranted further investigation was the effect of "necking down" the mixing flow area. The mixing section has been typically necked down in RQL combustors to promote better mixing and prevent backflow[8-11]. In Reference 2 it was experimentally shown that neckdown of the mixing section produced lower NO_x emissions. The experiments did not provide the data base to identify why neckdown produced lower NO_x emissions or how to optimize NO_x reduction. Hence, this study was undertaken to investigate the effects of area reduction on NO_x formation in the mixing section, and to develop design correlations to optimize mixing in reduced areas.

2. Approach

Parametric numerical calculations were performed to quantify potential improvement from neckdown and to understand the physical mechanisms causing low NO_x. Both 3-D CFD numerical analysis and 1-D analysis were employed. The 3-D numerical calculations were made using the CFD code named REFLEQS. REFLEQS has been developed to analyze turbulent reacting flows[12], and has undergone a considerable amount of systematic quantitative validation for both incompressible and compressible flows. Over 30 validation cases have been performed to date, and good to excellent agreement between data and predictions has been shown[13-14]. Further, it has been shown that REFLEQS is a viable tool in modelling complex geometries and intricate flow patterns involved in mixing concepts of low emission combustors[5-7].

The study was divided into four parts. First, a baseline mixing configuration was analyzed and assessed for grid independence. Second, the baseline configuration was optimized in terms of number of slots. Third, a parametric variation of the mixing diameter (from six inches down to four inches) was performed to understand the cause of NO_x reduction in reduced flow area. And finally, a 1-D computer code was used to calculate the overall pressure loss of a combustor and to assess the penalty of mixing in a neckdown section. Each part of the study will be discussed in the following sections.

3. Baseline Case

Geometry

A "no neckdown" case was selected as the baseline. The baseline configuration (see Figure 2) consisted of three components: inlet pipe, converging section, and mixing section. The inlet pipe was 6.0 inches (0.152 m) in diameter and 3.0 inches (0.0762 m) in length. The convergence section connected the inlet pipe to the mixing section and was 0.866 inches (0.022 m) in length. The mixing section had a diameter of six inches (*i.e.* no neckdown) and had twelve equally-spaced slots located on its perimeter. The slots' centerlines were located one mixing section diameter downstream of the exit plane of the converging section. The aspect ratio of each slot was 4-to-1, with the largest dimension of 1.31 inches (0.033 m) positioned in the direction of the mainstream. The mixing section extended two mixing section diameters downstream of the jet centerline.

Grid

The baseline grid had 20,160 cells (56×20×18 cells in x, r, θ directions). Figure 3 shows two views of the baseline grid. The grid distribution is non-uniform with greater grid density in the vicinity of the slot as well as the combustor wall. The domain in the θ-direction extends from the jet centerline to between the jets. Only a pie section with a central angle of 15° was analyzed to conserve grid points. The grid distribution in each direction is described below.

Axial Direction

$X_0 < x < X_1$	inlet pipe	4 cells	uniform
$X_1 < x < X_2$	converging section	2 cells	uniform

$X_2 < x < X_3$	pre-slot	10 cells	matched last cell to the 1st cell in the slot
$X_3 < x < X_4$	slot	8 cells	uniform
$X_4 < x < X_5$	post-slot to 1-D	22 cells	matched 1st cell to last cell in the slot
$X_5 < x < X_L$	1-D to exit	10 cells	matched 1st cell to last cell of previous domain

Radial Direction

$R_0 < r < R_L$	20 cells	grid refined at the combustor wall with algebraic packing factor of 1.4

Angular Direction

$\theta_0 < \theta < \theta_1$ slot	6 cells	uniform
$\theta_1 < \theta < \theta_L$	12 cells	matched 1st cell with last cell in the slot

The values of the grid variables in the different zones discussed above are given in Table 1.

Table 1. Grid Data

Dia	6"	5"	4"
X_0	-0.2506	-0.2252	-0.1998
X_1	-0.1744	-0.1490	-0.1236
X_2	-0.1524	-0.1270	-0.1016
X_3	-0.0167	-0.0139	-0.0111
X_4	0.0167	0.0139	0.0111
X_5	0.1524	0.1300	0.1016
X_L	0.3048	0.2540	0.2032
R_0	0.0000	0.0000	0.0000
R_L	0.0762	0.0762	0.0762
θ_0	0.0000	0.0000	0.0000
θ_1	3.1400	3.1400	3.1400
θ_L	15.0000	15.0000	15.0000

Units
x ~ m
R ~ m
θ ~ deg

Numerical Details

The numerical details of the baseline calculation (as well as all calculations in this paper) included:

1. Wholefield solution of u momentum, v momentum, w momentum, pressure correction, turbulent kinetic energy (k), turbulence dissipation (ε), total enthalpy, and mixture fraction.
2. Second order central differencing of convective and diffusive fluxes;
3. Variable fluid properties;
4. Adiabatic walls;
5. Standard k-ε model with wall functions;
6. Turbulent Prandtl number of 0.9;
7. Instantaneous heat-release model and one-step NO_x model (details of the reaction models are discussed in reference 7); and
8. Six chemical species.

Boundary Conditions

The baseline case had a jet-to-mainstream momentum flux ratio (J) of 36 and a jet-to-mainstream mass flow ratio of 1.94. Specific boundary conditions are stated below.

Mainstream Flow

Axial Velocity	=	35.4 m/s (116.2 ft/s)
Temperature	=	2221 °K (3538 °F)
Density	=	1.864 kg/m^3 (0.1163 lbm/ft^3)
Composition (mass fraction)	=	0.134 CO, 0.068 CO_2, 0.006 H_2, 0.096 H_2O, 0.696 N_2
Turbulent kinetic energy, k	=	300.0 m^2/s^2 (3.2x10^3 ft^2/s^2)
Dissipation of turbulent kinetic energy, ε	=	5.5x10^5 m^2/s^3 (5.92x10^6 ft^2/s^3)

The mass fractions of the species were equilibrium concentrations for propane and air at an equivalence ratio (ϕ) of 1.6. The turbulent kinetic energy corresponded to a high turbulence intensity (40%) typically encountered at the exit of combustor primary zones[15]. However, the solution has been shown to be relatively insensitive to inlet turbulent kinetic energy.

Jet Flow (Slot)

Radial Velocity	=	120.3 m/s (394.6 ft/s)
Temperature	=	811 °K (1000 °F)
Density	=	5.82 kg/m^3 (0.36 lbm/ft^3)
Composition (mass fraction)	=	0.232 O_2, 0.768 N_2
Turbulent kinetic energy, k	=	219.0 m^2/s^2 (2.3x10^3 ft^2/s^2)
Dissipation of turbulent kinetic energy, ε	=	1.2x10^5 m^2/s^3 (1.3x10^6 ft^2/s^3)

The radial velocity corresponded to a liner $\Delta p/p$ of 0.03. The assumed turbulent kinetic energy gave a turbulence intensity of 10%, typical of dilution jets[15].

Exit Boundary

The exit boundary condition was a fixed pressure boundary with pressure set at 200 psia (13.6x10^5 N/m^2). All other variables (velocity components, physical properties, turbulence variables, species concentrations, *etc.*) were zero gradient.

Transverse Boundaries

The transverse boundaries were assumed to be symmetry planes. As a check for potential asymmetric and/or periodic flow behavior, the transverse boundaries were moved between slots (doubling the computational grid) and periodicity was enforced. No discernible difference was observed between the two solutions. Hence, to conserve grid points, transverse boundaries were assumed to be symmetric, and positioned on the jet centerline and between jets.

Combustor Wall

The combustor wall was treated as a no-slip adiabatic wall (zero enthalpy gradient). Wall functions were used for the calculation of wall shear stress and near wall turbulent quantities (k and ε).

Centerline

The computational boundary at the centerline was assumed to be a symmetry plane.

Convergence

The summations of all error residuals were reduced five orders of magnitude, and continuity was conserved in each axial plane. Typically, convergence required approximately 300 iterations. Approximately 6 CPU hours were required on an Alliant FX/8 mini-supercomputer (configured one computational element per job). For comparison, the Alliant computer speeds are ~20 times slower than a Cray X-MP.

Results for Baseline Case

The calculated isotherm results are presented in Figure 4. Figure 4a shows isotherms in the x-r plane through the center of the slot (θ = 0). Although a 15° pie section was numerically analyzed, the results in Figure 4 are shown as a 30° pie section for ease of understanding. The cold jet has penetrated to about the center of the mixing section. Reaction is taking place at the interface of the two flowstreams as evidenced by isotherms near stoichiometric temperature. At x/D=0.15, Figure 4b shows kidney-shaped isotherms behind the jet. Figure 4c shows the velocity vectors at x/D=0.5. The velocity vectors show the vortex roll-up behind the jet which is a typical feature of a jet in crossflow.

In Figure 5, NO_x emissions are presented in terms of NO_x Emission Index (EI) as a function of axial distance. NO_x EI is derived from the sum of volume fractions of NO and NO_2, and expressed as equivalent grams of NO_2 per kilogram of fuel. The value of NO_x EI one diameter downstream of the jet centerline (x/D=1.0) is 8.14.

4. Grid Independence Study

Two sizes of grids were employed to check for grid independence. The baseline grid was 20,160 cells and the fine grid was 68,040 cells. The fine grid was obtained by increasing the grid density by 50% in each of the three directions and maintaining the same stretching factors.

Computational results for the two grids are presented in Figure 6. Quantitatively, they are nearly the same. However, the fine grid solution shows slightly greater jet penetration and less temperature dissipation.

To estimate numerical error caused by grid resolution, the Richardson extrapolation method was employed. The Richardson extrapolation method utilizes a Taylor series expansion on the baseline and fine grid solutions to obtain an approximate solution based on zero discretization error. The values of NO_x EI at x/D=1.0 are 8.14, 7.97, and 7.47 for the baseline grid, fine grid and zero error grid, respectively. Based on this finding, hundreds of thousands of grid cells would be required to obtain a grid independent solution. Such fine grids were not practical in this study. For a comparative study such as this, it was felt the baseline grid is sufficient in accuracy, and should give qualitative engineering answers.

5. Optimization on Number of Slots

It has been shown in the past[16-19] that temperature distributions are similar when J and orifice spacing are coupled. Since the number of orifices follows from orifice spacing, optimum mixing in a can occurs when the following expression is satisfied[4]:

$$n = \frac{\pi\sqrt{2J}}{C} \qquad (1)$$

where

n = optimum number of holes
C = experimentally derived constant ~ 2.5
J = jet-to-mainstream momentum flux ratio

Using equation 1, the optimum number of slots would be 10 or 11 depending on the roundoff. However, this correlation was developed for circular holed dilution jet mixing and jet-to-mainstream mass flow ratios (m_j/m_∞) of approximately 0.5. The accuracy of equation 1 for high aspect ratio slots (4-to-1) and high mass flow ratios (1.94) studied in this investigation is not certain.

Hence, as a preliminary step to studying flow area reduction on mixing, a parametric study was performed to determine the optimum number of slots for J=36. The number of slots was parametrically varied from 10 to 14 on the baseline geometry. As the number of slots was varied, the central angle of the pie section changed, but the jet-to-mainstream mass flow ratio (m_j/m_∞) was held constant by varying the slot open area. The slot aspect ratio was maintained at 4 for all cases.

The same number of grid cells was used in all cases, including the number of grid cells in the slot. However, since the slot width-to-transverse dimension varied in each case, cell density in the θ-direction varied between cases. This variation is thought to have minimal impact on the trends discussed below.

Figure 7 shows the predicted isotherms in the θ=0 plane for different numbers of slots. The jet penetration increased as an inverse function of the number of slots and led to backflow as the number of slots was reduced to 10. From previous experience in reference 6, jet backflow on the mixing section centerline leads to poor mixing and excessive NO_x formation in the combustor. So, further decrease in number of slots below 10 was not considered necessary for this analysis. As the number of jets was increased to 14, the individual jets did not penetrate to the mixing section centerline. Such underpenetration has been shown to be poor from a mixing viewpoint.

Table 2 shows NO_x and CO emissions at x/D of 1.0 as a function of number of slots. NO_x emissions decrease with the increase in the number of slots. Going by NO_x emissions alone, the 14 slot case would be judged to be the optimum mixing configuration. However, for the 13 and 14 slot cases, CO has gone unreacted on the centerline of the mixer due to underpenetration of the dilution jets. The 12 slot configuration has the lowest NO_x EI while exhibiting no CO at x/D=1.0.

Based on this analysis, the 12 slot configuration was selected as the optimum mixer for this geometry and these flow conditions.

Table 2. NO_x and CO Emissions at x/D = 1 for Variable Number of Slots

Slots	NO_x EI	CO EI
10	10.07	0.00
11	8.73	0.00
12	8.14	0.00
13	7.37	1.22
14	6.75	5.71

6. Parametric Study of Area Reduction

Using the optimized 12 slot geometry, three neckdown configurations were analyzed to assess the effect of flow area reduction on NO_x emissions. The three mixing section diameters were 6, 5, and 4 inches (0.1524, 0.127, and 0.0762 m). As the flow area was reduced, the velocity of the mainstream flow in the mixing section increased proportionately to the flow area reduction. The resulting reduction in mainstream static pressure in the mixing section increased the pressure drop across the slots, thus increasing the jet velocity. For incompressible flow, the increase in mainstream and jet velocities exactly counterbalanced, and the jet-to-mainstream momentum flux ratio (J) remained constant as the mixing flow area was reduced.

The slot size was adjusted according to the variation in diameter of the mixing section to ensure a constant mass flow ratio (m_j/m_∞). The turbulence parameters at the jet inlet had to be rescaled according to slot size and the jet velocity. The jet velocity and turbulence parameters at the jet inlet for each mixing diameter are given in Table 3. The rest of the boundary conditions were the same as the baseline case except the exit boundary condition.

Table 3. Jet Velocity and Turbulence Data

Diameter	6"	5"	4"
V_j (m/s)	120.3	173.2	270.6
K_j (m^2/s^2)	219.0	454.1	1098.0
ε_j (m^2/s^3)	1.2×10^5	4.3×10^5	2.0×10^6

The pressure at the exit plane for the 6 inch diameter case was set to be 200 psia (13.6×10^5 N/m^2). For the 5 inch and 4 inch neckdown diameters, the exit pressure was set at 198.8 psia (13.52×10^5 N/m^2) and 195.3 psia (13.28×10^5 N/m^2), respectively. The lower pressures were determined by assuming isentropic flow expansion from the five or four inch diameter mixer to a 6 inch diameter exit. This precluded the necessity of modeling a diffuser at the exit of the five or four inch mixer in the CFD calculations.

The grid distribution in the axial and the radial direction was identical except for the size of the slot. The grid distributions for the three configurations are given in Table 1.

Figure 8 shows the isotherms in the plane through the jet centerline (θ=0) for all three cases. Figure 9 shows isotherms at an r-θ plane one mixing section diameter downstream of the jet inlet (x/D=1.0). In this figure, a full 360° plane is displayed, although the computations were performed on a 15° pie section. The identical nature of the flow patterns shows that the mixing characteristics were identical for each case.

There was some concern that flow separation was not predicted at the inlet to the four-inch diameter mixing section. To investigate this concern, a number of cases were run with fine grid in the converging section and immediately downstream. Cases were run with and without dilution jets. Without dilution jets, flow separation was predicted for laminar flow, but not for turbulent flow (although a somewhat thick boundary layer

was calculated downstream of the contraction). However, with dilution jets, the mainstream flow "sensed" the jet blockage and started accelerating at the entrance of the mixing section. Hence, flow separation (and a thick boundary layer) was avoided in the neckdown mixing sections.

In Figure 10, NO_x EI is plotted as a function of axial location for the three different neckdown diameters. NO_x decreased as the mixing section diameter decreased. For all the cases, CO was completely depleted by x/D of 1.0. The NO_x EI for the six inch diameter mixing section was 8.14 at x/D of 1.0, while the NO_x EI for the four inch diameter mixing section was 2.43, a 3.35-to-1 reduction.

The formation of NO_x is controlled by local temperature, local oxygen concentration, and local residence time. Since mixing was identical for the three mixing diameters analyzed, the local temperatures and oxygen concentrations must be identical. This left residence time as the parameter causing reduced NO_x levels. Residence time is reduced in neckdown mixers in two ways: higher velocities and shorter mixing lengths.

An engineering correlation was developed to approximate NO_x emissions attainable by reduced flow areas. The correlation (based on residence time considerations) is expressed below:

$$\frac{NO_{x\ neckdown}}{NO_{x\ no\ neckdown}} = \frac{A_{neckdown}}{A_{no\ neckdown}} \cdot \frac{H_{neckdown}}{H_{no\ neckdown}} \qquad (2)$$

where

A = flow area

H = height (diameter in can, duct height in annulus)

A comparison of CFD results with equation 2 is shown in Table 4.

Table 4. Neckdown Effect on NO_x Emissions

$NO_{x\ neckdown}/NO_{x\ no\ neckdown}$		
Neckdown Diameter	3-D Calculations	Eq. 2
6"	1.0	1.0
5"	1.73	1.75
4"	3.35	3.38

A flow area reduction of 4.0 appears to be possible in conventional combustor designs (see next section for details), giving a potential NO_x reduction of 16-to-1 in an annular combustor (8-to-1 in a can combustor).

7. 1-D Pressure Loss Analysis

There is a penalty involved in reducing the flow area of the mixing section. By necking down the mixing section, a total pressure drop occurs across the mixer, backpressuring the combustor. The backpressure causes a reduced pressure drop across the combustor swirler. The reduced swirler air pressure drop results in lower atomizing velocities and worse atomization quality.

To investigate this backpressure effect, a 1-D flow model of a combustor was developed. This model was similar to the 1-D model discussed in reference 2 that showed good agreement with experimental pressure loss measurements. Figure 11 shows the basic elements of the model, consisting of 1) primary zone section, 2) converging section, 3) constant-area mixing section, and 4) diffuser. The primary zone was six inches in diameter, and the mixing section diameter was varied between six and three inches.

The hot mainstream gases in the primary zone section were isentropically accelerated into the mixing section. In the mixing section, the 1-D momentum equation was used to solve for static pressure at the exit of the mixing section. The jet velocity was assumed to enter radially, and complete (*i.e.* uniform) mixing and reaction was assumed. An iterative solution procedure was used, in which the inlet pressure of the hot gases was iterated until a combustor exit pressure of 200 psia was attained.

To better understand the relationship of combustor loading parameter on backpressure penalty, calculations were performed with two reference velocities: 50 and 100 f/s. The reference velocity is defined as

$$V_{rel} = \frac{\dot{m}}{\rho A} \qquad (3)$$

where

$\dot{m}$ = total combustor airflow
ρ = combustor inlet density
A = area of the inlet (6 in. diameter)

A combustor reference velocity of 50 f/s corresponds to conventional combustor design practice.

Figure 12 presents the predictions of swirler pressure drop versus mixing flow area. For demonstration purposes, a six percent $\Delta p/p$ was assumed across the swirler for no mixing neckdown. As the mixing flow area was reduced, the pressure drop across the swirler was reduced. For a combustor reference velocity of 50 f/s, a 4-to-1 flow area reduction produced a four percent $\Delta p/p$ across the swirler. Such a swirler pressure drop should be acceptable to combustor designers. However, for a combustor reference velocity of 100 f/s, it is evident that excessive backpressure would result, making the three-inch diameter mixing design impractical.

To get confidence in the 1-D model, results from the 3-D CFD calculations were compared with the 1-D predictions. Figure 13 shows the comparison and good agreement between 1-D and 3-D calculations.

8. Conclusions

The overall conclusions of this study are :

1. By reducing residence time at high flame temperatures, mixing in a "neckdown" mixing section significantly reduces NO_x formation. A design correlation was developed for NO_x reduction attainable by area reduction, as shown in equation 2.

   Area reduction of 4.0 appears to be possible in conventional combustor designs, giving a potential NO_x reduction of 16-to-1 in an annular combustor (8-to-1 in a can combustor).

2. The penalty for neckdown manifests itself in reduced pressure drop across the combustor swirler. This backpressure effect is caused by increased total pressure loss across the mixing section. Analysis showed the penalty for neckdown to be relatively minor for conventional combustor loading parameters.

9. Acknowledgements

The authors wish to thank NASA Lewis Research Center for funding this work under NASA Contract NAS3-25967. Our thanks also are extended to Ms. Kathy W. Rhoades for preparing this typescript.

10. References

1. Mosier, S.A., and Pierce, R.M., "Advanced Combustion Systems for Stationary Gas Turbine Engines," Vol. I, EPA Contract 68-02-2136, 1980.
2. Pierce, R.M., Smith, C.E., and Hinton, B.S., "Advanced Combustion Systems for Stationary Gas Turbine Engines," Vol. III, EPA Contract 68-02-2136, 1980.
3. Holdeman, J.D., "Summary of NASA-Supported Experiments and Modeling of the Mixing of Multiple Jets with a Confined Crossflow for Controlling Exit Temperature Profiles in Gas Turbine Combustors," AIAA Paper 91-2458, 1991.
4. Holdeman, J.D., Srinivasan, R., and White, C.D., " An Empirical Model of the Effects of Curvature and Convergence on Dilution Jet Mixing", AIAA Paper 88-3180 (NASA TM 100896), July 1988.
5. Smith, C.E., "Mixing Characteristics of Dilution Jets in Small Gas Turbine Combustors," AIAA-90-2728,1990.
6. Talpallikar, M.V., Smith, C.E., and Lai, M.-C., "Rapid Mix Concepts for Low Emission Combustors in Gas Turbine Engines," NASA CR-185292, 1990.
7. Talpallikar, M.V., Smith, C.E., Lai, M.-C., and Holdeman, J.D., "CFD Analysis of Jet Mixing in Low NO_x Flametube Combustors," *36th* ASME International Gas Turbine and Aeroengine Conference, 1991.
8. Russell, P.L., *et al.*, "Evaluation of Concepts for Controlling Exhaust Emissions from Minimally Processed Petroleum and Synthetic Fuels," ASME Paper 81-GT-157, 1981.

9. Rosfjord, T.J., "Evaluation of Synthetic-Fuel-Character Effects on Rich-Lean Stationary-Gas-Turbine Combustion Systems, Vol. 1: Subscale Test Program," EPRI-AP-2822-Vol-1, 1981.
10. Novick, A.S., and Troth, D.L., "Low NO_x Heavy Fuel Combustor Concept," NASA CR-165367, 1981.
11. Lew, H.G., Carl, D.R., Vermes, G., DeZubay, E.A., "Low NO_x Heavy Fuel Combustor Concept Program, Phase 1: Combustion Technology Generation," NASA CR-165482, 1981.
12. Przekwas, A.J., Habchi, S.D., Yang, H.Q., Avva, R.K., Talpallikar, M.V., and Krishnan, A., "REFLEQS-3D: A Computer Program for Turbulent Flows With and Without Chemical Reaction, Volume 1: User's Manual," CFD Research Corp., Huntsville, AL, CFDRC Report GR-89-4, 1990.
13. Smith, C.E., Ratcliff, M.L., Przekwas, A.J., Habchi, S.D., and Singhal, A.K., "Modeling of Turbulent Combustion in Liquid Rocket Engine Components," NASA Contract NAS8-37619, 1988.
14. Smith, C.E., Ratcliff, M.L., Przekwas, A.J., and Habchi, S.D., "Validation of an Advanced Turbulent Combustion Code: REFLEQS," *7th* ASME CFD Workshop, NASA MSFC, 1989.
15. Smith, C.E., Graves, C.B., Johnson, B.V., and Roback, R., "Advanced Fuel Injector Characterization," Phase I Design Report, Navy Contract N00140-83-8899, 1986.
16. Holdeman, J.D., Srinivasan, R., and Berenfeld, A., "Experiments in Dilution Jet Mixing, " *AIAA Journal*, vol. 22, No. 10, Oct. 1984, pp. 1436-1443.
17. Holdeman, J.D., and Srinivasan, R., Modeling Dilution Jet Flowfields, *J. Propulsion and Power*, Vol. 2, No. 1, Jan-Feb 1986, pp 4-10.
18. Holdeman, J.D., Srinivasan, R., Coleman, E.B., Meyers, G.D., and White, C.D., "Effects of Multiple Rows and Non-Circular Orifices on Dilution Jet Mixing," *J. of Propulsion and Power*, Vol. 3, No. 3, May-Jun 1987, pp. 219-226.
19. Holdeman, J.D., Srinivasan, R., Reynolds, R., and White, C.D., "Studies of the Effects of Curvature on Dilution Jet Mixing", *J.of Propulsion and Power*, vol. 7 No. 2, Mar-Apr 1991.

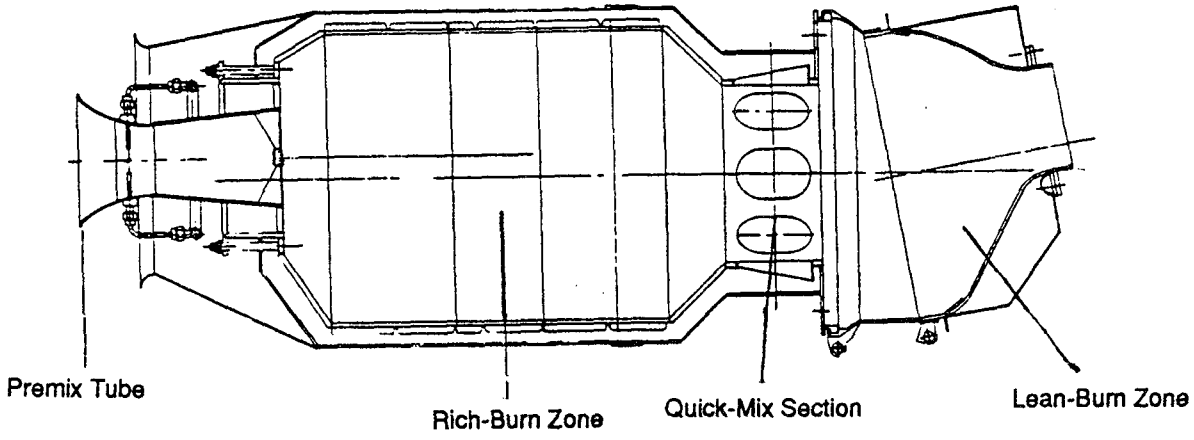

Figure 1. Industrial Rich/burn/Quick-mix/Lean-burn (RQL) combustor[2].

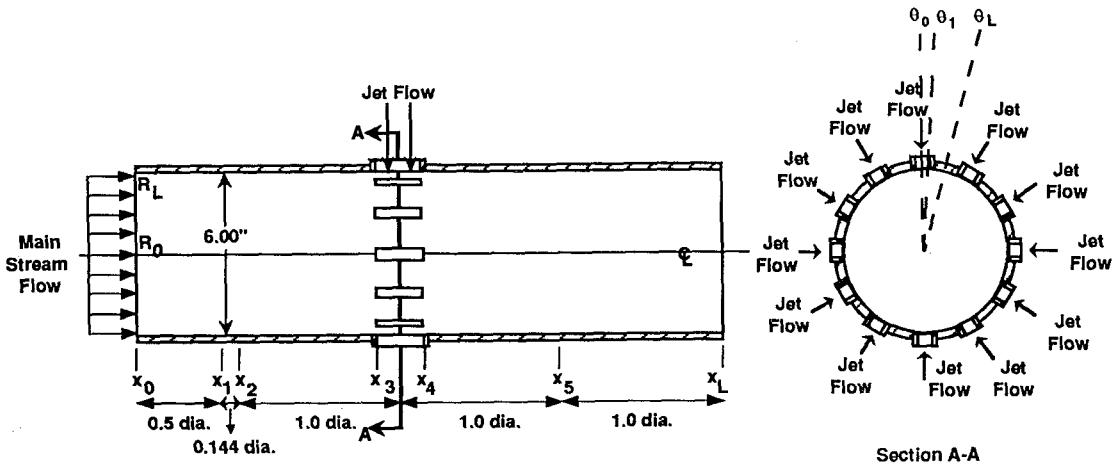

Figure 2. Schematic of baseline geometry.

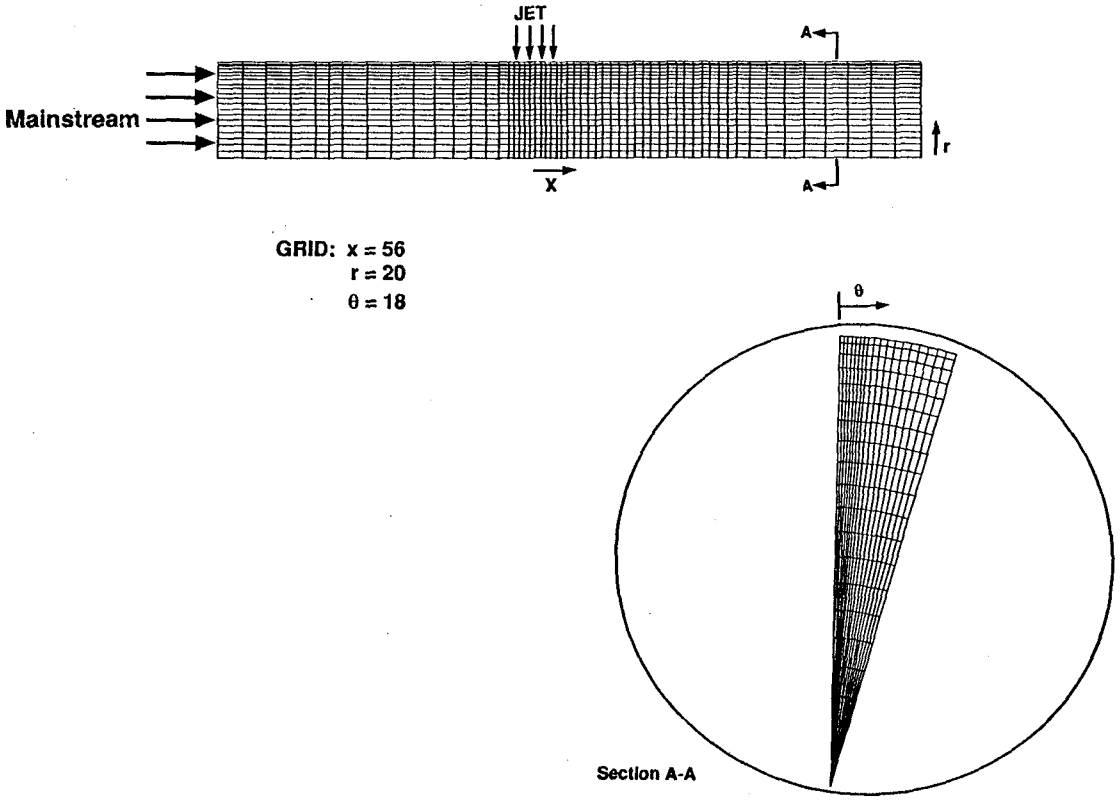

Figure 3. Numerical grid for baseline configuration.

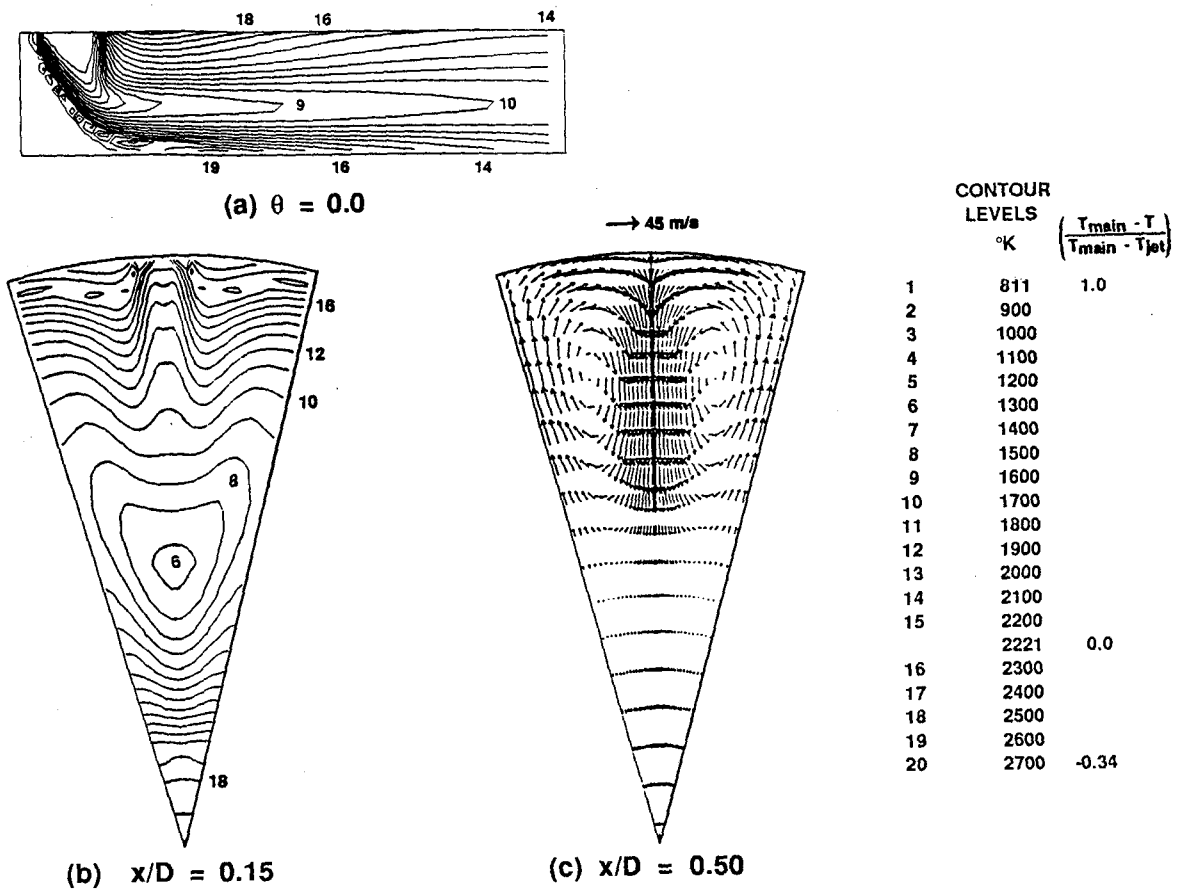

Figure 4. Computational results for baseline configuration.

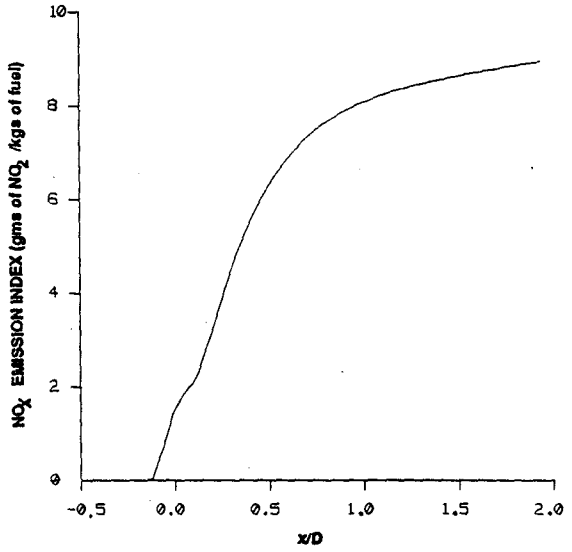

Figure 5. NO_x emission index for baseline configuration.

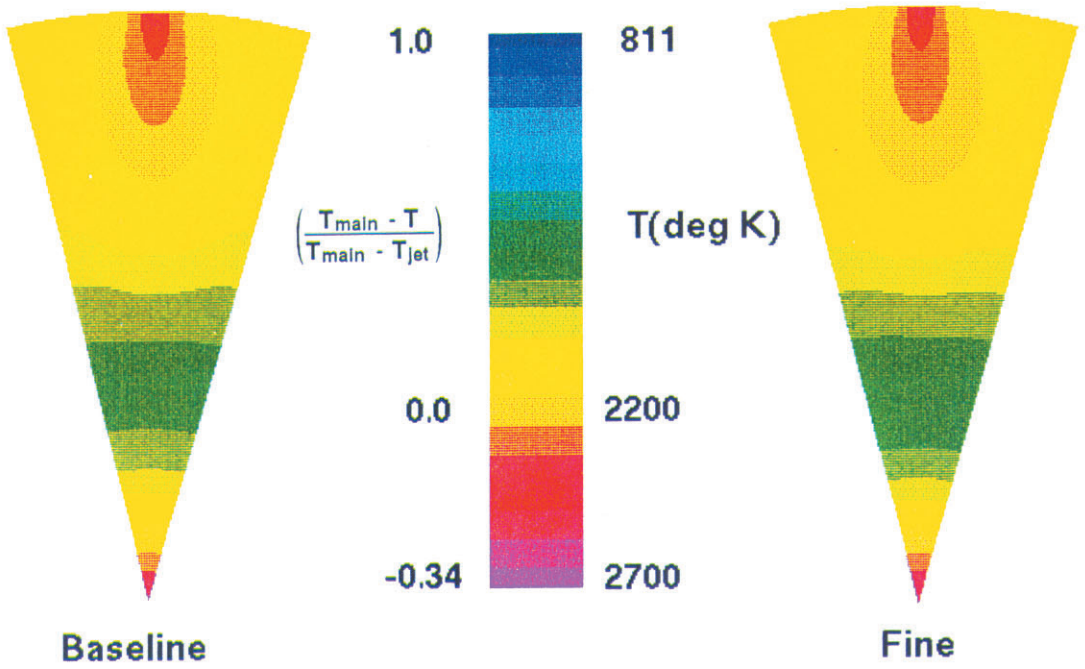

Figure 6. Isotherms predicted for baseline and fine grids: x/D=1.0.

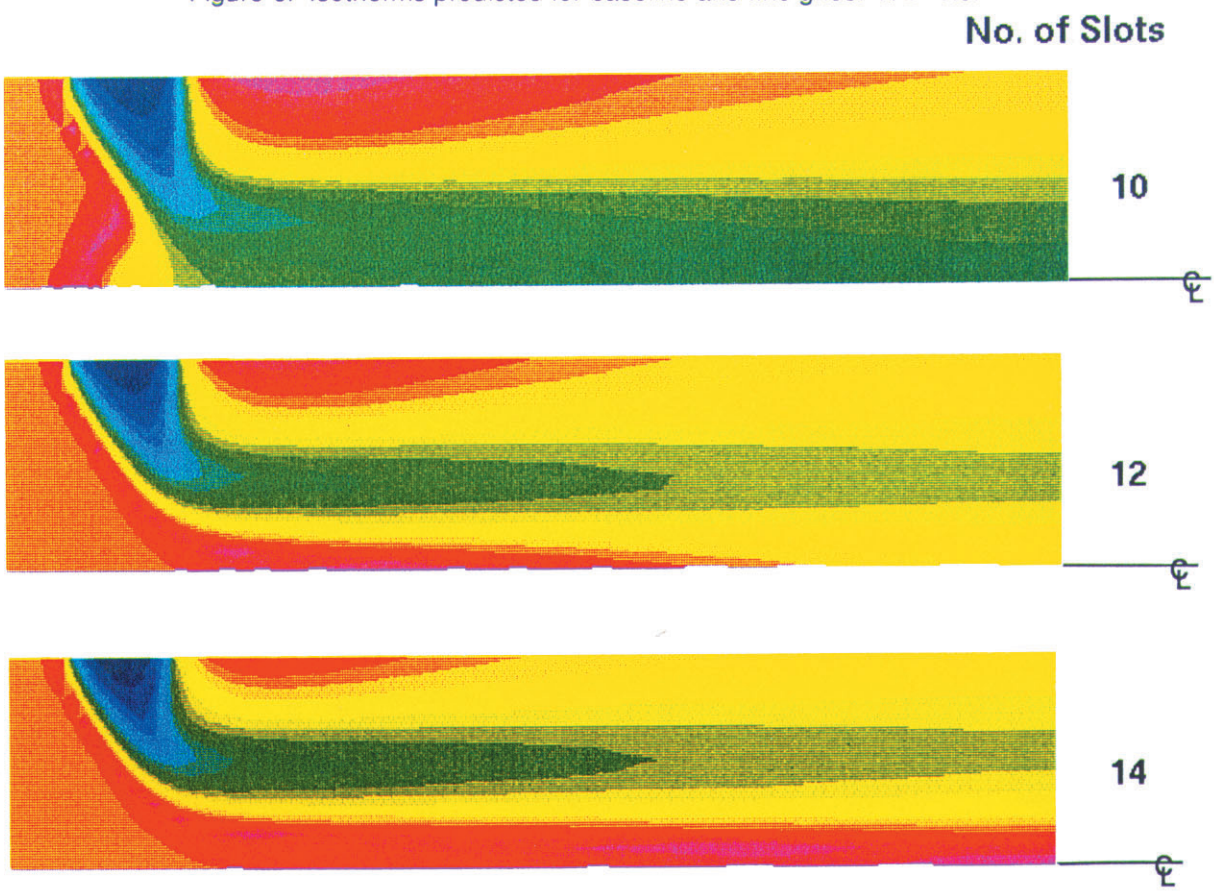

Figure 7. Predicted isothermal maps (θ=0) for J=36; variation in number of slots. Temperature scale same as shown in Figure 8.

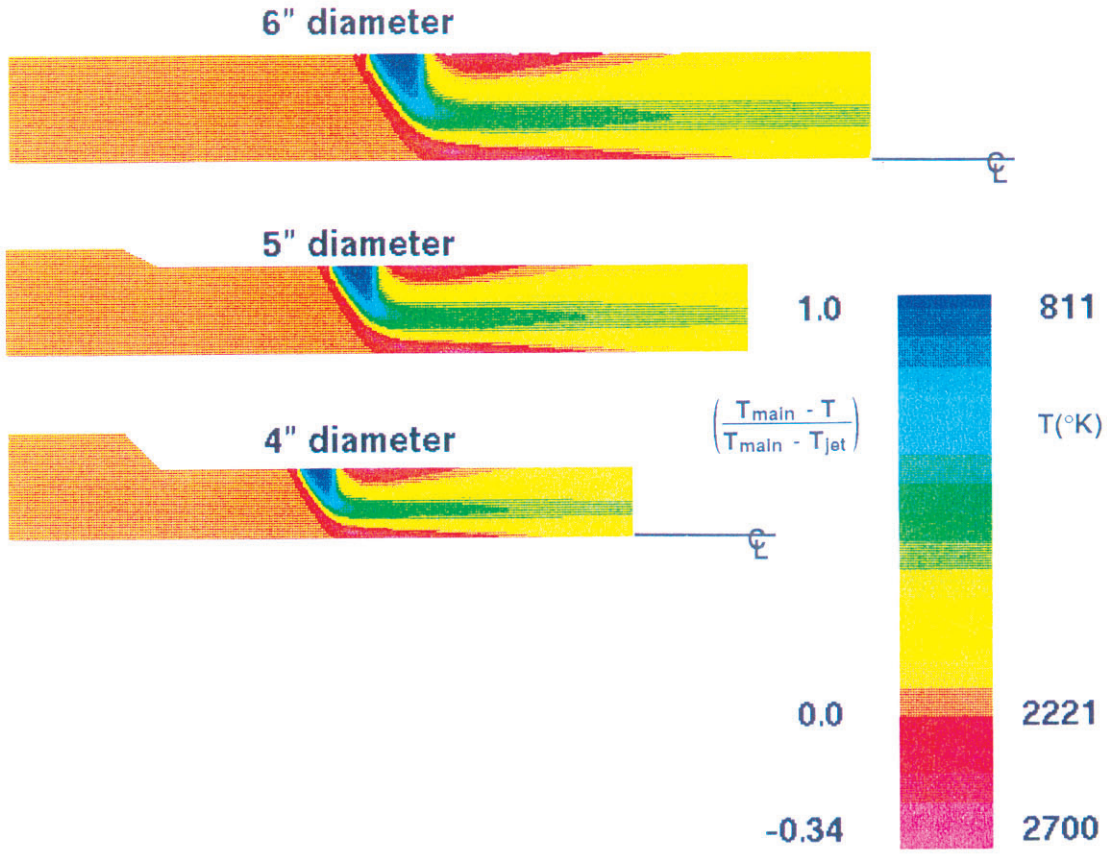

Figure 8. Predicted isothermal maps (θ=0) for J = 36; variation in mixing diameter.

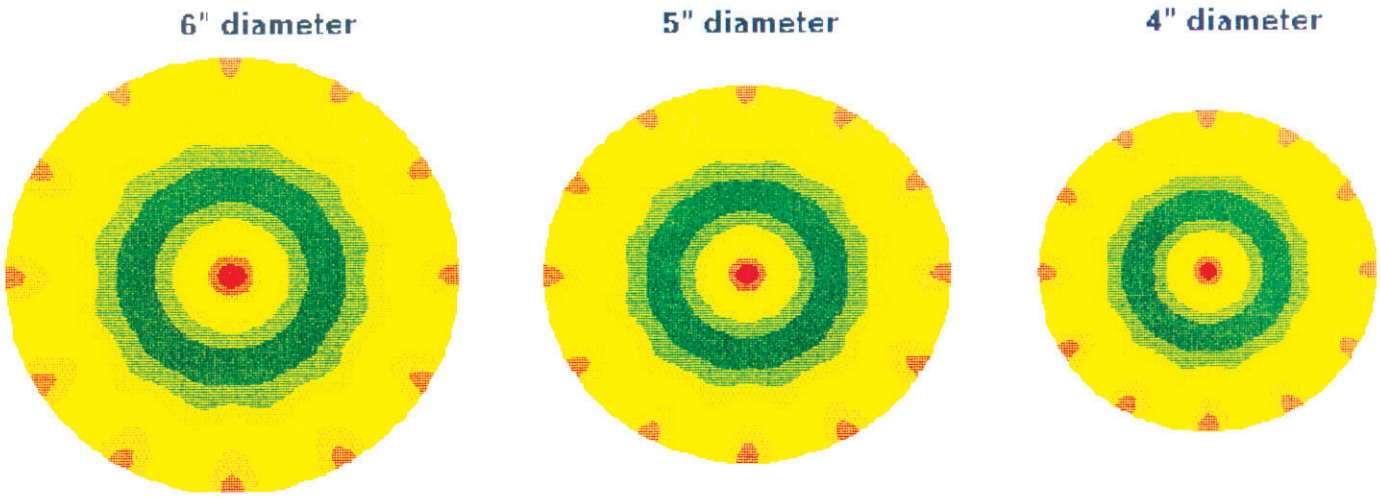

Figure 9. Predicted isothermal maps (x/D=1.0) for J=36; variation in mixing diameter.

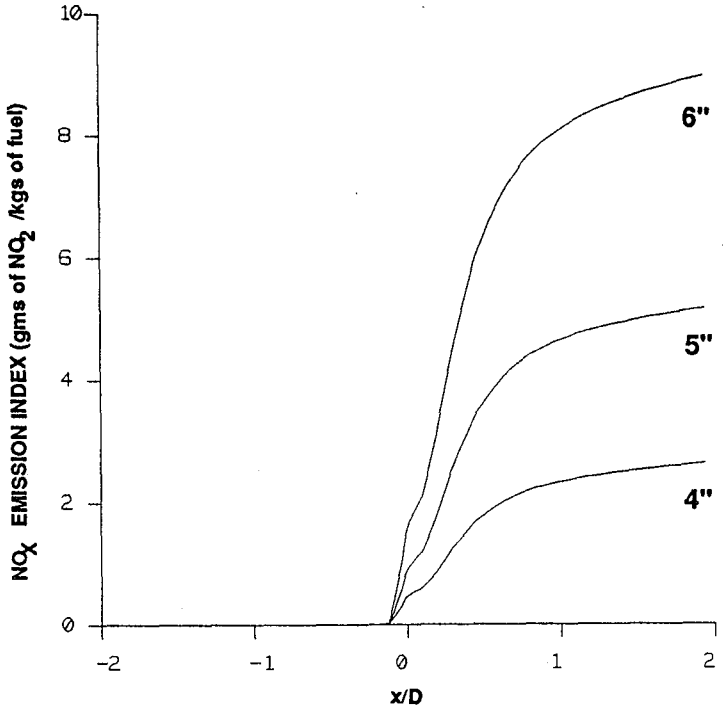

Figure 10. NO_x emission index for mixing diameters of 6", 5", and 4".

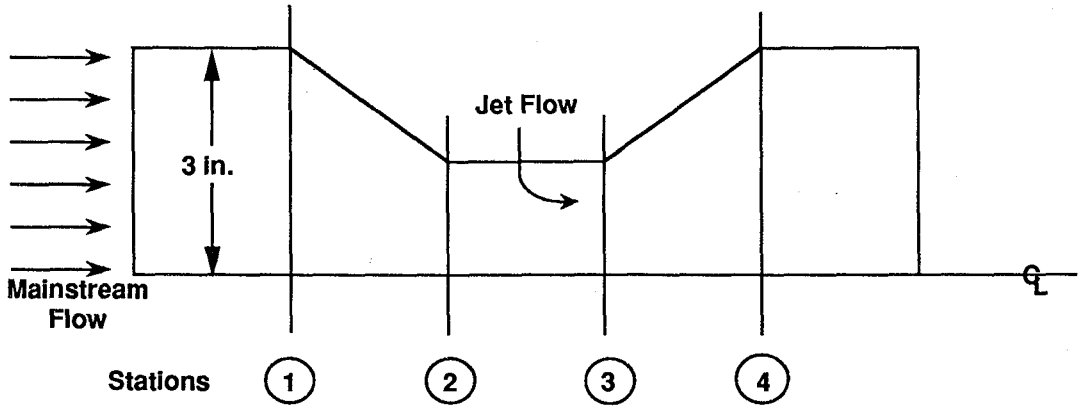

Figure 11. Schematic showing stations of 1-D pressure loss code.

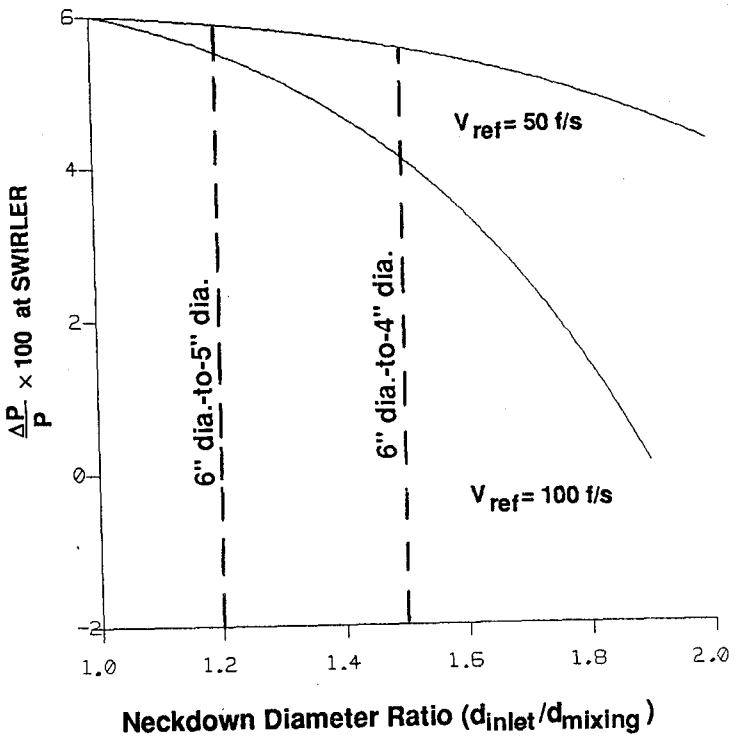

Figure 12. Percentage pressure drop available across the swirler as predicted by 1-D pressure loss code.

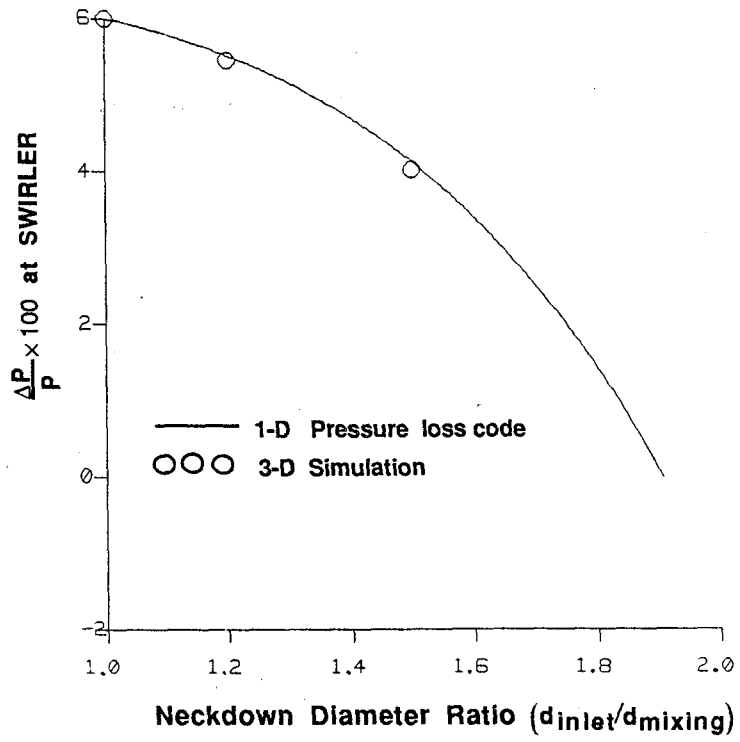

Figure 13. Pressure drop predicted by 1-D pressure loss code compared to 3-D calculations.

REPORT DOCUMENTATION PAGE

Form Approved
OMB No. 0704-0188

1. AGENCY USE ONLY (*Leave blank*)	2. REPORT DATE	3. REPORT TYPE AND DATES COVERED
	June 1991	Technical Memorandum

4. TITLE AND SUBTITLE

A CFD Study of Jet Mixing in Reduced Flow Areas for Lower Combustor Emissions

5. FUNDING NUMBERS

WU–537–02–21–00

6. AUTHOR(S)

C.E. Smith, M.V. Talpallikar, and J.D. Holdeman

7. PERFORMING ORGANIZATION NAME(S) AND ADDRESS(ES)

National Aeronautics and Space Administration
Lewis Research Center
Cleveland, Ohio 44135–3191

8. PERFORMING ORGANIZATION REPORT NUMBER

E–6238

9. SPONSORING/MONITORING AGENCY NAME(S) AND ADDRESS(ES)

National Aeronautics and Space Administration
Washington, DC 20546–0001

10. SPONSORING/MONITORING AGENCY REPORT NUMBER

NASA TM–104411
AIAA–91–2460

11. SUPPLEMENTARY NOTES

Prepared for the 27th Joint Propulsion Conference cosponsored by the AIAA, SAE, ASME, and ASEE, Sacramento, California, June 24–27, 1991. C.E. Smith and M.V. Talpallikar, CFD Research Corporation, Huntsville, Alabama 35805 (work funded by NASA Contract NAS3–25967). J.D. Holdeman, NASA Lewis Research Center. Responsible person, J.D. Holdeman, (216) 433–5846.

12a. DISTRIBUTION/AVAILABILITY STATEMENT

Unclassified - Unlimited
Subject Category: 07

Available electronically at http://gltrs.grc.nasa.gov/GLTRS

This publication is available from the NASA Center for AeroSpace Information, (301) 621–0390.

12b. DISTRIBUTION CODE

13. ABSTRACT ***(Maximum 200 words)***

The Rich-burn/Quick-mix/Lean-burn (RQL) combustor has the potential of significantly reducing NO_x emissions in combustion chambers of High Speed Civil Transport (HSCT) aircraft. Previous work on RQL combustors for industrial applications suggested the benefit of "necking down" the mixing section. In this study, a 3D numerical investigation was performed to study the effects of neckdown on NO_x emissions and to develop a correlation for optimum mixing designs in terms of neckdown area ratio. The results of the study showed that jet mixing in reduced flow areas does not enhance mixing, but does decrease residence time at high flame temperatures, thus reducing NO_x formation. By necking down the mixing flow area by four, a potential NO_x reduction of sixteen-to-one is possible for annular combustors. However, there is a penalty that accompanies the mixing neckdown: reduced pressure drop across the combustor swirler. At conventional combustor loading parameters, the pressure drop penalty does not appear to be excessive.

14. SUBJECT TERMS	15. NUMBER OF PAGES
Dilution; Can; Emissions; Jet mixing flow; Gas turbines; Combustion chamber	22
	16. PRICE CODE A03

17. SECURITY CLASSIFICATION OF REPORT	18. SECURITY CLASSIFICATION OF THIS PAGE	19. SECURITY CLASSIFICATION OF ABSTRACT	20. LIMITATION OF ABSTRACT
Unclassified	Unclassified	Unclassified	

Appendix F

NASA Technical Memorandum 106976

NASA Technical Memorandum 106976
AIAA–95–2995

Jet Mixing and Emission Characteristics of Transverse Jets in Annular and Cylindrical Confined Crossflow

D.B. Bain and C.E. Smith
CFD Research Corporation
Huntsville, Alabama

J.D. Holdeman
Lewis Research Center
Cleveland, Ohio

Prepared for the
31st Joint Propulsion Conference and Exhibit
cosponsored by AIAA, ASME, SAE, and ASEE
San Diego, California, July 10–12, 1995

National Aeronautics and
Space Administration

Jet Mixing and Emission Characteristics of Transverse Jets in Annular and Cylindrical Confined Crossflow

D. B. Bain* and C. E. Smith**
CFD Research Corporation
Huntsville, Alabama

J. D. Holdeman***
NASA Lewis Research Center
Cleveland, Ohio

Abstract

3-D turbulent reacting CFD analyses were performed on transverse jets injected into annular and cylindrical (can) confined crossflows. The goal of this study was to identify and assess mixing differences between annular and can geometries. The approach was to optimize both annular and can configurations by systematically varying orifice spacing until lowest emissions were achieved, and then compare the results. Numerical test conditions consisted of a jet-to-mainstream mass-flow ratio of 3.2 and a jet-to-mainstream momentum-flux ratio (J) of 30.

The computational results showed that the optimized geometries had similar emission levels at the exit of the mixing section although the annular configuration did mix-out faster. For lowest emissions, the design correlation parameter ($C=(S/H)\sqrt{J}$) was 2.35 for the annular geometry and 3.5 for the can geometry. For the annular geometry, the constant was about twice the value seen for jet mixing at low mass-flow ratios (i.e. MR < 0.5). For the can geometry, the constant was about 1 1/2 times the value seen for low mass-flow ratios.

Nomenclature

f	Mixture Fraction
h	Enthalpy
k_∞	Turbulent Kinetic Energy of Mainstream
m_j	Mass Flow of Jets
m_∞	Mass Flow of Mainstream
x	Axial Coordinate, x=0 at leading edge of the orifice
x/H	Axial Distance-to-Duct Height Ratio
y	Vertical Coordinate
z	Lateral Coordinate
C	$(S/H)\sqrt{J}$ (see Eq. 1)
H	Duct Height
J	Momentum-Flux Ratio $\left(\rho_j V_j^2\right)/\left(\rho_\infty U_\infty^2\right)$
MR	Mass-Flow Ratio m_j/m_∞
P	Static Pressure (N/m^2)
P_{jet}	Static Pressure of Jet
P_∞	Static Pressure of Mainstream
S	Orifice Spacing
S/H	Orifice Spacing-to-Duct Height Ratio
T	Temperature (K)
T_{exit}	Exit Temperature
T_{jet}	Temperature of Jet
T_∞	Temperature of Mainstream
U_∞	Mainstream Flow Velocity (m/s)
V_j	Jet Velocity (m/s)

* Project Engineer, Member AIAA
** Vice President/Engineering, Member AIAA
*** Senior Research Engineer, Associate Fellow AIAA

ε_∞ Turbulent Energy Dissipation of Mainstream
ϕ_{rb} Rich-Burn Equivalence Ratio
ϕ_{lb} Lean-Burn Equivalence Ratio
ρ_j Density of Jet
ρ_∞ Density of Mainstream

1. Introduction

In recent years, the concern over the environmental impact of aircraft gas turbine technology has steadily increased. The need for the reduction of both carbon monoxide (CO) and oxides of nitrogen (NO_x) is quickly becoming a very sensitive issue. Past advancements to aircraft gas turbine engines have focused on increasing the overall thermodynamic cycle efficiency by implementing increases in pressure and temperatures. The increases tend to have an adverse effect on NO_x emission levels, necessitating the development of new ways of controlling NO_x.

In order to improve the emission signatures of combustors, the industry has departed from the standard single axial staged combustion to pursue staged burning. One such concept being evaluated both experimentally and numerically is the Rich-burn/Quick-mix/Lean-burn (RQL) combustor[1]. This combustor utilizes the staged burning concept in which the primary zone is designed to operate fuel rich.[2] The combustion products high in carbon monoxide concentration enter the quick-mix section where mixing is initiated with bypass air. The combustion process is then completed in the lean-burn region.

To achieve the low emission goals set for RQL combustors, high importance must be placed on attaining rapid and uniform mixing in the quick-mix section. Recent experimental and numerical studies have been completed that investigated and assessed improved mixing concepts[3-18].

2. Background

For quite some time the importance of research on jet mixing in a confined crossflow has been recognized as having a significant impact on a variety of practical applications. Within gas turbine technology, jet mixing plays a particularly important role in the dilution zone of the combustor. The dilution zone is the aft zone where the products of combustion are mixed with air to produce a temperature profile acceptable to the turbine.[19-21]

As of late, many studies have been conducted relative to jet mixing in gas turbine applications[22-27]. These studies have concentrated on both rectangular and cylindrical geometric configurations. The results of these studies have identified two significant design parameters that influence the mixing pattern: 1) jet-to-mainstream momentum-flux ratio (J) and 2) orifice spacing-to-duct height ratio (S/H). Optimum mixing relationships were determined to be a function of the product of S/H and square root of J for the range of conditions tested and analyzed[19]:

$$C = (S/H)\sqrt{J} \qquad (1)$$

These studies summarized in Ref. 19 examined both two-sided and single-sided injection in rectangular geometries. Table 1 shows the constants derived from these studies. The optimum C value was shown to be 1.25 for inline, two-sided injection, while single-sided injection produced a C value of 2.5. It was determined that the best mixing occurred when the dilution jet reached a penetration level of 1/4 duct height for two-sided injection. Previous dilution jet work focused on conditions where the jet-to-mainstream mass-flow levels were less than 0.50. More recent numerical and experimental research has examined the effect of increased mass-flow ratios, more typical of RQL combustors (i.e. MR > 2.0). The results for MR > 2.0 have concluded that the C value is about twice (2.5 vs.

1.25) that of the lower mass-flow ratio cases for two-sided, rectangular configurations.

Presently, the design of the mixing section is pursuing two options. The first employs a full annular geometry, while the second consists of a can mixing section. The basic questions that needed to be addressed were: 1) is there an inherent difference between the way can and annular configurations mix, 2) does one of these produce higher NO_x than the other, and 3) can one be optimized based on knowledge of the other? Although many factors (i.e. liner cooling considerations, structural requirements, etc.,) will play a role in the decision making process, the input of geometry on emission signature is an equally important factor. This study sought to address these issues by a systematic computational analysis. A complete description of the work follows.

3. CFD Code

The approach in this study was to perform 3-D numerical calculations on generic geometry sections. The CFD code named CFD-ACE[28] was used to perform the computations. The basic capabilities/methodologies in CFD-ACE include:

(1) co-located, fully implicit and strongly conservative finite volume formulation;
(2) solution of two- and three-dimensional Navier-Stokes equations for incompressible and compressible flows;
(3) non-orthogonal curvilinear coordinates;
(4) multi-block grid topology;
(5) upwind, central (with damping), second order upwind and Osher-Chakravarthy differencing schemes;
(6) standard[29], extended[30], RNG and low Reynolds number[31] k-ε turbulence models;
(7) instantaneous, one-step, two-step, and four-step heat release and emission combustion models;
(8) spray models including trajectory, vaporization, etc.; and
(9) pressure-based solution algorithms including SIMPLE and a variant of SIMPLEC.

4. Details of Numerical Calculations

The analysis was divided up into two parametric studies. The first parametric study focused on the annular geometries, while the second concentrated on the can geometries. A schematic of the annular geometry is shown in Figure 1. The inner radius of the annulus measured 0.3896m with the outer radius measuring 0.4404m. The height of the mixing section was 0.0508m. The computation domain extended 0.152m from the leading edge of the orifice (x/H=3.0). The walls were modeled as being 0.0064m thick. Above each orifice a plenum 0.076m long was constructed. The annular model consisted of two-sided injection from the top and bottom orifices into the mainstream crossflow.

A constant shape orifice was selected for use in both of the parametric studies. The orifice was a slot with rounded ends and had a 2:1 length-to-width aspect ratio. The selection of the 2:1 rounded slot was made to ensure enough orifices would be able to fit on the ID of the annular configuration for an underpenetrated jet configuration. The 2:1 rounded slots were aligned with the long dimension in the direction of the mainstream flow.

The can configurations were made comparable to the annular configuration by making the can cross-sectional area equal to a one-nozzle sector of the annular geometry. Thus for a 24-nozzle annular combustor, the diameter for the equivalent-area can geometry was 0.084m. A schematic of the can geometry is presented in Figure 2.

To enhance the computational efficiency of the numerical calculations, only one set of orifices (top and

bottom) was modeled. Similarly, only one orifice was modeled for the can geometry. For the annular geometry, the orifices were located on the inner and outer diameter in the same axial plane, and inline in the transverse direction. The transverse calculation domain extended from midplane to midplane between the jets' centerlines. Periodic boundary conditions were assumed on the transverse boundaries. For the can geometry, a single orifice was located on the outer liner with periodic boundary conditions being specified on the transverse boundaries.

Four parametric cases were analyzed for the annular geometry, while six cases were performed for the can geometry. For each case, the orifice spacing, S/H, was varied parametrically while maintaining all other design variables constant. Note that as the orifice spacing was varied, the size of the orifice was changed to maintain constant flow area. The intent of this method was to optimize each geometry based on the lowest emission signature. A full range of jet penetration levels was studied, including under, optimum, and over-penetrating cases.

Tables 2 and 3 show the geometry specifics for the can and annular cases, respectively. The six can cases are designated C1-C6. These cases correspond to 5, 6, 7, 8, 10, and 12 holes on the can liner. For the annular analysis, the cases are labeled as AN1-AN4. Test case AN1 corresponds to 3 orifices on the inner and outer diameter (6 orifices in a one-nozzle sector) and continues to 6 orifices on ID&OD (12 orifices in the nozzle sector). Since the areas of the annular 15 degree sector and the can are set equal, the orifices are identical when there are the same number of orifices in the can and annular configurations (e.g. AN1 & C2 have identical orifices).

To determine the jet-to-mainstream momentum-flux ratio (J), the jet velocity had to be calculated. The pressure drop across the orifice was determined by using the total pressure at the plenum inlet and the mass-averaged static pressure across the orifice exit. It should be mentioned that the static pressure and radial velocity at the orifice exit were highly non-uniform in the axial direction. From this pressure drop, the velocity of the jet at the orifice exit was calculated, as well as the orifice discharge coefficient (C_d). The C_d for the orifice was calculated to be 0.685. Using the jet velocity based on the pressure drop, the momentum-flux ratio was calculated to be 30.

The turbulence boundary conditions, k & ε, were determined in the following manner. For the mainstream (rich-burn) flow, the turbulence parameters were determined from unreported CFD calculations of the rich-burn section. For the jets, the turbulence levels were determined by the CFD analysis as the flow proceeded from the plenums into the orifices. The inlet turbulence into the plenum had no effect on the turbulence through the orifices; hence the inlet turbulence to the plenums were set at nominal values.

The flow conditions of the mainstream and jets were:

Mainstream		Jets	
U_∞	= 43.5 m/s	P_{jet}	= 9.72×10^5 N/m^2
T_∞	= 2035 K	T_{jet}	= 777 K
P_∞	= 9.72×10^5 N/m^2		
k_∞	= 118.0 m^2/sec^2		
ε_∞	= 5.4×10^4 m^2/sec^3		

J = 30
m_j/m_∞ = 3.20
T_{exit} = 1755 K
ϕ_{rb} = 2.0
ϕ_{lb} = 0.425

Grids

The computational mesh was created using CFD-GEOM[32], an interactive three-dimensional geometry modeling and mesh generation software. A typical

annular case consisted of approximately 63,000 cells. The breakdown of the cell distribution was as follows:

Top and Bottom Plenums	42x10x28 [x,y,z direction]
Mixing Region	77x20x28

The can grid was separated into:

Top Plenum	42x10x28
Mixing Region	77x20x28

The orifices were composed of 28 x 14 uniformly distributed cells. The orifice was modeled with 5 cells in the vertical direction to represent the wall thickness of 0.0064m. A typical annular grid is shown in Figure 3. The grid upstream and downstream of the orifice region was expanded/contracted so that each cell adjacent to the orifice region matched the cell size in the slot region. The cells in the vertical direction were compressed in the vicinity of the wall to more accurately capture any wall effects.

Numerics & Models

The following conservation equations were solved: u momentum, v momentum, w momentum, mass (pressure correction), turbulent kinetic energy (k), turbulent energy dissipation (ε), enthalpy (h), and mixture fraction (f). The convective fluxes were calculated using upwind differencing, and the diffusive fluxes were calculated using central differencing. The standard k-ε turbulence model was employed and conventional wall functions were used. The walls were assumed to be adiabatic. The turbulent Schmidt and Prandtl numbers were set to 0.5. A fast chemistry (instantaneous) model was assumed. Equilibrium products were also assumed. The use of a fast chemistry model was based on LSENS[33] calculations using a 63-step, 33 species reaction model; the chemical reaction times were small compared to flow times at the conditions being studied.

Convergence

All error residuals were reduced at least 4 orders of magnitude, and continuity was conserved in each axial plane to the fifth decimal. A converged solution required approximately 8-12 CPU hours on a CRAY C-90 computer.

Rich-Burn Inlet Conditions

The inlet to the rich-burn section was assumed to be premixed fuel and air. The fuel used in this analysis was $C_{10}H_{19}$, representative of Jet A fuel. The inlet premixed equivalence ratio (ϕ_{rb}) was specified to 2.0. As the inlet flow entered the first cell of the computational domain, it burned immediately to equilibrium products. The resulting downstream flow was representative of rich-burn conditions entering the quench zone.

5. Data Postprocessing

Graphics postprocessing was performed using CFD-VIEW[34-35], an interactive graphical visualization tool. The NO_x results were calculated using a post-processing tool named CFD-POST.[36] Using the equilibrium species calculated in the CFD-ACE solution, NO_x was calculated using an extended Zeldovich thermal NO_x model shown below in equation (2).[37,38] The effect of turbulent fluctuations was included by using a prescribed, beta function pdf.

$$\frac{d(NO)}{dt} = 2k_1(O)(N_2)\frac{1-\dfrac{(NO)^2}{K(O_2)(N_2)}}{1+\dfrac{k_{-1}(NO)}{[k_2(O_2)+k_3(OH)]}} \qquad (2)$$

where, $K=(k_1/k_{-1})(k_2/k_{-2})$ is the equilibrium constant for the reaction between N_2 and O_2.

6. Results and Discussion

The results for the parametric cases are presented using three variables; equivalence ratio, temperature, and NO_x production.

Annular Geometry

The effect of orifice spacing on jet penetration is presented in Figures 4 and 5. Plotted in Figure 4 are the temperature contours in a lateral plane through the orifice centerline. Similarly, the equivalence ratios are shown in Figure 5. The 6ID/6OD configuration (case AN4 in Table 3) is clearly underpenetrated, represented by a core of mainstream fluid passing through the center of the duct. In contrast, the 3ID/3OD case (AN1 in Table 3) exhibits overpenetration of the jet; the mainstream flow is deflected to the outer wall. This is seen by the higher temperature along the OD and ID wall for the 3ID/3OD (AN1) case. The 4ID/4OD (AN2 in Table 3) and 5ID/5OD (AN3 in Table 3) configurations exhibit near-optimum characteristics. The jet penetrates to approximately 1/4 duct height for these cases. From the equivalence ratio contours shown in Figure 5, the 5ID/5OD (AN3) appears to show the most uniform downstream mixing characteristics at the exit.

Shown in Figure 6 are axial planes at x/H=1.0 for temperature and equivalence ratios. The high temperatures along the wall in the 3ID/3OD (AN1) case indicate the over-penetrating jets, while the 6ID/6OD (AN4) case shows the hot mainstream flow in the duct center typical of under-penetrating jets. Note that the OD near-wall temperature is hotter than the ID near-wall temperature for each case. This occurs because the orifice spacing is greater for the OD liner, resulting in more mainstream (rich-burn) flow passing between the jets.

Figure 7 shows the NO_x production for the annular parametric cases. NO_x is mainly produced in regions where there is near-stoichiometric temperature and oxygen available. The high NO_x production along the OD wall in the 3ID/3OD (AN1) case results from excessive mainstream flow passing between the jets and then mixing with the jet airflow. When the jets underpenetrate, as in the 6ID/6OD (AN4) case, excessive NO_x is produced along the center of the duct. The lowest amount of NO_x production occurs when the jets have optimum penetration, i.e., 4ID/4OD (AN2) case and the 5ID/5OD (AN3) case.

Can Geometry

Figures 8 and 9 show the corresponding temperature and equivalence ratio contour plots for the can parametric. Note, only a single jet is shown for the can configurations; the bottom of the plot represents the can centerline. As seen in the previous annular results, an increase in the number of orifices translates into a corresponding decrease in jet penetration levels. It can be seen in Figures 8 and 9 that the jets are overpenetrated for the 5 orifice case (C1 in Table 2), underpenetrated for the 8 orifice case (C4 in Table 2), and near optimally penetrated for the 6 (C2 in Table 2) and 7 (C3 in Table 2) orifice cases.

Figure 10 shows the axial planes at x/R=1.0 for temperature and equivalence ratios. It can be seen that stoichiometric burning occurs near the liner for the 5 orifice case (C1), near the centerline for the 8 orifice case (C4), and near both the liner and centerline for the 6 (C2) and 7 orifice (C3) cases. Once again, the 6 (C2) and 7 orifice (C3) cases appear to be near optimum in terms of jet penetration and mixing.

Figure 11 presents the NO_x production for the can cases. By comparing Figure 11 with Figure 8, it can be seen that the highest NO_x production locations correspond to areas of near stoichiometric flame temperatures. For the overpenetrating, 5 orifice case (C1), most of the NO_x is produced next to the liner. For the underpenetrating, 8 orifice case (C4), there is almost no NO_x being formed on the liner; all of the NO_x is formed on the centerline.

Emissions

To effectively quantify the emissions results, both the NO_x and CO signature must be considered in the analysis. In some cases low NO_x levels can be predicted, but significant concentrations of CO can still be present in the gas flow. High levels of CO translates into combustion inefficiency, and is undesirable. Low NO_x that is achieved due to combustion inefficiency is not an acceptable design.

Figure 12 presents normalized NO_x as a function of x/H for the annular cases. Up to x/H=0.5, all configurations produce a comparable amount of NO_x. NO_x continues to be produced all the way to x/H of 3.0 for the 3ID/3OD (AN1) and 6ID/6OD (AN4) cases, and will continue being produced downstream of x/H of 3.0 due to lack of mixing. Both the 4ID/4OD (AN2) and 5ID/5OD (AN3) cases show the NO_x leveling off by x/H of 3.0. This "leveling off" is an indication of good mixing. At the mixed-out temperature of these cases (1755 K), no additional NO_x should be formed once near-complete mixing has occurred. If there are pockets of higher equivalence ratio (and thus higher temperatures), NO_x will continue to be formed, as shown by the 3ID/3OD (AN1) and 6ID/6OD (AN4) cases. Figure 13 shows contour plots of both the equivalence ratios and temperatures for the annular parametric at x/H=3.0. These contour plots show that the 4ID/4OD (AN2) and 5ID/5OD (AN3) cases have the most complete mixing, while the 3ID/3OD (AN1) and 6ID/6OD (AN4) cases still exhibit significant radial variations.

Figure 14 presents a plot of CO emissions index (EI) versus x/H for each of the annular cases. Note that the CFD analysis assumes a fast chemistry approximation, and any CO that is present in the flowfield is a direct result of lack of mixing. Each CO EI figure is divided into two graphs. The first graph shows the overall CO EI levels for the parametric cases. The inserted graph shows an enlarged view of the lower end of the CO EI scale. Equilibrium CO EI for ϕ_{lb}=0.425 is 2, and a combustion efficiency of 99.5% corresponds to a CO EI of 20. A horizontal line is shown on the graphs to represent the 99.5% combustion efficiency level. All the cases reach a CO EI of 20 well before reaching the exit (x/H > 3.0). Of the four cases, the 3ID/3OD (AN1) has the highest CO, not falling below 20 until x/H of 1.8.

Figures 15 and 16 show the normalized NO_x and CO EI as a function of x/R for the can parametric. The NO_x curves all have positive slopes at x/R > 3.0 indicating ongoing NO_x production. Only the 6 (C2) and 7 (C3) orifice cases are starting to level off. The CO curves shown in Figure 16 take a much longer axial distance to reach the 99.5% combustion efficiency level than the annular cases (x/R=2.0- 2.5-can vs. x/H=1.5-annular), and even then only the 5 (C1), 6 (C2), and 7 (C3) orifice cases attain the 99.5% level. For the other cases the positive slopes of the NO_x curves and the presence of CO remaining in the flowfield suggest the need of a longer lean-burn section to achieve the necessary combustion efficiency.

Based on the emission curves, the optimum configurations are the 5ID/5OD (AN3) case for the annular geometry, and the 7 orifice case (C3) for the can geometry. These two configurations were selected as being optimum because 1.) they showed the lowest overall NO_x at the exit plane, and 2.) reached a combustion efficiency of 99.5% before the end of the mixing section. A comparison of the two optimum configurations is shown in Figure 17. Note the x/R_{eq} used for the annular geometry is based on the radius of an equal area can. From Figure 17, both configurations show similar trends of NO_x production. The NO_x production in the first x/R=2.25 is approximately the same. Towards x/R=4.0, the annular geometry shows a slightly lower value of NO_x. In addition, both curves are "leveling off", indicating good overall mixing and no NO_x production (i.e. no significant NO_x contribution farther downstream). Therefore, from a design standpoint, there is no significant emission

advantage gained by the selection of either the annular or can geometry.

Design Correlation Constant for Annular and Can Configuration

The last columns of Tables 2 & 3 show the optimum mixing design correlation constants based on the equation, $C = (S/H)\sqrt{J}$.

For the can cases (Table 2), the constant were determined using two different spacing methods;

1. Orifice spacing at the OD
2. Orifice spacing at a radius corresponding to equal flow areas in the can

These methods are illustrated at the bottom of Table 2. Similarly, these methods exist for the annular geometry. For the annular cases, the constants were calculated based on orifice spacing at the ID and OD (Method 1), and equivalent area spacing (Method 2). Method 2 has been reported to be the appropriate method for both can and annular configurations.[19]

Based on the emission results, the optimum configuration for the annular geometry is the 5ID/5OD (AN3) case. The design constant for this case is 2.35. This C value is consistent with results from previously performed high jet-to-mainstream mass-flow ratio (MR > 2.0) analyses. It is about twice the value reported for low MR's (< 0.5).

The can emission results indicate that the 7 orifice case (C3) has the best emission signature. Using the equal area approach, the C constant is 3.5, or 40% higher than that reported for mixing at lower MR (< 0.5).

7. Conclusions

A CFD parametric analysis was performed on transverse jets injected into both annular and can confined crossflow. The slot spacing was systematically varied while maintaining all other design variables constant. Optimum configurations were determined based on jet penetration, and NO_x and CO emissions. The conclusions that can be drawn are as follows;

1. Optimum annular and can geometries have similar emission characteristics at the end of a mixing section and lean-burn section (x/H=3.0) as long as jet penetration/mixing is optimized.
2. For the MR of 3.2 evaluated in this study, the design correlation constant $[C = (S/H)\sqrt{J}]$ was 2.35 for the annulus and 3.5 for the can. The value for the annulus is about twice the value for low MR's (< 0.5). The value for the can is about 40% higher than that for the low MR.

8. Acknowledgement

This work was supported by NASA Contract NAS3-25967, and NAS computer time was provided by NASA Lewis Research Center. The authors would like to thank Mr. Gary Hufford and Dr. Bhavin Patel for their expertise and help in the use of CFD-GEOM. In addition, thanks are also extended to Dr. Andy Leonard and the CFD-ACE development and support staff for their assistance in using the combustion model. Last but not least, thanks are given to Ms. Marni Kent for preparing this typescript.

9. References

1. R. J. Shaw, "Engine Technology Challenges for a 21st Century High Speed Civil Transport," *AIAA Tenth International Symposium on Air Breathing Engines*, September 1-6, 1991 (Also NASA TM 104363).
2. S. A. Mosier and R. M. Pierce, "Advanced Combustion Systems for Stationary Gas Turbine Engines," Vol. 1, EPA Contract 68-02-2136, 1980.

3. C. E. Smith, M. V. Talpallikar, and J. D. Holdeman, "A CFD Study of Jet Mixing in Reduced Flow Areas for Lower Combustor Emissions," AIAA 91-2460, June, 1991 (Also NASA TM 104411).
4. A. Vranos, D. S. Liscinsky, B. True, and J. D. Holdeman, "Experimental Study of Cross-Stream Mixing in a Cylindrical Duct," AIAA 91-2459, June, 1991 (Also NASA TM 105180).
5. M. V. Talpallikar, C. E. Smith, M. C. Lai, and J. D. Holdeman, "CFD Analysis of Jet Mixing in Low NO_x Flametube Combustors," ASME Paper 91-GT-217, Vol. 114, pp. 416-424, ASME Transactions, Journal of Engineering for Gas Turbines and Power, 1992 (Also NASA TM 104466).
6. G. W. Howe, Z. Li, T. I.-P. Shih, and H. L. Nguyen, "Simulation of Mixing in the Quick Quench Region of a Rich Burn-Quick Quench-Lean Burn Combustor," AIAA 91-0410, 1991.
7. M. S. Hatch, W. A. Sowa, G. S. Samuelsen, and J.D. Holdeman, "Jet Mixing Into a Heated Cross Flow in a Cylindrical Duct: Influence of Geometry and Flow Variations," Accepted for publication in Journal of Propulsion and Power. (See also AIAA 92-0773, January 1992 and NASA TM 105390).
8. D. B. Bain, C. E. Smith, and J. D. Holdeman, "CFD Mixing Analysis of Jets Injected from Straight and Slanted Slots into Confined Crossflow in Rectangular Ducts," AIAA 92-3087, (Also NASA TM 105699).
9. D. S. Liscinsky, B. True, A. Vranos, and J. D. Holdeman, "Experimental Study of Cross-Stream Mixing in a Rectangular Duct," AIAA 92-3090, (Also NASA TM 106194).
10. M. S. Hatch, W. A. Sowa, G. S. Samuelsen, and J. D. Holdeman, "Influence of Geometry and Flow Variations on NO Formation in the Quick Mixer of a Staged Combustor," Accepted for publication in Journal of Engineering for Gas Turbine and Power, (See also NASA TM 105639, July 1992).
11. V. L. Oechsle, H. C. Mongia, and J. D. Holdeman, "A Parametric Numerical Study of Mixing in a Cylindrical Duct," AIAA 92-3088, (Also NASA TM 105695).
12. G. Zhu and M.-C. Lai, "A Parametric Study of Penetration and Mixing of Radial Jets in Necked-Down Cylindrical Crossflow," AIAA 92-3091.
13. J. T. Kroll, W. A. Sowa, G. S. Samuelsen, and J. D. Holdeman, "Optimization of Circular Orifice Jets Mixing into a Heated Crossflow in a Cylindrical Duct," AIAA 93-0249, (Also NASA TM 105984).
14. D. S. Liscinsky, A. Vranos, and R. P. Lohmann, "Experimental Study of Crossflow Mixing in Cylindrical and Rectangular Ducts," NASA CR 187141, March 1993.
15. Th. Doerr and D. K. Hennecke, "The Mixing Process in the Quenching Zone of the Rich-Lean Combustion Concept," *AGARD 81st Symposium on Fuels and Combustion Technology for Advanced Aircraft Engines*, Colleferro, NR Rome, Italy, May 10-14, 1993.
16. D. S. Liscinsky, B. True, and J. D. Holdeman, "An Experimental Study of Crossflow Jet Mixing in Rectangular Ducts," AIAA-93-2037 (also TM 106152).
17. D. B. Bain, C. E. Smith, and J. D. Holdeman, "CFD Mixing Analysis of Axially Opposed Rows of Jets Injected in Confined Crossflow," Accepted for publication in Journal of Propulsion and Power, (See also AIAA Paper 93-2044 and NASA TM 106179).

18. V. L. Oechsle, H. C. Mongia, and J. D. Holdeman, "An Analytical Study of Jet Mixing in a Cylindrical Duct", AIAA 93-2043, (Also NASA TM 106181).
19. J. D. Holdeman, "Mixing of Multiple Jets with a Confined Subsonic Crossflow," *Progress in Energy and Combustion Sciences*, Vol. 19, pp. 31-70, 1993. (also NASA TM 104412, 1991 and AIAA 91-2458, 1991).
20. J. D. Holdeman, R. Srinivasan, R. Reynolds, and C. D. White, "Studies of the Effects of Curvature on Dilution Jet Mixing, Journal Propulsion and Power, Vol. 8, No. 1, p. 209, 1992. (Also, AIAA Paper 87-1953; NASA TM –89878 and AIAA Paper 88-3180; NASA TM–00896).
21. D. S. Crocker and C. E. Smith, "Numerical Investigation of Enhanced Dilution Zone Mixing in a Reverse Flow Gas Turbine Combustor," ASME 93-GT-129, 1993.
22. D.B.Bain, C.E. Smith, and J.D. Holdeman, (1994). "CFD Assessment of Orifice Aspect Ratio and Mass Flow Ratio on Jet Mixing in Rectangular Ducts. AIAA Paper 94-0218 (also NASA TM 106477).
23. D.S. Liscinsky, B. True, and J.D. Holdeman, (1994) "Mixing Characteristics of Directly Opposed Rows of Jets Injected Normal to a Crossflow in a Rectangular Ducts. AIAA Paper 94-0217 (also NASA TM 106477).
24. V.L. Oechsle, H.C. Mongia, and J.D. Holdeman, (1994). "Comparison of the Mixing Calculations of Reacting and Non-Reacting Flows in a Cylindrical Duct." AIAA Paper 94-0865 (also NASA TM 106436).
25. W.A. Sowa, J.T. Kroll, G.S. Samuelsen, and J.D. Holdeman, (1994). "Optimization of Orifice Geometry for Crossflow Mixing in a Cylindrical Duct." AIAA Paper 94-0219 (also NASA TM 106436)
26. D.S. Liscinsky, B. True, and J.D. Holdeman, (1995). "Crossflow Mixing of Noncircular Jets. Accepted for publication in Journal of Propulsion and Power, (see also AIAA Paper 95-0732 and NASA TM 106865).
27. V.L. Oechsle and J.D. Holdeman, (1995). Numerical Mixing Calculations of Confined Reacting Jet Flows in a Cylindrical Duct. AIAA Paper 95-0733 (also NASA TM 106736).
28. S. F. Owens, "CFD-ACE: Command Language Reference Manual," CFD Research Corporation, Huntsville, AL, CFDRC Report GR-92-6, 1992.
29. B. E. Launder and D. B. Spalding, "The Numerical Computation of Turbulent Flows," *Computer Methods in Applied Mechanics and Engineering*, Vol. 3, pp. 269-289, 1974.
30. Y. S. Chen and S. W. Kim, "Computation of Turbulent Flows Using an Extended k–ε Turbulence Closure Model," NASA CR-179204, 1987.
31. K. Y. Chien, "Predictions of Channel and Boundary-Layer Flows with a Low-Reynolds Number-Turbulence Model," *AIAA Journal*, Vol. 23, No. 2, 1985.
32. CFD-GEOM User Manual, Version 1.3, March 1995.
33. K. Radhakrishnan and D. A. Bittker, LSENS, A General Chemical Kinetics and Sensitivity Analysis Code for Gas-Phase Reactions: User's Guide, NASA Technical Memorandum 105851, January 1993.
34. V. J. Harrand, "CFD VIEW: A 3D Computer Graphics Software; Volume 1: Technical Manual," August 1992.
35. V. J. Harrand, "CFD VIEW: A 3D Computer Graphics Software; Volume 2: User's Manual," August 1, 1992.
36. CFD-POST User Manual, Version 1.06, July 1994.
37. W. Bartok and A. F. Sarofim, Fossil Fuel Combustion, New York, p. 233, 1991.

38. D. G. Nicol, R. C. Steele, N. M. Marinov, and P. C. Malte, "The Importance of the Nitrous Oxide Pathway to NO_x in Lean-Pre-Mixed Combustion," ASME Paper 93-GT-342, ASME Transactions, Cincinnati, May 1993.

Table 1. Spacing and Momentum-Flux Ratio Relationships

Configuration	$C = (S/H)\sqrt{(J)}$
Single-side injection:	
Under-penetration	<1.25
Optimum	2.5
Over-penetration	>5.0
Opposed rows of jets:	
In-line optimum	1.25
Staggered optimum	5.0

Case	Can Sector Angle	Wall Diameter	Orifice Aspect Ratio	Orifice Width	# of Orifices Modeled	Orifice Spacing 1	Orifice Spacing 2	Orifice Spacing 3	Momentum Flux Ratio,J	Design C Values 1	Design C Values 2
C1	72°	3.306" (0.0838m)	2:1 Rounded Slot	0.01738m	1 (5 holes)*	0.0527m S/H 1.26	0.0263m S/H 0.63	0.0372m S/H 0.88	30	6.9	4.87
C2	60°	3.306" (0.0838m)	2:1 Rounded Slot	0.01578m	1 (6 holes)*	0.0439m S/H 1.05	0.0219m S/H 0.52	0.03102m S/H 0.74	30	5.75	4.05
C3	51.43°	3.306" (0.0838m)	2:1 Rounded Slot	0.01464m	1 (7holes)*	0.0376m S/H 0.90	0.0188m S/H 0.45	0.0266m S/H 0.63	30	4.93	3.48
C4	45°	3.306" (0.0838m)	2:1 Rounded Slot	0.0137m	1 (8 holes)*	0.0329m S/H 0.78	0.0165m S/H 0.39	0.0233m S/H 0.56	30	4.27	3.07
C5	36°	3.306" (0.0838m)	2:1 Rounded Slot	0.0122m	1 (10 holes)*	0.0263m S/H 0.63	0.0132m S/H 0.31	0.01862m S/H 0.44	30	3.45	2.41
C6	30°	3.306" (0.0838m)	2:1 Rounded Slot	0.0112m	1 (12 holes)*	0.0219m S/H 0.52	0.0101m S/H 0.26	0.0155m S/H 0.37	30	2.85	2.03

Method 1 * per 360° **Method 2**

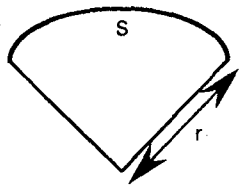

Outer Radius

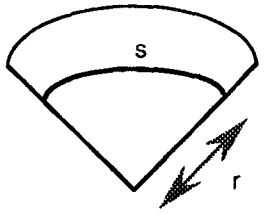

Equal Area

Table 2. Can Geometry Parameters

Case	# of Orifices Pairs	Sector Angle per Orifice Pair	Sector Height	Orifice Aspect Ratio	Orifice Width	# of Orifices Modeled	Orifice Spacing		Momentum-Flux Ratio,J	Design C Values		
							ID	OD		ID	OD	Equal Area
AN1	3 * (3ID/3OD)	5°	2" (0.0508m)	2:1 Rounded Slot	0.01578m	1 OD 1 ID	0.0340m S/H 0.67	0.0384m S/H 0.76	30	3.67	4.16	3.91
AN2	4 * (4ID/4OD)	3.75°	2" (0.0508m)	2:1 Rounded Slot	0.0137m	1 OD 1 ID	0.0255m S/H 0.50	0.0283m S/H 0.57	30	2.74	3.12	2.93
AN3	5 * (5ID/5OD)	3°	2" (0.0508m)	2:1 Rounded Slot	0.0122m	1 OD 1 ID	0.0204m S/H 0.40	0.0231m S/H 0.45	30	2.19	2.46	2.35
AN4	6 * (6ID/6OD)	2.5°	2" (0.0508m)	2:1 Rounded Slot	0.0112m	1 OD 1 ID	0.0170m S/H 0.33	0.0192m S/H 0.38	30	1.81	2.08	1.96

* # of Orifice Pairs per 15° Nozzle Sector

Table 3. Annular Geometry Parameters

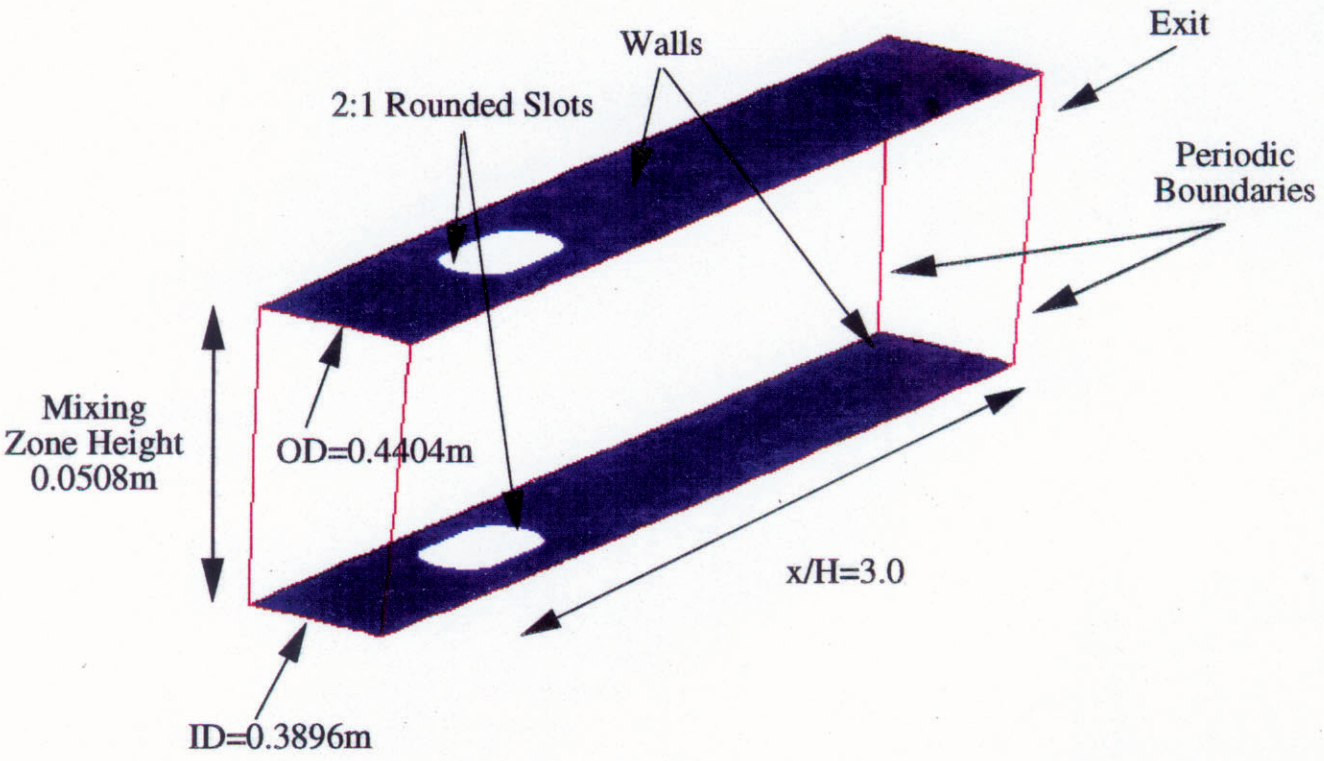

Figure 1. Schematic of the Annular Geometry

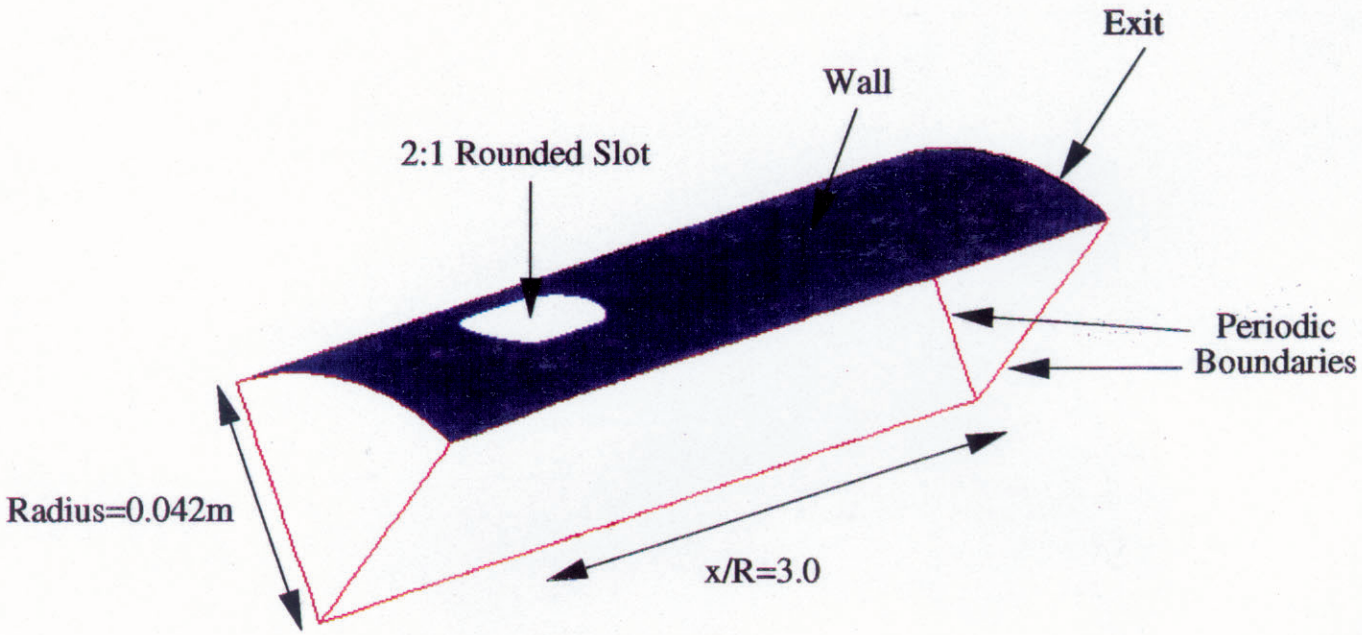

Figure 2. Schematic of the Can Geometry

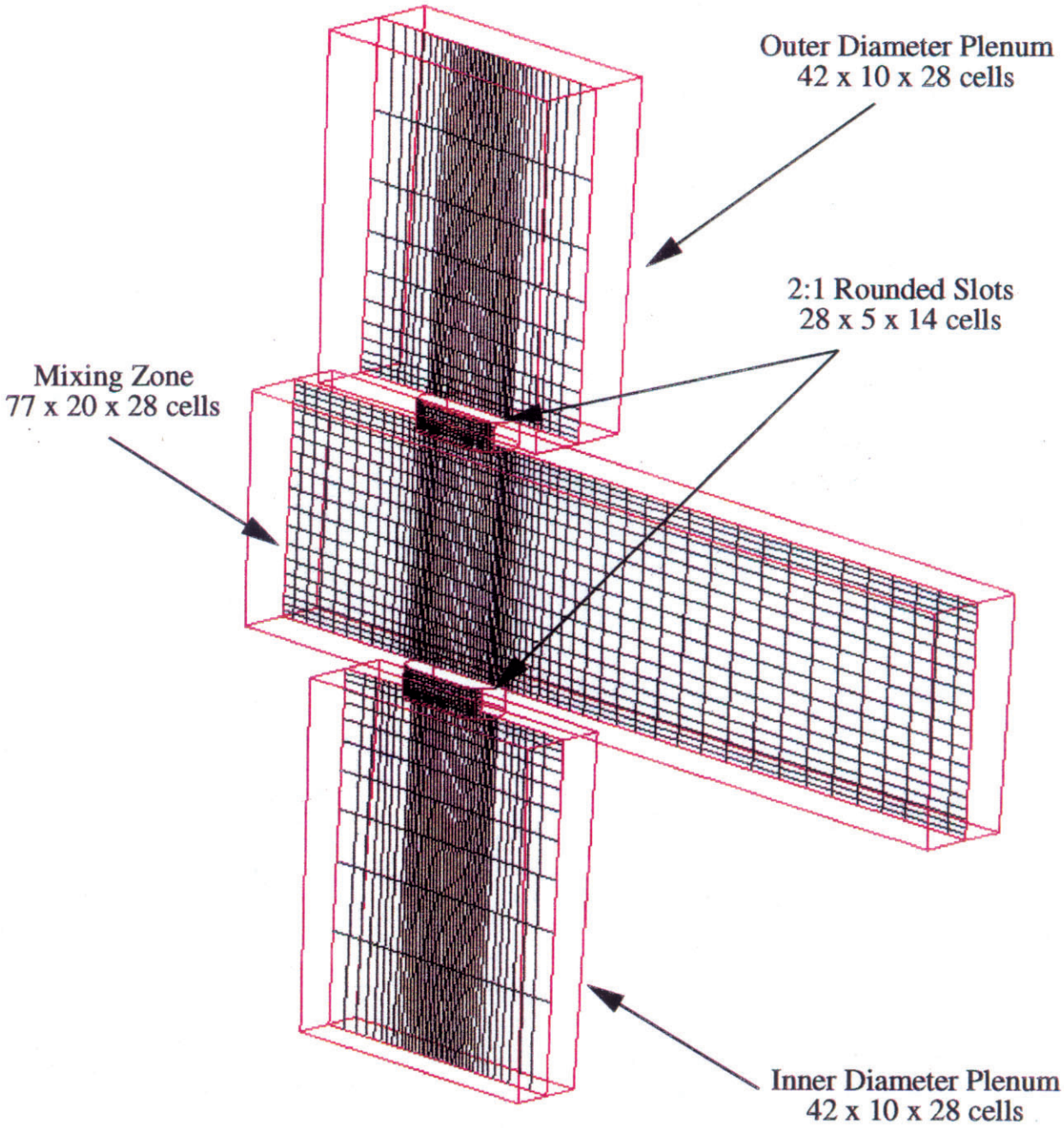

Figure 3. Typical Computational Mesh Used for Annular Parametric Analysis

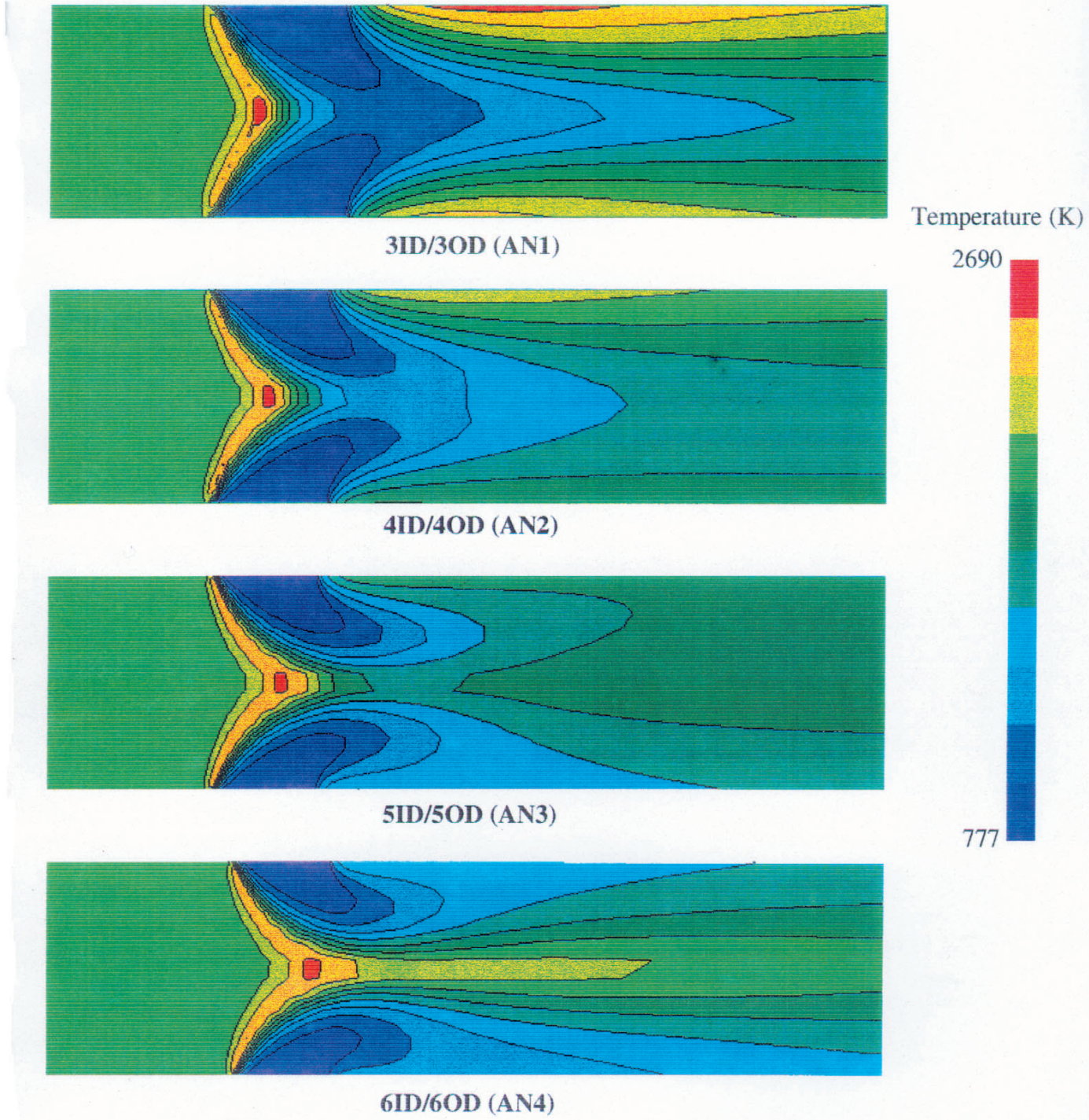

Figure 4. Temperature Transverse Slices Taken at the Slot Centerline;Annular Geometry

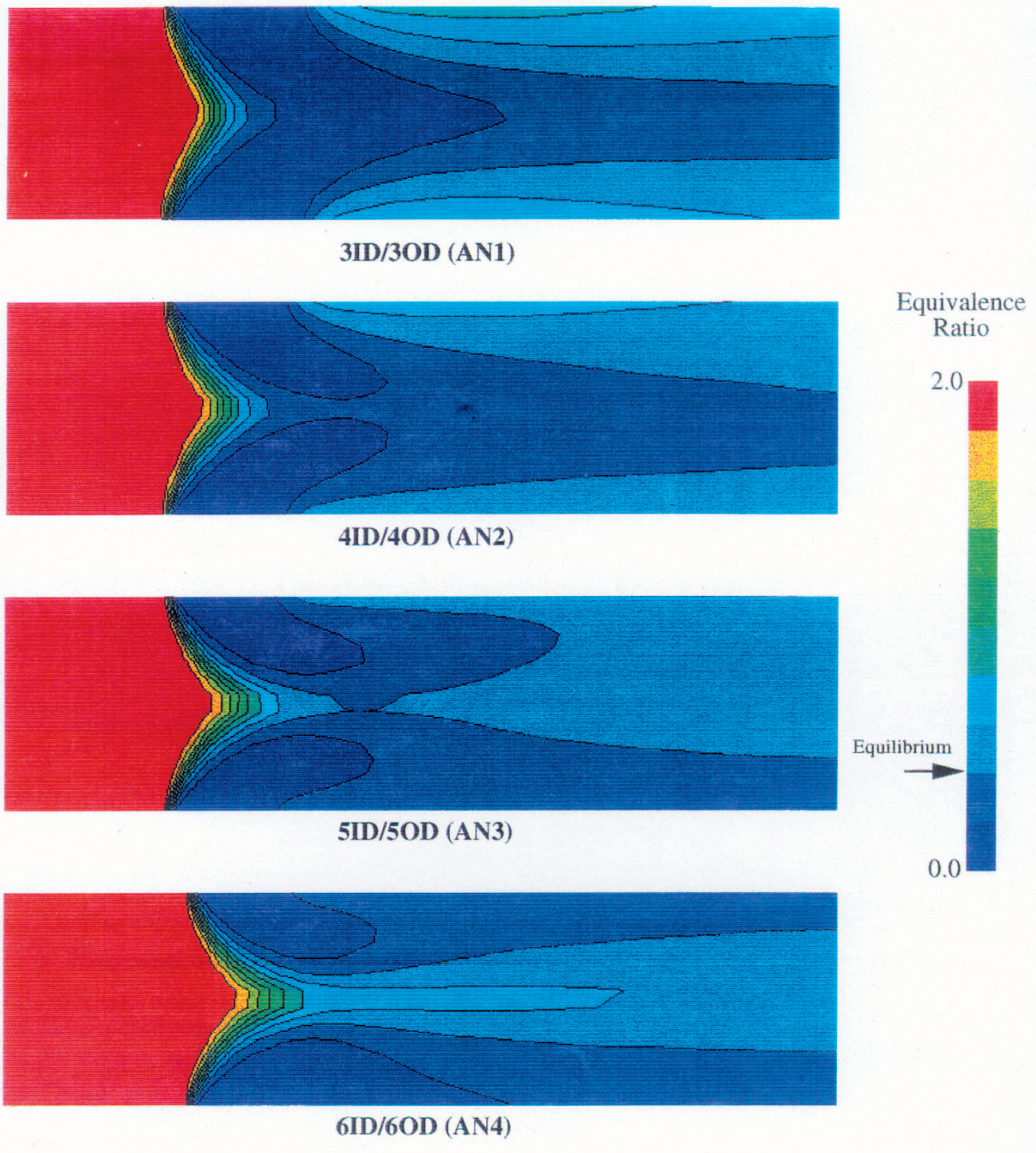

Figure 5. Equivalence RatioTransverse Slices Taken at the Slot Centerline;Annular Geometry

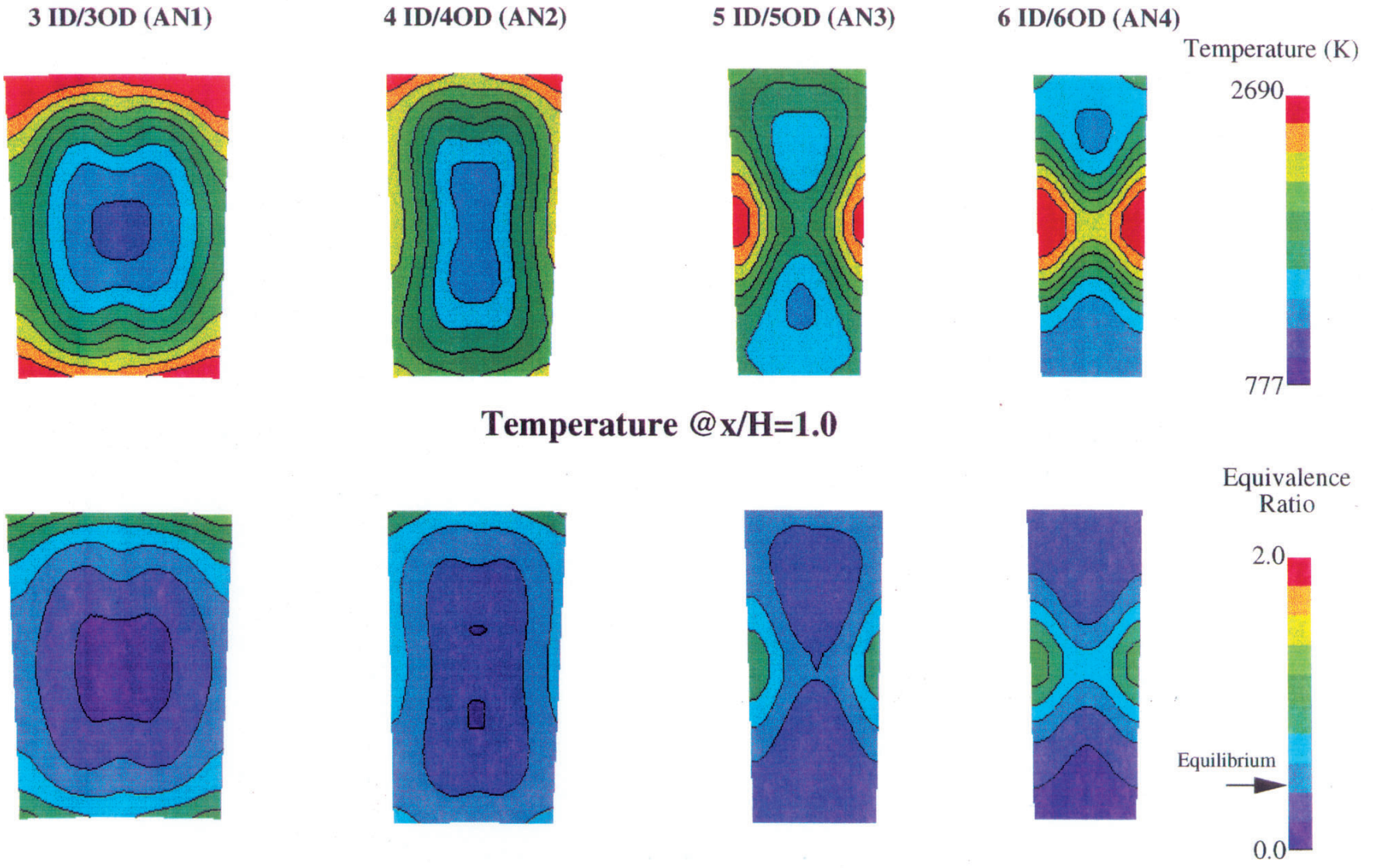

Figure 6. Equivalence Ratio and Temperature Contours (Annular Geometry) @ x/H=1.0

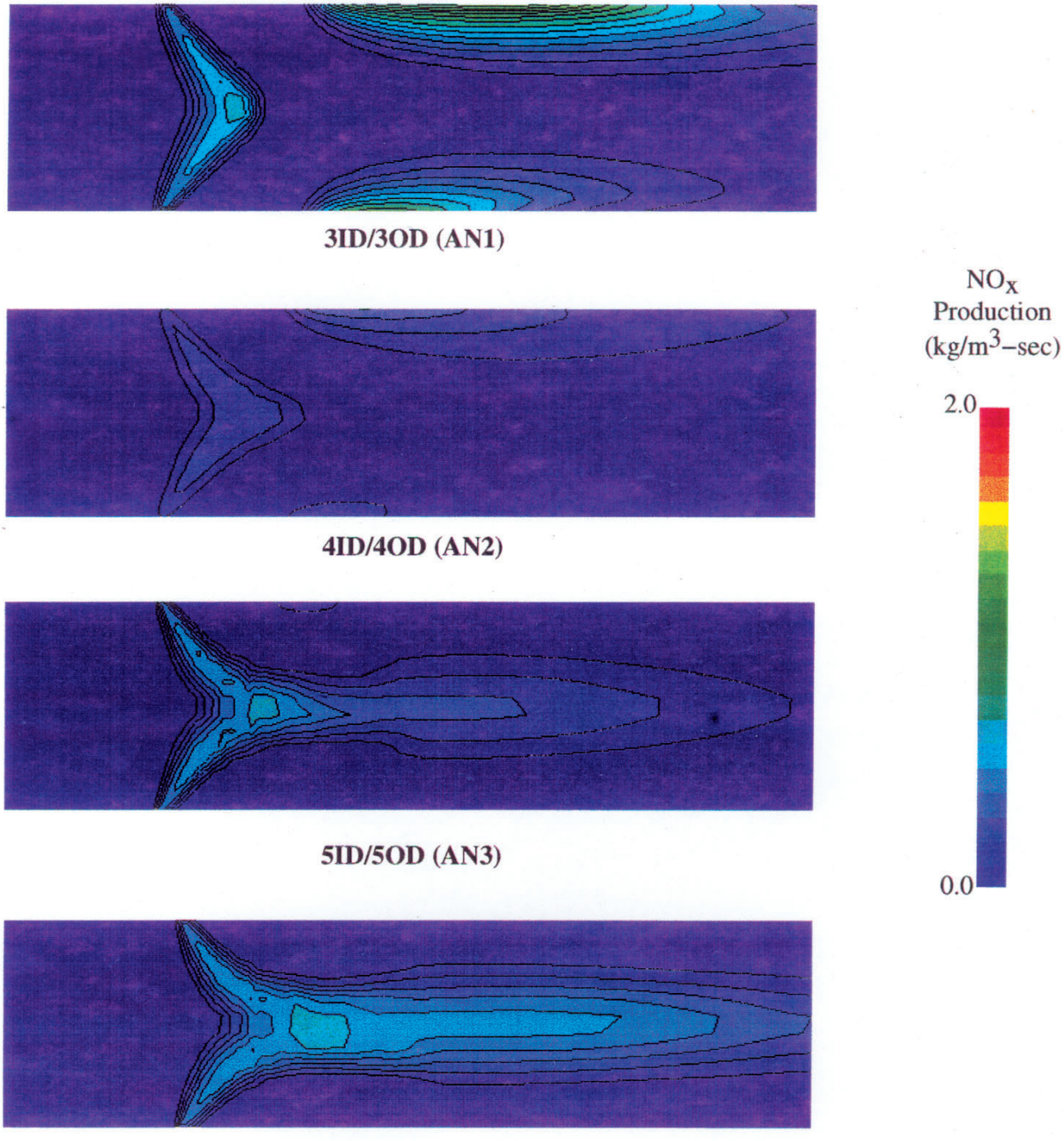

Figure 7. NO_x Production Contours for Annular Geometry

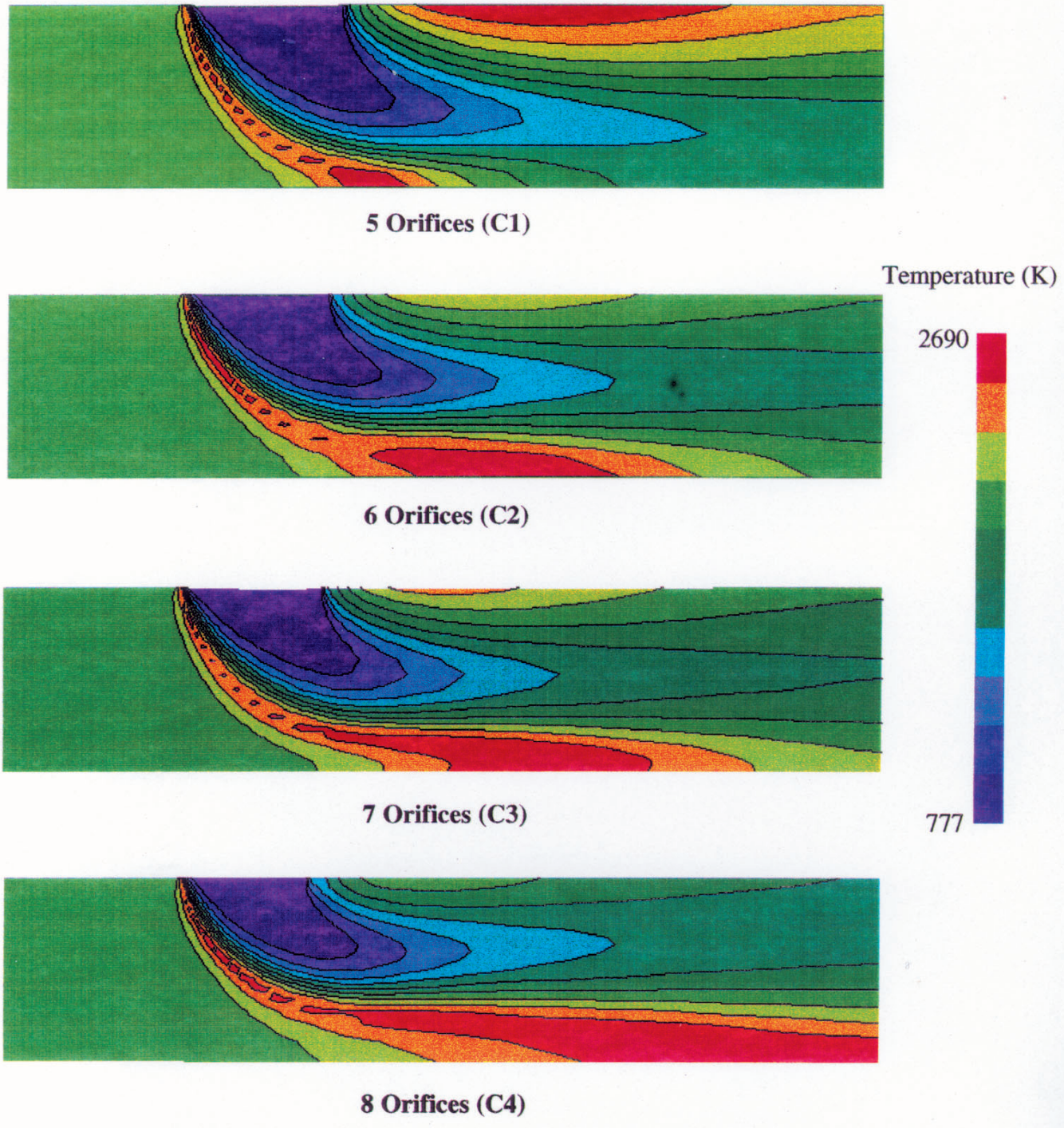

Figure 8. Temperature Transverse Slices Taken at the Slot Centerline; Can Geometry

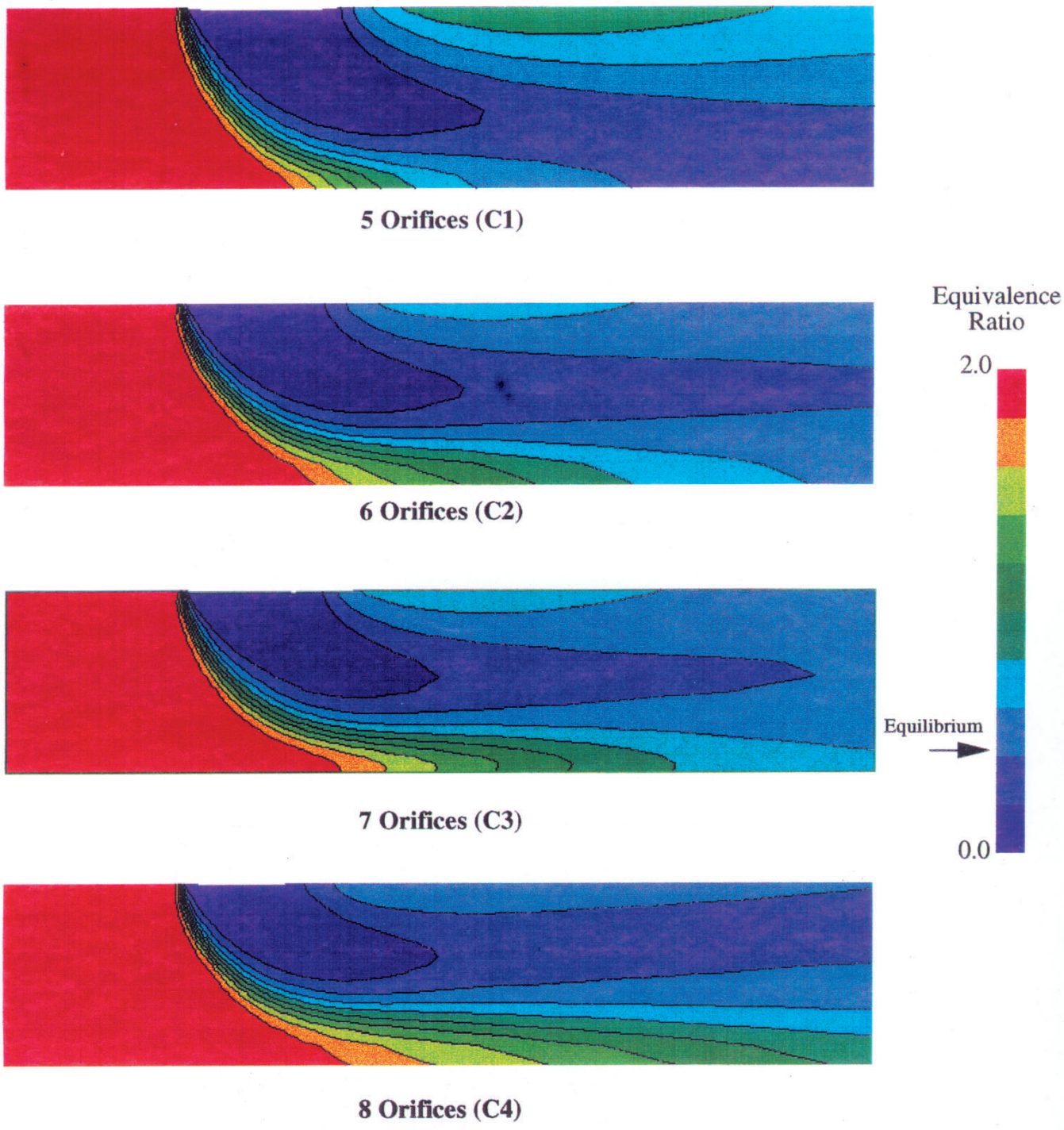

Figure 9. Equivalence Ratio Transverse Slices Taken at the Slot Centerline; Can Geometry

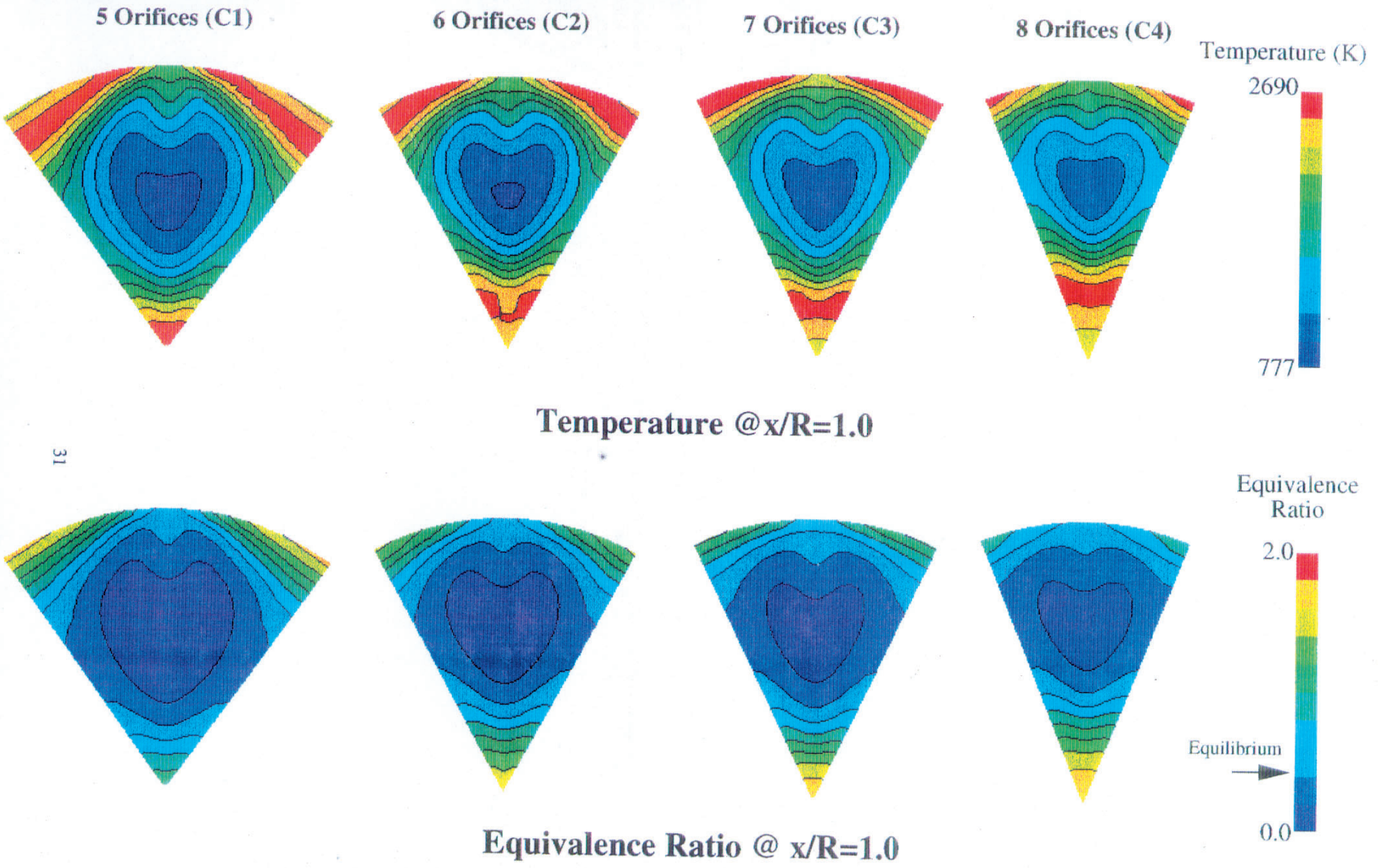

Figure 10. Equivalence Ratio and Temperature Contours (Can Geometry) @ x/R=1.0

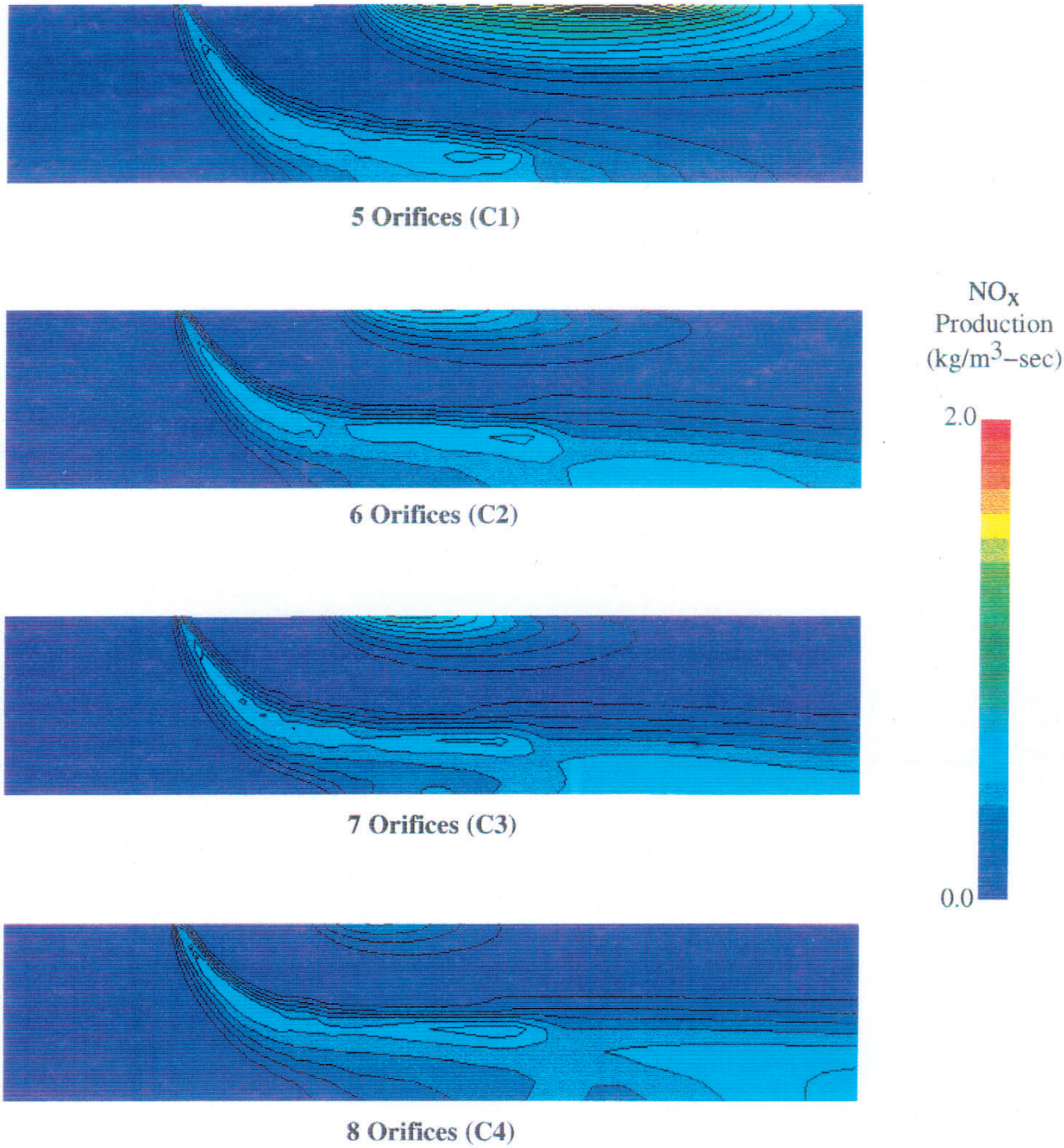

Figure 11. NO_X Production Terms Contours for Can Geometry

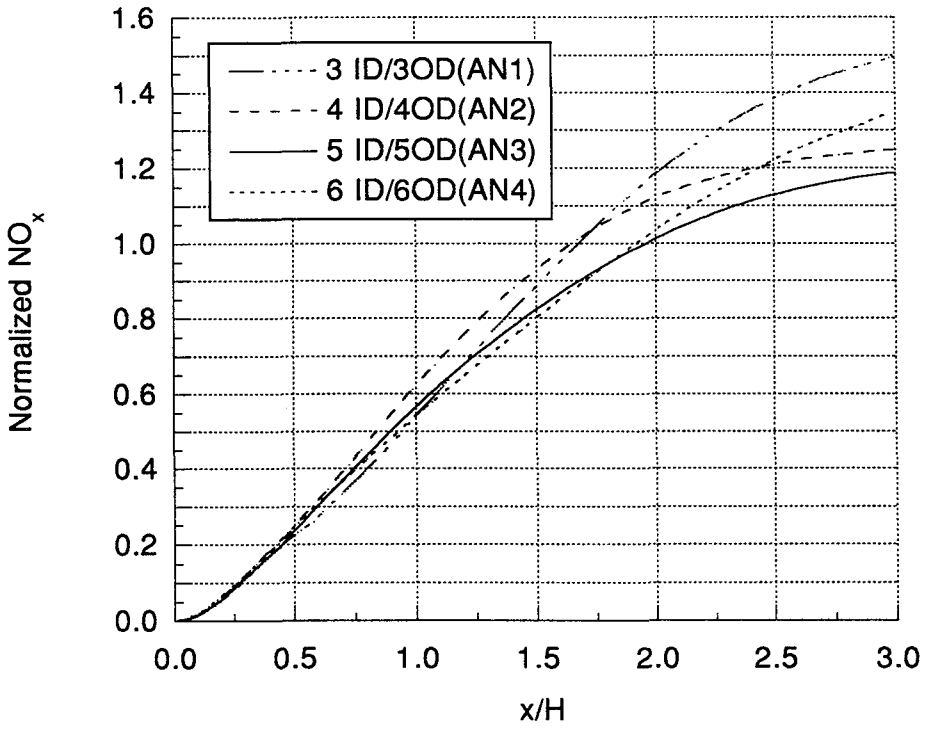

Figure 12. Normalized NO_x Curves for Annular Geometry

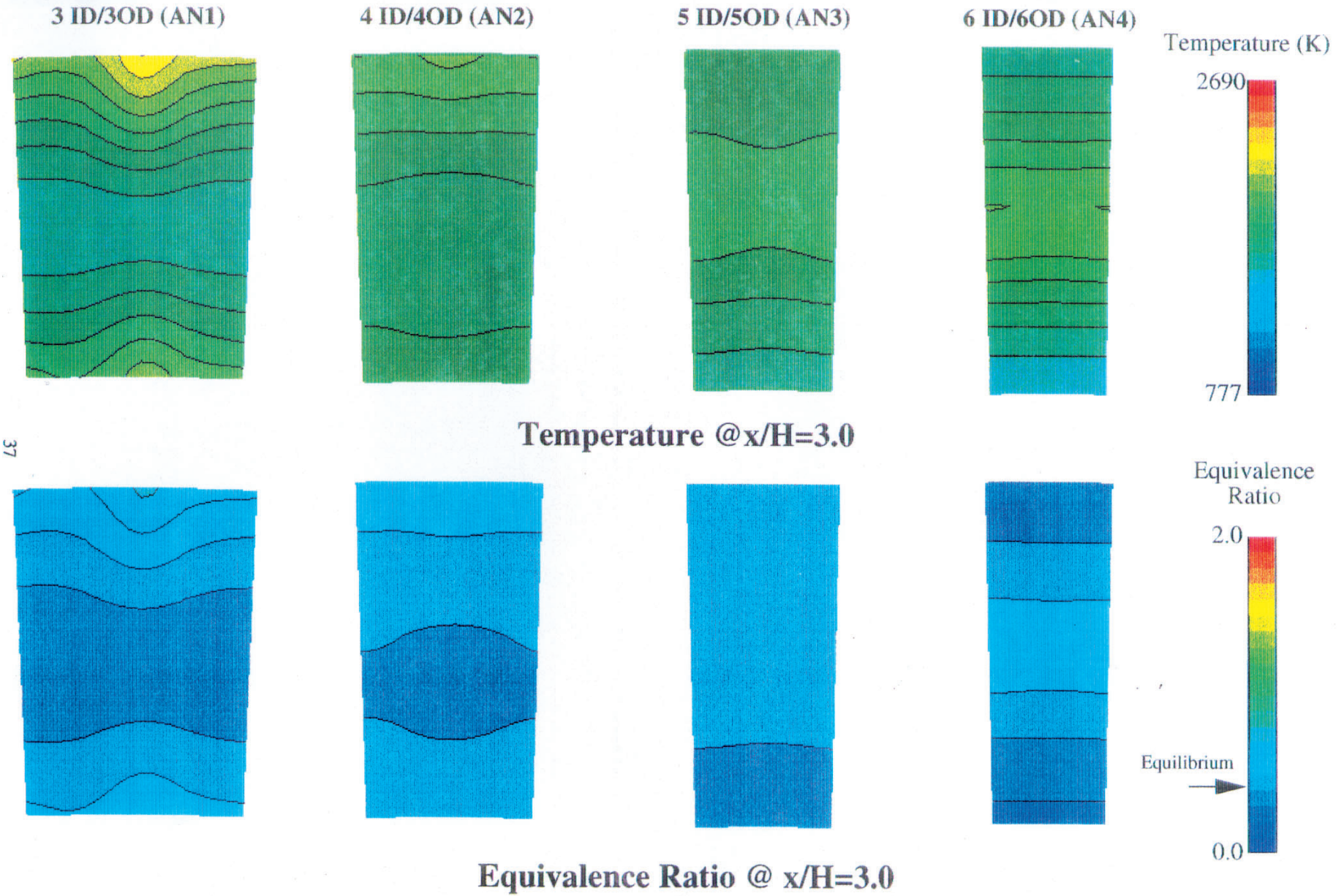

Figure 13. Equivalence Ratio and Temperature Contours (Annular Geometry) @ x/H=3.0

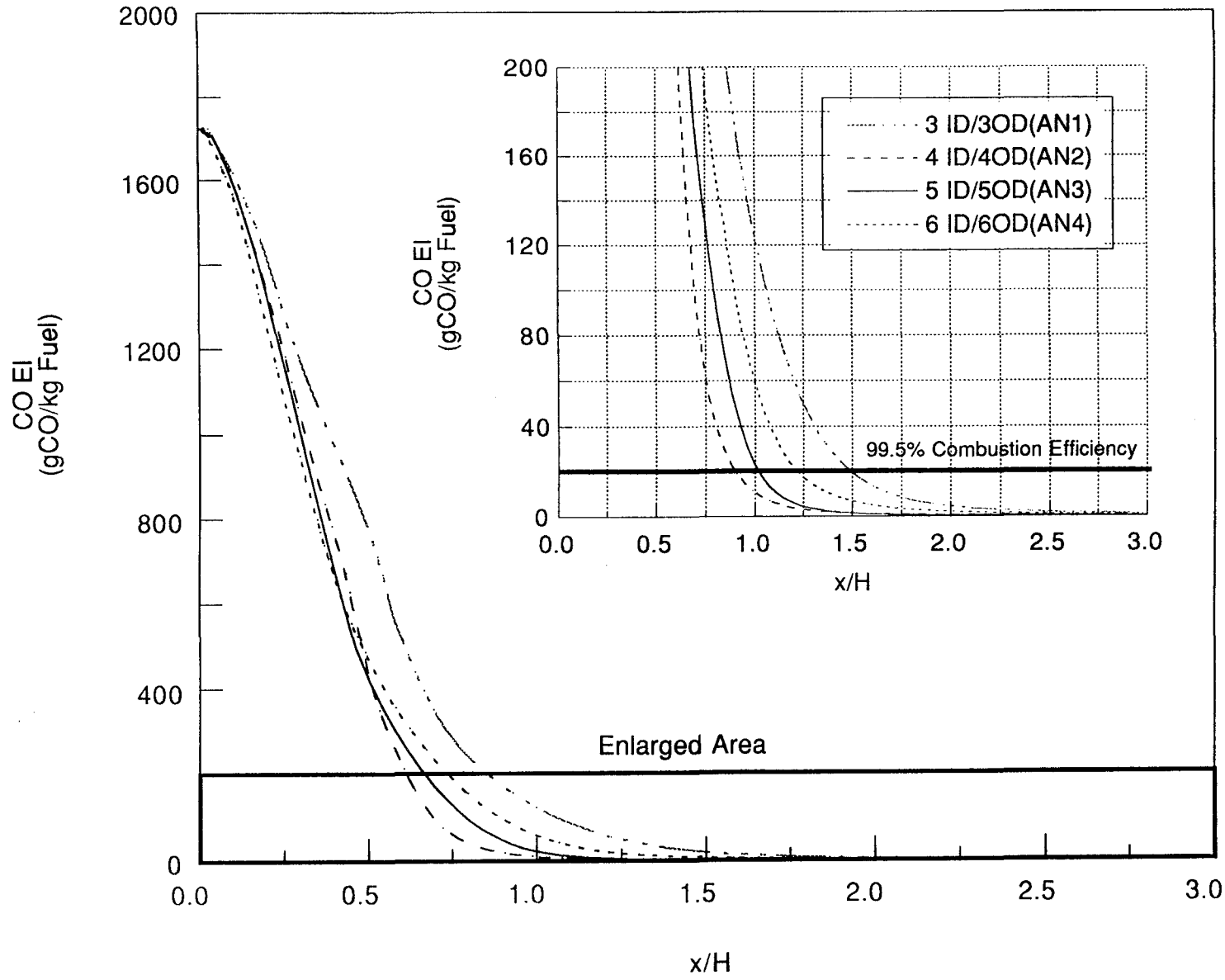

Figure 14. CO EI Curves for Annular Geometry

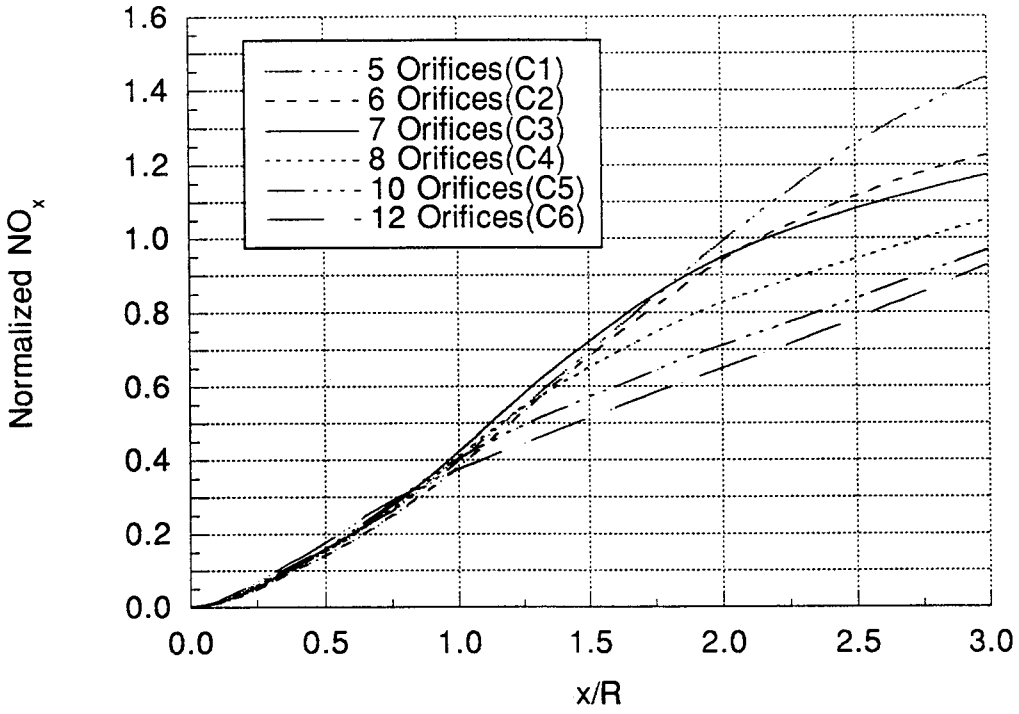

Figure 15. Normalized NO_x Curves for Can Geometry

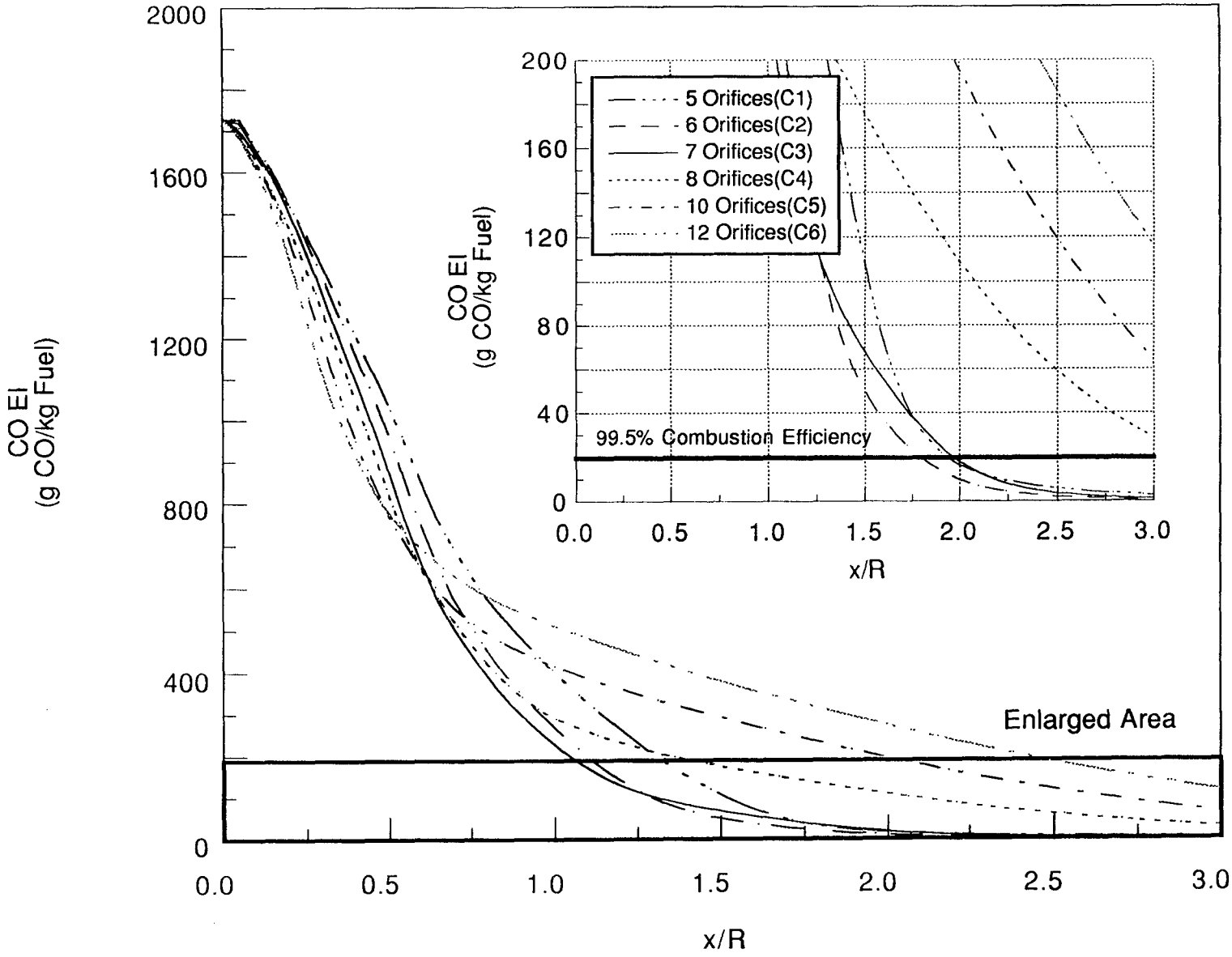

Figure 16. CO EI Curves for Can Geometry

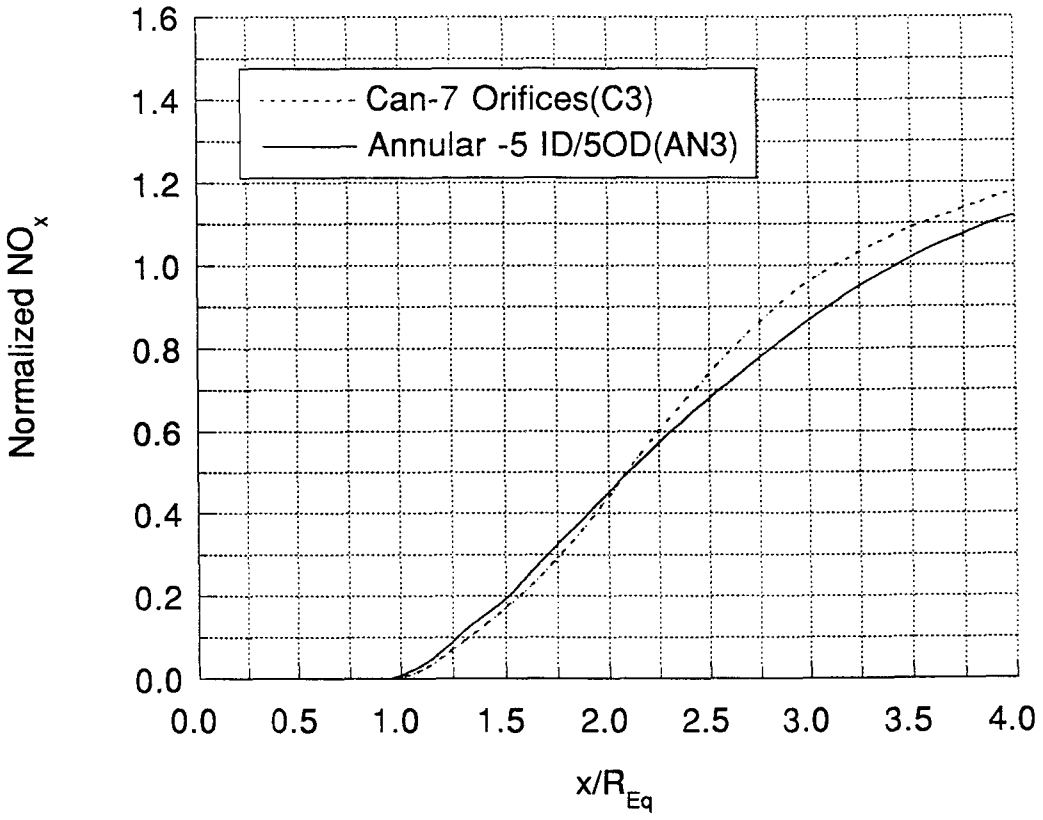

Figure 17. Comparison of Optimum Can and Annular Normalized NO_x

REPORT DOCUMENTATION PAGE

Form Approved
OMB No. 0704-0188

1. AGENCY USE ONLY (*Leave blank*)	2. REPORT DATE	3. REPORT TYPE AND DATES COVERED
	July 1995	Technical Memorandum

4. TITLE AND SUBTITLE

Jet Mixing and Emission Characteristics of Transverse Jets in Annular and Cylindrical Confined Crossflow

5. FUNDING NUMBERS

WU–537–02–21–00

6. AUTHOR(S)

D.B. Bain, C.E. Smith, and J.D. Holdeman

7. PERFORMING ORGANIZATION NAME(S) AND ADDRESS(ES)

National Aeronautics and Space Administration
Lewis Research Center
Cleveland, Ohio 44135–3191

8. PERFORMING ORGANIZATION REPORT NUMBER

E–9737

9. SPONSORING/MONITORING AGENCY NAME(S) AND ADDRESS(ES)

National Aeronautics and Space Administration
Washington, DC 20546–0001

10. SPONSORING/MONITORING AGENCY REPORT NUMBER

NASA TM–106976
AIAA–95–2995

11. SUPPLEMENTARY NOTES

Prepared for the 31st Joint Propulsion Conference and Exhibit cosponsored by AIAA, ASME, SAE, and ASEE, San Diego, California, July 10–12, 1995. D.B. Bain and C.E. Smith, CFD Research Corporation, Huntsville, Alabama; J.D. Holdeman, NASA Lewis Research Center. Responsible person, J.D. Holdeman, organization code 2650, (216) 433–5846.

12a. DISTRIBUTION/AVAILABILITY STATEMENT

Unclassified - Unlimited
Subject Category: 07

Available electronically at http://gltrs.grc.nasa.gov/GLTRS
This publication is available from the NASA Center for AeroSpace Information, (301) 621–0390.

12b. DISTRIBUTION CODE

13. ABSTRACT ***(Maximum 200 words)***

3-D turbulent reacting CFD analyses were performed on transverse jets injected into annular and cylindrical (can) confined crossflows. The goal of this study was to identify and assess mixing differences between annular and can geometries. The approach was to optimize both annular and can configurations by systematically varying orifice spacing until lowest emissions were achieved, and then compare the results. Numerical test conditions consisted of a jet-to-mainstream mass-flow ratio of 3.2 and a jet-to-mainstream momentum-flux ratio (J) of 30. The computational results showed that the optimized geometries had similar emission levels at the exit of the mixing section although the annular configuration did mix-out faster. For lowest emissions, the design correlation parameter ($C=(S/H),\sqrt{J}$) was 2.35 for the annular geometry and 3.5 for the can geometry. For the annular geometry, the constant was about twice the value seen for jet mixing at low mass-flow ratios (i.e. MR < 0.5). For the can geometry, the constant was about 1 1/2 times the value seen for low mass-flow ratios.

14. SUBJECT TERMS

Dilution; Jet mixing flow; Gas turbines; Combustion chamber; Emissions

15. NUMBER OF PAGES

32

16. PRICE CODE

A03

17. SECURITY CLASSIFICATION OF REPORT	18. SECURITY CLASSIFICATION OF THIS PAGE	19. SECURITY CLASSIFICATION OF ABSTRACT	20. LIMITATION OF ABSTRACT
Unclassified	Unclassified	Unclassified	

Appendix G

NASA Technical Memorandum 107257

NASA Technical Memorandum 107257
AIAA–96–2762

Flow Coupling Effects in Jet-In-Crossflow Flowfields

D.B. Bain and C.E. Smith
CFD Research Corporation
Huntsville, Alabama

D.S. Liscinsky
United Technologies Center
East Hartford, Connecticut

J.D. Holdeman
Lewis Research Center
Cleveland, Ohio

Prepared for the
32nd Joint Propulsion Conference
cosponsored by AIAA, ASME, SAE, and ASEE
Lake Buena Vista, Florida, July 1–3, 1996

National Aeronautics and
Space Administration

FLOW COUPLING EFFECTS IN JET-IN-CROSSFLOW FLOWFIELDS

D.B. Bain
C.E. Smith
CFD Research Corporation
Huntsville, Alabama

D.S. Liscinsky
United Technologies Center
East Hartford, Connecticut

J.D. Holdeman
NASA Lewis Research Center
Cleveland, Ohio

Abstract

The combustor designer is typically required to design liner orifices that effectively mix air jets with crossflow effluent. CFD combustor analysis is typically used in the design process; however the jets are usually assumed to enter the combustor with a uniform velocity and turbulence profile. The jet-mainstream flow coupling is usually neglected because of the computational expense. This CFD study was performed to understand the effect of jet-mainstream flow coupling, and to assess the accuracy of jet boundary conditions that are commonly used in combustor internal calculations.

A case representative of a plenum-fed quick-mix section of a Rich Burn/Quick Mix/Lean Burn combustor (i.e. a jet-mainstream mass-flow ratio of about 3 and a jet-mainstream momentum-flux ratio of about 30) was investigated. This case showed that the jet velocity entering the combustor was very non-uniform, with a low normal velocity at the leading edge of the orifice and a high normal velocity at the trailing edge of the orifice. Three different combustor-only cases were analyzed with uniform inlet jet profile. None of the cases matched the plenum-fed calculations. To assess liner thickness effects, a thin-walled case was also analyzed. The CFD analysis showed the thin-walled jets had more penetration than the thick-walled jets.

Nomenclature

$A_{orifice}$	Geometric Area of Orifice
A_{tot}	Total Flow Area in Each Axial Plane
A_i	Flow Area of Cell i
C_{avg}	$m_j/(m_j+m_\infty) = \theta_{EB}$
C_i	Jet Mass Fraction in Cell i
c_{var}	$(1/A_{TOT})\sum_i A_i (C_i - C_{avg})^2$
DR	Density Ratio ρ_j/ρ_∞
f	Mixture Fraction
h	Enthalpy
H	Duct Height
J	Momentum-Flux Ratio $(\rho_j V_j^2)/(\rho_\infty U_\infty^2)$
k_∞	Turbulent Kinetic Energy of Mainstream
m_j	Mass-Flow of Jets
MR	Mass-Flow Ratio m_j/m_∞
m_∞	Mass-Flow of Mainstream
P	Static Pressure (N/m^2)
P_{exit}	Static Pressure at Combustor Exit
P_{jet}	Static Pressure of Jet
P_{s_1}	Static Pressure Upstream of Quick-Mix Orifices
P_t	Total Pressure at Plenum Entrance
P_∞	Static Pressure of Mainstream
T	Temperature (K)
T_{exit}	Exit Temperature
T_{jet}	Temperature of Jet
T_∞	Temperature of Mainstream
U_∞	Mainstream Flow Velocity (m/s)
V_j	Jet Velocity (m/s)
x	Axial Coordinate, x=0 at leading edge of the orifice
x/H	Axial Distance-to-Duct Height Ratio
y	Vertical Coordinate

z	Lateral Coordinate
ε_∞	Turbulent Energy Dissipation of Mainstream
ϕ_{rb}	Rich-Burn Equivalence Ratio
ϕ_{lb}	Lean-Burn Equivalence Ratio
ρ_{jet}	Density of Jet
ρ_∞	Density of Mainstream

Introduction

The mixing of jets with mainstream flow is very significant in many gas turbine combustor applications. In conventional combustor design, air is injected through primary and dilution orifices to mix with hot gas effluent. The design of the orifices is important in combustor performance and durability (i.e. exit temperature pattern factor, exit radial temperature profile, combustion efficiency, emissions, liner hot streaks, etc.). Dilution jet mixing has received a lot of attention as discussed by Holdeman[1]. More recently, jet mixing has drawn a lot of attention in regards to low emission combustor design, especially the Rich Burn/ Quick Mix/Lean Burn (RQL)[2] combustor design. The RQL combustor requires a large amount of bypass air (typically a jet-to-mainstream mass-flow ratio of 3) to be efficiently mixed with rich burn effluent so that NO_x emissions are kept to a minimum.[3] The optimization of this type of mixing process has received a lot of study.[4-16]

CFD analysis is typically used to help design the orifice pattern for effective mixing. To conserve computer resources, CFD analysis is usually performed on the interior of the combustor; the inlet boundary conditions for the air jets are specified by the designer. The jets are typically input with uniform velocity and turbulence levels, and the flow direction is determined by 1D annulus models. Usually, an effective orifice flow area is modeled, corresponding to the geometric area multiplied by the discharge coefficient. Other research[17-21] has shown that there is a coupling effect between the annulus airflow and combustor interior flow, and the prediction of jet penetration and mixing is strongly affected by including the annulus flow in the CFD analysis. Indeed, in the next five years as parallel computers are utilized, CFD analysis will be performed starting from the compressor exit and going all the way to the combustor exit. But, for now, only the interior of the combustor is usually analyzed, and ways of defining the jet boundary conditions are needed.

McGuirk's[20-21] work focussed on primary and dilution hole airflows that had jet-to-mainstream mass-flow ratios less than 0.5. This paper studies mass-flow ratios more commonly used in RQL combustors. Instead of annulus flow, the air jets are fed by a plenum as a first step in understanding the coupling effect between jet and mainstream. A baseline plenum case is discussed first, and the nonuniformity of the jet exiting the orifice is presented. The CFD analysis is then verified by comparing isothermal numerical predictions with experimental measurements. Next, three cases of the combustor interior are analyzed to try and identify ways to specify jet boundary conditions that capture the flow coupling effects. And last, a thin-walled liner case is compared to a thick-walled liner case to assess the differences in flow coupling.

CFD Code

The approach in this study was to perform 3-D numerical calculations on generic combustor geometries with and without the addition of plenums. The code named CFD-ACE[22] was used to perform all of the computations. The basic capabilities/methodologies in CFD-ACE include:

(1) co-located, fully implicit and strongly conservative finite volume formulation;

(2) solution of two-and three-dimensional Navier-Stokes equations for incompressible and compressible flows;

(3) non-orthogonal curvilinear coordinates;

(4) multi-block grid topology;

(5) upwind, central (with damping), second order upwind and Osher-Chakravarthy differencing schemes;

(6) standard[23], extended, RNG[24] and low Reynolds number[25] k-ε turbulence models;

(7) instantaneous, one-step, two-step, and four-step heat release and emission combustion models;

(8) spray models including trajectory, vaporization, etc.; and

(9) pressure-based solution algorithms including SIMPLE and a variant of SIMPLEC.

Details Of Numerical Calculations

The focus of this study was to analyze the flow coupling effect that can occur in jet-in-crossflow geometries. The baseline configuration, shown in Figure 1, can be described as having an annular quick-mix zone section with orifices located on both the inner and outer diameter liner. The orifices are fed by plenums. The orifice length-to-diameter ratio, L/d, was greater than one, representative of a thick-walled combustor. The inner radius of the quick-mix zone annulus measured 0.3896m and the outer radius measuring 0.4404m. The height of the quick-mix zone was 0.0508m. The axial length of the calculation extended 0.152m from the leading edge of the orifice (x/H=3.0). The walls (i.e. thickness of the orifices) were modeled as being 0.0064m thick. Each orifice was fed by a plenum that was 0.065m in length and 0.076m in height. The orifices were slots with semi-circular ends and had 2:1 length-to-width aspect ratios.

To enhance the computational efficiency of the numerical calculations, only one set of orifices (top and bottom) were modeled. The orifices were located on the inner and outer diameter in the same axial plane, and inline in the transverse direction. The transverse calculation domain extended from midplane to midplane between the jets' centerline. The included angle was 3.75 degrees. Periodic boundary conditions were assumed on the transverse boundaries.

For the combustor-only calculations only the quick-mix zone was used. The quick-mix orifices were modeled as inlets with a uniform velocity profile. The velocity magnitude was determined via three different methods (Figure 2). The first method used the velocity calculated from the plenum to mixer exit pressure drop. The second method determined the pressure drop by using the total pressure in the plenum and the average static pressure across the quick-mix zone. The third method calculated a velocity based on the mass-flow through the geometric area of the orifice. The jet velocities for the three method were calculated to be; 155 m/sec, 135 m/sec, and 92 m/sec respectively.

To assess the effects of orifice thickness, a thin-walled geometry was also analyzed. The thin-walled case was identical to the baseline case except for the orifice thickness. For the thin-walled geometry the wall thickness was reduced to be 0.000889m.

The flow conditions of the mainstream and the jets were:

Mainstream		Jets	
U_∞	= 43.5 m/s	P_{jet}	= 1.03 x 10^6 N/m^2
T_∞	= 2035 K	T_{jet}	= 777 K
P_∞	= 9.72 x 10^5 N/m^2		
k_∞	= 118.0 m^2/sec^2		
ε_∞	= 5.4 x 10^4 m^2/sec^3		

MR = 3.20
DR = 3.20
T_{exit} = 1755 K
ϕ_{rb} = 2.0
ϕ_{lb} = 0.425

Grids

The computational mesh was created using CFD-GEOM[26], an interactive three-dimensional geometry modeling and mesh generation software. The baseline case consisted of approximately 86,500 cells. The grid shown in Figure 1 was created with 5 domains. Each plenum was modeled as a domain as well as each orifice. The quick-mix zone was also specified as a domain and was composed of 28,329 cells, 71 cells in the axial direction (x), 19 cells in the vertical direction (y), and 21 cells in the transverse direction (z). The plenum grid was distributed as 42x29x21 cells (x,y,z, direction). The 2:1 slots were composed of 28x11 uniformly distributed cells, with 7 cells in the vertical direction to represent the combustor wall thickness (0.0064m). The grid upstream and downstream of the slots was expanded/contracted so that each cell adjacent to the slot matched the cell size in the interior of the slot. The cells in the vertical direction were compressed in the wall regions to more accurately capture wall effects.

For the combustor-only case a single domain mesh consisting of solely the quick-mix section was used. Finally, the thin-walled case was the same as the baseline case except the thickness of the orifices was reduced.

Numerics & Models

The following conservation equations were solved: u momentum, v momentum, w momentum, mass (pressure correction), turbulent kinetic energy (k), turbulent energy dissipation (ε), and mixture fraction (f). The convective fluxes were calculated using upwind differencing, and the diffusive fluxes were calculated using central differencing. The standard k-ε turbulence model was employed and conventional wall functions were used. The walls were assumed to be adiabatic. The turbulent Schmidt and Prandtl numbers were set to be 0.5. A fast chemistry (instantaneous) model was assumed. Equilibrium products were also assumed. The inlet to the rich-burn section was assumed to be the equilibrium products of a fully-burned 1.8 equivalence ratio. The fuel used was $C_{10}H_{19}$, representative of Jet A fuel.

Convergence

All error residuals were reduced at least 6 orders of magnitude, and continuity was conserved in each axial plane to the fifth decimal. A converged solution required approximately 5-7 CPU hours on a IBM RS6000 Model 560 computer. Although the cases reported in this paper were performed using the IBM RS6000, additional cases were run using the NAS C-90 computer.

Results and Discussion

Baseline Plenum-Fed Case

Figure 3 shows the temperature contours for the baseline plenum-fed case. The temperature contours are plotted in a lateral plane through the orifice centerline. The jets show near optimum jet penetration, penetrating to approximately 1/4 duct height. There is a slight difference in penetration between the outer diameter and inner diameter jets; this difference is caused by geometric differences. The coupling effect causes a non-uniformity of the jet flowfield as it exits the orifice. By examining the velocity vectors and profile at the orifice exit (Figure 4), the jet velocity non-uniformity in the jet flowfield can be seen. Because of the large L/d of the orifice, the jet velocity is essentially normal to the crossflow. A low normal velocity at the leading edge of the orifice and a high normal velocity at the trailing edge is evident.

Similarly, the static and total pressure at the orifice discharge was also non-uniform as seen in Figure 5 and 6. There is a high total pressure core in the center of the orifice, but at the edges of the orifice there is a total pressure loss. The non-uniform static pressure is further illustrated in the axial static pressure plot presented in Figure 7. The static pressure varies from 30,000 N/m^2 above combustor exit pressure to -15,000 N/m^2 below the combustor exit pressure.

Non-Reacting Validation Case

To validate the plenum-fed baseline case, it was decided to perform a thick-orifice isothermal case for which jet mixing data existed. The case selected is described below, with the comparison between numerical predications and experimental measurements.

Geometry

For the validation case, the geometry consisted of a cylindrical mixing zone with 8 round holes uniformly spaced on the can circumference. Figure 8 shows a schematic of the test geometry. The diameter of each hole was 0.0178m (0.7 inches) and diameter of the can was 0.0792m (3.88 inches). The thickness of each round hole was 0.0792m (3.12 inches). Figure 8 shows the plenum which is approximately 0.529m (6 inches) in length. The mainstream flow enters from an inlet section 0.3048m long and 0.079m in diameter. The inlet section had a divergence angle of 2 degrees with an initial diameter of 0.079m that diverges to the mixing section diameter of 0.0986m. The orifices are located 0.0508m downstream of the bulkhead that connects the mainstream inlet feed into the quick-mix region. The experimental procedure is described in, for example, Reference 14.

The computational grid is shown in Figure 9. To enhance the computational efficiency of the numerical calculations, only one orifice was modeled (45 deg. sector) and periodic boundaries were assumed. The grid was separated into three distinct blocks. The first block represented the quick-mix zone, consisting of 78 cells in the axial direction (x), 19 cells in the vertical direction (y), and 29 cells in the transverse (z) direction. The second block was the plenum; it was composed of 11 x 14 x 11 cells (x,y,z). The third block represented the orifice, composed of 29 x 29 uniformly distributed cells. The orifice was modeled with 14 cells in the

vertical direction to represent the thickness of the combustor wall. In the quick-mix section, the grid upstream and downstream of the orifice region was expanded/contracted so that each cell adjacent to the orifice region matched the cell size in the slot region. The cells in the vertical direction were compressed in the vicinity of the wall to more accurately capture wall effects.

Flow Conditions

The flow conditions of the mainstream and jets were specified to be:

Mainstream		Jets	
U_∞	= 4.637 m/s	P_{jet}	= 106,166 N/m^2
T_∞	= 291.67 K	T_{jet}	= 291.67 K
P_∞	= 101,341 N/m^2		
k_∞	= 2.9027 x 10^{-2} m^2/sec^2		
ε_∞	= 3.2063 x 10^{-1} m^2/sec^3		

The mass-flow ratio was specified to be 1.0 corresponding to a momentum-flux ratio of 30.

Validation Case Results

Shown in Figure 10 are the jet mixture fraction axial slices measurements. The comparable numerical results are also presented in Figure 10. Axial slices were extracted at x/R locations of 1.28, 1.54, and 2.05 downstream of the leading edge of the round hole. The same color bar was used for the calculated results and experimental measurements. The numerical results show very good agreement with the experimental results at all of the downstream stations. At the closest station (x/R=1.28), the computational results capture the center mainstream core along with the slight bluish contour levels present at about mid-radius. Moving to the farther downstream locations, the numerical results show a slightly slower mixing rate than seen in the experimental results.

Figure 11 shows the spatial unmixedness curves for the CFD and experimental results. Planar unmixedness, U_s,[27] is a parameter that quantifies the unmixedness of a distribution and can be defined as:

$$U_s = c_{var} / [c_{avg} (1-c_{avg})]$$

Good overall agreement can be seen. Thus, from an engineering viewpoint, the plenum-fed calculations capture the overall characteristics of the jets-in-crossflow.

Combustor-Only Calculations

Shown in Figure 12 are the results of the combustor-only calculations for three specified uniform inlet velocities: 1) jet velocity corresponding to the overall pressure drop velocity, 155 m/sec; 2) jet velocity corresponding to the average pressure drop velocity, 135 m/sec; and 3) jet velocity corresponding to the mass-flow through the orifice geometric area, 92 m/sec. Compared to the baseline calculation (Figure 3), each combustor-only case predicted jet overpenetration. The highest jet velocity produced the greatest amount of overpenetration, as evidenced by the mainstream flow being deflected to the outer wall. This is illustrated by the hotter temperatures near the ID and OD walls. The results of the lowest jet velocity (Method 3) still predicted overpenetrating jets, but gave the closest overall agreement to the baseline case results. Note that the OD near wall temperatures are hotter than the ID temperature for each case. This occurs because the office spacing is greater for the OD wall, resulting in more mainstream flow passing between the jets.

Thus it appears that there is no simple way to capture the flow coupling that occurs with plenum-fed flowfields. As discussed previously for the baseline plenum geometry, there exists non-uniformity in the jet flow at the discharge orifice plane. In order to use an inlet boundary condition for the orifice, one would have to devise a way to determine the velocity profile that correctly produces the flow non-uniformity at the orifice discharge. This includes correctly modeling the non-uniform velocity profile, turbulence quantities, and the flow angle. The determination of these factors creates potential problems because of their variation across the orifice cross-sectional area. If it was possible to ascertain an acceptable method of capturing the flow non-uniformity, there is no guarantee that this method would be generally applicable to a variety of different orifices (i.e. round holes, slanted slots, etc...,). Therefore from a design standpoint, it probably would be very difficult to accurately capture the jet coupling effect without the use of the plenums.

Effect of Wall Thickness

For completeness, analysis was performed on a thin-walled liner to asses the effect of wall thickness on the flow coupling effect. Presented in Figure 13 are the temperature contour results of the thin-walled case. Compared to the thick-walled case (Figure 3), the thin-walled geometry showed higher jet penetration and higher overall downstream mixing.

Based on the work performed by Lichtarowicz, Duggins, and Markland[28], the discharge coefficient for orifices with length/diameter ratios (L/d) between 0 and 1 vary significantly as a function of L/d. From these results, it would be safe to assume that the thin-walled configuration (L/d = 0.04) would have a smaller discharge coefficient than the thick-walled design (L/d > 1). The lower Cd in the thin-walled case would then result in an increased pressure drop across the orifice for the same mass-flow ratio. The total pressure variation for the two geometries is presented in Figure 14. The pressure drop, plenum total pressure-combustor total pressure, for the thin-walled case is about 6.5% whereas the thick-walled case has a pressure drop around 5.8%. Despite the variation in Cd, the normal velocity levels were essentially the same for both cases. The comparable normal velocity levels for both the thin and thick-walled cases are shown in Figure 15. The differences in the penetration levels for the thick and thin-walled cases can be addressed by examining the velocity profiles. The velocity flowfield for both cases exhibit similar characteristics, but one significant difference seen is that the velocity profiles for the thin-walled case are pushed farther into the mainstream flow. This inboard translation of the velocity profiles results in more jet penetration into the quick-mix zone for the thin-walled case. Thus the increased jet penetration can be directly attributed to the lower discharge coefficient and subsequently the higher pressure drop evident in the thin-walled case. The importance of modeling the flow through the orifice is thereby shown.

Conclusions

CFD analyses were performed on air jets injected into rich-burn effluent flowing in an annulus. Jet-to-mainstream mass-flow ratios (~3) typical of RQL combustors were analyzed. Two types of calculations were performed: 1) only the combustor was modeled, with the jet flow specified at the orifice discharge plane, and 2) the jet plenum and orifice were included in the calculation domain. Results from the CFD analysis showed:

1) There exists a strong coupling between the jet flow and mainstream flow evidenced by the large velocity profile at the orifice exit.

2) This coupling effect could not be easily captured by specifying commonly-used uniform jet velocity boundary conditions for combustor-only CFD calculations.

3) The only way to accurately predict jet-in-crossflow flowfields is to include both the interior and exterior (plenums) flowfields in the CFD analysis. To do this, an order of magnitude increase in the number of computational cells is needed over conventional computational grid sizes.

4) CFD analysis was able to capture the effect of liner thickness on jet penetration and mixing, provided the calculation domain included the external and internal combustor geometry.

Acknowledgements

This work was supported by NASA Contract NAS3-25967, and NAS computer time was provided by NASA Lewis Research Center. The authors would like to thank the CFDRC software development and support staff for implementing improvements to the software. In addition thanks are given to Ms. Marni Kent for preparing this typescript.

References

1. J. D. Holdeman, "Mixing of Multiple Jets with a Confined Subsonic Crossflow," *Progress in Energy and Combustion Sciences*, Vol. 19, pp. 31-70, 1993. (See also NASA TM 104412, 1991 and AIAA 91-2458, 1991.)
2. R. J. Shaw, "Engine Technology Challenges for a 21st Century High Speed Civil Transport," *AIAA Tenth International Symposium on Air Breathing Engines*, September 1-6, 1991 (Also NASA TM 104363).

3. S. A. Mosier and R. M. Pierce, "Advanced Combustion Systems for Stationary Gas Turbine Engines," Vol. 1, EPA Contract 68-02-2136, 1980.
4. J. D. Holdeman, D. S. Liscinsky, V. L. Oechsle, G. S. Samuelsen, and C. E. Smith, "Mixing of Multiple Jets with a Confined Subsonic Crossflow in a Cylindrical Duct," Accepted for publication in *Journal of Engineering for Gas Turbines and Power*, 1996 (Also ASME Paper-GT-482 & NASA TM 107185).
5. C. E. Smith, M. V. Talpallikar, and J. D. Holdeman, "A CFD Study of Jet Mixing in Reduced Flow Areas for Lower Combustor Emissions," AIAA 91-2460, June 1991 (Also NASA TM 104411).
6. D. B. Bain, C. E. Smith, and J. D. Holdeman, "CFD Mixing Analysis of Jets Injected from Straight and Slanted Slots into Confined Crossflow in Rectangular Ducts," AIAA 92-3087, June 1992 (Also NASA TM 105699).
7. D. S. Liscinsky, B. True, A. Vranos, and J. D. Holdeman, "Experimental Study of Cross-Stream Mixing in a Rectangular Duct," AIAA 92-3090, June 1992 (Also NASA TM 106194).
8. D. S. Liscinsky, A. Vranos, and R. P. Lohmann, "Experimental Study of Crossflow Mixing in Cylindrical and Rectangular Ducts," NASA CR 187141, March 1993.
9. D. S. Liscinsky, B. True, and J. D. Holdeman, "An Experimental Study of Crossflow Jet Mixing in Rectangular Ducts," AIAA-93-2037, June 1993 (Also TM 106152).
10. D. B. Bain, C. E. Smith, and J. D. Holdeman, "CFD Mixing Analysis of Axially Opposed Rows of Jets Injected in Confined Crossflow," *Journal of Propulsion and Power*, Vol. 11, No. 5, p. 885-893, September-October 1995 (See also AIAA Paper 93-2044 and NASA TM 106179).
11. D. B. Bain, C. E. Smith, and J. D. Holdeman, "CFD Assessment of Orifice Aspect Ratio and Mass Flow Ratio on Jet Mixing in Rectangular Ducts," AIAA Paper 94-0218, January 1994 (Also NASA TM 106477).
12. D. S. Liscinsky, B. True, and J. D. Holdeman, "Mixing Characteristics of Directly Opposed Rows of Jets Injected Normal to a Crossflow in a Rectangular Ducts," AIAA Paper 94-0217, January 1994 (Also NASA TM 106477).
13. D.S. Liscinsky, B. True, and J.D. Holdeman, "Crossflow Mixing of Noncircular Jets," *Journal of Propulsion and Power*, Vol. 12, No. 2, pp. 225-230, January-February 1996 (See also AIAA Paper 95-0732 and NASA TM 106865).
14. Th. Doerr and D. K. Hennecke, "The Mixing Process in the Quenching Zone of the Rich-Lean Combustion Concept," *AGARD 81st Symposium on Fuels and Combustion Technology for Advanced Aircraft Engines*, Colleferro, NR Rome, Italy, May 10-14, 1993.
15. Th. Doerr, M. Blomeyer, and D. K. Henneke, "Optimization of Multiple Jets Mixing with a Confined Crossflow," ASME Paper 95-GT-313, 1995.
16. Th. Doerr, M. Blomeyer, and D. K. Henneke, "Experimental Investigation of Optimum Jet Mixing Configurations for RQL-Combustors," 12th ISABE, Melborne, Aus., 1995.
17. J. F. Carrotte, and S. J. Stevens, "The Influence of Dilution Hole Geometry on Jet Mixing," *J. of Engineering for Gas Turbines and Power*, Vol. 112, No. 1, pp. 73-75, January 1990 (See also ASME Paper 89-GT-292).
18. S. J. Stevens, and J. F. Carrotte, "Experimental Studies of Combustor Aerodynamics, Part I: Mean Flowfields," *J. of Propulsion and Power*, Vol. 6, No. 3, pp. 297-304, May-June 1990 (See also AIAA Paper 87-1827, The Influence of Dilution Hole Aerodynamics on the Temperature Distribution in a Combustor Dilution Zone).
19. S. J. Stevens, and J. F. Carrotte, "Experimental Studies of Combustor Dilution Zone Aerodynamics, Part II: Jet Development," *J. of Propulsion and Power*, Vol. 6, No. 4, pp. 503-511, July-August 1990 (See also AIAA Paper 88-3274).
20. J. J. McGuirk and S. J. Baker, "Multi-Jet Annulus/ Core-Flow Mixing-Experiments and Calculations," ASME 92-GT-111, 1992.
21. J. J. McGuirk and A. Spencer, "CFD Modeling of Annulus/Port Flows," ASME 93-GT-185, 1993.
22. S. F. Owens, "CFD-ACE: Command Language Reference Manual," CFD Research Corporation, Huntsville, AL, CFDRC Report GR-92-6, 1992.
23. B. E. Launder and D. B. Spalding, "The Numerical Computation of Turbulent Flows," *Computer Methods in Applied Mechanics and Engineering*, Vol. 3, pp. 269-289, 1974.

24. Y. S. Chen and S. W. Kim, "Computation of Turbulent Flows Using an Extended k–ε Turbulence Closure Model," NASA CR-179204, 1987.
25. K. Y. Chien, "Predictions of Channel and Boundary-Layer Flows with a Low-Reynolds Number-Turbulence Model," *AIAA Journal*, Vol. 23, No. 2, 1985.
26. CFD-GEOM User Manual, Version 1.3, March 1995.
27. P. V. Danckwertz, "The Definition and Measurement of Some Characteristics of Mixtures," *Appl. Sci. Res.*, Sec. A., Vol. 3, pp. 279-296, 1952.
28. S. Lichtarowicz, R. K. Duggins, and E. Markland, "Discharge Coefficients for Incompressible Non-Cavitating Flow Through Long Orifices," *Journal Mechanical Engineering Science*, Vol. 7, No. 2, pp. 210-219, 1965.

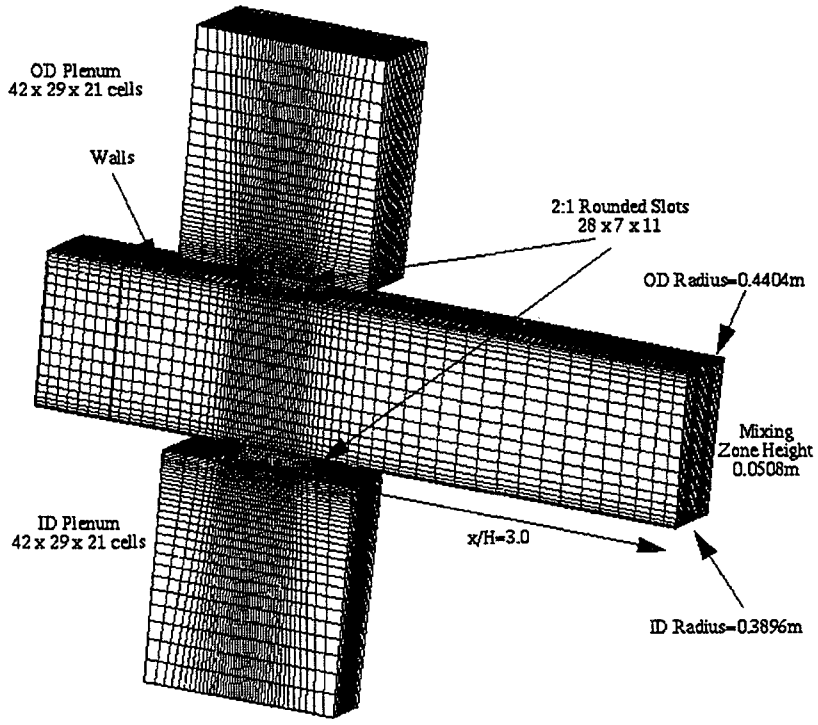

Figure 1. Baseline Annular Geometry and Grid

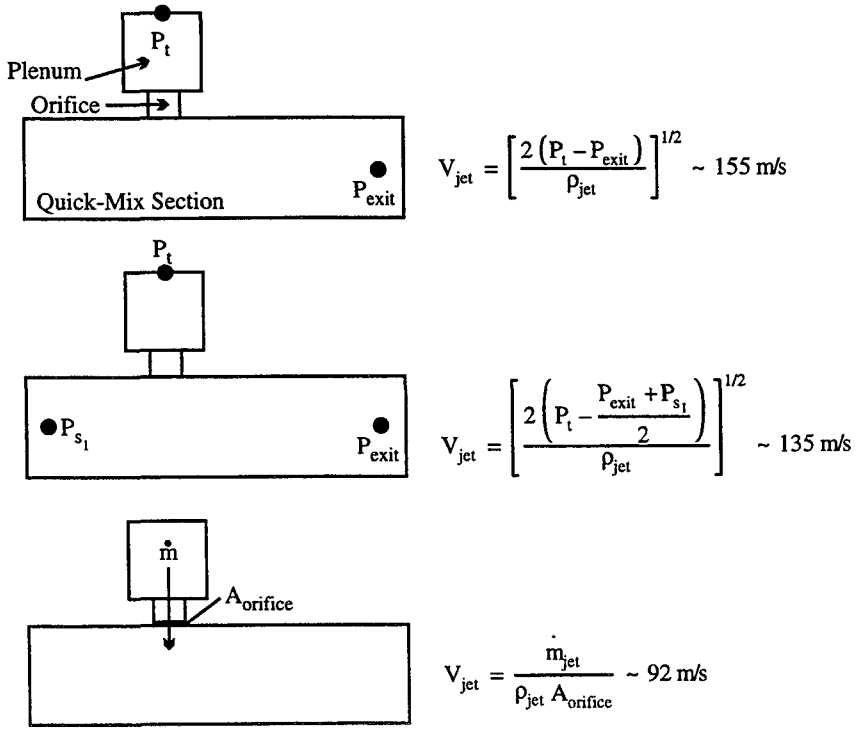

Figure 2. Three Methods Used to Determine Jet Velocity for Combustor-Only Calculations

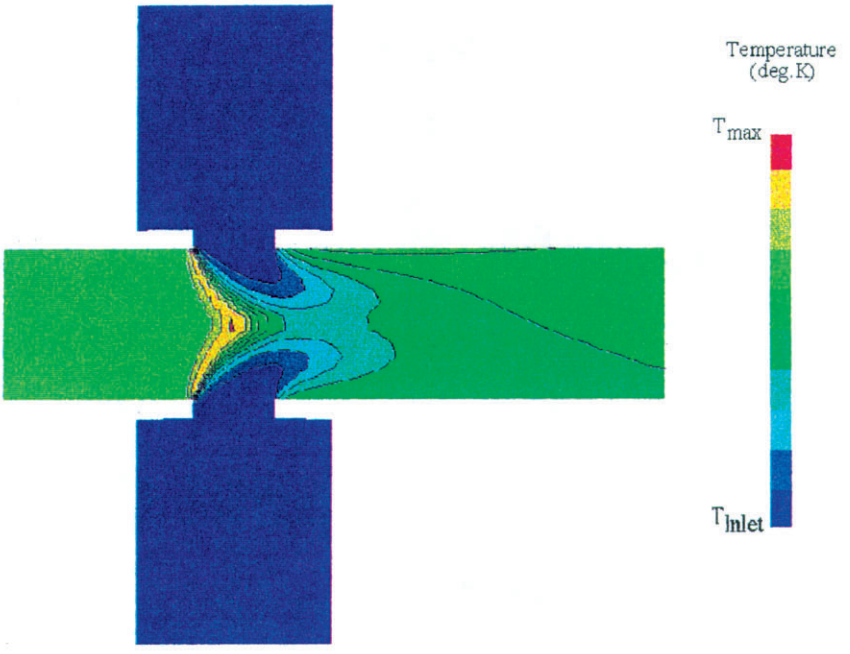

Figure 3. Temperature Contours for Baseline Plenum-Fed Geometry

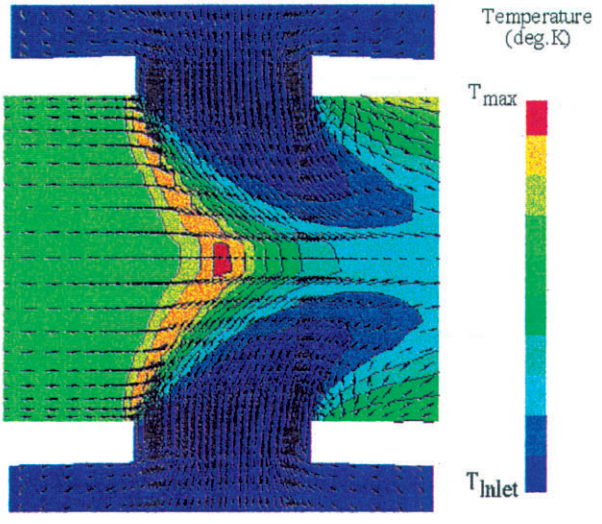

Figure 4. Close-Up of Velocity Flowfield through Thick-Walled Combustor

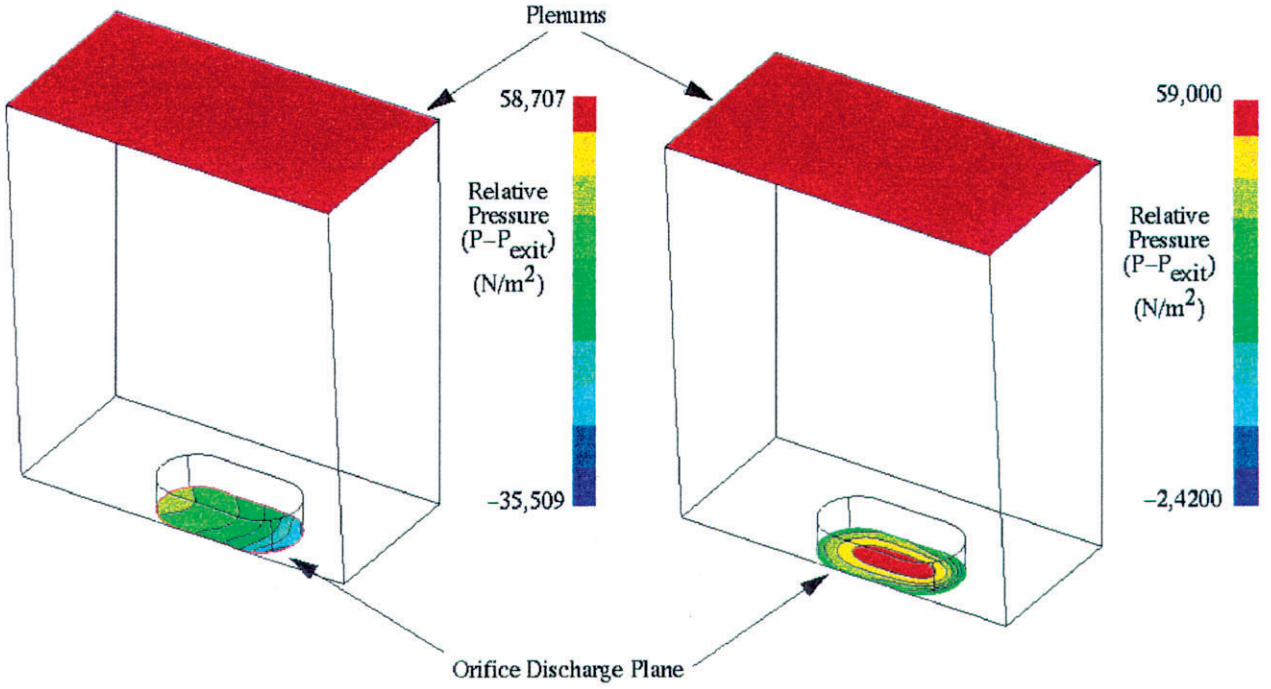

Figure 5. Non-Uniform Static Pressure Distribution Across the Orifice Exit Plane

Figure 6. Non-Uniform Total Pressure Distribution Across the Orifice Exit Plane

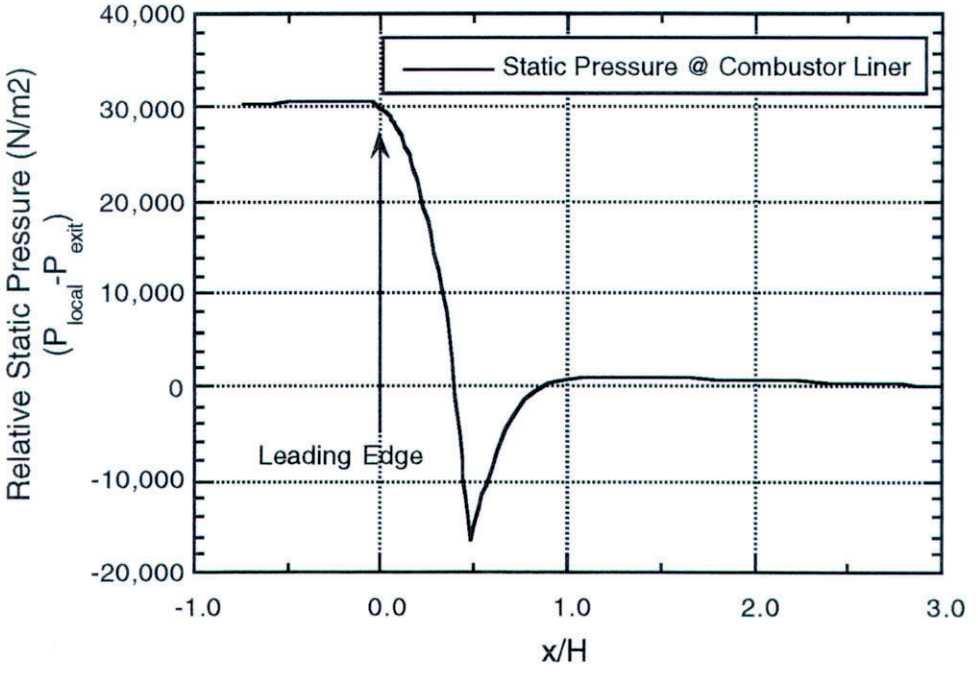

Figure 7. Non-Uniform Static Pressure at Combustor Liner (Orifice extends from 0<x/H<0.5)

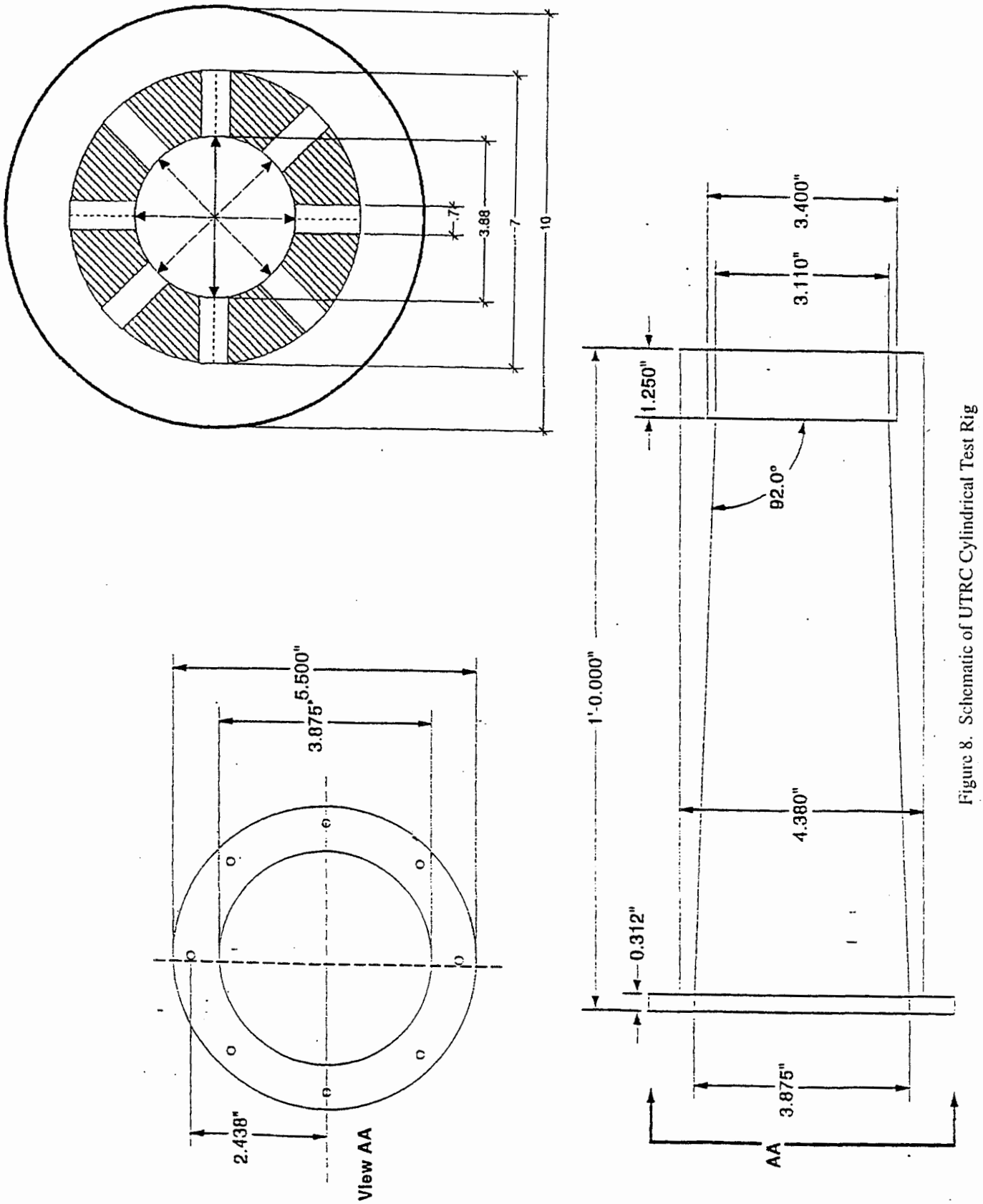

Figure 8. Schematic of UTRC Cylindrical Test Rig

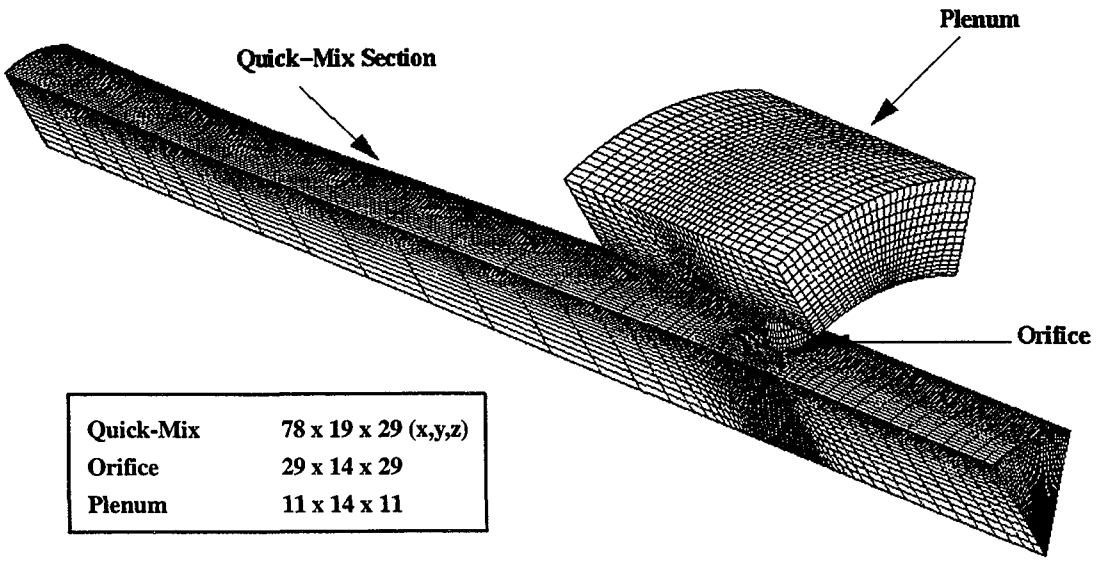

Figure 9. Computational Mesh of UTRC Cylindrical Geometry

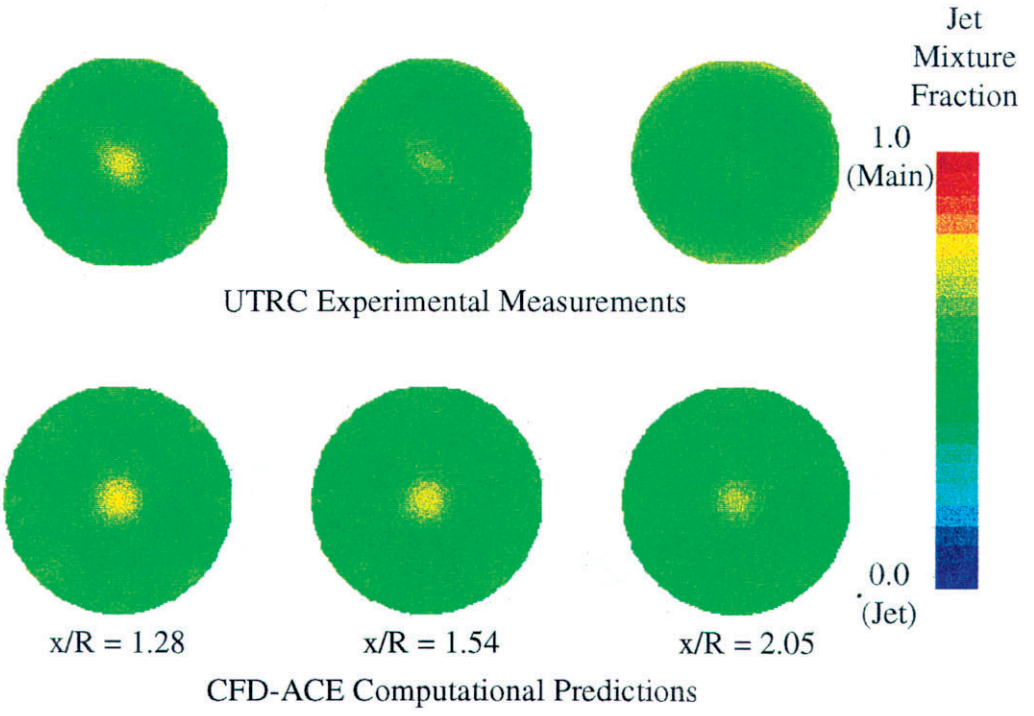

Figure 10. Comparison of CFD-ACE and Experimental Measurements

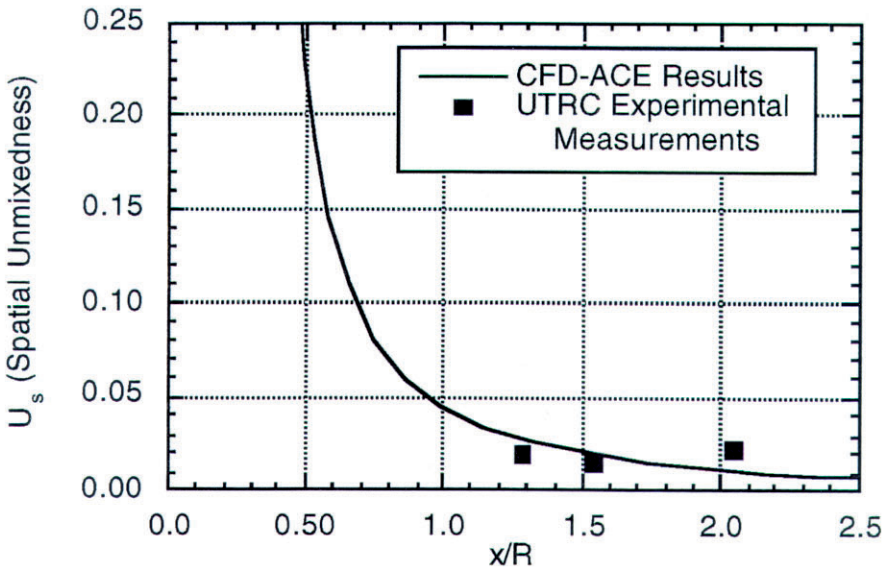

Figure 11. Numerical and Experimental Comparison of Spatial Unmixedness

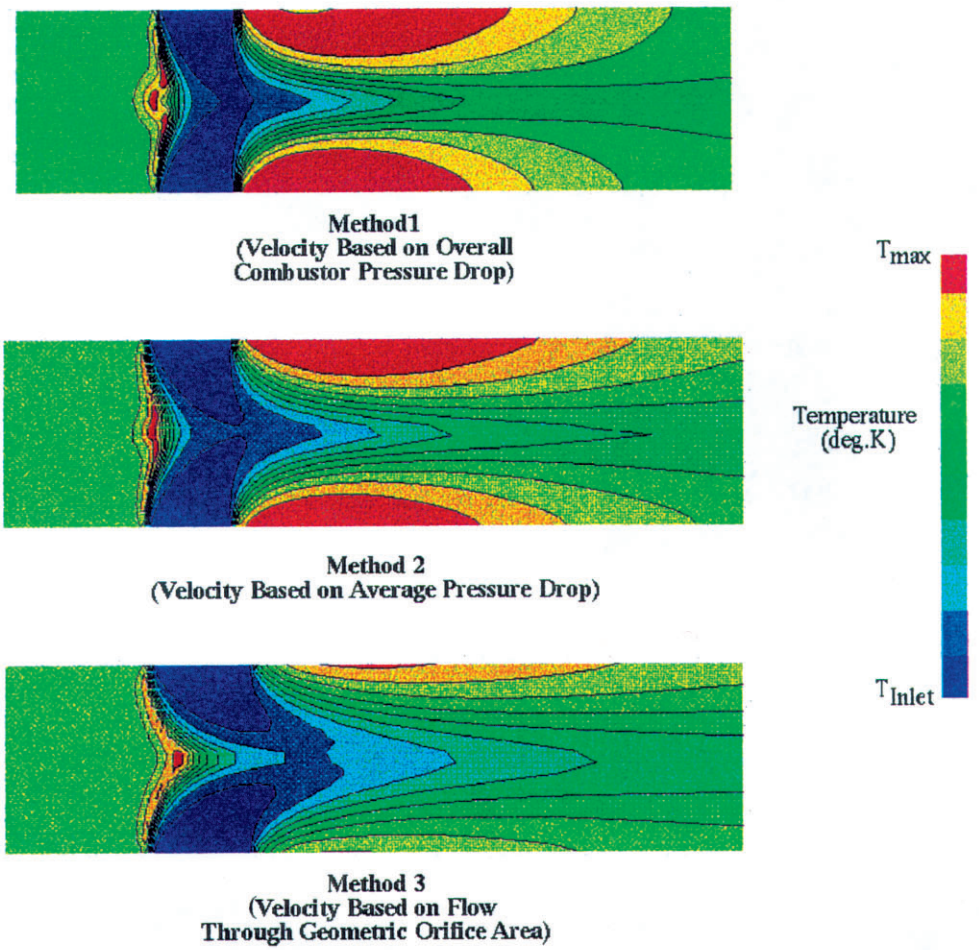

Figure 12. Combustor – Only Analysis for 4 Orifices ID & OD in 15 deg. Sector

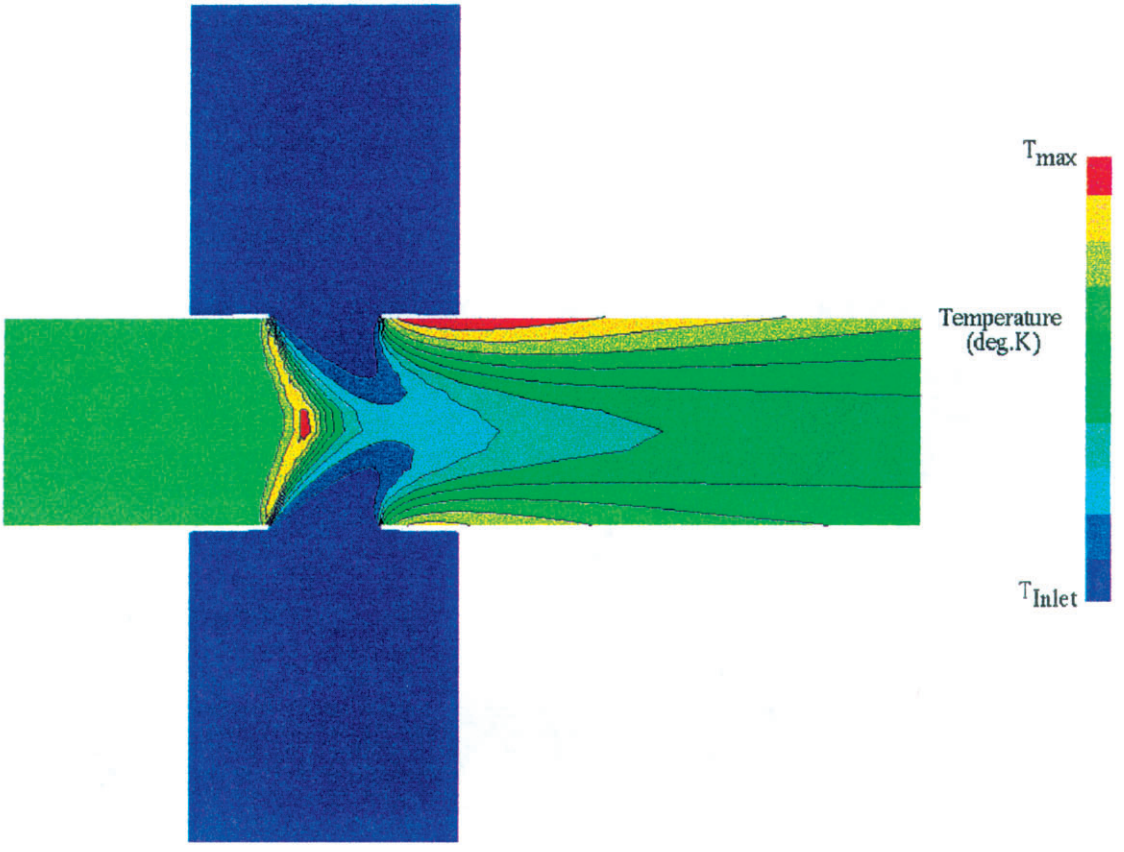

Figure 13. Temperature Contours for the Thin-Walled Geometry

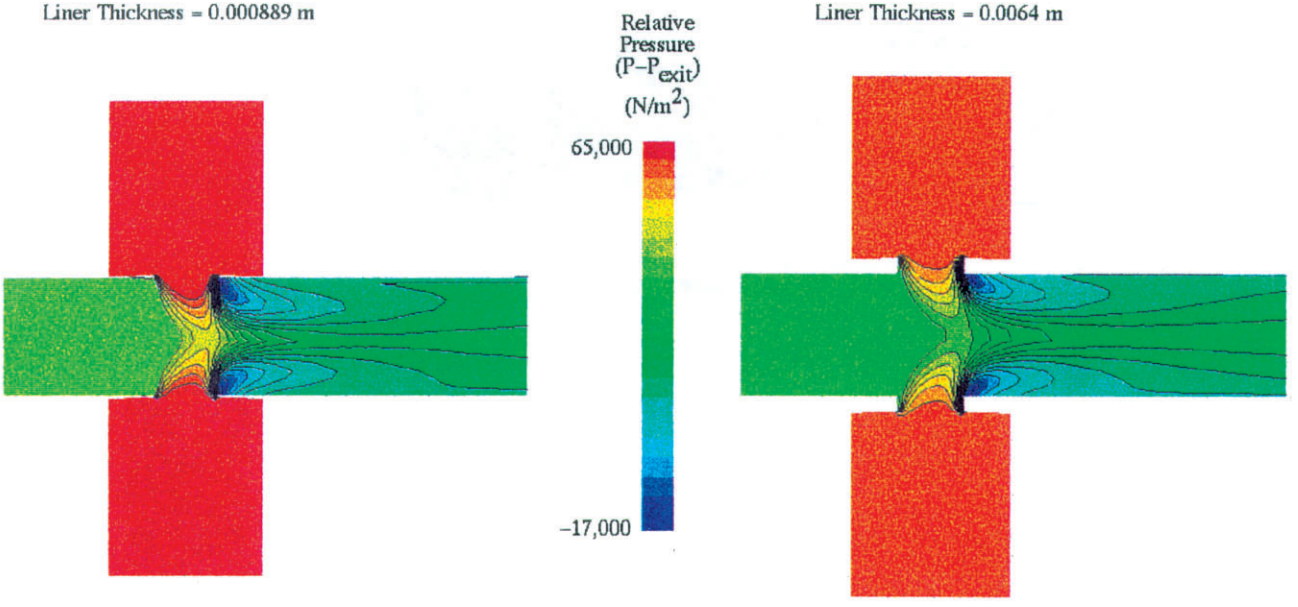

Figure 14. Total Pressure Centerline Slices for Thin and Thick-Walled Geometry

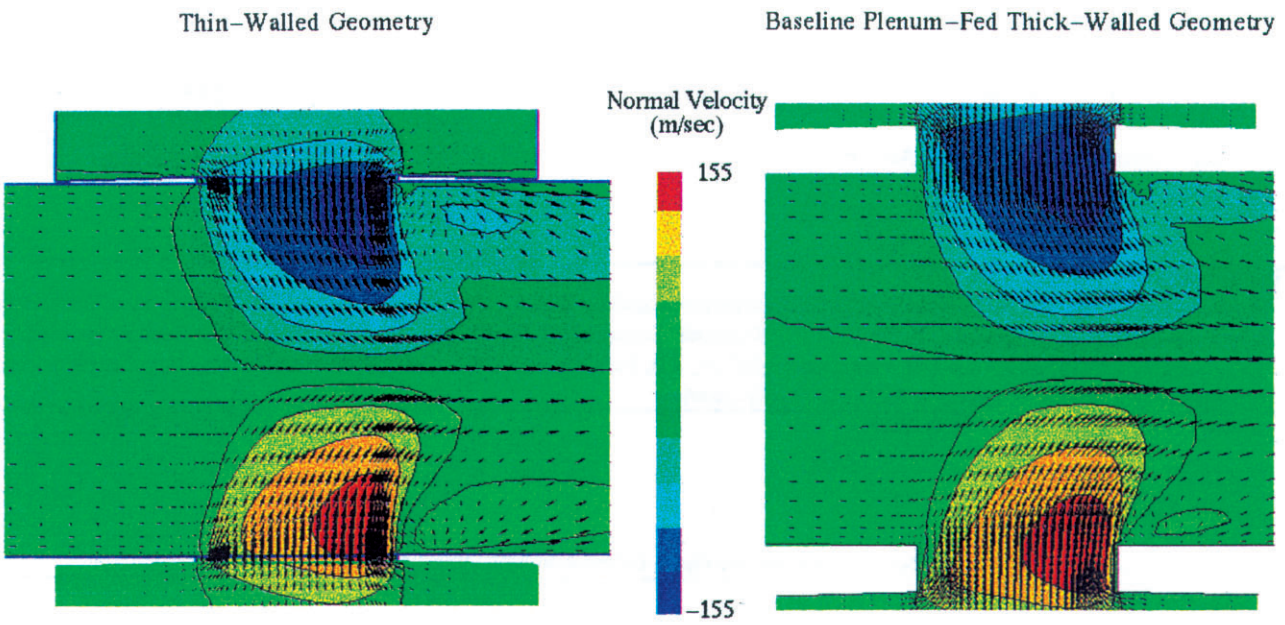

Figure 15. Velocity Profile Comparison Between Thick-Walled and Thin-Walled Combustor

REPORT DOCUMENTATION PAGE

Form Approved
OMB No. 0704-0188

1. AGENCY USE ONLY (*Leave blank*)	2. REPORT DATE	3. REPORT TYPE AND DATES COVERED
	June 1996	Technical Memorandum

4. TITLE AND SUBTITLE

Flow Coupling Effects in Jet-In-Crossflow Flowfields

5. FUNDING NUMBERS

WU–537–02–20–00

6. AUTHOR(S)

D.B. Bain, C.E. Smith, D.S. Liscinsky, and J.D. Holdeman

7. PERFORMING ORGANIZATION NAME(S) AND ADDRESS(ES)

National Aeronautics and Space Administration
Lewis Research Center
Cleveland, Ohio 44135–3191

8. PERFORMING ORGANIZATION REPORT NUMBER

E–10318

9. SPONSORING/MONITORING AGENCY NAME(S) AND ADDRESS(ES)

National Aeronautics and Space Administration
Washington, DC 20546–0001

10. SPONSORING/MONITORING AGENCY REPORT NUMBER

NASA TM–107257
AIAA–96–2762

11. SUPPLEMENTARY NOTES

Prepared for the 32nd Joint Propulsion Conference cosponsored by AIAA, ASME, SAE, and ASEE, Lake Buena Vista, Florida, July 1–3, 1996. D.B. Bain and C.E. Smith, CFD Research Corporation, Huntsville, Alabama 35805; D.S. Liscinsky, United Technologies Research Center, East Hartford, Connecticut 06108; J.D. Holdeman, NASA Lewis Research Center. Responsible person, J.D. Holdeman, organization code 2650, (216) 433–5846.

12a. DISTRIBUTION/AVAILABILITY STATEMENT

Unclassified - Unlimited
Subject Category: 07

Available electronically at http://gltrs.grc.nasa.gov/GLTRS
This publication is available from the NASA Center for AeroSpace Information, (301) 621–0390.

12b. DISTRIBUTION CODE

13. ABSTRACT ***(Maximum 200 words)***

The combustor designer is typically required to design liner orifices that effectively mix air jets with crossflow effluent. CFD combustor analysis is typically used in the design process; however the jets are usually assumed to enter the combustor with a uniform velocity and turbulence profile. The jet-mainstream flow coupling is usually neglected because of the computational expense. This CFD study was performed to understand the effect of jet-mainstream flow coupling, and to assess the accuracy of jet boundary conditions that are commonly used in combustor internal calculations. A case representative of a plenum-fed quick-mix section of a Rich Burn/Quick Mix/Lean Burn combustor (i.e., a jet-mainstream mass-flow ratio of about 3 and a jet-mainstream momentum-flux ratio of about 30) was investigated. This case showed that the jet velocity entering the combustor was very non-uniform, with a low normal velocity at the leading edge of the orifice and a high normal velocity at the trailing edge of the orifice. Three different combustor-only cases were analyzed with uniform inlet jet profile. None of the cases matched the plenum-fed calculations. To assess liner thickness effects, a thin-walled case was also analyzed. The CFD analysis showed the thin-walled jets had more penetration than the thick-walled jets.

14. SUBJECT TERMS

Emissions; Dilution jet mixing; Gas turbine engine; Combustion chamber

15. NUMBER OF PAGES

19

16. PRICE CODE

A03

17. SECURITY CLASSIFICATION OF REPORT	18. SECURITY CLASSIFICATION OF THIS PAGE	19. SECURITY CLASSIFICATION OF ABSTRACT	20. LIMITATION OF ABSTRACT
Unclassified	Unclassified	Unclassified	

REPORT DOCUMENTATION PAGE

Form Approved
OMB No. 0704-0188

1. AGENCY USE ONLY (*Leave blank*)	2. REPORT DATE	3. REPORT TYPE AND DATES COVERED
	June 2003	Final Contractor Report

4. TITLE AND SUBTITLE

Analysis of Combustion Systems

5. FUNDING NUMBERS

WBS–22–714–01–38
NAS3–25967

6. AUTHOR(S)

Daniel B. Bain and Clifford E. Smith

7. PERFORMING ORGANIZATION NAME(S) AND ADDRESS(ES)

CFD Research Corporation
215 Wynn Drive
Huntsville, Alabama 35805

8. PERFORMING ORGANIZATION REPORT NUMBER

E–13905

9. SPONSORING/MONITORING AGENCY NAME(S) AND ADDRESS(ES)

National Aeronautics and Space Administration
Washington, DC 20546–0001

10. SPONSORING/MONITORING AGENCY REPORT NUMBER

NASA CR—2003-212317

11. SUPPLEMENTARY NOTES

This research was originally published internally as HSR043 in August 1996. Project Manager, James D. Holdeman, Turbomachinery and Propulsion Systems Division, NASA Glenn Research Center, organization code 5830, 216–433–5846.

12a. DISTRIBUTION/AVAILABILITY STATEMENT

Unclassified - Unlimited
Subject Category: 07 Distribution: Nonstandard

Available electronically at http://gltrs.grc.nasa.gov

This publication is available from the NASA Center for AeroSpace Information, 301–621–0390.

12b. DISTRIBUTION CODE

13. ABSTRACT ***(Maximum 200 words)***

This five year project focused on identifying quick-mix methods that would reduce NO_x emissions in RQL combustors. The work included study of mixing concepts, and the development of design methodology. 3–D CFD analysis was the primary tool used in assessing concepts and developing design methodology for low emissions. Isothermal and reacting CFD calculations were performed on cylindrical, rectangular, and annular generic geometries. Systematic parametric studies were performed to isolate key design parameters and their influence on mixing and emissions. In addition to the CFD analysis, software was written to interpret experimental isothermal mixing results in terms of NO_x emissions. The software, called NO_x Inference Code (NIC), took planar experimental jet mass fraction data and inferred NO_x emissions assuming: 1) the jet mass fraction fields were the same for reacting and non-reacting flows if the momentum-flux ratio and mass-flow ratio were maintained, and 2) fast equilibrium chemistry occurred for heat release. Thermal NO_x was predicted using the extended Zeldovich mechanism. The code was validated using the experimental data of Anderson. NIC was then used to assess the effect of jet penetration on NO_x emissions and to compare emission for optimum inline and staggered orifices in a rectangular geometry. Overall, this project produced an improved understanding of the jet-in-crossflow mixing process and emission production in RQL combustor applications. Improved design methodology was developed that assisted in the design and evaluation of RQL combustors for High-Speed Civil Transport Aircraft engines. Close interaction was maintained with United Technology Research Center (UTRC) and Pratt & Whitney (P&W) for the duration of the project.

14. SUBJECT TERMS

Dilution; Jet mixing flow; Gas turbine; Combustion chamber; Emissions; CFD

15. NUMBER OF PAGES

256

16. PRICE CODE

17. SECURITY CLASSIFICATION OF REPORT	18. SECURITY CLASSIFICATION OF THIS PAGE	19. SECURITY CLASSIFICATION OF ABSTRACT	20. LIMITATION OF ABSTRACT
Unclassified	Unclassified	Unclassified	